SYNTHESIS AND CRYSTALLOGRAPHIC STUDIES OF NOVEL ORGANOTIN ACENAPHTHENE COMPOUNDS

Kasun S. Athukorala Arachchige

A Thesis Submitted for the Degree of PhD
at the
University of St Andrews

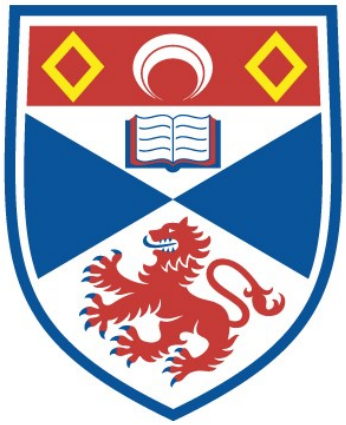

2014

Synthesis and Crystallographic Studies of Novel Organotin Acenaphthene Compounds

by

Kasun S. Athukorala Arachchige

Thesis submitted in partial fulfilment for the degree of

Doctor of Philosophy

The University of St Andrews

April 2014

Under the supervision of Professor A. M. Z. Slawin

Declaration

I, Kasun S. Athukorala Arachchige, hereby certify that this thesis, which is approximately 31, 800 words in length, has been written by me, and that it is the record of work carried out by me or principally by myself in collaboration with others as acknowledged, and that it has not been submitted in any previous application for a higher degree.

I was admitted as a research student in September 2010 and as a candidate for the degree of Ph.D. in August 2011; the higher study for which this is a record was carried out in the University of St Andrews between 2010 and 2014.

Date ….....…... Signature of Candidate ….....….....

I hereby certify that the candidate has fulfilled the conditions of the Resolution and Regulations appropriate for the degree of Ph.D. in the University of St Andrews and that the candidate is qualified to submit this thesis in application for that degree.

Date ….....…... Signature of Supervisor ….....….....

In submitting this thesis to the University of St Andrews I understand that I am giving permission for it to be made available for use in accordance with the regulations of the University Library for the time being in force, subject to any copyright vested in the work not being affected thereby. I also understand that the title and the abstract will be published, and that a copy of the work may be made and supplied to any bona fide library or research worker, that my thesis will be electronically accessible for personal or research use unless exempt by award of an embargo as requested below, and that the library has the right to migrate my thesis into new electronic forms as required to ensure continued access to the thesis. I have obtained any third-party copyright permissions that may be required in order to allow such access and migration, or have requested the appropriate embargo below.

The following is an agreed request by candidate and supervisor regarding the electronic publication of this thesis:

Embargo on both all of printed copy and electronic copy for a period of two years on the following grounds:

Publication would preclude future publication

Date ….....….. Signature of Candidate ….....….....

Signature of Supervisor ….....….....

Acknowledgements

The past 3 years of my academic life in St Andrews have been full of adventures and new challenges. I have faced the most difficult period in my life during my studies in St Andrews. During this time of difficulty, my supervisors, friends and university staff have been most helpful in helping me to overcome so many hurdles and I am ever grateful to them for their enormous help and support.

First of all I would like to thank my supervisor Professor Alex Slawin, who has given me her full support and encouragement during my PhD. Also Professor Derek Woollins, who has guided me throughout my time in St Andrews, shadowing my studies and leading me through my PhD work to make me who I am today. Thank you so much to both of you for your enormous support and I am ever in debt to both of you.

My biggest thanks go to Dr Fergus Knight; my Post Doc who helped me a lot during my personal difficulties and his support, encouragement and proof reading skills have been most helpful in allowing me to complete my work on time. Many thanks should also go to Dr Katie for the support given to me during my stay in St Andrews. Also, Louise who started her PhD at the same time as me has helped me a lot during my time in St Andrews and with formatting this thesis.

I would also like to thank Rebecca and Joy, my crystallography friends, for your help and support with my PhD work. I have enjoyed working with the Woollin's group and I have made so many new friends throughout my PhD work. Dr Petr Kilian, Dr Hua and Dr Marie thank you so much for your support with chemistry lab work and technical support.

I must also thank my research group friends, Andreas, Brain C, Jackie, Matthew, Paula, Lawrence and all the members of the Woollins and Kilian group, for your help and fun filled company over the past 3 years. They have given me so many crystals to run and it has helped me solve new structures which in turn has helped me to grow my crystallography knowledge much wider every day.

I would like to take this opportunity to give thanks to St Andrews University Chaplin, Donald MacEwan and Rob Warren who have helped me to find university accommodation during my difficult time in St Andrews. Also I would like to thank all the university accommodation, student service and chemistry staff members for your understanding and generosity during my time in St Andrews.

My thanks also goes to all my Sri Lankan friends in UK and Sri Lanka they have been really helpful to overcome the difficult time. Special thanks also go to Wellawaththe Seelagawesee Thero, Rewatha Thero, Upulani, Kushan, Chamila, Madu, Pradeep, Kannan, Geetha, Yasith, Sachith, Anusha, Rani and David for looking after me during my time in St Andrews.

I would like to thank each and everybody who has given me any kind of help and support for me to come this far in my academic life.

Finally, I would like to thank to my family, Amma, Thaththa, Sister, Brother, Brother-in-law and my wife, without your moral support and encouragement I won't be who I am today. Thank you all again.

Collaboration statement with regards to the Chapter 3 manuscript

I am grateful to Michael Buhl for DFT calculations, Dr Fergus R. Knight and Dr Marie Lechner for the day to day support in the laboratory. Elemental analyses were performed by Stephen Boyer at the London Metropolitan University. Mass spectrometry was performed by Caroline Horsburgh at the University of St. Andrews Mass Spectrometry Service and by the EPSRC National Mass Spectrometry Service in Swansea.

Abstract

Organic frameworks with rigid backbones, such as acenaphthene, are highly suitable for the study of interatomic interactions. The short "natural" *peri*-distance (2.44 Å) and the rigidity of the aromatic system causes considerable steric strain between *peri*-substituted heteroatoms. As a consequence, substitution at both *peri*-positions leads to in- and out-of-plane distortions, which often result in buckling of the ring system. In order to relax this geometric strain, weak bonding interactions can also exist between the *peri*-substituents.

This thesis focuses on the synthesis, structural characterisation and investigation of a range of sterically crowded *peri*-substituted acenaphthene compounds. This involves the study of the acenaphthene geometry, through X-ray crystallography when different *peri*-substituents occupy the close 5,6-positions; our main focus is to study weak non-bonded interactions that can occur across the *peri*-gap, for example weakly attractive three-centre four-electron (3c-4e) type interactions which are known to prevail in such compounds under the appropriate conditions. Repulsion within these systems, resulting from the steric crowding of the *peri*-space is also investigated, employing changes in bond lengths, bay-region angle splay, displacement of atoms from the mean plane and central acenaphthene torsion angles to help quantify the degree of acenaphthene distortion, which are all conveniently probed by the *peri*-distance.

To this end we have synthesised a range of novel sterically crowded mixed bromo-tin acenaphthene derivatives (Chapter 3), chalcogen-tin acenaphthene molecules (Chapter 4), phosphorus–tin derivatives (Chapter 5) and a series of homologous tin-tin acenaphthenes (Chapter 6). All the compounds studied in this thesis were characterised by multinuclear NMR spectroscopy and X-ray crystallography in an effort to gain a greater understanding of the deformation that

occurs when disparate functionalities are located in close proximity and explore the potential for weak non-covalent intramolecular interactions to occur.

Contents

Abbreviations

Å	Ångström, 1 x 10^{-10} m
Acenap	acenaphthene
br s	broad singlet
°C	degrees Celsius
c.a.	*circa*
CCD	charge coupled device
CIF	crystallographic information file
CSD	Cambridge structural database system
cm^{-1}	wavenumber
COSY	correlation spectroscopy
d	doublet
DFT	density functional theory
DMF	dimethylformamide
E	chalcogen i.e. sulfur, selenium, tellurium
equiv	equivalent
et. al	*et alii*
g	grams
h	hour
Hz	Hertz
HSQC	heteronuclear single quantum coherence
*i*Pr	isopropyl
IR	infra red
J	coupling constant
m	multiplet
Me	methyl, CH_3
min	minutes
mp	melting point
MS	mass spectrometry
m/z	mass to charge ratio
*n*BuLi	*n*-butyllithiuym

nap	naphthalene
NBS	N-bromosuccinimide
nm	nanometer, 1 x10^{-9} m
NMR	nuclear magnetic resonance
Ph	phenyl, C_6H_5
ppm	parts per million
r_{vdW}	van der Waals radius
s	singlet
Σr_{vdw}	sum of the van der Waals radii
tert	tertiary
THF	tetrahydrofuran
TMEDA	N,N,N',N'-tetramethyl-1,2-ethanediamine
TMS	tetramethylsilane
WBI	Wiberg bond index

Chapter 1

An introduction to X-ray crystallography

Introduction

X-ray crystallography is a technique used to determine the structure of molecular and non-molecular materials in the solid state. Each individual crystal is made up of atoms which are uniquely arranged in a repetitive manner, like building blocks in a three dimensional space, the smallest pattern is called an asymmetric unit.[2]

Single crystal X-ray diffraction is a technique in which the arrangement of atoms in a crystal is determined. It is a very powerful technique. X-ray structure determination has become more common with the development of area detectors in the 1990s.[1] Initially, crystal structure determination was carried out by experts, but software developments of the last couple of decades have enabled scientists not formally trained in crystallography to also determine crystal structures. The rapid advancement of crystallography software has enabled crystal structures to be determined very efficiently. X-ray crystallography is useful for structure determination of a wide range of compounds such as complex minerals, inorganic and organometallic complexes, natural products, biological macromolecules, proteins and viruses.[3] Crystallography is used to study a variety of structural features such as bond lengths and angles, torsion angles, non-bonded distances, weak interactions and the packing of molecules.

Background - A Crystal

A crystal can be defined as a pattern of arranged atoms that repeats periodically in three dimensions.[4] This pattern can consist of a single atom, a group of atoms, a molecule or a group of molecules. The key feature of a crystal is the periodicity or regularity of the arrangement of these patterns.

Unit cell

The unit cell can be defined as the smallest repeating unit found within a crystal. It is possible that more than one repeating unit is present in the crystal (Figure 1.1).

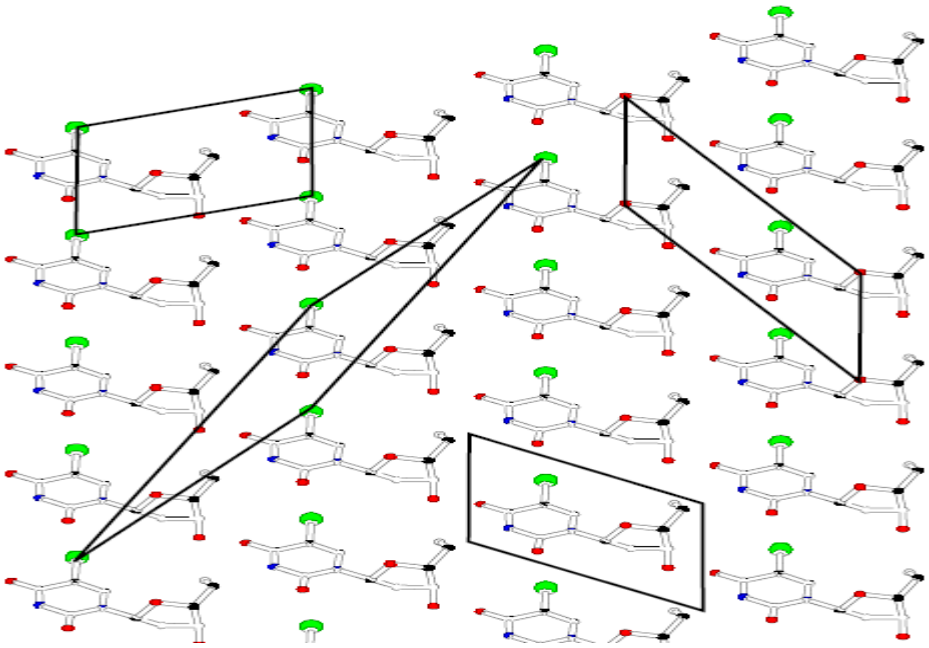

Figure 1.1 Four possible two dimensional unit cells.[5]

Each unit cell is defined in terms of lattice points. Lattice points are the points in space about which the particles are free to move in a crystal. There are six parameters of the unit cell, three defining distances within the three dimensions (a, b and c) and one for each angle associated as shown in Figure 1.2.[4]

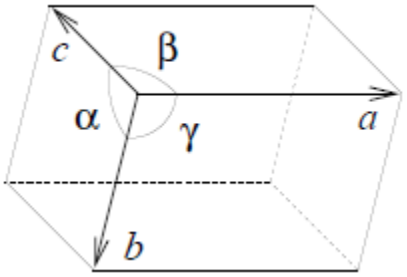

Figure 1.2 Parameters of a unit cell.[5]

The Seven Crystal Systems

There are seven basic unit cell geometries which are called crystal systems. The most commonly seen crystal systems are triclinic, monoclinic and orthorhombic (Figure 1.3).

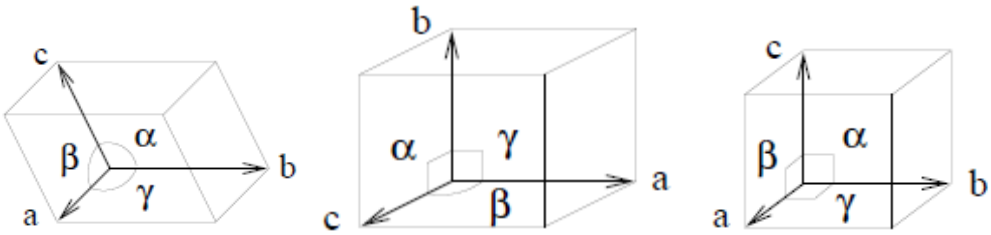

Triclinic Monoclinic Orthorhombic

Figure 1.3 Most common unit cell geometries.[5]

There are 230 space groups defined from the combination of 32 crystallographic point groups and the 14 Bravais lattices.[6] The space group is a tool that describes the symmetry of the molecule within the unit cell. Two types of symmetry element exist in a crystal system known as point group symmetry and space group symmetry. Point group symmetry includes the inversion centres (-1) two fold axes (2), or mirror planes (m). Space group symmetry includes unit lattice centring (P, primitive; C, side-centred; I body centred or F; face centred) screw axes (21) and glide planes (a,b,c or n).[6] Every crystal structure is explained by a combination of these symmetry operations. There is a specific notation for describing space groups: the first descriptor defines the lattice type (P, C, F, I), the next descriptors describe the point group symmetry of which the principal axis is noted first. For the remaining characters, different rules apply for different crystal systems.

Table 1.1 The seven crystal systems.

Crystal systems	Lattice centring	Axial lengths	Axial angles
Triclinic	P	$a \neq b \neq c$	$\alpha, \beta, \gamma \neq 90^o$
Monoclinic	PC	$a \neq b \neq c$	$\beta \neq 90^o$ and $\alpha, \gamma = 90^o$
Orthorhombic	PICF	$a \neq b \neq c$	$\alpha, \beta, \gamma = 90^o$
Hexagonal	P	$a = b \neq c$	$\alpha = \beta = 90^o$ and $\gamma = 120^o$
Trigonal	PR	$a = b = c$	$\alpha = \beta = \gamma \neq 90^o$
Tetragonal	PI	$a = b \neq c$	$\alpha, \beta, \gamma = 90^o$
Cubic	PIF	$a = b = c$	$\alpha, \beta, \gamma = 90^o$

The Bragg Equation

X-rays are a form of electromagnetic radiation with a wavelength about as long as the distance between neighbouring atoms which are regularly placed in crystals. Thus atoms in a crystal act as

scattering centres and thereby diffract X-rays. Diffraction can be constructive or destructive. As a result of this varying intensities can be observed in a diffraction pattern. X-ray diffraction can be understood by considering the Bragg equation.[7]

A section of a crystal with atoms arranged on a set of parallel planes (*h k l*) and spaced distance *d* apart is shown in Figure 1.4. When a beam of monochromatic X-ray with wave length **λ** strikes through the planes of the crystal at an angel **θ**, the rays reflected by the lower plane travel a longer distance than those reflected from the upper plane (Equation 1.1; **n** is an integer).

$$n\lambda = 2d\ sin\theta \qquad (1.1)$$

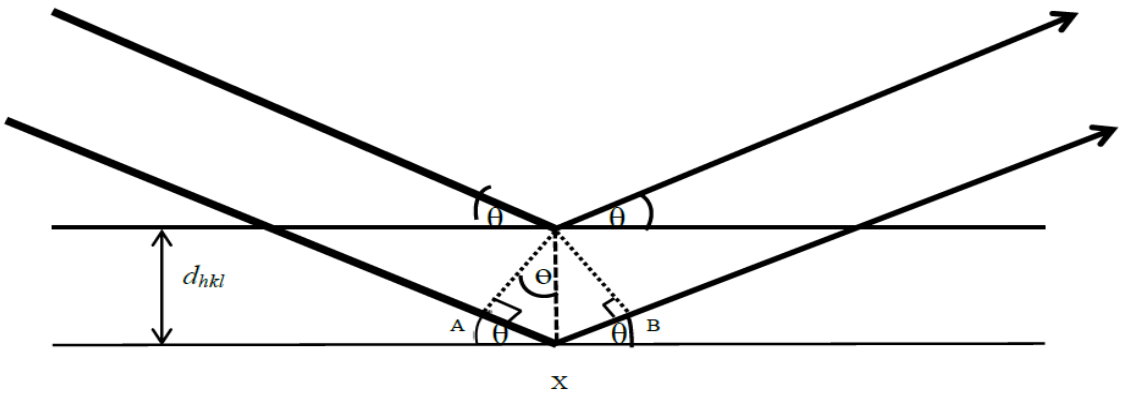

Figure 1.4 Bragg's law form reflections of incident radiation from successive lattice planes.

This theory was first formulated by Sir William Lawrence Bragg and known as the Bragg equation. The **n** in the Bragg equation is known as the order of reflection.[7] This equation states the essential conditions which must be met if diffraction is to occur and a diffraction pattern is recorded as images of spots. (Figure 1.5).

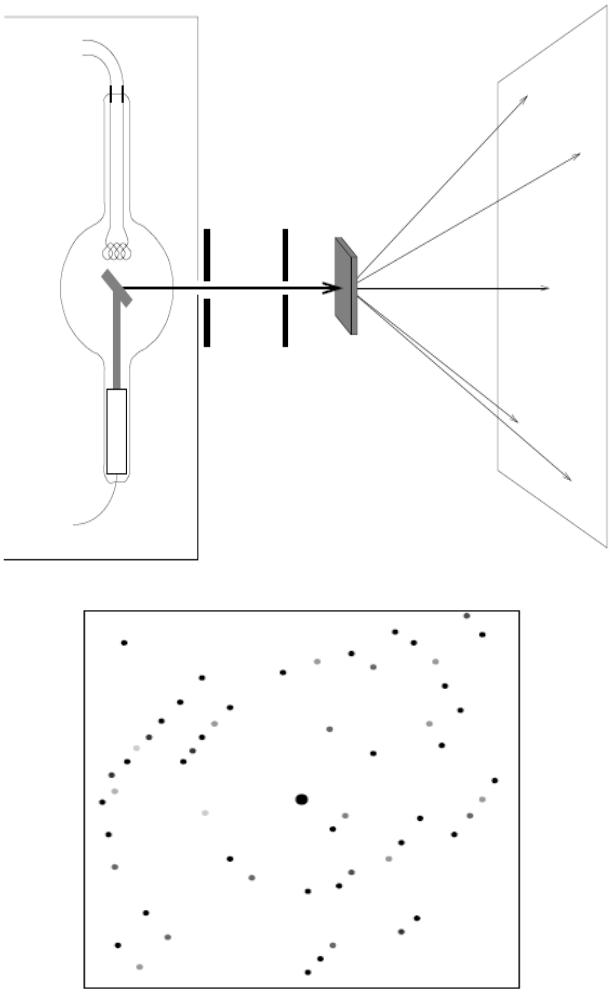

Figure 1.5 Schematic of single crystal X-ray diffraction; the diffracted X-rays produce a diffraction pattern.[5]

Obtaining a Crystal Structure

Crystal structure determination consists of several steps.[1] The initial step is generally performed by the experimental chemist to grow an X-ray quality crystal. The crystal should be large enough (approximately 0.1-0.2 mm in each dimension for organic samples), regular in shape and ideally pure in composition as this will help to obtain the best possible data.[6] The crystal is mounted in a

small loop onto a goniometer in the diffractometer. The crystal is then rotated whilst being irradiated with X-rays and multiple diffraction patterns are collected from each angle.

The diffraction pattern is then processed and spots of intensity are integrated and collected using e.g. CrystalClear software.[2] This gives a set of hkl values and intensities which are used to deduce where peaks of electron density are situated.

The following steps are performed by a crystallographer: unit cell determination, data collection, data reduction, space group determination, structure solution and structure refinement.[1]

Growing a crystal

In order to form crystals, a nucleation should take place followed by crystal growth. But still growing good quality crystals is a difficult task. Different techniques can be applied to grow crystals. The most common methods used today are vapour diffusion, evaporation, solvent layering and cooling.

Generally, the best technique to grow good quality crystals is the vapour diffusion method. It uses a binary solvent system. Here the sample is dissolved in a suitable solvent and placed in a vial of a secondary solvent usually in which the product is less soluble. This secondary solvent is allowed to diffuse across into the initial solvent, changing the solubility of the product in this new solution allowing it to precipitate out, potentially in crystalline form. This process is usually carried out in a closed system (Figure 1.6(c)).[1]

In the slow evaporation method, the sample is dissolved in a suitable solvent, generally one which can make a saturated solution, and then it is evaporated slowly over a period of time. Usually this is carried out at room temperature and the crystal may form when the solution has achieved supersaturation (Figure 1.6(a)).[6]

In the slow cooling crystallisation, prepare a saturated solution of the product at room temperature and place in a cold place, preferably in a freezer or in a dry-ice acetone bath. This is good for the moderately soluble substances.

Solvent layering is also commonly used in growing crystals. The compound should be fully dissolved in one solvent before a secondary solvent is layered carefully on the top without breaking the surface. If the compound does not dissolve it should be miscible with the first solvent. This should be placed gently above the solute. Crystals are formed, when the solvents diffuse into one other.[6]

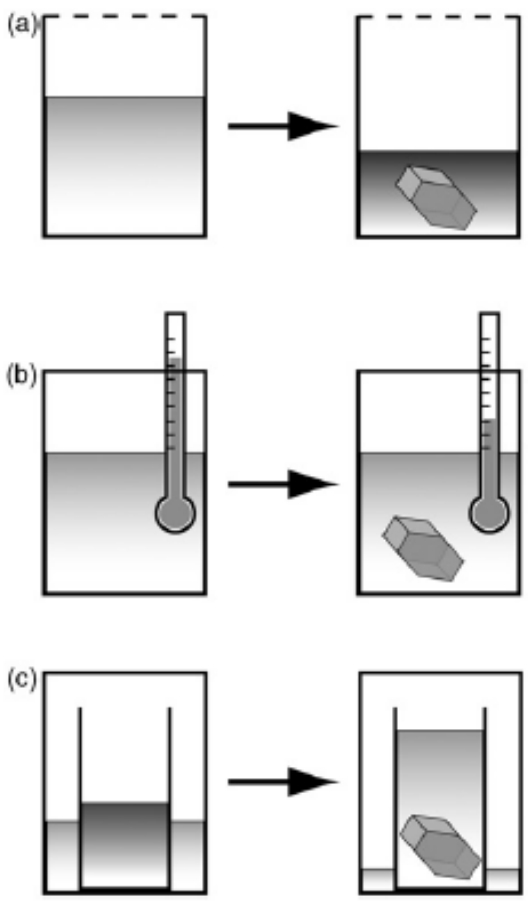

Figure 1.6 Schematics of three popular methods of crystal growth. (a) Slow evaporation of the solvent, (b) slow cooling of the solution and (c) gas-phase diffusion of a precipitant into a solution. (Adopted from Müller, 2009[1]).

A flowchart for the steps involved in a crystal structure determination

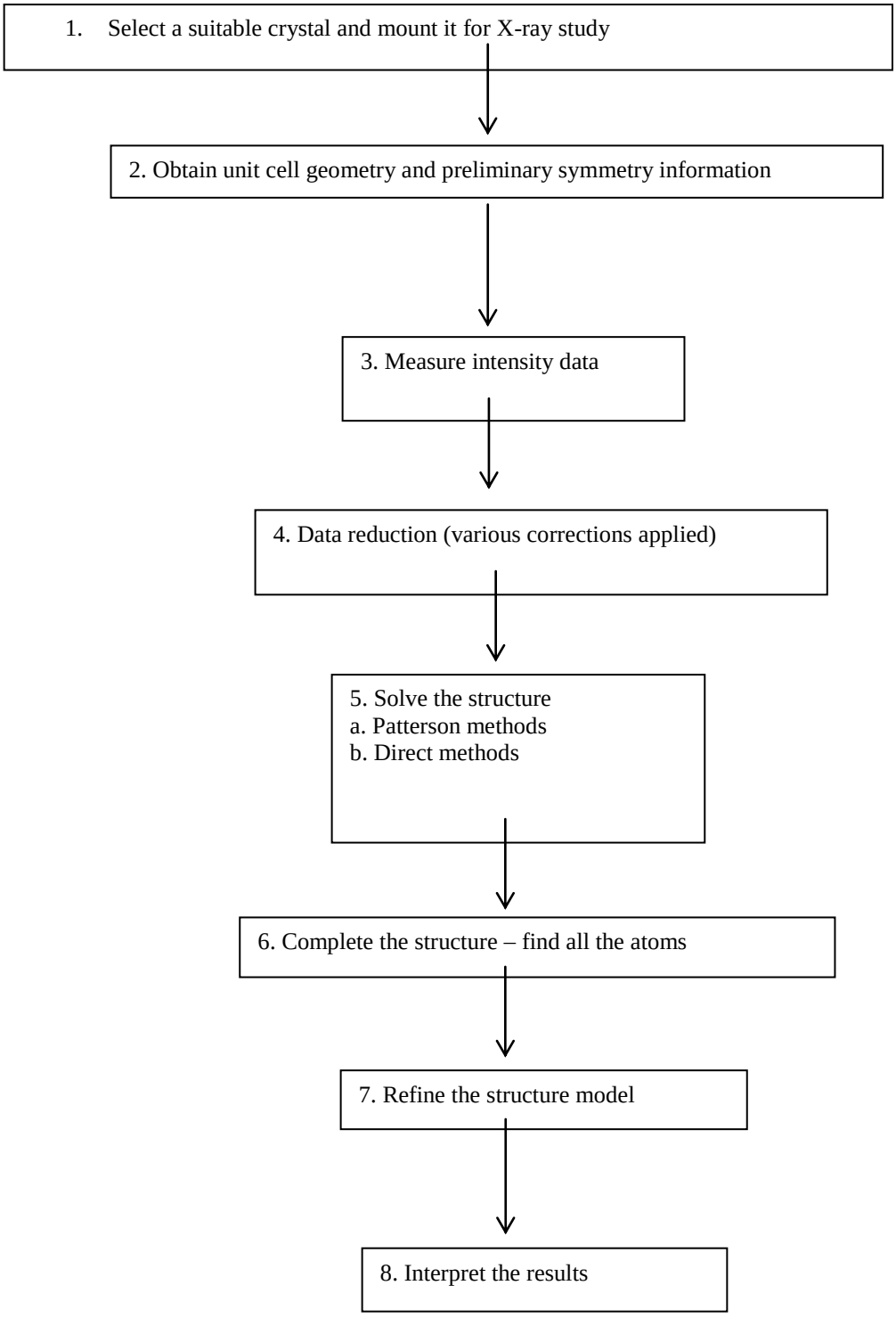

Collecting data

The X-ray crystallographic data is obtained by introducing a single crystal to the X-ray diffractometer (Figure 1.7). Inside the diffractometer the X-rays are diffracted and the scattered beams are plotted against the refractive angle. A video camera is used to magnify the crystal in order to help the crystallographer to move the crystal to the correct position in the X-ray beam. A stream of e.g. cold gaseous N_2 is passed over the crystal to lower the thermal vibrations of the atoms and also to minimize the solvent diffusion out of the crystal during the data collection.[2] This stream can be stopped to allow room temperature data collection to occur if this is of interest to the crystallographer, for example studying phase changes.

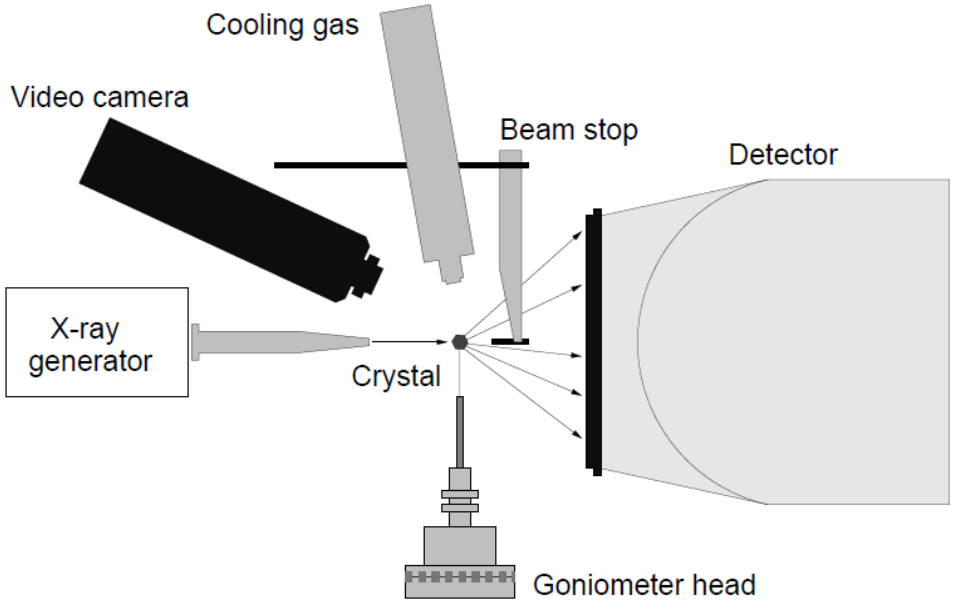

Figure 1.7 Schematic of an X-ray diffractometer.[5]

When a crystal is irradiated with a monochromatic beam it scatters the waves and results a specific diffraction pattern. These diffracted rays are then recorded, e.g. on a charge coupled device (CCD) area detector in the form of images. These images consist of different spots known as reflections. Valuable structural information can be revealed from the intensity and the position of each spot in a diffraction pattern. This includes the information on atomic positions, bond lengths and angles, torsion angles, etc.

Structure solution

There are two structure solution methods for solving the crystal structures using the electron density map, to overcome the phase problem; either Patterson methods or direct methods can be used.[8] In the overall crystallographic process one of these methods is used. Once the process is successful, an electron density map is drawn.

Refining the structure

Refinement can include the addition or deletion of atoms, alteration of elements or accounting for thermal parameters. The aim is to optimize the fit of the model to the diffraction data. The fit is measured by the residual factor also called the *R*-factor. In general the lower the *R*-factor the better the model fits the collected data. Refinements are usually carried out until the lowest *R*-factor is obtained. The R factor is defined as follows:

$$R = \frac{\sum| \ |F_o| - | \ |Fc| \ |}{\sum |F_o|} \qquad (1.2)$$

Where ;
Fo = observed structure factor
Fc = calculated structure factor

Once the thermal parameters of the atoms look reasonable and the R1 and *w*R2 values are close to 0 a CIF file (crystallographic information file) can be generated and from this other structural information can be looked studied. The structure model contains information including atom positions in the unit cell and distances and angles between atoms. The CIF file is checked using CheckCif (provided as an online service by the International Union of Crystallography) for any errors that may have been written into the CIF. Throughout this thesis, PLATON software has been used to generate data for packing interactions and hydrogen bonding. The molecular pictures and interactions images have been visualised and generated using SHELXTL software.

References

1. P. Müller, *Crystallogr. Rev.*, 2009**, 15**, 57.

2. A. L. Fuller, "*Application of X-ray Crystallography: studies into the structural perturbations of peri-substituted naphthalene derivatives*", Ph.D. Thesis, University of St Andrews, 2009.

3. C. F. Campana, *Analytical application note*. BRUKER AXS Inc. : 2000.

4. D. E. Sands, in *Introduction to Crystallography*, W. A. Benjamin Inc., New York, 1969.

5. H. Kooijman, Interpretation of Crystal Structure Determination, version 2.3, undergraduate course notes, Utrecht University, 2005.

6. L. Ooi, *Principles of X-ray Crystallography*, Oxford University Press, Oxford, 2010.

7. A. R. West, *Solid state Chemistry and its applications*, John Wiley and Sons Ltd., New York, 1984.

8. W. Clegg, *Crystal Structure determination*, Oxford University Press, New York, 1998.

Chapter 2

An introduction to *peri*-substituted systems

Introduction

Peri-substitution is a "double substitution of atoms or groups at the *peri*-positions" of naphthalene systems;[1] positions 1- and 8- on the naphthalene ring or 5- and 6- on the acenaphthene backbone.[1,2] In unsubstituted ("ideal") naphthalene the *peri*-positions, occupied by two hydrogen atoms, are at a distance of *ca*. 2.5 Å.[1-5] The naphthalene backbone is planar with unequal bond lengths, but internal angles are *ca*. 120°,[1-5] with the exocyclic *peri*-bonds aligned parallel to each other.[2,5] The presence of the CH_2CH_2 linker at the 1,2-positions in acenaphthene, however, results in a slight deviation in the planarity of the carbon framework.[5] Therefore, the internal angles in acenaphthene deviate from those in naphthalene, with angles ranging from 111-127°.[5] The smallest angle is observed near to the CH_2CH_2 bridge (C1-C1a-C2, Figure 2.1), whilst the splay angle has widened in the *peri*-region (C5-C5a-C6, Figure 2.1). Accordingly, the exocyclic bonds lean away from each other in different directions, thus increasing the *peri*-gap to a *ca*. 2.7 Å, compared to naphthalene.[5]

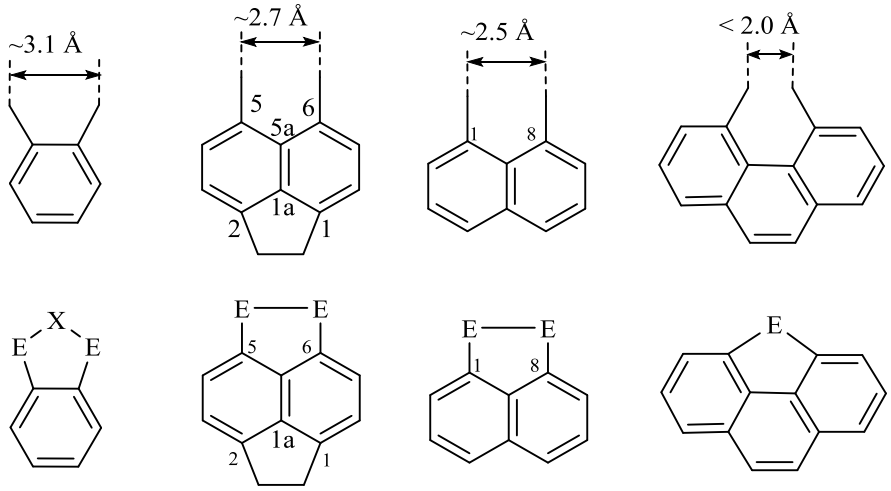

Figure 2.1 The geometry of *peri*-functionalities in naphthalenes, ortho-substitution in benzenes and *peri*-region disubstitution in phenanthrene. The 'relaxed' configuration of each system is shown at the bottom.[5-9]

The *peri*-distances in acenaphthene and naphthalene are large enough to comfortably accommodate the two hydrogen atoms (Σr_{vdW} 2.18 Å),[5,6] however, when larger atoms or groups are located at the *peri*-positions they can experience greater steric compression.[2-5] This steric strain can be released *via* four different possibilities; elongation of the *peri*-atom bonds (Figure 2.2,a), in-plane distortions (Figure 2.2,b), out-of-plane deflections (Figure 2.2,c) and buckling of the acenaphthene backbone (Figure 2.2,d).[2-5] Further relaxation of steric strain can be achieved through attractive interactions between *peri*-functionalities. X-ray crystallography is a widely used tool for the highly accurate determination of molecular structures. It can therefore be used to identify distortion of the acenaphthene backbone, as well as any changes in bond lengths and the *peri*-distance, which are indications for the existence of weak intramolecular interactions. One particular interest of this thesis is to gain a thorough understanding of the structural features of *per*i-substituted acenaphthenes.

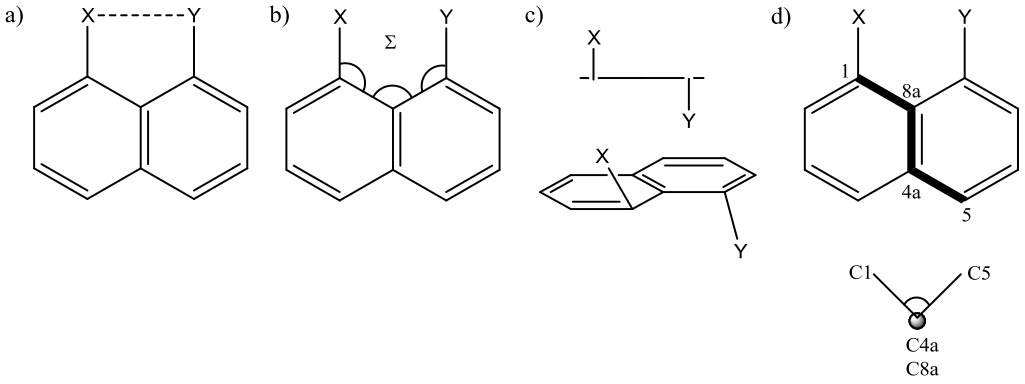

Figure 2.2 The degree of steric strain and naphthalene deformation is determined by comparing a) *peri*-distances, b) sum of the *peri*-region angles, c) in-plane and out-of-plane distortions and d) dihedral angles around the C(5)-C(10) bond.[3,11]

Relieving steric pressure by elongating *peri*-atom bonds

Considering a large amount of energy is associated with only a small change in bond length,[2,3,11] the elongation of bonds as a means of releasing the steric pressure in *peri*-substituted systems is uncommon (Figure 2.3). To get a better understanding of the C-X, C-Y bond lengthening in acenaphthene molecules, a Cambridge structural database system (CSD) search was narrowed down to acenaphthene structures containing a sulfur at one *peri*-substituent and the other position occupied with any atom other than hydrogen.

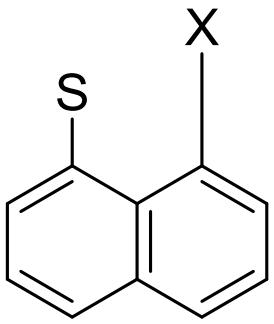

Figure 2.3 CSD search for *peri*-substituted acenaphthenes with the *peri*-positions containing one sulfur atom and any atom other than hydrogen.

The CSD search revealed 28 hits, in which the S-C bond length varied from 1.75 Å to 1.81 Å (Figure 2.3). As the difference between the bond lengths is less than 0.06 Å, it suggests that steric strain occurring between *peri*-substituents does not greatly affect the C-X bond length, but rather the other three modes of distortion are more prominent in relaxing the molecule. The release of steric strain by one or more of these atomic displacements is referred to as "decentralization of steric strain"[12] or "distribution of deformation over many coordinates".[3]

In-plane distortions

In-plane distortion of *peri*-functionalities can be deduced by looking at the angles around the bay region. In acenaphthene, the bay-region angles are C5-C5a-C6 (128°), C5a-C5-H (119°) and C5a-C6-H (113°) and sum to 360°. Therefore the degree of in-plane distortion occurring in substituted systems can be determined by comparing the splay angle (sum of the bay-region angles - 360°) to acenaphthene.[4,6]

In order to reduce the steric tension in these systems imposed by the close proximity of the substituents, the *peri*-bonds can bend outward to minimise the repulsive interactions (Figure 2.4 a). In-plane distortion can also be used to indicate the presence of a weak or strong bonding interaction between the *peri*-substituents if the exocyclic bonds bend inwards (Figure 2.4 b), compared to the parallel arrangement in acenaphthene (Figure 2.4 c).

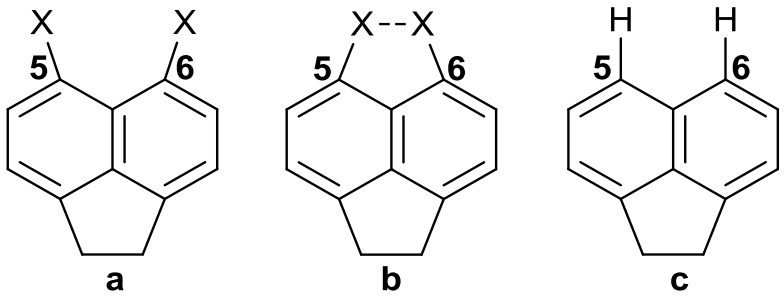

Figure 2.4 In-plane deflections of the *peri*-functionalities at the 5 and 6 positions in acenaphthenes: repulsive interactions (a), attractive interactions (b), and parallel alignment in acenaphthene (c).

A limited search in the CSD of *peri*-substituted acenaphthene molecules with one substituent as a sulfur atom and any atom in the other position was used to determine how the bond angles of the

bay-region deviate from ideal values. The largest splay angle (13.2°) was observed in an acenaphthene compound substituted with S-Ph and $(SeMePh)^+$ moieties[13] (Figure 2.5), showing the substituents lean outward to release steric tension. Conversely, the smallest splay angle was found in a disulfide acenaphthene derivative (-11.9°), illustrating that the substituents bend inward as a result of forming a strong covalent bond, thus reducing the sum of the bay angles (Figure 2.5).

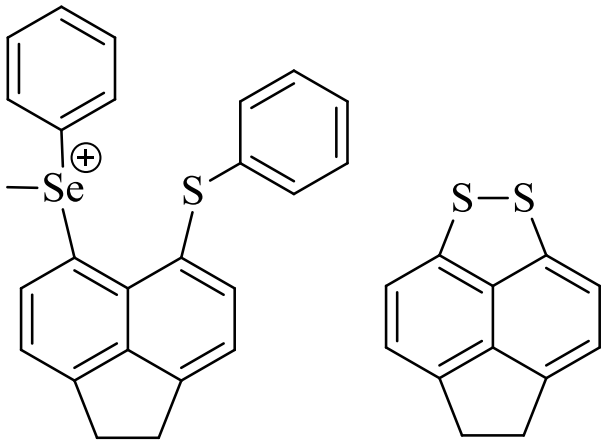

Figure 2.5 In-plane distortion indicates the extent of both repulsive and attractive interactions between substituents.[13]

Out-of-plane distortions

Out-of-plane deformation is calculated by measuring how far the *peri*-atoms reside from the mean acenaphthene plane (Figure 2.6). Due to the steric crowding of the substituents, *peri*-atoms can be forced to sit above or below the mean acenaphthene plane in order to achieve a relaxed geometry. Out-of-plane distortion is dependent upon the size of the atoms and also the size of the groups attached to the *peri*-atom.[1,3] In order to get a better understanding of how the size of the atom affects the out-of-plane displacement, a CSD search was limited to chalcogen groups attached to

the acenaphthene backbone. Unsurprisingly it was found that the largest distortion occurred for the acenaphthene backbone containing bulky TePh-TePh as substituents (-0.404(1) Å Te1, 0.310(1) Å Te2; Figure 2.7).[6] Much smaller deviations from the mean plane are observed when lighter congeners occupy the close 5,6-position, for example when SPh-SPh are substituents (-0.132(1) Å S1, 0.161(1) Å S2; Figure 2.7).[6]

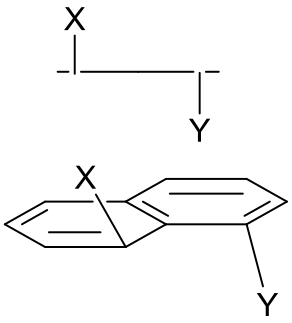

Figure 2.6 Out-of-plane distortion: distance of the *peri*-substituents occupy relative to the acenaphthene mean plane.

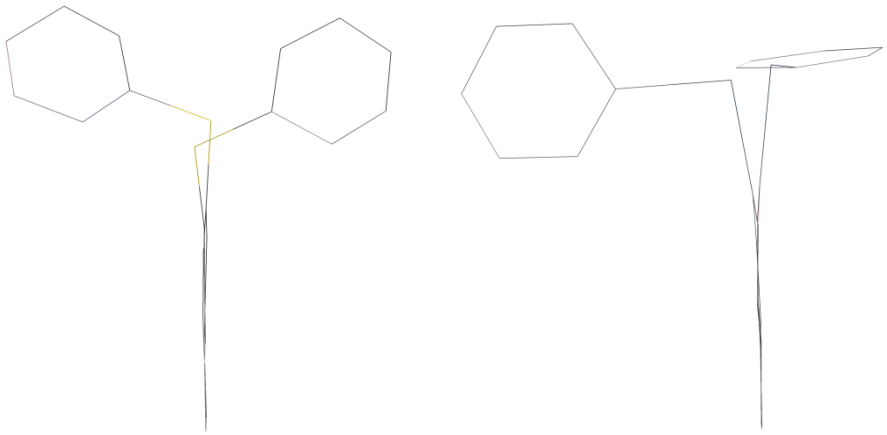

A **B**

Figure 2.7 Line drawing of **A** Acenap$(SPh)_2$ and **B** Acenap$(TePh)_2$ showing the difference in out-of-plane displacement and the planarity of the two acenaphthene backbones.[6]

Buckling in the acenaphthene ring

In addition to in- and out-of-plane distortions, the carbon framework may also undergo twisting to relieve the steric strain induced by the bulky *peri*-functionalities. Torsion angles associated with central bridging carbon atoms in acenaphthene (C5-C10) give a good indication of the amount of buckling taking place in the acenaphthene backbone; in acenaphthene the backbone is planar with angles *ca*. 0° or 180° (Figure 2.8).

A CSD search of torsion angles for S containing acenaphthene structures resulted 28 hits, with the disulfide structure displaying the least amount of distortion from planarity (179.84° and 179.55°). The largest torsion angles are observed for a Ag coordinated SPh acenaphthene derivative (AgS_2 (SPh-SPh-AgS_2acenap)$_2$)[14] with torsion angles of 172.24° and 172.42° indicating the backbone has undergone a significant degree of distortion away from the ideal planar structure in order to relieve the steric tension .

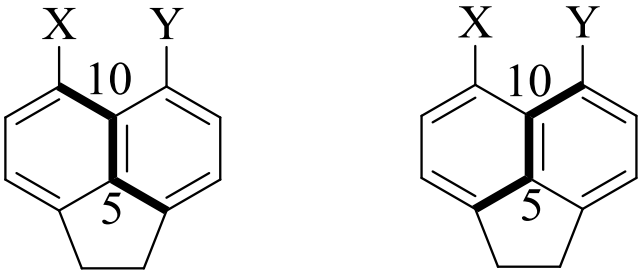

Figure 2.8 Torsion angles in bold, run through the C5-C10 central bond and indicate the planarity of the backbone.

Three centre-four electron (3c-4e) type interactions

Recently the Woollins group has carried out extensive studies using acenaphthene molecules in which the *peri*-positions are occupied by larger heteroatoms, in order to gain a greater understanding of non-bonded interactions. This has been achieved by introducing chalcogen, phosphorus or halide substituents into the *peri*-positions.[4-6] It has been suggested that the linear arrangement and the close proximity of the *peri*-positions (within the sum of the van dar Waals radii) which can occur in such systems, provides the correct geometry for promoting a three-centre four-electron (3c-4e) type interaction. When the three atoms are closely accommodated and linearly arranged, it is possible for a lone-pair orbital of one heteroatom to interact with an empty σ* anti-bonding orbital on the adjacent heteroatom. This attractive interaction has been shown to greatly influence the geometry of the *peri*-region (Figure 2.9).[4-6]

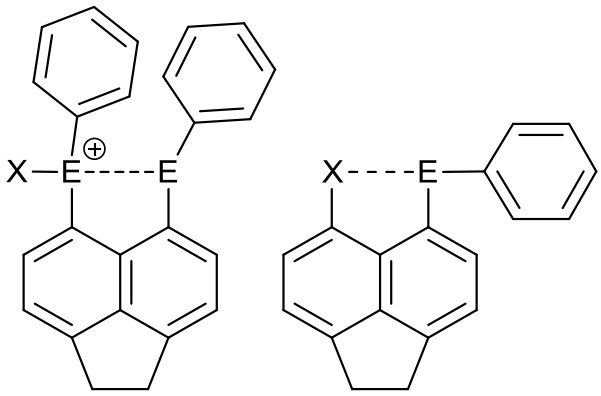

Figure 2.9 An illustration of the linear arrangement and 3c-4e type interactions, where X is a halide and E is a chalcogen.

Previous work on *peri*-substituted organotin compounds

In 1979, Mislow and co-workers[15] reported the first example of an organotin substituted naphthalene compound, containing trimethyltin at both *peri*-positions (Figure 2.10). In their studies, they concluded that positioning the large tin moieties ($\sum r_{vdW}$ Sn 4.34 Å) in close proximity caused significant changes to the geometry of the compound. As might be expected, the compound displayed a significant degree of deformation away from that of naphthalene, with a notably large Sn···Sn *peri*-distance of 3.864 Å, accompanied by exceptional in-plane and out-of-plane deviations of the *peri*-substituents, suggesting a large amount of steric strain is introduced between the bulky trimethyltin groups.

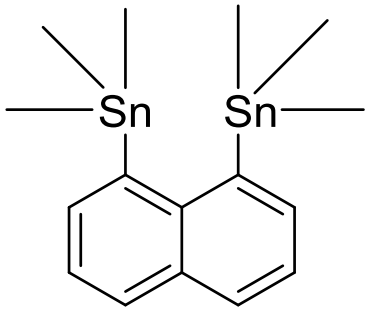

Figure 2.10 The structure of 1,8-bis(trimethylstannyl)naphthalene.[15]

Later in 2002, Gabbai *et al*., demonstrated that trimethyltin containing naphthalenes can be used for the preparation of heteronuclear *peri*-substituted compounds such as dimesitylboranes.[16] These compounds readily undergo transmetallation reactions with Group 13 halides.

Due to the large size of tin, substituting organotin functional groups onto an acenaphthene backbone is difficult. Only two similar compounds have been reported in literature up until now. Brune *et al*. prepared 5-tributylstannylacenaphthene in 1989[17] by reacting 5-bromoacenaphthene

with the sodium salt of tributylstannane and Fry *et al*. synthesized 5,5,12,12-tetramethyldiacenaphtho[5,6-*bc*:5',6'-*fg*]-(1,5)distannocin in 1991 by reacting 5,6-dilithioacenaphthene with dimethyldichlorostannane (Figure 2.11).[18] Nevertheless no crystal structure data for an organotin substituted acenaphthene was found in the Cambridge Structure database (CSD) at the start of this work.

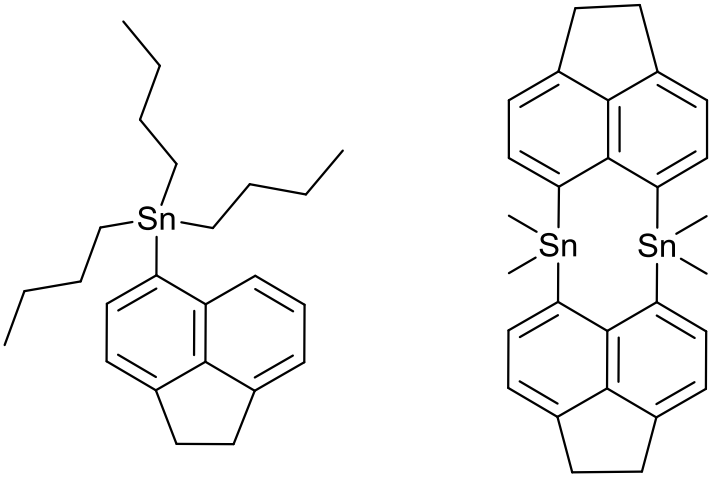

Figure 2.11 The structures of 5-tributylstannylacenaphthene and 5,5,12,12-tetramethyldiacenaphtho[5,6-*bc*:5',6'-*fg*]-(1,5)distannocin.[17,18]

This thesis focuses on the synthesis, structural characterisation and investigation of a range of sterically crowded *peri*-substituted acenaphthene compounds. This involves the study of the acenaphthene backbone through X-ray crystallography when different *peri*-substituents occupy the close 5,6-positions; our main focus is to study weak non-bonded interactions that can occur across the *peri*-gap, for example weakly attractive three-centre four-electron (3c-4e) type interactions which are known to prevail in such compounds under the appropriate conditions. Repulsion within these systems, resulting from the steric crowding of the *peri*-space is also

investigated, employing changes in bond lengths, bay-region angle splay, displacement of atoms from the mean plane and central acenaphthene torsion angles to help quantify the degree of acenaphthene distortion, which are all conveniently probed by the *peri*-distance. We are particularly interested in these compounds as there are only two reported examples of organotin acenaphthene compounds in the literature so far. As an extension to this, weak interactions, including H-bonding, π-π stacking and H-Cg bonding are also investigated.

To this end we have synthesised a range of novel sterically crowded mixed bromo-tin acenaphthene derivatives (Chapter 3), chalcogen-tin acenaphthene molecules (Chapter 4), phosphorus–tin derivatives (Chapter 5) and a series of homologous tin-tin acenaphthenes (Chapter 6). All the compounds studied in this thesis were characterised by multinuclear NMR spectroscopy and X-ray crystallography in an effort to gain a greater understanding of the deformation that occurs when disparate functionalities are located in close proximity and explore the potential for weak non-covalent intramolecular interactions to occur.

References

1. P. Kilian, F. R. Knight and J. D. Woollins, *Chem. Eur. J.*, 2011, **17**, 2302.

2. A. L. Fuller, "*Synthesis and Structural studies of group 16 peri-substituted naphthalenes and related compounds*", Ph.D. Thesis, University of St Andrews, 2010.

3. V. Balasubramaniyan, Chem. Rev., 1966, **66**, 567.

4. M.-L. Lechner, K. S. Athukorala Arachchige, R. A. M. Randall, F. R. Knight, M. Bühl, A. M. Z. Slawin and J. D. Woollins, *Organometallics*, 2012, **31**, 2922.

5. C. A. Coulson, R. Daudel and J. M. Robertson, *Proc. R. Soc. London,Ser. A*, 1951, **207**, 306; D. W. Cruickshank, *Acta Crystallogr*., 1957,**10**, 504.

6. L. K. Aschenbach, F. R. Knight, R. A. M. Randall, D. B. Cordes, A. Baggott, M. Bühl, A. M. Z. Slawin and J. D. Woollins, *Dalton Trans*., 2012, **41**, 3141.

7. A. C. Hazell, R. G. Hazell, L. Norskov-Lauritsen, C. E. Briant and D.W. Jones, *Acta Crystallogr., Sect. C: Cryst. Struct. Commun*., 1986, **42**, 690.

8. G. E. Bacon, N. A. Curry and S. A. Wilson, *Proc. R. Soc. London, Ser.A*, 1964, **279**, 98.

9. A. Budzianowski and A. Katrusiak, *Acta Crystallogr*., *Sect. B: Struct. Sci*., 2006, **62**, 94.

10. M. I. Kay, Y. Okaya and D. E. Cox, *Acta Crystallogr., Sect. B*: *Struct. Crystallogr. Cryst. Chem.*, 1971, **27**, 26.

11. F. R. Knight, *"Synthesis and structural studies of group 16 peri-substituted naphthalenes and related compounds"* Ph.D. Thesis, University of St Andrews, 2010.

12. R. L Avoyan, A.I Kitaigorodskii, and Yu.T Struchkov, *Struct. Chem. (USSR)*, 1963, **4**, 581.

13. C. G. M. Benson, Catherine M. Schofield, Rebecca A. M. Randall, Lucy Wakefield, Fergus R. Knight, Alexandra M. Z. Slawin and J. Derek Woollins, *Eur. J. Inorg. Chem.* 2013, 427.

14. F. R. Knight, Rebecca A. M. Randall, Lucy Wakefield, Alexandra M. Z. Slawin and J. Derek Woollins, *Molecules* 2012, **17**, 13307.

15. J.F. Blount, F. Cozzi, J.R. Damewood, D.L. Iroff, U. Sjöstrand and K. Mislow, *J. Am. Chem. Soc.*, 1980, **102**, 99.

16. M. Schulte and F.P. Gabbao, *Chem. Eur. J*. 2002, **8**, No. 16.

17. C.Weisemann, G.Schmidtberg and H.A Brune, *J. Organomet. Chem.* 1989, **365**, 403.

18. R. H. Mitchell, M. Chaudhary, R. V.Williams, R. Fyles, Gibson, J. A. Smith and M, J. Fry, *Can. J. Chem.* 1992, **10**, 1015.

Chapter 3

Synthetic and structural studies of sterically crowded 5-bromo-6(organostannyl)acenaphthenes

The work undertaken in this chapter contributed to the manuscript 'Sterically Crowded Tin Acenaphthenes', published in the journal *Organometallics* in 2012.[1] (Please see Collaboration Statement at the beginning of this thesis).

Introduction

The study of molecular bonding is of key importance in chemistry, biochemistry and materials science.[1,2] Great advances have been made towards the understanding of covalent and ionic bonds, however, the large field of weak inter- and intramolecular interactions still holds mysteries. Organic frameworks with rigid backbones, such as acenaphthene, are highly suitable for the study of interatomic interactions. The short "natural" *peri*-distance (2.44 Å) and the rigidity of the aromatic system causes considerable strain between the *peri*-substituents.[3] Only the hydrogen substituted acenaphthene is 'relaxed'.[2-5] As a consequence, substitutions in the *peri*-position lead to in- and out-of-plane distortions, which often result in buckling of the ring system. In order to relax this geometric strain, weak bonding interactions can exist between the *peri*-substituents.[5] We speculated that due to the large van der Waals radius of tin (2.17 Å) organo-tin acenaphthenes could be expected to be good candidates to demonstrate weak interactions.

Up to this point there has been limited research on organo-tin acenaphthene compounds, however, the X-ray structure of a naphthalene bearing iodine and $SnPh_3$ at the *peri*-positions has recently been reported, exhibiting a Sn···I distance of 3.46 Å. Other studies of group 14 *peri*-substituted compounds, however, has involved carbon or silicon substituted systems, for example disilyl compounds ($Nap(SiR_3)_2$) have been described[6-7] (SiR_3 = SiH_3, $SiMe_3$, SiH_2Ph). In addition,

systems containing group 15/16 *peri*-atoms have been thoroughly investigated with intramolecular donor-acceptor interactions across the *peri*-gap leading to 3c-4e type bonding (Figure 3.1).

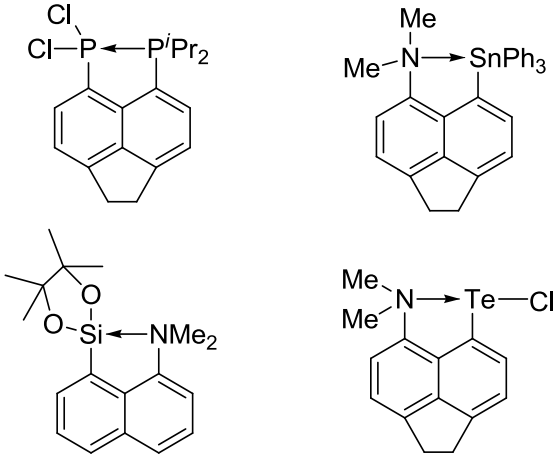

Figure 3.1 Examples of *peri*-substituted molecules stabilized by weak intramolecular interactions.[8-10]

Here we report the synthesis and structural studies of *peri*-substituted 5-bromo-6(organostannyl) acenaphthene compounds, in which elements from group 17(Br) and 14(Sn) occupy the close 5,6-positions on the acenaphthene backbone, but which are formally non-bonded. For their synthesis, 5,6-dibromoacenaphthene was treated with a selection of different organo-tin reagents (Ph_3SnCl, Ph_2SnCl_2, Bn_2SnCl_2, Bu_2SnCl_2, $SnCl_4$), affording the series of mixed bromo-tin derivatives **1** (Acenap[$SnPh_3$][Br], **2** (Acenap[$SnPh_2Cl$][Br] and **3-6** bis (Acenap[SnX_2][Br_2] (X= Cl, Bu, Ph, Bz)) (Figure 3.2).

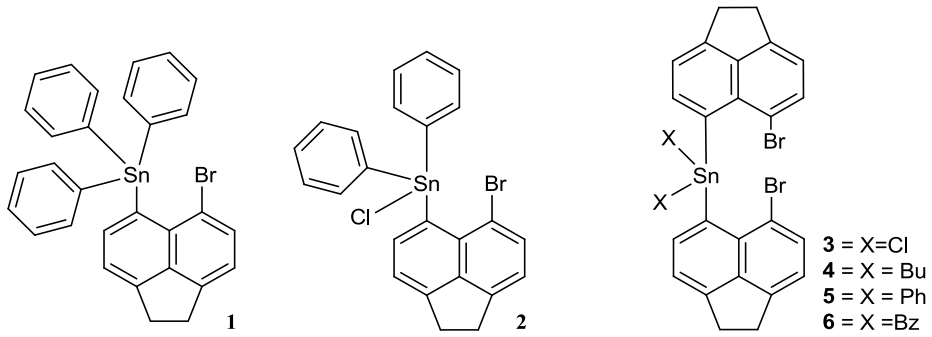

Figure 3.2 Compounds **1-6**, which will be discussed in this chapter.

Section 1

Synthesis and structural studies of mono-substituted 6-bromoacenaphth-5-yl-triphenyltin (1)

and

6-bromoacenaphth-5-yl-diphenyltin chloride (2)

6-bromoacenaphth-5-yl-triphenyltin (**1**) and 6-bromoacenaphth-5-yl-diphenyltin chloride (**2**) were synthesized by reacting 5,6-dibromoacenaphthene with a one equivalent of *n*-butyllithium at −40 °C in diethyl ether, followed by subsequent addition of $SnPh_3Cl$ and $SnPh_2Cl_2$, respectively, [yield: 32% (**1**), 23% (**2**); Scheme 3.1 and 3.2].

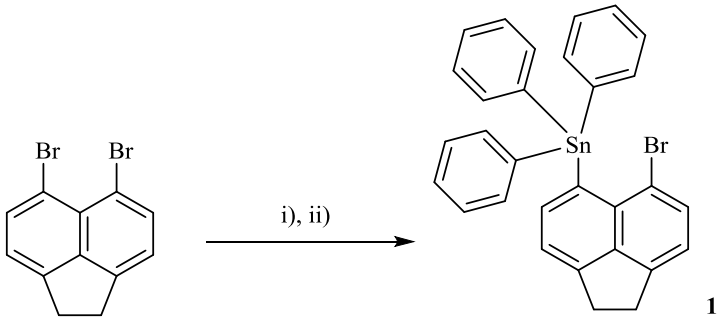

Scheme 3.1 The preparation of 6-bromoacenaphth-5-yl-triphenyltin **1** from 5,6-dibromoacenaphthene.

Conditions: i) *n*BuLi (1 equiv), Et_2O, -40 ºC, 1 h; ii) $SnPh_3Cl$ (1 equiv), Et_2O, 1 h.

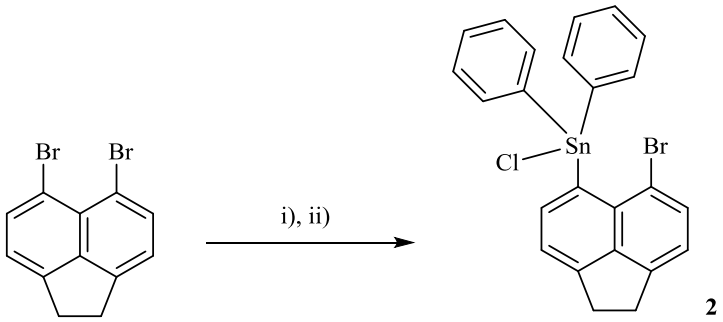

Scheme 3.2 The preparation of 6-bromoacenaphth-5-yl-diphenyltin chloride **2** 5,6-dibromoacenaphthene. Conditions: i) *n*BuLi (1 equiv), Et_2O, -40 ºC, 1 h; ii) $SnPh_2Cl_2$ (1 equiv), Et_2O, 1 h.

Compounds **1** and **2** were characterised by elemental analysis, ^{1}H, ^{13}C and ^{119}Sn NMR spectroscopy. The ^{119}Sn NMR spectra of **1** and **2** display the expected singlets at -82 ppm and -70 ppm, respectively. To date there are no tin-substituted acenaphthene structures known in the literature for comparison with the compounds studied here. While the ^{119}Sn NMR shifts of **1** and **2** are actually higher than for the phenyl analogue (Ph_4Sn), a large upfield shift can be seen for **2**, in comparison to Ph_3SnCl (Table 3.1), consistent with a higher coordination number at the tin atom as a result of the interaction between the *peri*-substituents.

Table 3.1 ^{119}Sn NMR spectroscopy data for compounds **1**-**2** and analogous compounds where the acenaphthene is replaced by a phenyl group; all spectra run in $CDCl_3$, δ (ppm).

Compound	**δ (ppm)**	**Compound**	**δ (ppm)**
1	-82	Ph_4Sn	-137
2	-70	Ph_3SnCl	-45

X ray investigations

Crystals for **1** suitable for X-ray crystallography were obtained by diffusion of hexane into a saturated solution of the product in tetrahydrofuran (THF); the data refined in the *Pbca* space group (R1 = 3.59% (**1**)). Suitable single crystals for **2** were obtained by slow evaporation of hexane into a saturated solution of the compound in dichloromethane; crystallising in the *P*21/*n* space group (R1 = 7.53% (**2**)). Both compounds crystallise with only one molecule in the asymmetric unit (Figures 3.3, 3.4). Selected interatomic distances, angles and torsion angles are listed in Table 3.2, further crystallography data for **1** and **2** can be found in Appendix 3.

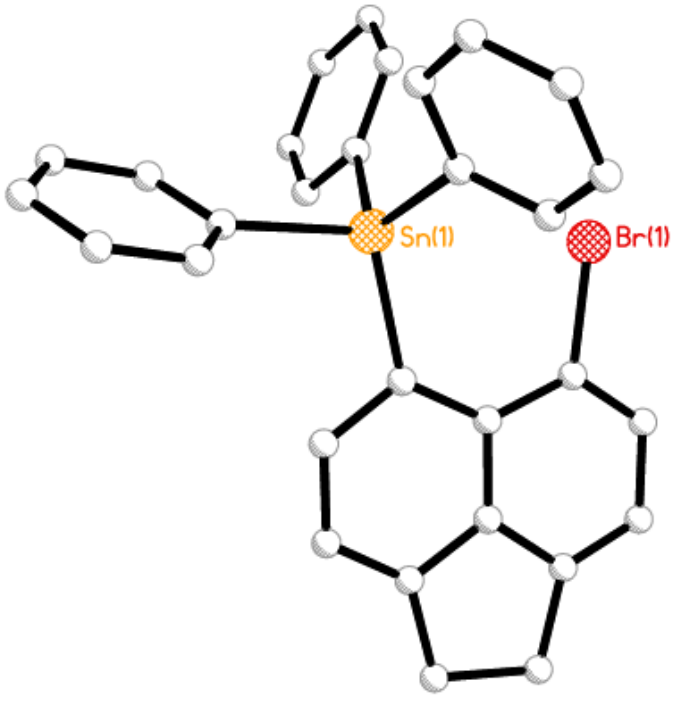

Figure 3.3 The crystal structure of *6-bromoacenaphth-5-yl-triphenyltin **1*** (hydrogen atoms omitted for clarity).

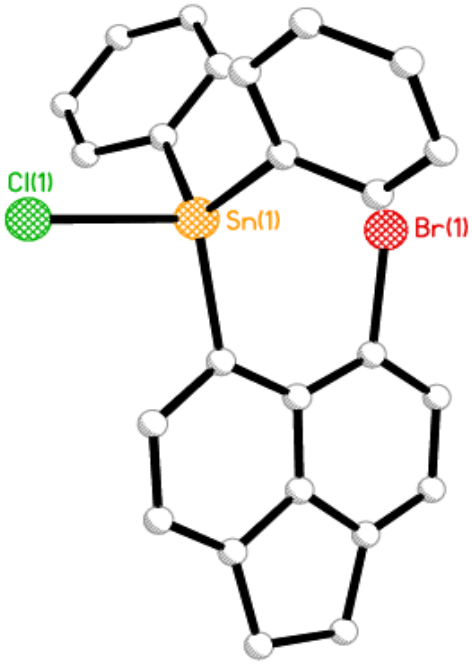

Figure 3.4 The crystal structure of *6-bromoacenaphth-5-yl-diphenyltin chloride* **2** (hydrogen atoms omitted for clarity).

The steric repulsion imposed in **1** and **2**, by the crowded tin moieties located in the bay region is relieved by in-plane and out-of-plane deviation supplemented by significant buckling of the acenaphthene skeleton (see the central C-C-C-C torsion angles of the acenaphthene framework Table 3.1). The magnitude of geometrical deformation of acenaphthene is related to the bulkiness of the tin functionalities which occupy the *peri*-positions in the acenaphthene molecules. This can be identified when comparing the *peri*-distances for the two compounds. In **1**, substituents reside in close proximity, with a non-bonded distance of 3.340(3) Å whereas **2** displays a much shorter *peri*-distance of 3.143(2) Å, due to less bulkier substituents residing at the *peri*-positions and additionally the presence of the highly electronegative chlorine atom ($SnPh_2Cl$), which enhances the donor-acceptor type interaction. However, the *peri*-distances are still much shorter than the

sum of the van der Waals radii for tin and bromine for both compounds (sum of vdW of Sn and Br, 4.02 Å), with distances 83% (**1**) and 78% (**2**) of the vdW sum (Table 3.1). These short weak interatomic *peri*-distances indicate the possible existence of non-covalent interactions.[3]

The bromine and tin atoms show greater deviations from the acenaphthene ring plane in **1** with the Sn lying -0.121(1) Å below the plane and Br displaced 0.1494 Å above, which is explained by the presence of the bulky triphenyl tin moiety sitting at one of the *peri*-positions. Minor out-of-plane distortion, however, is observed in **2** with the Sn and Br atoms sitting 0.076(1) Å and -0.094(1) Å from the mean plane respectively (Figure 3.2). Further distortion is provided by in-plane deviations of the exocyclic *peri*-bonds, with angles around the bay region affording a splay angle for **2** of 15.6° (sum of the *peri*-region angles - 360°), noticeably smaller than that observed in **1** (20.1°). The increase in in-plane distortion in **1** indicates the two *peri*-bonds are moving further apart due to repulsion between the large tin and bromine moieties. Moreover, central acenaphthene ring C-C-C-C torsion angles in the range 1- 4° also indicates significant buckling of the acenaphthene ring in each compound.

Table 3.2 Selected bond lengths (Å) and angles (°) for **1** to **2**.

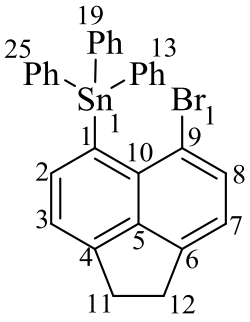

1

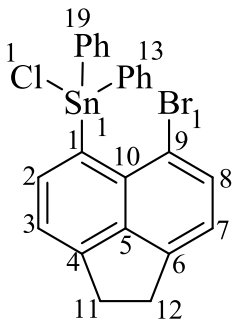

2

Peri-region-distances		
Br(1)···Sn(1)	3.340(3)	3.145(2)
Σr_{vdW} - Br(1)···Sn[a]	0.680	0.875
$\%r_{vdW}$[a]	83	78
Br(1)-C(9)	1.907(4)	1.918(11)
Sn(1)-C(1)	2.157(5)	2.147(11)
Acenaphthene bond lengths		
C(1)-C(2)	1.395(6)	1.425(15)
C(2)-C(3)	1.413(6)	1.411(17)
C(3)-C(4)	1.361(6)	1.372(16)
C(4)-C(5)	1.415(6)	1.428(15)
C(5)-C(10)	1.423(6)	1.417(15)
C(5)-C(6)	1.413(6)	1.422(15)
C(6)-C(7)	1.361(6)	1.334(16)
C(7)-C(8)	1.421(6)	1.458(18)
C(8)-C(9)	1.359(6)	1.375(16)
C(9)-C(10)	1.429(6)	1.418(15)
C(10)-C(1)	1.437(6)	1.417(15)
C(4)-C(11)	1.509(6)	1.522(16)
C(11)-C(12)	1.560(7)	1.529(17)
C(12)-C(6)	1.507(6)	1.522(17)
Peri-region bond angles		
Br(1)-C(9)-C(10)	120.2(3)	119.7(8)
C(1)-C(10)-C(9)	130.9(4)	130.5(10)
Sn(1)-C(1)-C(10)	129.0(3)	125.4(8)
Σ of bay angles	**380.1(6)**	**375.6(15)**
Splay angle[b]	20.1	15.6
C(4)-C(5)-C(6)	111.4(4)	111.3(10)

In and out-of-plane displacement		
Br(1)	0.149(1)	-0.094(1)
Sn(1)	-0.121(1)	+0.076(1)
C:(6)-(5)-(10)-(1)	-179.3(4)	178.9(9)
C:(4)-(5)-(10)-(9)	-176.5(4)	176.9(9)

[a] van der Waals radii used for calculations: rvdW (Sn) 2.17 Å, rvdW (Br) 1.85 Å [b] Splay angle: Σ of the three bay region angles – 360.

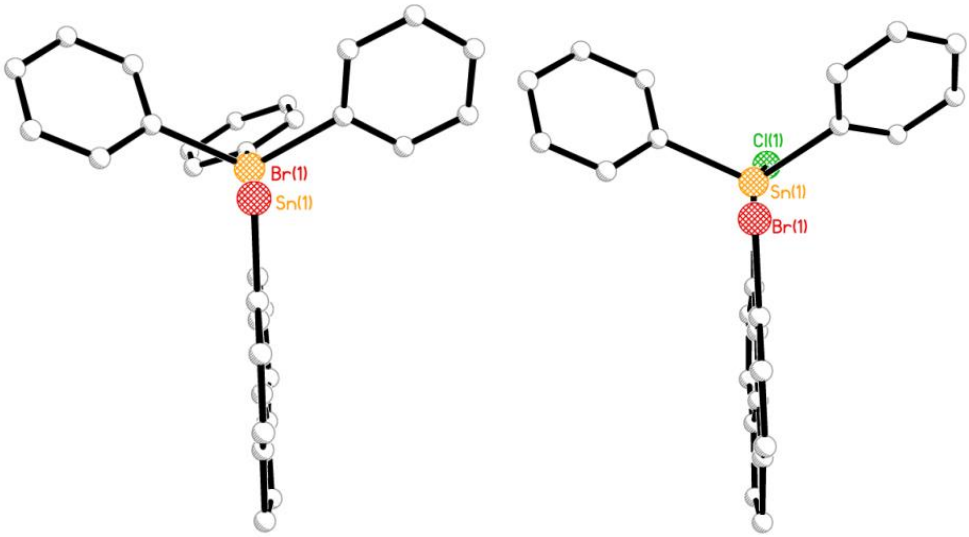

Figure 3.5 The structures **1** and **2** showing the planarity of the acenaphthene backbone.

The Sn-C1 distances (2.1 Å) are within the standard range for typical Sn-C bonds found in CSD search (2.1 ± 0.5 Å) for both **1** and **2**. This shows that despite the steric effects caused by the large *peri*-substituents the Sn-C distance is not greatly affected. The geometry around the tin centre, however, shows a significant deviation away from that of an ideal tetrahedron, with the most acute angle (C13-Sn1-C25) 96.1(3)º and the most obtuse angle (C19-Sn1-C25) 121.1(4)º, illustrating the

degree of distortion enforced by the rigid acenaphthene backbone (Table 3.2). It is interesting to note that the sum of the C(1)-Sn(1)-C(19), C(1)-Sn(1)-C(25), and C(19)-Sn(1)-C(25) angles in **1** is 345°; wider than the tetrahedral (328.5°) but not large enough (360°) for a perfect trigonal bipyramid. The main reason for these distortions appears to be the presence of weak Sn···Br interactions in these systems coupled with the rigidity of the acenaphthene backbone.

Table 3.3 Bond angles [°] categorising the geometry around Sn in **1** and **2**.

Angles around the Sn atom	**1**	**2**
C(1)-Sn(1)-C(13)	107.73(15)	-
C(1)-Sn(1)-C(19)	114.37(15)	-
C(1)-Sn(1)-C(25)	111.15(15)	-
C(13)-Sn(1)-C(19)	99.82(15)	-
C(13)-Sn(1)-C(25)	102.26(15)	-
C(19)-Sn(1)-C(25)	119.34(15)	-
Cl(1)-Sn(1)-C(1)	-	100.7(3)
Cl(1)-Sn(1)-C(13)	-	96.1(3)
Cl(1)-Sn(1)-C(19)	-	100.3(3)
C(1)-Sn(1)-C(13)	-	121.1(4)
C(1)-Sn(1)-C(19)	-	114.2(4)
C(13)-Sn(1)-C(19)	-	117.5(4)

The Sn-C_{Ph} and Sn-Cl moieties in **1** and **2** lie in a similar location producing *quasi*-linear three-body fragments; Br···Sn-C_{Ph} in **1** (179.88^{o}) and Br···Sn-Cl in **2** (172.06°) (Figure 3.6). The observed *peri*-distances between tin and bromine are well within van der Waals radii of the atoms by 0.68 Å for **1** and 0.875 Å for **2** [**1** 3.34(3) Å, (4.02) Å ; **2** 3.145(2) Å, (4.02) Å]. The linear arrangement and the close proximity of the two *peri*-atoms provides the correct geometry for promoting a 3c-4e type interaction.[2,3] This is supported by the Wiberg bond indices (WBIs),[5] which measure covalent bond order, calculated for the Br···Sn interactions present in both

structures. The WBI for **2** is 0.11 which indicates the presence of a weakly attractive interaction between the Sn···Br *peri* substituents, and as expected much more significant than in **1** (0.07). This is due to the presence of the highly electronegative chlorine atom on the Sn atom in **2**, which enhances the weak Sn···Br interaction, formed by electron donation from the bromine atom into low-lying empty orbitals on tin.

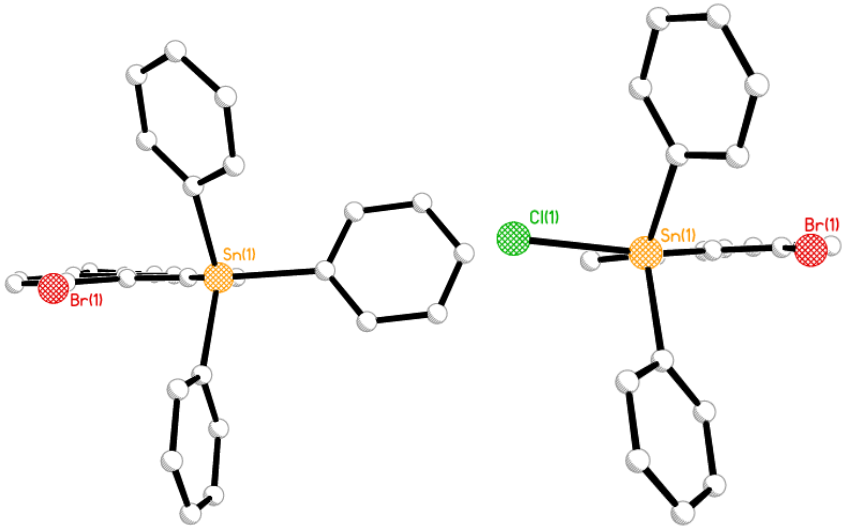

Figure 3.6 The molecular configurations of **1** and **2** showing the orientation of the substituents bound to acenaphthene.

The phenyl rings attached to the tin metal sit in different orientations for **1** *cf.* **2,** which makes for different packing within the structure. There are no significant π-π stacking interactions; when the molecules are packed the distances between the centroids exceed 3.80 Å[11], the recognised distance under which π-π stacking is considered to occur. There are no standard H-bonds found in the

structure, however centroid (Cg) hydrogen bonds (H-Cg) are present (Table 3.4, Figure 3.7 and 3.8). In **1** and **2**, the H atom attached to C11 interacts with the centroid of a separate molecule and due to the orientation of the second molecule the C11-H11A atom can similarly interact with a centroid from the first molecule, resulting in a back interaction (Figure 3.7 and 3.8). In **1** and **2**, the hydrogen atoms from both the acenaphthene and the attached phenyl rings interact with centroids of further phenyl rings from different molecules. In contrast to the structure of **1**, compound **2** exhibits a weak donor–accepter type interaction due to the close proximity of the large Cl atom and H2, with the H2-Cl1 distance 2.72 Å (Figure 3.8).

Table 3.4 H – Cg interactions for **1** and **2**; Cg2: 6 membered C5-C6-C7-C8-C9-C10; Cg3: 6 membered C1-C2-C3-C4-C5-C10; Cg4: 6 membered C5-C6-C7-C8-C9-C10; Cg6: 6 membered C19-C20-C21-C22-C23-C24; generated in Platon.

Compound	X	H	Cg	H...Cg Distance /Å	X...Cg Distance /Å	Angle /°
1	C11	H11A	2	2.72	3.4942	136
	C15	H15	3	2.82	3.6398	145
2	C11	H11B	4	2.93	3.7105	136
	C15	H15	6	2.86	3.6585	142

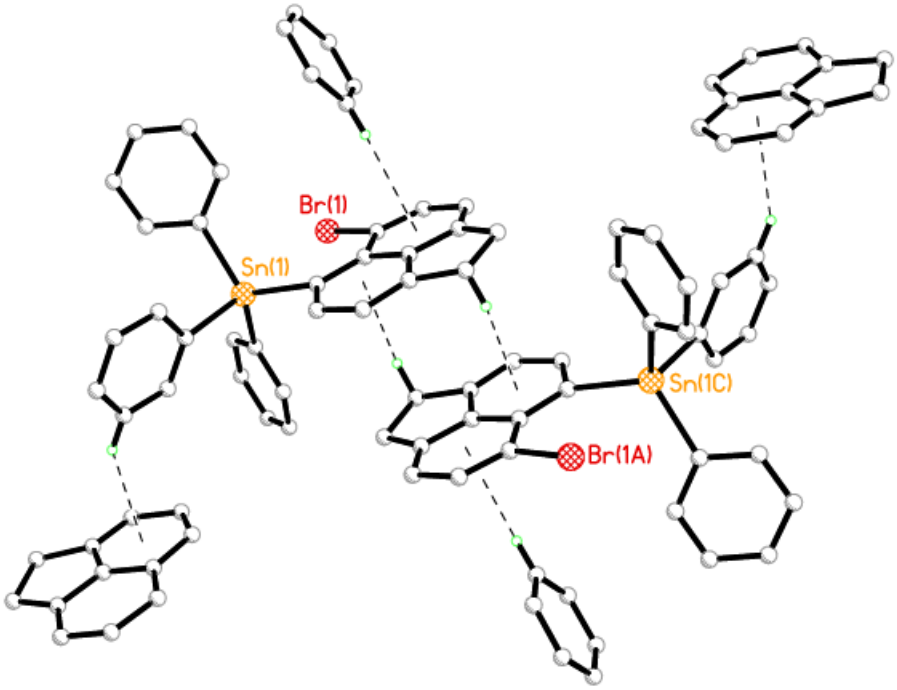

Figure 3.7 H- Centroid interactions within the structure of **1**.[12,13]

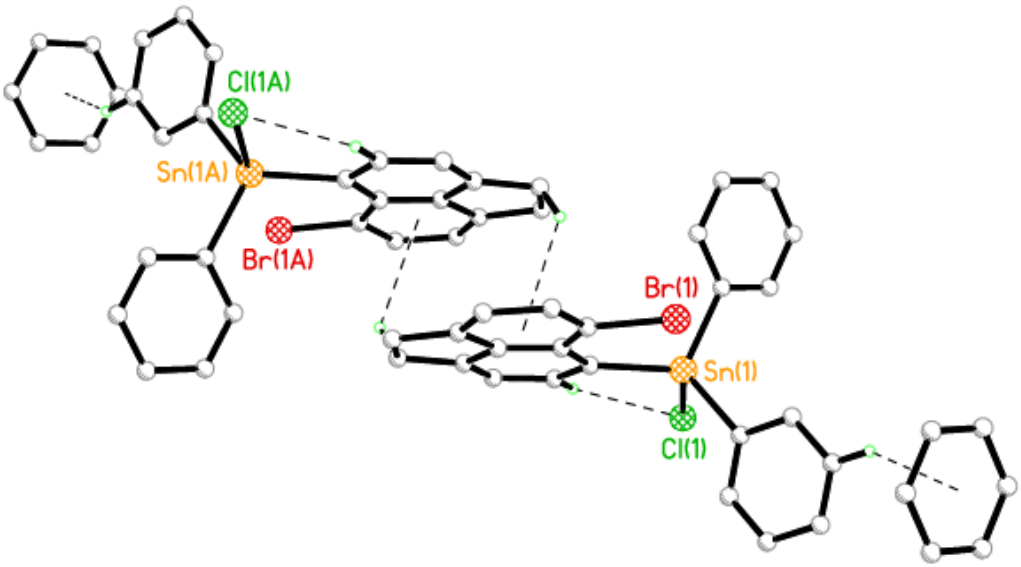

Figure 3.8 H- Centroid and donor-acceptor interactions within the structure of **2**.[12,13]

Section 2

Synthesis and structural studies of bis(6-bromoacenaphth-5-yl)tin dichloride

and

bis(6-bromoacenaphth-5-yl)dibutyltin

Single substitution reactions of 5,6-dibromoacenapthene, *via* lithium halogen exchange followed by treatment of a suitable tin dichloride, yielded compounds of the type bis ({AcenapBr}$_2$SnX$_2$ (X= Cl (**3**), Bu (**4**)) (Scheme 3.3). For their synthesis, 5,6-dibromoacenapthene was independently reacted with *n*-butyllithium (1 equivalent) at −40 °C in diethyl ether and subsequent addition of a ½ equivalent of $SnCl_2$ and $SnBu_2Cl_2$, respectively, **3** and **4** [35% (**3**), 14% (**4**); Scheme 3.1 and 3.2].

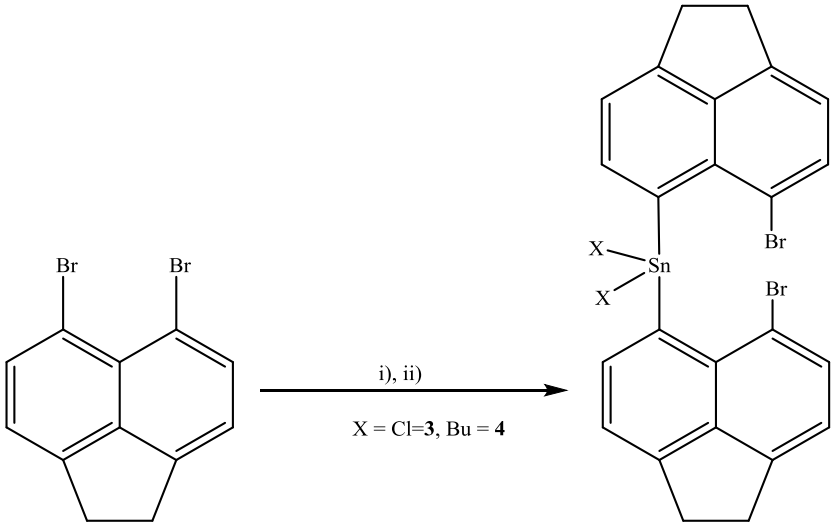

Scheme 3.3 The preparation of bis(6-bromoacenaphth-5-yl)tin dichloride **3** and bis(6-bromoacenaphth-5-yl)dibutyltin **4** from 5,6-dibromoacenaphthene. Conditions: i) *n*BuLi (1 equiv), Et_2O, -40 ºC, 1 h; ii) $SnCl_2$ and $SnBu_2Cl_2$ respectively (1 equiv), Et_2O, 1 h.

Both compounds were fully characterised by elemental analysis, ^{1}H, ^{13}C and ^{119}Sn NMR spectroscopy. The ^{119}Sn NMR spectra of **3** and **4** display single peaks at -132.2 ppm and -31.4 ppm, respectively, with the presence of the two highly electronegative chlorine atoms producing a substantial upfield shift compared to the two butyl groups.

X ray investigations

Colourless crystals, suitable for characterisation by single crystal X-ray crystallography were obtained for **3** and **4** from THF at −30 °C. The data for both **3** and **4** refined in the *P-1* space group, with the final refinement of **4** containing one independent molecule plus an additional 5-bromoacenapthene molecule in the asymmetric unit, whilst compound **3** had one independent molecule and one solvent (THF) molecule in the asymmetric unit, (R1 = 4.98 **(3),** 6.33 **(4**) %). The crystal structures of **3** and **4** are shown in Figures 3.9 and 3.10. Selected interatomic bond lengths and angles are listed in Table 3.5, and further crystal structure data is found in Appendix 3.

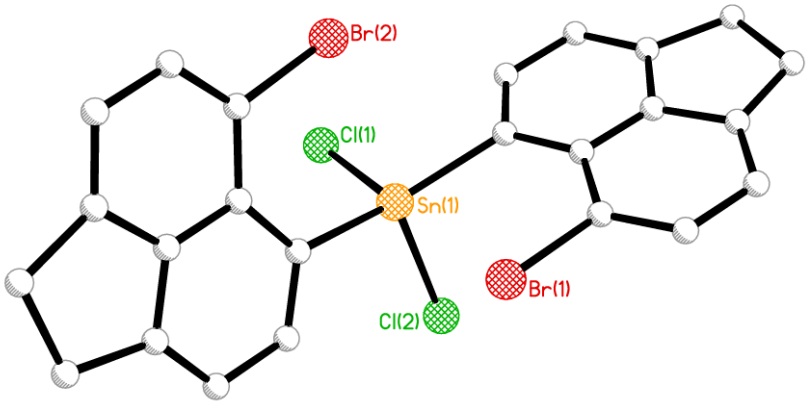

Figure 3.9 The crystal structure of *bis(6-bromoacenaphth-5-yl)dichlorotin* **3** (hydrogen atoms omitted for clarity).

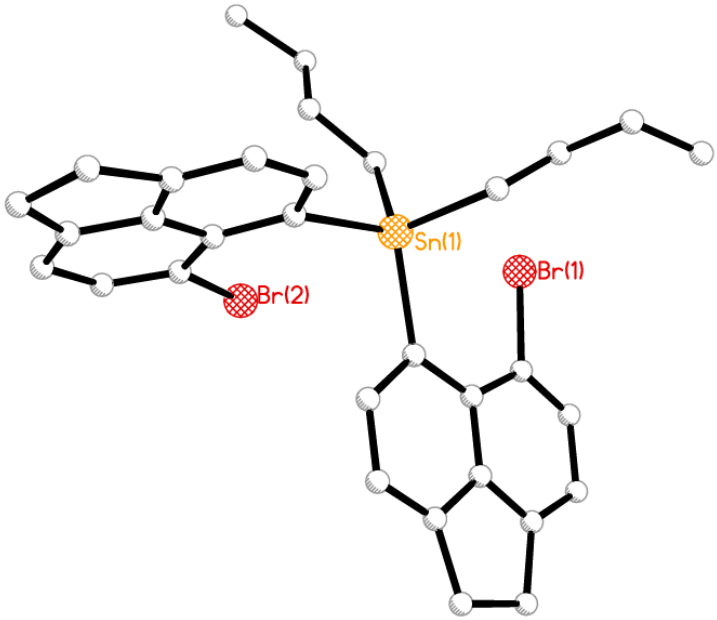

Figure 3.10 The crystal structure of *bis(6-bromoacenaphth-5-yl)dibutyltin* **4** (hydrogen atoms omitted for clarity).

The molecular structures of bis-tin derivatives **3** and **4** are constructed from two crystallographically different acenaphthene fragments which couple through a central *pseudo*-tetracoordinated tin atom in a geminal fashion (Figure 3.9 and 3.10). In **3** and **4**, the acenaphthene fragments lie with angles of 37° and 61° respectively between the two mean planes, keeping the Br atoms at a close distance to the tin center. The steric strain forced upon the *peri*-substituents by the rigid acenaphthene scaffolds is released by the formation of weakly attractive intermolecular 3c-4e type interactions which are presumably between the lone pair of electrons on Br and the electropositive Sn atom. This results in short Sn···Br distances within the sum of van der Waals radii (Sn1-Br1 3.174 (1) Å **3**, Sn1-Br 3.398(1) Å **4**). This is supported by the alignment of the Sn-C_{Bu} , Sn-C_{acenap} and Sn-Cl moieties in **3** and **4**, which sit in a linear arrangement, leading to the construction of comparable three-body fragments; Br···Sn-Cl in **3** (179.23°) and Br···Sn-C_{Bu} in **4** (175.72°) (Figure 3.12).

In both compounds the geometry around the Sn atom deviates significantly from an ideal tetrahedral geometry, with angles in the range 98.74°-142.1° (Table 3.4). In dichloride **3**, the tin geometry is somewhat complicated, which can be described as either 2-coordinate (linear), 4-coordinate (square planar) or 6-coordinate (octahedral) depending upon the interpretation of the Sn-Y bonding interactions (Figure 3.12). If the two Sn-Br interactions are classified as non-bonding and the Sn-Cl bond thought of as having ionic character due to the electronegativity difference between the Sn and Cl atoms, the tin center would be coordinated to just the two acenaphthene fragments, with a C_{acenap}-Sn-C_{acenap} bond angle of 179.23(4)° displaying linear geometry. However, if we consider the Sn-Cl interaction as a covalent bond the arrangement of atoms around Sn is now best described as distorted see-saw geometry. Finally, the weakly

attractive donor-acceptor interactions between Br and Sn complete a distorted octahedral geometry around the tin center.

Table 3.4 Bond angles [°] categorising the geometry around Sn in **3** and **4**.

Angles around the Sn atom		**3**		**4**
C(1)-Sn(1)-C(13)	142.1(4)	142.1(4)	-	-
C(1)-Sn(1)-Cl(1)	103.6(3)	103.6(3)	-	-
C(1)-Sn(1)-Cl(2)	98.9(2)	98.9(2)	-	-
Cl(1)-Sn(1)-Cl(2)	98.74(10)	98.74(10)	-	-
C(13)-Sn(1)-Cl(1)	102.4(3)	102.4(3)	-	-
C(13)-Sn(1)-Cl(2)	103.7(3)	103.7(3)	-	-
C(1)-Sn(1)-C(13)	-	-	104.7(3)	104.7(3)
C(1)-Sn(1)-C(25)	-	-	125.8(3)	125.8(3)
C(1)-Sn(1)-C(29)	-	-	102.6(4)	102.6(4)
C(13)-Sn(1)-C(25)	-	-	107.5(3)	107.5(3)
C(13)-Sn(1)-C(29)	-	-	104.9(4)	104.9(4)
C(25)-Sn(1)-C(29)	-	-	109.6(4)	109.6(4)

The degree of steric hindrance operating between the *peri*-substituents of **3** and **4** is substantially larger than compared to the mono-compounds of Section 1. The out-of-plane displacement of the *peri*-atoms above and below the mean acenaphthene plane is unequal in the two acenaphthene fragments of each molecule (see Table 3.5). However, the tin atoms are displaced to a similar degree in each structure, lying -0.390(1) Å **3a** and -0.400(1) Å **4a** from the mean plane respectively. In order to further accommodate the steric congestion of the Sn and Br atoms, deviation *via* in-plane distortions occurs in the C-C-C group between the *peri*-region, as observed by the sum of the bay-region angles (374.6(11)° **3a** and 380.3(12)° **4a**). Moreover, central C-C-C-C torsion angles around the C5-C10 bond also suggest the acenaphthene backbone is twisted in both compounds, but to a greater extent in **4** than in **3.**

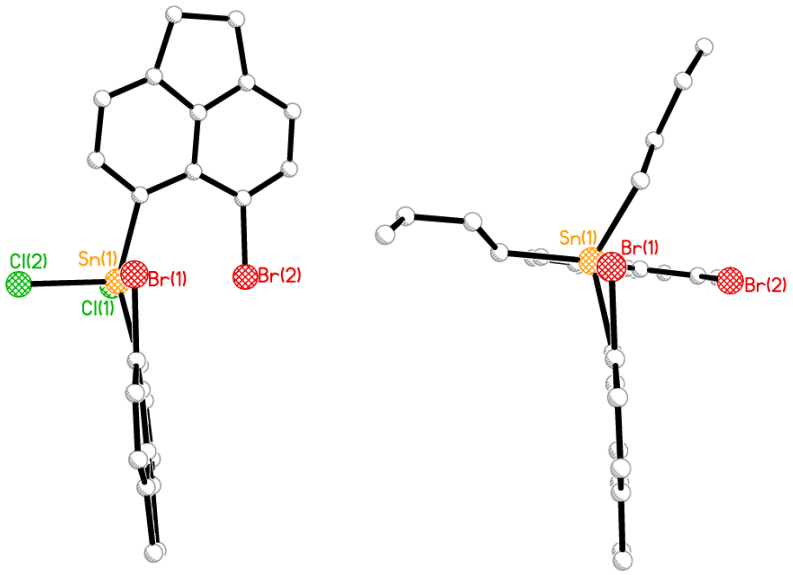

Figure 3.12 The structures of **3** and **4** showing the planarity of the acenaphthene backbone.

Table 3.5 Selected bond lengths (Å) and angles (°) for **3** to **4**.

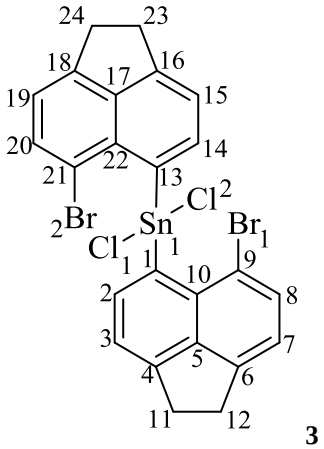

3

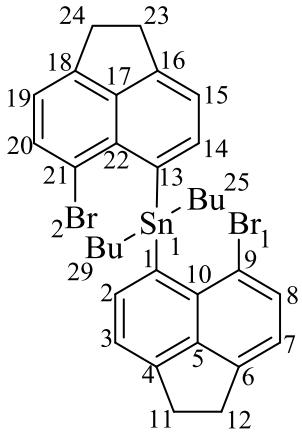

4

Fragment	**3a**	**3b**	**4a**	**4b**
Peri-region-distances				
Br(1)···Sn(1)	**3.174(2)**	**3.174(2)**	**3.398(1)**	**3.370(1)**
Σr_{vdW} - Br(1)···Sn[a]	0.846	0.846	0.622	0.650

$\%r_{vdW}$[a]	79	79	85	84
Br(1)-C(9)	1.910(8)	1.919(9)	1.911(9)	1.904(7)
Sn(1)-C(1)	2.125(8)	2.142(9)	2.163(8)	2.211(8)
Acenaphthene bond lengths				
C(1)-C(2)	1.393(13)	1.383(12)	1.405(13)	1.374(11)
C(2)-C(3)	1.423(12)	1.438(13)	1.416(13)	1.430(10)
C(3)-C(4)	1.363(13)	1.368(11)	1.353(11)	1.364(13)
C(4)-C(5)	1.423(13)	1.410(11)	1.407(12)	1.424(12)
C(5)-C(10)	1.411(11)	1.410(12)	1.423(12)	1.419(10)
C(5)-C(6)	1.413(11)	1.406(11)	1.399(10)	1.417(13)
C(6)-C(7)	1.354(13)	1.382(12)	1.375(12)	1.377(13)
C(7)-C(8)	1.420(12)	1.399(12)	1.429(13)	1.422(11)
C(8)-C(9)	1.381(11)	1.374(10)	1.360(11)	1.368(13)
C(9)-C(10)	1.435(13)	1.443(11)	1.436(12)	1.419(12)
C(10)-C(1)	1.436(11)	1.439(10)	1.450(10)	1.447(13)
C(4)-C(11)	1.542(12)	1.523(12)	1.507(12)	1.511(11)
C(11)-C(12)	1.549(14)	1.573(11)	1.556(11)	1.552(13)
C(12)-C(6)	1.518(12)	1.530(13)	1.499(13)	1.506(10)
Peri-region bond angles				
Br(1)-C(9)-C(10)	119.8(6)	119.6(6)	120.5(6)	121.4(6)
C(1)-C(10)-C(9)	129.4(7)	130.1(8)	129.8(8)	131.1(7)
Sn(1)-C(1)-C(10)	125.4(6)	125.3(6)	130.0(7)	128.0(6)
Σ of bay angles	**374.6(11)**	**375.0(12)**	**380.3(12)**	**380.5(11)**
Splay angle[b]	14.6	15.0	20.3	20.5
C(4)-C(5)-C(6)	112.3(7)	112.0(8)	111.8(8)	110.8(7)
In and out-of-plane displacement				
Br(1)	+0.177(1)	+0.072(1)	-0.002(1)	-0.002(1)
Sn(1)	-0.390(1)	-0.176(1)	-0.400(1)	-0.011(1)
C:(6)-(5)-(10)-(1)	-175.9(6)	-179.7(7)	179.9(8)	179.0(7)
C:(4)-(5)-(10)-(9)	179.9(6)	179.7(7)	-179.0(7)	178.7(7)

[a] van der Waals radii used for calculations: rvdW (Sn) 2.17 Å, rvdW (Br) 1.85 Å [b] Splay angle: Σ of the three bay region angles – 360.

It is interesting to note that in **4**, one acenaphthyl group attached to Sn is perpendicular to the other acenaphthene backbone to relieve the repulsion caused by the two butyl groups; this feature is not seen in compound **3**. In addition, the Sn–C bond distance is 2.211(8) Å, which is slightly elongated

to accommodate the repulsion caused by the *peri* substituents, but nevertheless is concurrent with standard Sn-C distances from a CSD search for typical Sn-C bond lengths (2.10 Å).[1]

In **4**, in addition to the H-Cg interactions, there is a weak H-bond between the hydrogen of the acenaphthene and the bromine atom. This suggest that the addition of the butyl group instead of the phenyl group, allows the substituents to get close enough to make a weak H···Br bond (Figure 3.14). Whilst there is no π-π stacking seen in **3** and **4** (as the closest centroids are 3.82 Å and 3.89 Å in distance), there are H-Cg interactions seen in each structure (Table 3.6). In both these structures the molecules pack in pairs with one molecule rotated through 180°, lying on top of the other, allowing for the acenaphthene of one molecule to interact through the C11 and C12 hydrogens (Figure3.13 and 3.14). In addition, there are two weak donor-accepter interactions present in **3**, due to the alignment of the bromine atoms in the *peri*-region (C30-H30B···Br1 - 2.80 Å, C41-H41···Br3 – 2.92 Å), and similarly, **4** displays two donor-acceptor interactions with H-Cl (C2-H2···Cl1, 2.76 Å and C14-H14···Cl2, 2.76 Å).

Table 3.6 H – Cg interactions for **3** and **4**, Cg1: 6 membered C1-C2-C3-C4-C5-C10; Cg2: 6 membered C5-C6-C7-C8-C9-C10; Cg3: 6 membered C13-C14-C15-C16-C17-C22; Cg4: 6 membered C17-C18-C19-C20-C21-C22, generated in Platon.

Compound	X	H	Cg	H...Cg Distance /Å	X...Cg Distance /Å	Angle /°
	C11	H11B	2	2.80	3.6495	144
1	C12	H12A	1	2.77	3.5813	140
	C25	H25B	3	2.81	3.5887	136
	C11	H11B	2	2.95	3.7815	143
	C12	H12A	3	2.92	3.6352	129
2	C23	H23A	4	2.67	3.5080	143
	C24	H24B	3	2.60	3.4661	146

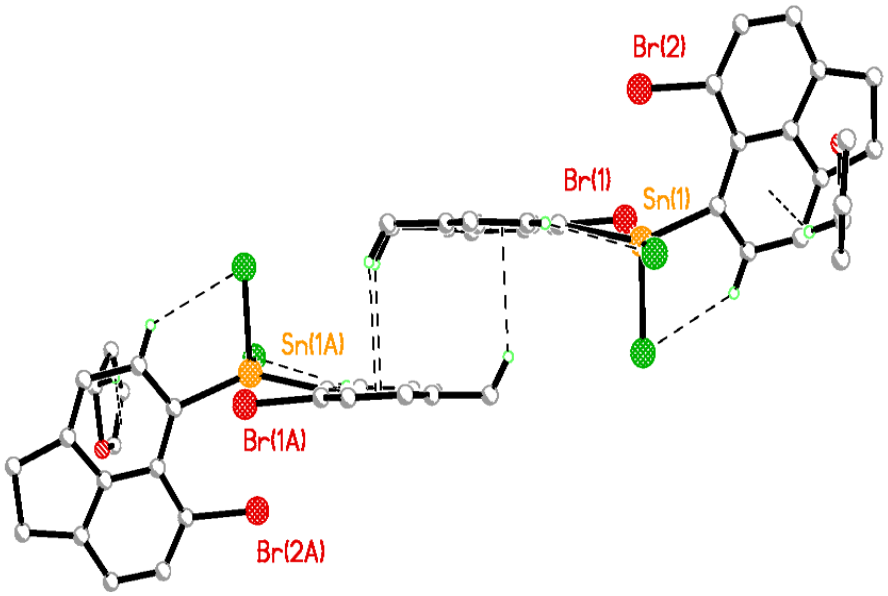

Figure 3.13 H- Centroid and donor-acceptor interactions within the structure of **3**.[12,13]

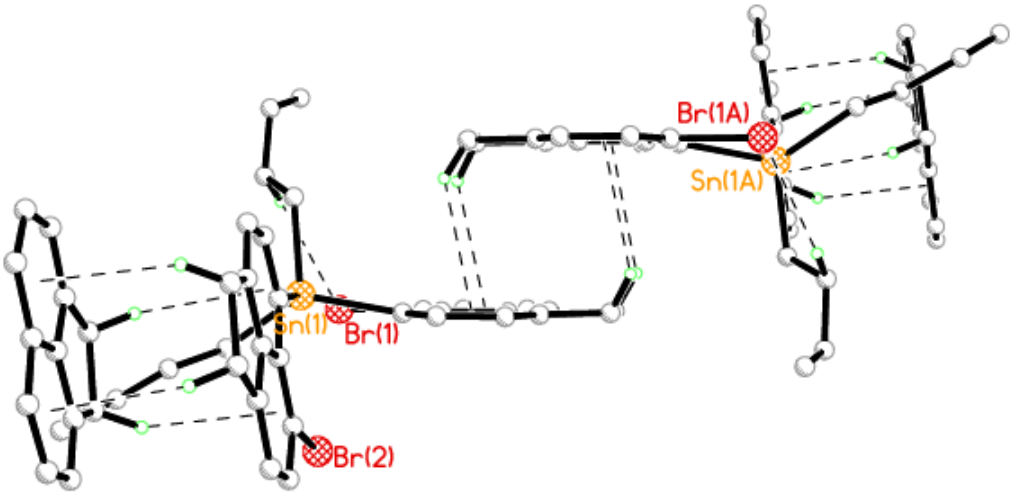

Figure 3.14 H- Centroid interactions and donor-acceptor within the structure of **4**.[12,1]

Section 3

Synthesis and structural studies of bis(6-bromoacenaphth-5-yl)diphenyltin

and

bis(6-bromoacenaphth-5-yl)dibenzyltin

To complete the series, analogues of compounds **3** and **4** containing the bulkier diphenyltin (**5**) and dibenzyltin (**6**) moieties at the *peri*-positions were prepared following the same procedure. 5,6-dibromoacenapthene was treated with a single equivalent of *n*-butyllithium at −40 °C in diethyl ether followed by addition of ½ equivalent of $SnPh_2$ and $SnBz_2Cl_2$, respectively [10% (**5**), 60% (**6**); Scheme 3.4]

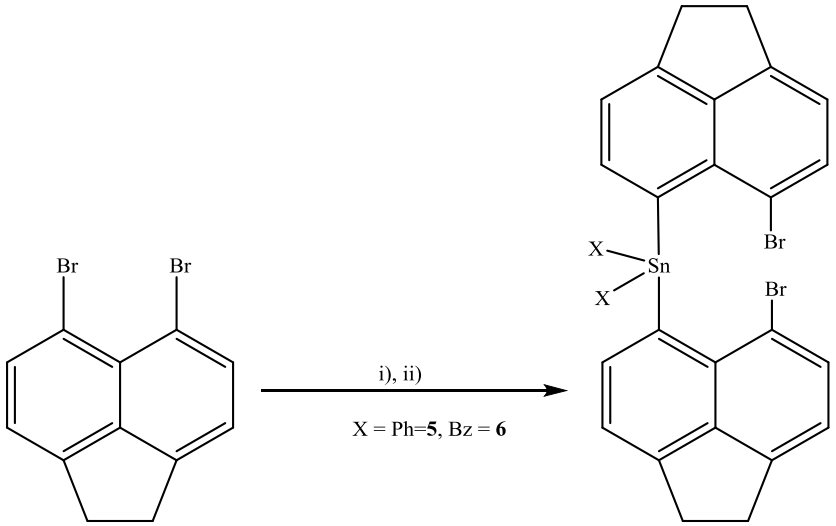

Scheme 3.4 The preparation of bis(6-bromoacenaphth-5-yl)diphenyltin **5** and bis(6-bromoacenaphth-5-yl)dibenzyltin **6** from 5,6-dibromoacenaphthene. Conditions: i) *n*BuLi (1 equiv), Et_2O, -40 ºC, 1 h; ii) $SnPh_2$ and $SnBz_2Cl_2$ respectively (1 equiv), Et_2O, 1 h.

Both compounds were characterised by elemental analysis, ^{1}H and ^{13}C NMR spectroscopy. **5** was additionally characterised by ^{119}Sn NMR spectroscopy, however due to poor solubility this was not possible for **6**. As expected, the ^{119}Sn NMR spectrum of **5** exhibited a single peak at -116 ppm, lying between the values observed for **3** and **4**.

X ray investigations

Colourless crystals, suitable for characterisation by single crystal X-ray crystallography were obtained for **5** and **6** from hexane diffusion into saturated solutions of dichloromethane. Diphenyltin derivative **5** (Figure 3.15) crystallises in the monoclinic system with space group P-1 (R1 = 5.12%), whilst benzyltin **6** (Figure 3.16) crystallises in the monoclinic system with space group of $P2_1/_C$ (R1 = 5.04%). Both compounds crystallise with one molecule in the asymmetric unit. Selected interatomic bond lengths and angles are listed in Tables 3.7 and further details of refinement data for **5** and **6** can be found in Appendix 3.

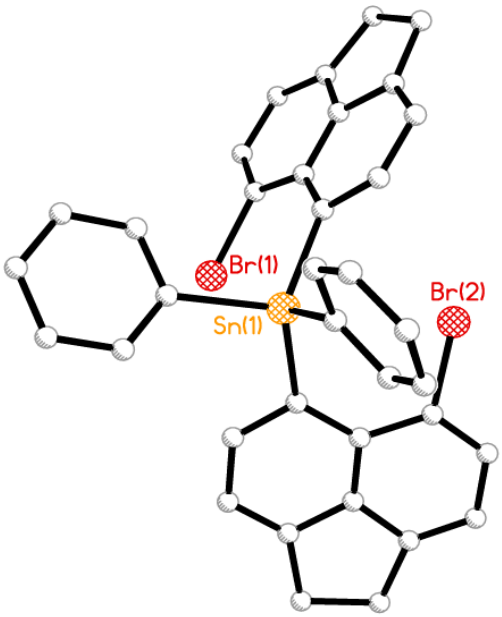

Figure 3.15 The crystal structure of *bis(6-bromoacenaphth-5-yl)diphenyltin* **5** (hydrogen atoms omitted for clarity).

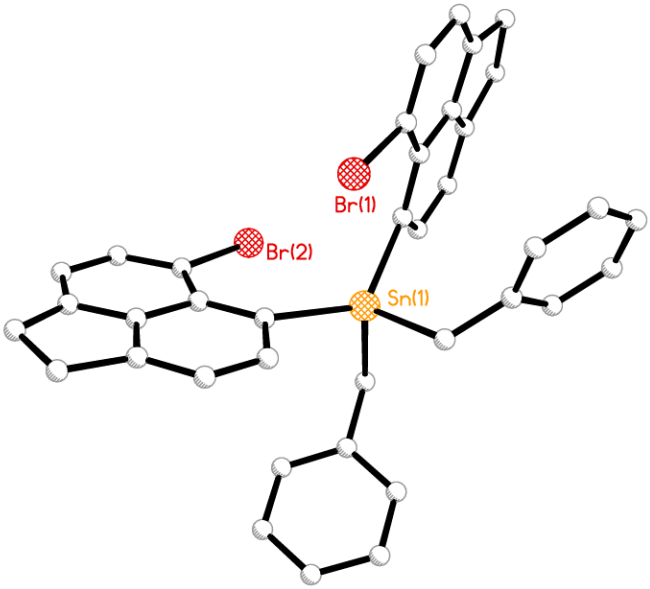

Figure 3.15 The crystal structure of *bis(6-bromoacenaphth-5-yl)dibezyltin* **6** (hydrogen atoms omitted for clarity).

The increased size of the substituents bound to Sn in **5** and **6** is accommodated by greater in- and out-of-plane distortion of the exocyclic *peri*-bonds. This is illustrated by looking at the angles between the *peri*-substituents, with the sum of the bay region angles increasing to 380.4(10)° in **5** and 378.8(9)° in **6**, much larger than the distortion exhibited by **2** (375.6(15) Å). A significant increase is also observed in the degree of out-of-plane displacement compared to **2**, with Br experiencing the greatest displacement from the plane (~0.2 Å). In both molecules, Br sits above the plane whilst Sn lies above and below the mean acenaphthene plane, respectively [**Sn (1)** 0.054(1) Å **5**, -0.306(4) Å **6**; **Br (1)** 0.311(5) Å **5**, 0.126(4) Å **6**]. The mean plane deviations can be seen in Figure 3.17. Further distortion from planarity can be seen *via* buckling of the C-C-C-C torsion angles. Whilst the C(6)-C(5)-C(10)-C(1) torsion angle almost approaches 180° (179.2(7)°), the C(4)-C(5)-C(10)-C(9) angle in contrast is 176.8(8)° demonstrating the degree of buckling occurring in the carbon backbone in order to relieve the steric strain caused by the bulkier Sn moiety. In addition, the C11-C12 bond (1.570(10) Å) has elongated to relieve the twisting of the acenaphthene ring, and it is larger than that of 5,6-dibromoacenaphthene (1.549(9)Å). The other difference is the C5-C10 distance which increases from 1.42 Å to 1.44 Å.

The Sn···Br distance in **5** (3.339(3) Å) is notably longer than that of **2** (3.1451(15) Å), but it is statistically indistinguishable from the distance in **1** (3.340(6) Å). However, the *peri*-distance in **6** (3.299(1) Å) is smaller than in **5**, implying the addition of the benzyl groups cause less steric strain compared to the diphenyl moiety. Nevertheless, *peri*-distances are less than the sum of the van der Waals radii for the two interacting atoms [SnBr = 4.02 Å] suggesting non-covalent interactions could exist between these atoms.

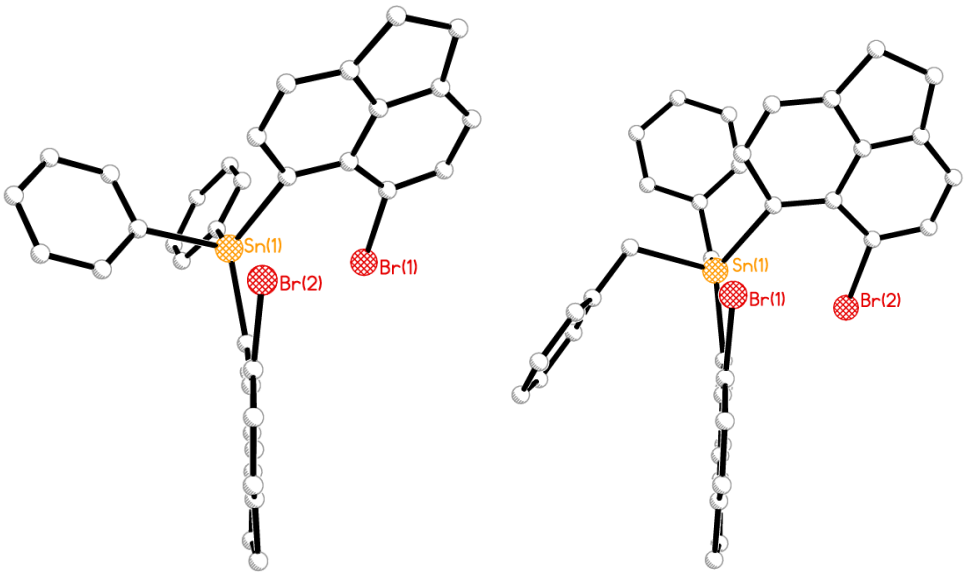

Figure 3.16 The structures of compounds **5** and **6** showing the planarity of the acenaphthene backbone.

Table 3.7 Selected bond lengths (Å) and angles (°) for **5** to **6**.

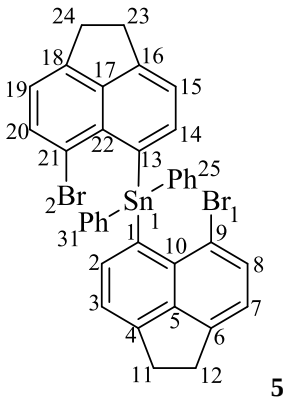

5

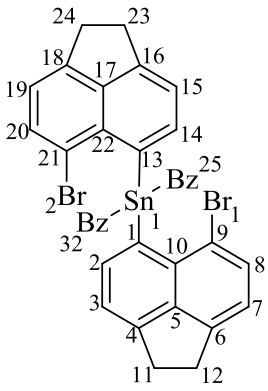

6

Fragment	**5a**	**5b**	**6a**	**6b**
Peri-region-distances				
Br(1)···Sn(1)	**3.328(1)**	**3.338(1)**	**3.299(1)**	**3.393(1)**
Σr_{vdW} - Br(1)···Sn[a]	0.692	0.682	0.721	0.627
$\%r_{vdW}$[a]	83	83	82	84

Br(1)-C(9)	1.913(8)	1.899(9)	1.902(6)	1.908(8)
Sn(1)-C(1)	2.161(7)	2.129(9)	2.168(6)	2.171(7)
Acenaphthene bond lengths				
C(1)-C(2)	1.430(10)	1.411(10)	1.386(8)	1.423(10)
C(2)-C(3)	1.413(11)	1.407(13)	1.432(9)	1.371(12)
C(3)-C(4)	1.374(10)	1.356(12)	1.352(9)	1.361(12)
C(4)-C(5)	1.394(10)	1.411(11)	1.420(8)	1.432(10)
C(5)-C(10)	1.446(10)	1.391(12)	1.415(9)	1.441(10)
C(5)-C(6)	1.417(9)	1.404(12)	1.416(9)	1.380(10)
C(6)-C(7)	1.359(11)	1.358(11)	1.370(9)	1.388(13)
C(7)-C(8)	1.407(12)	1.414(13)	1.417(9)	1.384(13)
C(8)-C(9)	1.368(10)	1.366(12)	1.372(10)	1.368(11)
C(9)-C(10)	1.416(11)	1.446(10)	1.424(8)	1.421(10)
C(10)-C(1)	1.413(9)	1.451(11)	1.422(9)	1.420(9)
C(4)-C(11)	1.513(11)	1.511(13)	1.516(9)	1.516(11)
C(11)-C(12)	1.570(10)	1.545(12)	1.567(10)	1.517(12)
C(12)-C(6)	1.512(11)	1.513(13)	1.505(9)	1.477(12)
Peri-region bond angles				
Br(1)-C(9)-C(10)	119.7(5)	120.2(6)	120.1(5)	120.0(5)
C(1)-C(10)-C(9)	130.0(7)	127.1(8)	130.1(6)	130.8(6)
Sn(1)-C(1)-C(10)	130.7(6)	131.6(6)	128.4(4)	131.3(5)
Σ of bay angles	**380.4(10)**	**378.9(12)**	**378.6(9)**	**382.1(9)**
Splay angle[b]	20.4	18.8	18.6	22.1
C(4)-C(5)-C(6)	111.9(7)	112.4(8)	110.9(6)	111.0(7)
In and out-of-plane displacement				
Br(1)	+0.311(1)	+0.266	+0.126	-0.043
Sn(1)	+0.054(1)	-0.374(1)	-0.306	-0.053
C:(6)-(5)-(10)-(1)	179.2(7)	-175.2(6)	179.5(5)	177.4(6)
C:(4)-(5)-(10)-(9)	-176.8(8)	179.9(6)	-175.7(5)	179.4(6)

[a] van der Waals radii used for calculations: rvdW (Sn) 2.17 Å, rvdW (Br) 1.85 Å [b] Splay angle: Σ of the three bay region angles – 360.

The four ligands are arranged around the tin atom to form a tetrahedral coordination sphere; however, C-Sn-C angles in the range 101.1°-126.7°, illustrate the degree of distortion away from that of an ideal tetrahedron (109.5°). The deformation of the Sn geometry is most probably due to the steric demand of the acenaphthene/phenyl groups attached to the tin centre. The angle between

the two acenaphthenyl groups C(1)-Sn(1)-C(13) (123.8 (3)° **5**, 126.7(3)° **6**) is significantly larger than the typical 109.5°. As a result of this the other angles are reduced in size (~4-6°) compared to **1** and **2**.

Table 3.8 Bond angles [°] categorising the geometry around Sn in **5** and **6**.

Angles around the Sn atom	**5a**	**5b**	**6a**	**6b**
C(1)-Sn(1)-C(13)	123.8(3)	123.8(3)	126.7(3)	126.7(3)
C(1)-Sn(1)-C(25)	107.8(3)	107.8(3)	106.2(3)	106.2(3)
C(1)-Sn(1)-C(31)	104.2(3)	104.2(3)	-	-
C(13)-Sn(1)-C(25)	109.2(3)	109.2(3)	106.7(3)	106.7(3)
C(13)-Sn(1)-C(31)	108.5(3)	108.5(3)	-	-
C(25)-Sn(1)-C(31)	101.1(3)	101.1(3)	-	-
C(1)-Sn(1)-C(32)	-	-	106.4(3)	106.4(3)
C(13)-Sn(1)-C(32)	-	-	104.2(3)	104.2(3)
C(25)-Sn(1)-C(32)	-	-	104.9(3)	104.9(3)

The favourable *quasi*-linear arrangement can be seen in both structures, with Br(1)···Sn(1)-C-(benzyl) and Br···Sn(1)-C(phenyl) aligning along the plane and angles approaching 180° (176.0(2)° **5,** 172.1(2)° **6**), suggesting the possibility of 3c-4e type interactions.

In **6**, in addition to the H-Cg interactions, there is a weak H-bond between the hydrogen of the acenaphthene and bromine which is not seen in the **5**. This implies that the addition of the benzyl group instead of the phenyl group, allows the substituents to get close enough to make a weak H···Br bond, these non-covalent attractions can be described as 'hydrogen-bond type' interactions[3-4], these are weak interactions occurred in soft acid and soft base system. There are no significant π-π stacking interactions in either compound; when the molecules are packed the distances between the centroids exceed 3.80 Å[11], the recognised distance under which π-π stacking

is known to occur. In **5** and **6**, hydrogen atoms from both the acenaphthene and the attached phenyl rings interact with phenyl rings from neighbouring molecules in a slipped conformation.

Table 3.9 H – Cg interactions for **5** and **6**, Cg1: 6 membered C1-C2-C3-C4-C5-C10; Cg2: 6 membered C5-C6-C7-C8-C9-C10; Cg3: 6 membered C13-C14-C15-C16-C17-C22; Cg4: 6 membered C17-C18-C19-C20-C21-C22, generated in Platon.

Compound	X	H	Cg	H...Cg Distance /Å	X...Cg Distance /Å	Angle /°
	C8	H5	5	2.63	3.5250	161
5	C15	H15	6	2.60	3.3959	144
	C20	H15	6	2.88	3.7476	156
	C27	H27	4	2.81	3.5554	138
	C34	H34	4	2.71	3.5434	149
	C24	H24B	4	2.78	3.6473	146
6	C32	H32B	5	2.91	3.7272	141

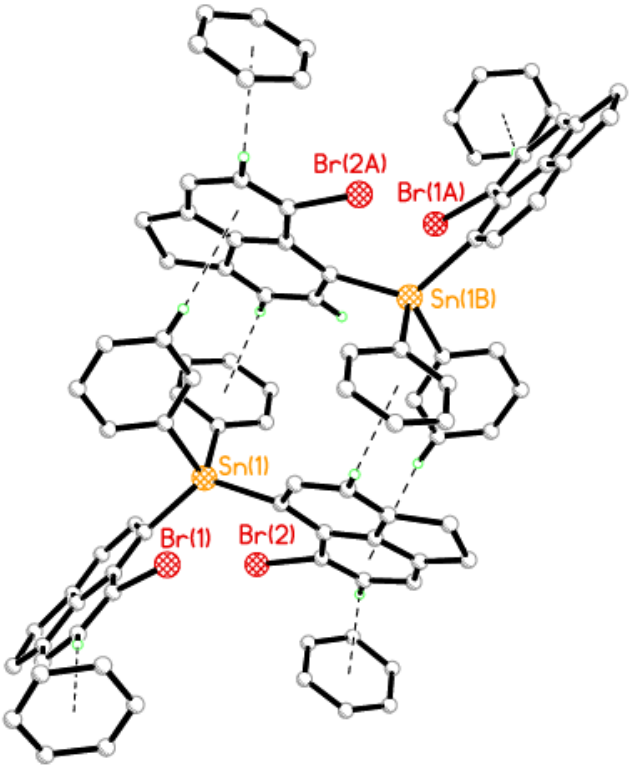

Figure 3.17 H- Centroid interactions within the structure of **5**.[12,13]

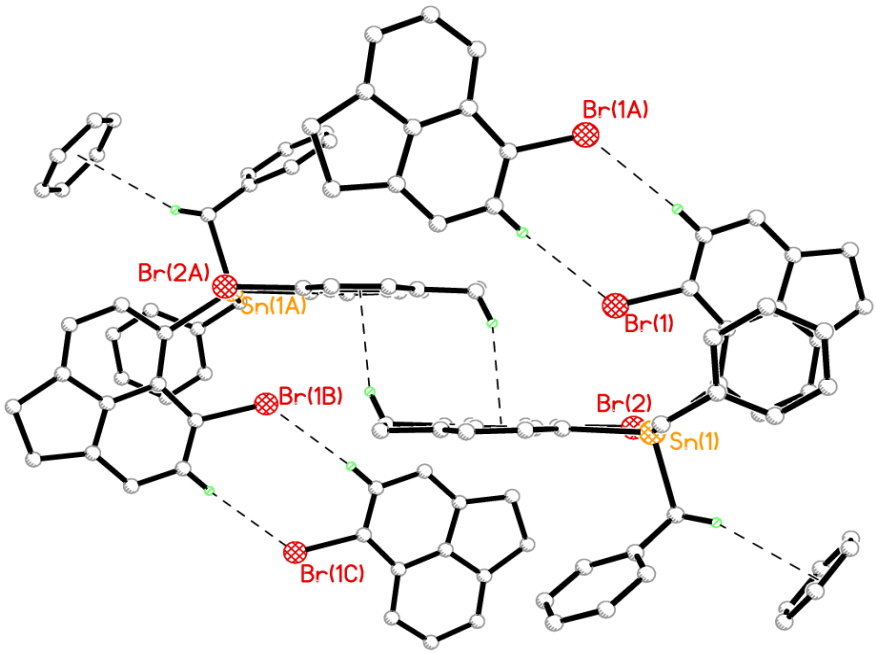

Figure 3.18 H- Centroid and donor-acceptor interactions within the structure of **6**.[12,13]

DFT calculations were performed for compounds **1**-**6** at the B3LYP/SBKJC level, chosen for its good performance during initial tests on 1,8-bis(trimethylstannyl)naphthalene.[1] In this case, the structure in the crystal was used as a starting geometry. The calculated structures and crystal structures are in good agreement.

The WBIs for **1**, **3**, **4**, **5** and **6** are in the range 0.07 to 0.09, indicating only a very minor interaction between the Sn and Br atoms, however a much larger value was observed in **2**, (0.11). This suggests the presence of the chlorine atoms on the tin centre in **2** help to strengthen the Sn···Br interaction. In fact, when an isomer of **2** containing a *trans* Br···Sn–Cl moiety is optimized with a corresponding *cis* orientation (by interchanging the Cl and one Ph substituent), the resulting minimum is 2.2 kcal/mol higher in energy.[1] On going from the *cis* isomer to the more

stable *trans* form, the Br···Sn distance decreases from 3.44 to 3.31 Å, with a corresponding increase in the WBI from 0.07 to 0.11. Therefore, a chlorine in a *trans* position strengthens the Br···Sn interaction.[1]

Conclusion

Steric strain caused by larger atoms occupying the *peri*-positions of acenaphthene, is relieved by buckling of the acenaphthene backbone and in- and out-of-plane displacements. All the compounds studied here show a significant deviation from the ideal acenaphthene structure. Compounds **1**, **4** and **5** show the greatest distortion of the acenaphthene ring, corresponding to the much bulkier *peri*-substituents.

Figure 3.19 shows all the *peri*-distances of the compounds studied in this chapter, with a noticeable increase in the *peri*-distance with bulkiness of the groups bound to the Sn atom. Compound **2** has the smallest *peri*-distance, and is much smaller than **1**. This shows that by replacing $SnPh_3$ in **1** with $SnPh_2Cl$ in **2** the bulkiness of the tin decreases, subsequently reducing the amount of steric strain, there is less repulsion, a stronger donor-acceptor interaction and thus overall a smaller *peri*-distance. A similar trend is observed in the bis-derivatives with dichloride **3** having a much smaller *peri*-distance compared to the butyl, phenyl and benzyl substituted compounds **4**-**6**.

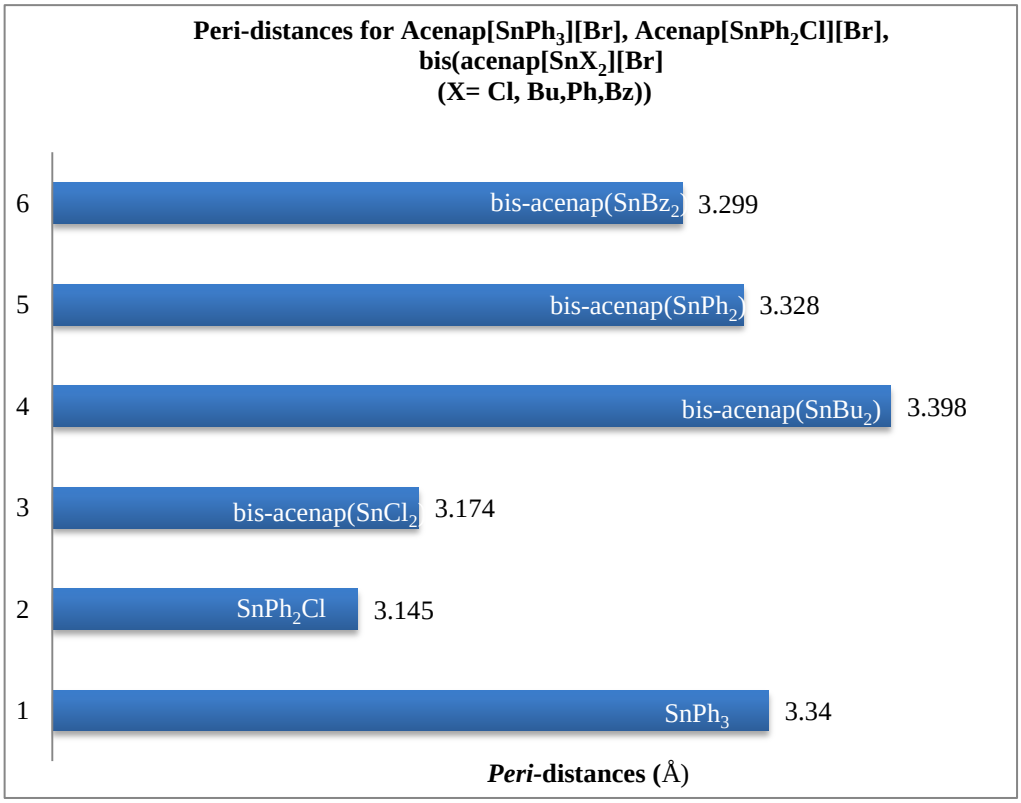

Figure 3.19 *peri*-distances for the compounds **1**-**6**.

The *quasi*-linear Br-Sn-Y three-body fragments present in the studied compounds, in which the Sn···Br *peri*-distances are within the sum of van der Waals radii (4.10 Å) and angles approach 180°, suggests the presence of weakly attractive 3c-4e type interactions. This is supported by DFT calculations with Wiberg bond indices of 0.07-0.1 calculated. According to NBA analysis, the charge on Sn atom is +2 in all compounds studied. Non-covalent interactions may thus be another significant source for the Br···Sn interactions, in addition to the contributions from the donor−acceptor interactions.[1]

Experimental

All experiments were carried out under an oxygen- and moisture-free nitrogen atmosphere using standard Schlenk techniques and glassware. Reagents were obtained from commercial sources and used as received. Dry solvents were collected from a MBraun solvent system. 5,6-Dibromoacenaphthene was prepared following standard literature procedures starting from acenaphthene.[2-4] Elemental analyses were performed by the London Metropolitan University School of Human Sciences Microanalysis Service. ^{1}H and ^{13}C NMR spectra of **2**, **3**, and **8** were recorded on a Bruker Avance 300 MHz spectrometer. ^{1}H and ^{13}C NMR spectra of **1**, **4**, **6**, and **7** were recorded on a JEOL GSX 270 MHz spectrometer. ^{119}Sn NMR spectra were recorded on a JEOL GSX 270 MHz spectrometer. δ(H) and δ(C) were referenced to external tetramethylsilane. δ(Sn) was referenced to external tetramethylstannane. Assignments of ^{13}C and ^{1}H NMR spectra were made with the help of H−H COSY and HSQC experiments, performed on a Bruker Avance 300 MHz spectrometer. All NMR shifts (δ) are given in ppm, and all couplings (J) are given in Hz.

6-bromoacenaphth-5-yl-triphenyltin (**1**):

To a solution of 5,6 dibromoacenaphthene (1.0 g, 3.2 mmol) in dry diethyl ether (30 mL) at −40 °C was added dropwise a 2.5 M solution of *n*-butyllithium in hexane (1.3 mL, 3.2 mmol) . The reaction mixture was warmed to room temperature and stirred at this temperature for 15 min after which a solution of Ph_3SnCl (1.2 g, 3.2 mmol) in diethyl ether (15 mL) was added dropwise to the reaction solution with ice cooling. The reaction mixture was then stirred overnight, the solvent removed *in vacuo*, and 40 mL of toluene was added. The solution was then filtered and the toluene removed *in vacuo*. Colourless crystals were obtained after recrystallisation from THF/hexane via the diffusion method (0.6 g, 32%); m.p. 116 °C; elemental analysis (Found: C, 61.8; H, 4.1. Calc.

for $C_{30}H_{23}BrSn$: C, 61.9; H, 4.0%); ^{1}H NMR (270 MHz, $CDCl_3$, Me_4Si): δ 7.74 (1 H, d, $^{3}J_{HH}$ = 7.2, $^{3}J_{HSn}$ = 64.4/61.0, Acenap 4-H), 7.68 (1 H, d, $^{3}J_{HH}$ = 7.2, Acenap 7-H), 7.61−7.56 (6 H, m, Sn*Ph-o*), 7.36-7.29 (9 H, m, Sn*Ph-m,p*), 7.23 (1 H, d, $^{3}J_{HH}$ = 7.4, Acenap 8-H), 7.17 (1 H, d, $^{3}J_{HH}$ = 7.2, Acenap 3-H), 3.37−3.28 (4 H, m, Acenap 2xCH_2); ^{13}C{^{1}H} NMR (67.9 MHz, $CDCl_3$, Me_4Si): δ 142.8(q), 142.5(q), 140.7(q), 137.4(s, $^{2}J_{CSn}$ = 36.4), 136.6(s, $^{2}J_{CSn}$ = 44.0), 136.4(s), 132.6(q), 130.2(q), 129.5(s), 129.0(s), 128.6(s), 128.4(s), 128.2(q), 121.1(q), 30.5(s, CH_2), 30.2(s, CH_2); ^{119}Sn{^{1}H} NMR (100.76 MHz, $CDCl_3$, Me_4Sn): δ −82.4(s).

6-bromoacenaphth-5-yl-diphenyltin chloride (**2**):

Experimental as for **1** but with 5,6-dibromoacenaphthene (1.0 g, 3.2 mmol), 2.5 M *n*-butyllithium (1.3 mL, 3.2 mmol) and Ph_2SnCl_2 (1.1 g, 3.2 mmol). Colourless crystals were obtained after recrystallisation from DCM/hexane via the diffusion method (0.4 g, 23%); m.p. 132 °C; elemental analysis (Found: C, 53.5; H, 3.4. Calc. for $C_{24}H_{18}BrClSn$: C, 53.3; H, 3.4%); ^{1}H NMR (300 MHz, $CDCl_3$, Me_4Si): δ 8.62 (1 H, d, $^{3}J_{HH}$ = 7.1, $^{3}J_{HSn}$ = 73.9/70.6, Acenap 4-H), 7.69−7.66 (4 H, m, Sn*Ph-o*), 7.60 (1 H, d, $^{3}J_{HH}$ = 7.0, Acenap 7-H), 7.47 (1 H, d, $^{3}J_{HH}$ = 7.1, Acenap 3-H), 7.34−7.29 (6 H, m, Sn*Ph-m,p*), 7.14 (1 H, d, $^{3}J_{HH}$ = 7.0, Acenap 8-H), 3.45−3.29 (4 H, m, Acenap 2xCH_2); ^{13}C{^{1}H} NMR (75.5 MHz, $CDCl_3$, Me_4Si): δ 150.1(q), 148.4(q), 147.5(s), 143.2(s), 141.7(q), 136.5(s), 136.3(s), 132.0(q), 130.1(s), 129.2(s), 121.7(q), 121.4(s), 121.1(q), 114.8(q), 30.9(s, CH_2), 30.3(s, CH_2); ^{119}Sn{^{1}H} NMR (100.76 MHz, $CDCl_3$, Me_4Sn): δ −70.3(s).

Bis(6-bromoacenaphth-5-yl) tin dichloride (**3**):

To a solution of 5,6-dibromoacenaphthene (3.0 g, 9.6 mmol) in dry diethyl ether (30 mL) at −40 °C was added dropwise a 2.5 M solution of *n*-butyllithium in hexane (3.9 mL, 9.6 mmol) . The reaction mixture was warmed to room temperature and stirred at this temperature for 15 min after

which $SnCl_4$ (2.45 g, 4.8 mmol) was added dropwise to the reaction solution with ice cooling. The reaction mixture was then stirred overnight, the solvent removed *in vacuo*, and 40 mL of toluene was added. The solution was then filtered and half of the solvent was removed. The product crystallised as small gray needles at −30 °C (1.1 g, 35%); m.p. >250 °C; elemental analysis (Found: C, 44.1; H, 2.5. Calc. for $C_{24}H_{16}Br_2SnCl_2$: C, 43.8; H, 2.3%); ^{1}H NMR (270 MHz, $CDCl_3$, Me_4Si): δ 8.68 (2 H, d, $^3J_{HH}$ = 7.3, $^3J_{HSn}$ = 109.6/104.9, Acenap 2x4-H), 7.64 (2 H, d, $^3J_{HH}$ = 7.3, Acenap 2x7-H), 7.54 (2 H, d, $^3J_{HH}$ = 7.7, Acenap 2x3-H), 7.23 (2 H, d, $^3J_{HH}$ = 7.3, Acenap 2x8-H), 3.54−3.34 (8 H, m, Acenap 4xCH_2); ^{13}C{^{1}H} NMR (67.9 MHz, $CDCl_3$, Me_4Si): δ 150.3 (q, $^1J_{CSn}$ = 19.7), 147.9(q), 137.8(s, $^2J_{CSn}$ = 45.6), 137.7(q), 131.9(s), 131.3(q), 126.2(s), 121.2(s, $^3J_{CSn}$ = 103.9), 121.1(s), 118.2(q), 30.5(s, *C*H_2), 30.0 (s, *C*H_2); ^{119}Sn{^{1}H} NMR (100.76 MHz, $CDCl_3$, Me_4Sn): δ −132.2(s).

Bis(6-bromoacenaphth-5-yl)dibutyltin (4):

Experimental as for **1** but with 5,6-dibromoacenaphthene (2g , 6.4 mmol), 2.5 M *n*-butyllithium (2.6 mL, 6.4 mmol and Bu_2SnCl_2 (1.1 g, 3.2 mmol). Colourless crystals were obtained after recrystallisation from THF at −30 °C (0.14 g, 13%) m.p. 114 °C; elemental analysis (Found: C, 55.2; H, 4.9. Calc. for $C_{32}H_{34}Br_2Sn$: C, 55.1; H, 4.9%); ^{1}H NMR (270 MHz, $CDCl_3$, Me_4Si): δ 8.12 (2 H, d, $^3J_{HH}$ = 7.0, $^3J_{HSn}$ = 69.5/66.4, Acenap 2x4-H), 7.68 (2 H, d, $^3J_{HH}$ = 7.3, Acenap 2x7-H), 7.30 (2 H, d, $^3J_{HH}$ = 7.0, Acenap 2x3-H), 7.23 (2 H, d, $^3J_{HH}$ = 6.3, Acenap 2x8-H), 3.45−3.25 (8 H, m, Acenap 4xCH_2), 1.56 (4 H, t, $^3J_{HH}$ = 6.9, 2xCH_2-α), 1.50−1.39 (4 H, m, 2xCH_2-β), 1.32 (4 H, quin, $^3J_{HH}$ = 7.1, 2xCH_2-γ), 0.77 (6 H, t, $^3J_{HH}$ = 7.3, 2xCH_3-δ); ^{13}C{^{1}H} NMR (67.9 MHz, $CDCl_3$, Me_4Si): δ 141.2(q), 140.3(s, $^2J_{CSn}$ = 33.1), 139.6(q), 135.6(q), 132.0(s), 131.0(q), 129.2(q), 121.8(q), 120.4(s), 119.9(s, $^3J_{CSn}$ = 29.0), 30.3(s, Acenap 2x*C*H_2), 29.8 (s, Acenap 2x*C*H_2), 29.5(s,

$^{2}J_{CSn}$ = 17.7, 2x*C*H_2-*β*), 27.4(s, $^{1}J_{CSn}$ = 73.2, 2x*C*H_2-*α*), 19.6(s, *C*H_2-*γ*), 13.6(s, *C*H_3-*δ*); ^{119}Sn{^{1}H} NMR (100.76 MHz, $CDCl_3$, Me_4Sn): *δ* −31.4(s).

Bis(6-bromoacenaphth-5-yl)diphenyltin (5):

Experimental as for **1** but with 5,6-dibromoacenaphthene (2.0 g, 6.4 mmol), 2.5 M *n*-butyllithium (2.6 mL, 6.4 mmol) and Ph_2SnCl_2 (1.1 g, 3.2 mmol). (Analysis of the residue revealed the presence of unreacted 5,6-dibromoacenaphthene, but increased reaction time did not improve the yield.) The crude solid was recrystallised from THF (0.23 g, 10%); m.p. 168−170 °C; elemental analysis (Found: C, 58.8; H, 3.7. Calc. for $C_{36}H_{26}Br_2Sn$: C, 58.7; H, 3.6%); ^{1}H NMR (300 MHz, $CDCl_3$, Me_4Si): *δ* 7.88 (2 H, d, $^{3}J_{HH}$ = 6.9, $^{3}J_{HSn}$ = 66.8/63.9, Acenap 2x4-H), 7.57 (2 H, d, $^{3}J_{HH}$ = 7.2, Acenap 2x7-H), 7.55−7.48 (4 H, m, Sn*Ph-o*), 7.30−7.18 (6 H, m, Sn*Ph-m,p*), 7.16 (2 H, d, $^{3}J_{HH}$ = 7.2, Acenap 2x3-H), 7.07 (2 H, d, $^{3}J_{HH}$ = 7.8, Acenap 2x8-H), 3.38−3.23 (8 H, m, 4xCH_2); ^{13}C{^{1}H} NMR (75.5 MHz, $CDCl_3$, Me_4Si): *δ* 148.1(q), 147.6(q), 145.7(q), 143.2(q), 140.8(q), 138.7(s), 137.6(s), 132.5(s), 128.9(s), 128.7(s), 128.4(s), 121.1(q), 120.6(s), 120.2(q), 30.7(s, *C*H_2), 30.2(s, *C*H_2); ^{119}Sn{^{1}H} NMR (100.76 MHz, $CDCl_3$, Me_4Sn): *δ* −116(s).

Bis(6-bromoacenaphth-5-yl)dibenzyltin (6):

Experimental as for **1** but with 5,6-dibromoacenaphthene (2.0 g, 6.4 mmol), 2.5 M *n*-butyllithium (2.6 mL, 6.4 mmol) and $SnPh_2Cl_2$ (1.1 g, 3.2 mmol). Colourless crystals were obtained after recrystallisation out of DCM/hexane via the diffusion method (1.1 g, 56%); m.p. 149 °C; elemental analysis (analysis (Found: C, 59.6; H, 4.1. Calc. for $C_{38}H_{30}Br_2Sn$: C, 59.6; H, 4.0%); ^{1}H NMR (270 MHz, $CDCl_3$, Me_4Si): *δ* 7.79 (2 H, d, $^{3}J_{HH}$ = 7.8, Acenap 2x4-H), 7.72 (2 H, d, $^{3}J_{HH}$ = 7.5, Acenap 2x7-H), 7.58 (2 H, d, $^{3}J_{HH}$ = 7.1, Acenap 2x8-H), 7.51 (2 H, d, $^{3}J_{HH}$ = 7.1, Acenap 2x3-H), 7.21−6.72 (10 H, m, $SnCH_2$*Ph*), 3.33−319 (8 H, m, 4xCH_2), 2.94 (4 H, s, 2xSnCH_2Ph);

$^{13}C\{^{1}H\}$ NMR (67.9 MHz, $CDCl_3$, Me_4Si): δ 147.2(q), 147.1(q), 139.2(s), 135.9(q), 135.0(q), 132.1(q), 131.8(s), 128.3(s), 128.0(s), 127.9(q), 123.3(s), 121.0(q), 120.7(s), 120.2(s), 30.3(s, Acenap 2x*C*H_2), 30.1(s, Acenap 2x*C*H_2), 29.7(s, 2xSn*C*H_2Ph).

X-ray Structure Analysis

X-ray crystal structures for **5** and **6** were determined at −148(1) °C on the St Andrews Robotic Diffractometer,[14] a Rigaku ACTOR-SM, Saturn 724 CCD area detector with graphite-monochromated Mo Kα radiation (λ = 0.710 73 Å). Data for compound **4** was collected at −180(1) °C by using a Rigaku MM007 high brilliance RA generator (Mo Kα radiation, confocal optic) and Mercury CCD system. Data for compounds **1**, **2 5** were collected at −148(1) °C on a Rigaku SCX Mini instrument with graphite-monochromated Mo Kα radiation (λ = 0.710 73 Å). All data had intensities corrected for Lorentz, polarization, and absorption. The data for the complexes was collected and processed using CrystalClear[15,16] (Rigaku). The structures were solved by Patterson or direct methods and expanded using Fourier techniques. Non-hydrogen atoms were refined anisotropically, and hydrogen atoms were refined using a riding model. All calculations were performed using CrystalStructure[17] and SHELXL-97.[18]

References

1. M.-L. Lechner, K. S. Athukorala Arachchige, R. A. M. Randall, F. R. Knight, M. Bühl, A. M. Z. Slawin and J. D. Woollins, *Organometallics*, 2012, **31**, 2922.

2. F. R. Knight, K. S. Athukorala Arachchige, R. A. M. Randall, M. Bühl, A. M. Z. Slawin and J. D. Woollins, *Dalton Trans.*, 2012, **41**, 3154.

3. F. R. Knight, R. A. M. Randall, K. S. Athukorala Arachchige, L. Wakefield, J. M. Griffin, S. E. Ashbrook, M. Bühl, A. M. Z. Slawin and J. D. Woollins, *Inorg. Chem.*, 2012, **51**, 11087.

4. L. K. Aschenbach, F. R. Knight, R. A. M. Randall, D. B. Cordes, A. Baggott, M. Bühl, A. M. Z. Slawin and J. D. Woollins, *Dalton Trans*., 2012, **41**, 3141.

5. P. Wawrzyniak, A. M. Z. Slawin, J. D. Woollins and P. Kilian, *Dalton Trans*., 2010, **39**, 85.

6. N. Meyer, S. Sivanathan and F. Mohr, *J. Organomet. Chem*., 2011, **696**, 1244.

7. R. Schroeck, K. Angermaier, A. Sladek and H. Schmidbaur, *Organometallics*, 1994, **13**, 3399.

8. F. H. Carre, R. J. P. Corriu, G. F. Lanneau and Y. Zhifang, *Organometallics*, 1991, **5**, 1237.

9. J. T. B. H. Jastrzebski, J. Boersma, P. M. Esch and G. van Koten, *Organometallics*, 1991, **10**, 930.

10. J. Beckmann, J. Bolsinger and A. Duthie, *Chem. Eur. J.*, 2011, **17**, 930.

11 A. L. Fuller, "*Synthesis and Structural studies of group 16 peri-substituted naphthalenes and related compounds*", Ph.D. Thesis, University of St Andrews, 2010.

12. A. L. Spek, *J. Appl. Cryst.*, 2003**, 36**, 7.

13. A. L. Spek, *Acta Crystallogr. Sect. D*, 2009**, 65**, 148.

14. A. L. Fuller, L. A. S. Scott-Hayward, Y. Li, M. Bühl, A. M. Z. Slawin and J. D. Woollins, *J. Am. Chem. Soc.*, 2010, **132**, 5799.

15. CrystalClear 2.0; Rigaku Corp., Tokyo, 2010. *CrystalClear Software User's Guide; Molecular Structure Corp.*: The Woodlands, TX, 2011.

16. J. W. P. Flugrath, *Acta Crystallogr., Sect. D*, 1999, **D55**, 1718.

17. CrystalStructure 4.0: *Crystal Structure Analysis Package; Rigaku and Rigaku/MSC*, The Woodlands, TX 77381, 200.

18. G. M. Sheldrick, *SHELX97, Acta Crystallogr., Sect. A: Fundam. Crystallogr*., 2008, **64**, 11.

Chapter 4

Synthetic and structural studies of sterically crowded tin-chalcogen acenaphthenes

Introduction

Peri-substituted naphthalenes and acenaphthenes with heavy atoms positioned at distances shorter than the sum of their van der Waals radii have attracted much attention in the past. These systems suffer considerable steric compression due to weak interactions, which are a result of overlapping orbitals.[1-3] Such non-covalent systems can be achieved by incorporating large heteroatoms of groups 14, 16 and 17 at the *peri*- positions.[2.3] During their extensive study of weak intramolecular interactions in sterically hindered mixed phosphorus-chalcogen[1] and chalcogen-chalcogen[3,4] systems, the Woollins group have illustrated that positioning heavy atoms in close proximity at the 5,6-positions in acenaphthene causes considerable steric strain enabling acenaphthene distortion and non-covalent *peri*-atom interactions to be studied.

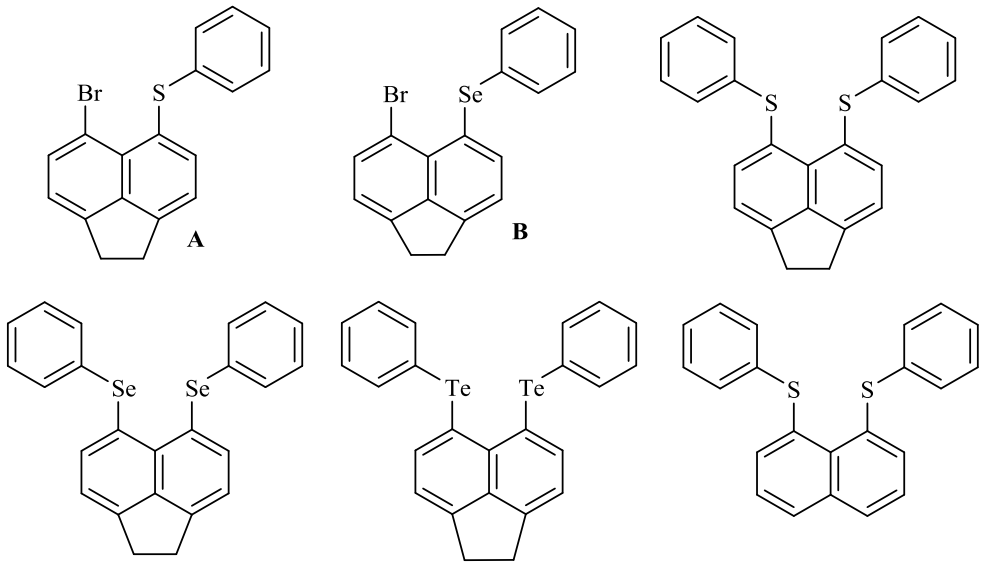

Figure 4.1 Line drawings of mixed chalcogen-chacogen and chalcogen-halogen acenaphthene and naphthalene compounds.[3,4]

Unlike chalcogen-halogen, chalcogen-chalcogen and chalcogen-phosphorous compounds, chalcogen–tin *peri*-substituted acenaphthenes have received limited attention in the literature. The synthesis of such systems might be considered extremely difficult due to their steric congestion.

This Chapter focuses on the synthesis and comprehensive structural analysis of four series of novel *peri*-substituted tin-chalcogen acenaphthenes containing heteronuclear tin-chalcogen moieties at the 5,6-positions in **7-9,** Acenap[$SnPh_3$][EPh] (E = S, Se, Te), **10-11** Acenap[$SnPh_2Cl$][EPh] (E = S, Se), **12-13,** bis Acenap[SnX_2][SPh] (X=Cl,Ph), and **14-15,** Acenap[$SnBu_2Cl$][EPh] (E = S, Se). In addition, the synthesis and structural study of 5-bromo-6-(ethylsulfanyl)acenaphthene (**16**), which was used as a precursor for preparing **17-18,** Acenap[SnX][SEt] (X=Bu_2Cl,Ph_3), is also discussed. The molecular structures of acenaphthenes **7-15** are compared with previously reported chalcogen substituted acenaphthene compounds[3] and **16** is compared with the analogous naphthalene compound.[5]

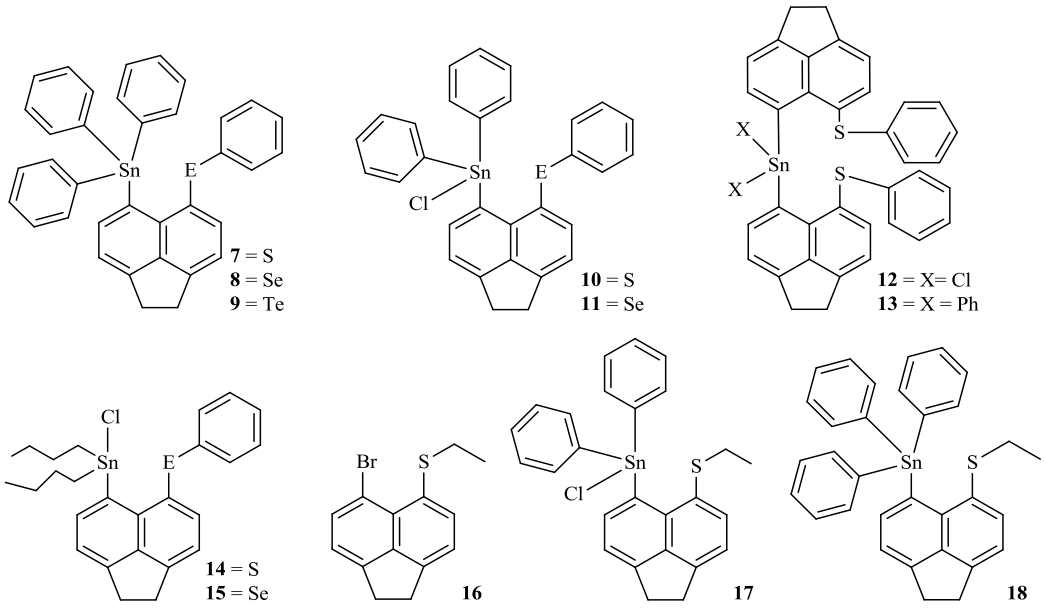

Figure 4.2 Compounds **7-18**, which will be discussed in this chapter.

Section 1

Synthetic and Structural Study of 5-(triphenylstannyl)-6-(phenylchalcogeno) acenaphthenes

Synthesis

Initially, 5-bromo-6-(phenylchalcogeno)acenaphthenes, **Acenap[$SnPh_3$][EPh] (E = S, Se),** were prepared following previously reported literature procedures.[3] These two analogous compounds were then individually treated with a single equivalent of *n*-butyllithium in diethyl ether to afford the respective 5-lithio-6-(phenylchalcogeno)acenaphthene precursor, which when treated with $SnPh_3Cl$ consequently affording **7** and **8** [yield: 39% (**7**), 44% (**8**); Scheme 4.1]. However, conversion to the 5-lithio-6-(phenyltelluro)acenaphthene was unsuccessful which may indicate that the Te-C_{Acenap} bond is more susceptible towards *n*-butyllithium as was reported previously in the chalcogen-chalgogen study.[3,4] In order to prepare **9**, 5-bromo-6-(triphenylstannyl)acenaphthene[6] was synthesised and then treated sequentially with a single equivalent of *n*-butyllithium followed by diphenyl ditelluride (yield:66%: Scheme 4.2).

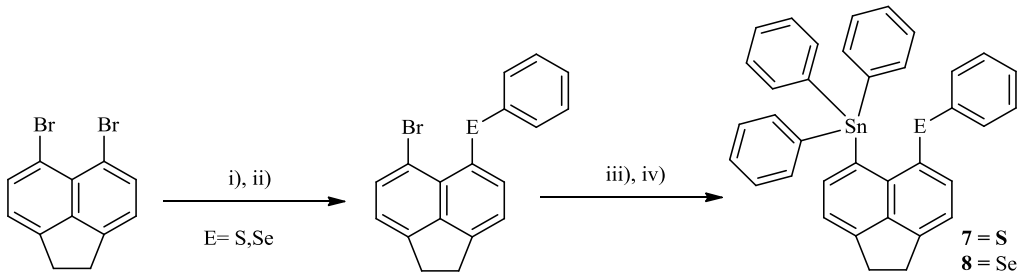

Scheme **4.1** The preparation of 5-(triphenylstannyl)-6-(phenylchalcogeno)acenaphthenes **7** and **8** from 5,6-dibromoacenaphthene. Conditions: i) *n*BuLi (1 equiv), Et_2O, -78 ºC, 1 h; ii) PhEEPh (1 equiv; E = S, Se), Et_2O, -78 ºC, 1 h. iii) *n*BuLi (1 equiv), Et_2O, -78 ºC, 1 h; iv) $SnPh_3Cl$ (1 equiv), Et_2O, -78 ºC, 1 h.

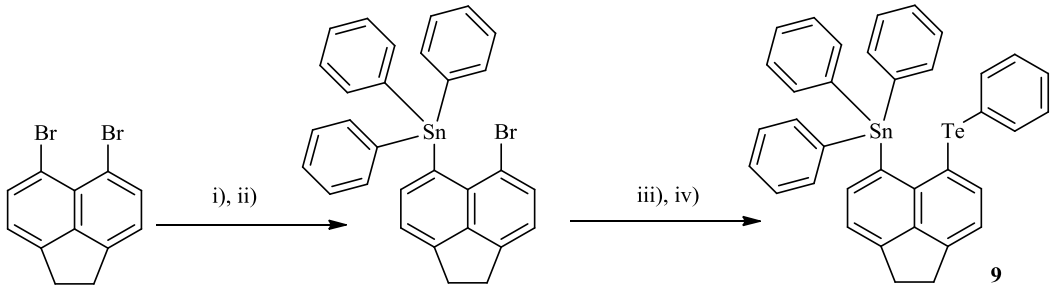

Scheme **4.2** The preparation of 5-(triphenylstannyl)-6-(phenyltelluro)acenaphthene **9** from 5,6-dibromoacenaphthene. Conditions: i) *n*BuLi (1 equiv), Et_2O, -78 ºC, 1 h; ii) $SnPh_3Cl$ (1 equiv), Et_2O, -78 ºC, 1 h. iii) *n*BuLi (1 equiv), Et_2O, -78 ºC, 1 h; iv) PhTeTePh (1 equiv), Et_2O, -78 ºC, 1 h.

Compounds **7**, **8** and **9** were characterised by multinuclear NMR spectroscopy and the homogeneity of the new compounds was, where possible, confirmed by microanalysis and mass spectrometry.

X ray investigations

Suitable single crystals were obtained for **7**, **8** and **9** by diffusion of hexane into a saturated solution of the compound in tetrahydrofuran (THF). All three compounds crystallise in the $P2_1/n$ space group (R1 = 4.69 (**7**), 4.57 (**8**), 4.54% (**9**)), with one molecule in the asymmetric unit (Figures 4.3, 4.4, 4.5). Selected interatomic distances, angles and torsion angles are listed in Table 4.2, further refinement data for **7**-**9** can be found in Appendix 3.

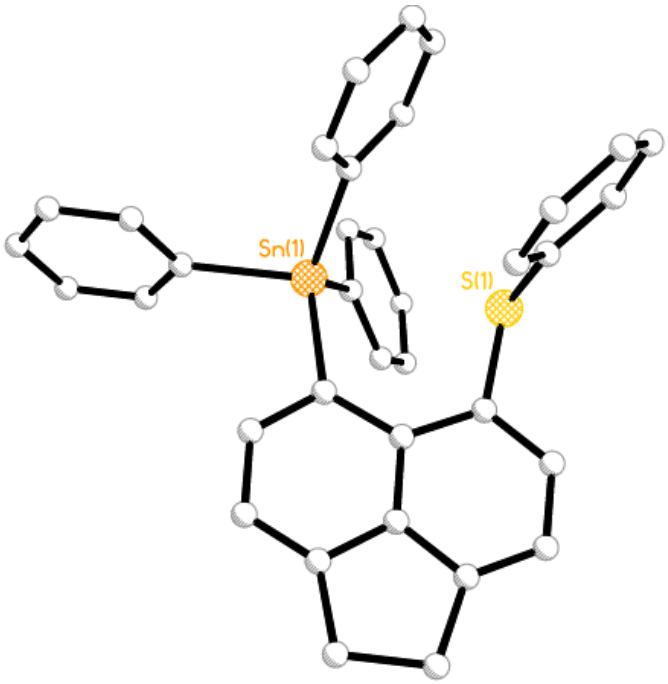

Figure 4.3 The crystal structure of *5-(phenylsulfanyl)-6-(triphenylstannyl)acenaphthene* **7** (hydrogen atoms omitted for clarity).

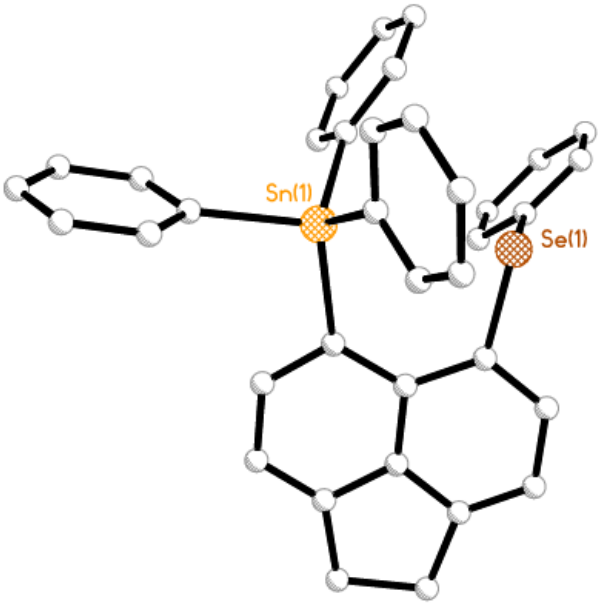

Figure 4.4 The crystal structure of *5-(phenylselanyl)-6-(triphenylstannyl)acenaphthene* **8** (hydrogen atoms omitted for clarity).

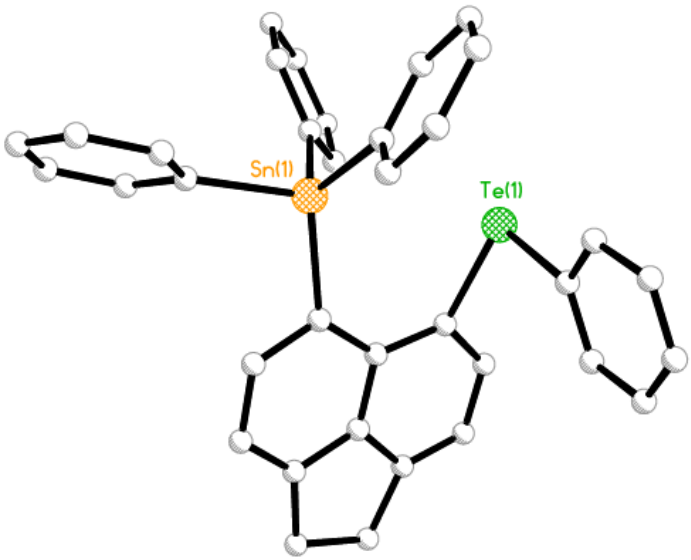

Figure 4.5 The crystal structure of *5-(phenyltelluro)-6-(triphenylstannyl)acenaphthene* **9** (hydrogen atoms omitted for clarity).

The structural similarities and differences in **7-9** can be demonstrated by comparing parameters such as the *peri*-distance, in-plane and out-of-plane deflections of the *peri*-substituents, torsion angles associated with buckling of the acenaphthene ring, the geometry around the Sn atom, the configuration adopted by the acenaphthene backbone and the intermolecular packing and interactions.

Deformation of the acenaphthene backbone in **7-9** involves further widening of the C1-C10-C9 bay angle (mean 131° compared with ideal 127°) [3,7]. The increased splay of the C1-C10-C9 angle does not greatly affect the bond length between C11-C12 (Table 4.2). Instead the central C5-C10 bond elongated from 1.41 Å[3], to an average of 1.43 Å, although the existence of the ethylene bridge ensures the C4-C5-C6 bond angle remains close to optimal (average 111.7° compared with

the ideal 111.3°)[3] and the remaining bonds in the acenaphthene backbone (average length 1.41 Å and 1.42 Å) retain their ideal length (average 1.418 Å and 1.423 Å)[3]. Additional separation is achieved by twisting in the acenaphthene ring by up to 4° as illustrated by torsion angles associated with the central C5-C10 bond (see Table 4.2).

The bond stretching and angle widening of the acenaphthene skeleton is insufficient to completely ease the "*peri*-space crowding"[3], so further distortion of the exocyclic *peri*-bonds is required in order to accommodate the large Sn and E *peri*-substituents. This distortion is accompanied by, in-plane distortion of the substituents that can be calculated by *peri*-region angles (splay angle). In the 'ideal' acenaphthene this would be 360°,[3] if the sum of the bay region angle is larger than this value it means the exocyclic bonds have moved away from each other due to repulsion or if sum of the splay angles decreases, then substituents reside closer to each other suggesting weak interaction between *peri*-atoms.[7]

Similarly, out-of-plane deviation can be measured from the distances of *peri*-atoms lie above and below the acenaphthene plane; in the 'ideal' situation the two hydrogen atoms on the *peri*-positions reside in the plane of the acenaphthene.[3] Thus, *peri*-distance increases as the size of the substituent increases but nevertheless are still shorter than the sum of vdWs. In all three compounds the $SnPh_3$ and EPh groups are located in close proximity to each other, with non-bonded Sn---E *peri*-distances increasing from 3.2710(19) Å in **7**, to 3.341(6) Å in **8** to 3.49(12) Å in **9**, correlating with the increasing size of the substituents, in respect to the van der Waals radii of (E). A similar trend is observed in the series of dichalcogen acenaphthenes, in which the *peri*-gap similarly elongates as a smaller congener is replaced by a larger member [**S-S** 3.274(4) Å, **Te-Te** 3.3674(19) Å][3].

Throughout the series, the chalcogen and tin atom lies in the *peri*-region pointing away from the acenaphthene plane to obtain a relaxed geometry. Minor out-of-plane displacement of the *peri*-substituents occurs in **7-9** (Figure 4.6, Table 4.2). However in all three compounds, the substituents reside on opposite sides of the acenaphthene plane. The largest distortions occur in **9**, in which the atoms sit at 0.4565 Å and -0.4676 Å above and below the mean plan, respectively.

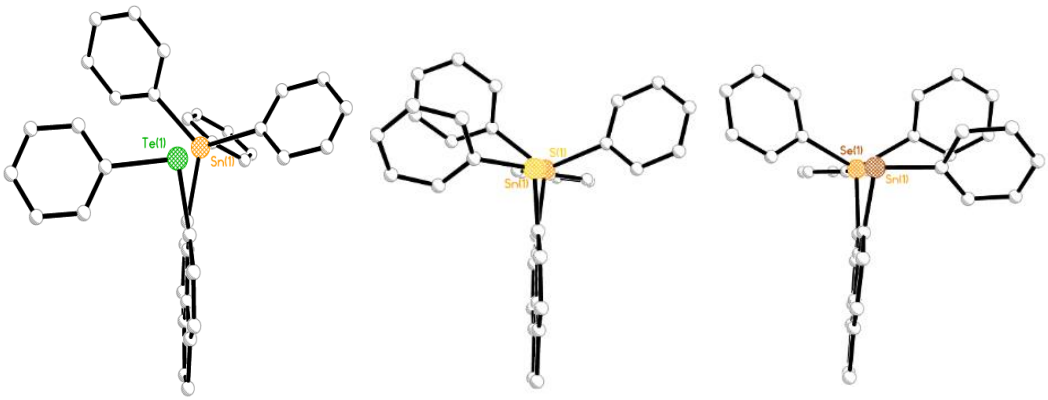

Figure 4.6 The structures **7-9** showing the planarity of the acenaphthene backbone.

As might be expected, the E1-C9 bond length increases as the size of E increases (Table 4.2). The C9-S1-C31 angle of 102.6(3)° also appears considerably larger than the that found in 5-bromo-6-(phenylsulfanyl)acenaphthene (C-S-C angle 94.8°),[3] due to the increased bulkiness of the tin ligand occupying one of the *peri*-positions.

For each of the compounds **7, 8** and **9** the bond angles within the tin coordination sphere slightly deviate from the expected tetrahedral angle of 109.5 ° (see Table 4.1), due to the steric demand of the phenyl groups. The angle between the two phenyl groups facing the bromine is widened to 121.1(3)° in **9**. Consequently the angles between the other phenyl groups are to some extent

smaller than the average tetrahedral angle ranging from 100.9° to 115.37(17)°. In **8** and **9** the largest tetrahedral angles are 115.37° and 111.44 ° respectively, resulting in a similar distorted tetrahedral geometry to that seen in **7**.

Table 4.1 Bond angles [°] categorising the geometry around Sn in **7-9.**

Angles around the Sn atom	**7**	**8**	**9**
C(1)-Sn(1)-C(13)	104.45(18)	105.2(2)	110.1(3)
C(1)-Sn(1)-C(25)	111.48(18)	115.1(2)	121.1(3)
C(13)-Sn(1)-C(25)	105.13(18)	104.0(2)	113.6(3)
C(1)-Sn(1)-C(19)	115.37(17)	111.4(2)	105.2(3)
C(13)-Sn(1)-C(19)	104.93(18)	104.2(2)	100.9(3)
C(19)-Sn(1)-C(25)	114.17(18)	115.4(2)	103.2(3)

Table 4.2 Selected bond lengths (Å) and angles (°) for **7 to 9.**

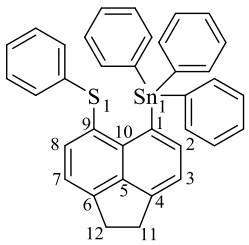

7

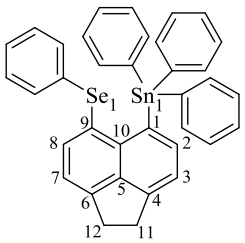

8

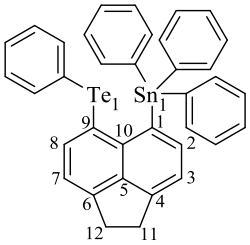

9

Peri-region-distances			
E(1)···Sn(1)	**3.27**	**3.341**	**3.49**
Σr_{vdW} - S···Sn[a]	0.70	0.73	0.74
$\%r_{vdW}$[a]	82	82	83
E(1)-C(9)	1.792(5)	1.932(6)	2.106(6)
Sn(1)-C(1)	2.156(5)	2.171(6)	2.166(5)
Acenaphthene bond lengths			
C(1)-C(2)	1.384(7)	1.394(8)	1.384(9)
C(2)-C(3)	1.418(7)	1.409(8)	1.411(8)
C(3)-C(4)	1.368(7)	1.368(8)	1.355(9)
C(4)-C(5)	1.418(7)	1.414(8)	1.389(9)
C(5)-C(10)	1.430(7)	1.422(8)	1.437(8)

C(5)-C(6)	1.403(7)	1.405(8)	1.422(8)
C(6)-C(7)	1.373(7)	1.369(8)	1.359(11)
C(7)-C(8)	1.407(7)	1.424(8)	1.403(9)
C(8)-C(9)	1.387(7)	1.391(8)	1.382(9)
C(9)-C(10)	1.426(7)	1.423(8)	1.424(9)
C(10)-C(1)	1.454(7)	1.440(8)	1.435(8)
C(4)-C(11)	1.515(7)	1.516(8)	1.520(8)
C(11)-C(12)	1.561(8)	1.569(9)	1.531(11)
C(12)-C(6)	1.529(7)	1.526(8)	1.498(9)
***Peri*-region bond angles**			
S(1)-C(9)-C(10)	121.7(4)	123.2(4)	122.9(4)
C(1)-C(10)-C(9)	129.0(4)	128.8(5)	129.9(5)
Sn(1)-C(1)-C(10)	127.0(4)	128.1(4)	127.9(5)
Σ of bay angles	**377.7**	**380.1**	**380.7**
Splay angle[b]	17.7	20.1	20.7
C(4)-C(5)-C(6)	111.9(5)	112.0(5)	112.2(5)
Out-of-plane displacement			
E(1)	0.1847	0.1990	-0.4676
Sn(1)	-0.2867	-0.2499	0.4565
C:(6)-(5)-(10)-(1)	-179.1	-179.0	-175.61
C:(4)-(5)-(10)-(9)	-176.4	-177.4	-177.92

[a] van der Waals radii used for calculations: rvdW(S) 1.80 Å, rvdW(Se) 1.90 Å, rvdW(Sn) 2.17 Å , rvdW(Te) 2.06 Å **[b]** Splay angle: Σ of the three bay region angles – 360.

In addition to the distortions associated with the acenaphthene backbone, the molecular geometry of **7**-**9** is also affected by the location and orientation of the phenyl groups bound to the *peri*-atoms with respect to the mean acenaphthene plane. The conformation of the molecule can be categorised from torsion angles (θ) which describe the orientation of the acenaphthene backbone with respect to the C(Ph)-Sn-C(Acenap) and C(Ph)-E-C(Acenap) planes, respectively.[2-5] When the dihedral angle approaches 90°, the orientation is denoted axial and when the angle shows a *quasi*-linear arrangement (close to 180°), they are named as equatorial.[2-5]

When the E–C_{Ph} bond is arranged perpendicular to the mean acenaphthene plane with an axial conformation the structure is defined as a type A,[2-5] whereas for equatorial angles of θ (~180°), the E–C_{Ph} bond is located on or close to the acenaphthene plane, and the conformation is denoted as type B.[2-5] When θ lies in between the values of equatorial and axial (~135°), the structure is called twist and relates to type C.[2-5]

From the classification system reported by Nakanishi *et al*.,[9] derivatives **7**-**9** are seen to adopt similar conformations which can be described as ABC-A (Figure 4.7). In all three compounds, one Sn-C_{ph} bond aligns along the acenaphthene mean plane (type B), affording a *quasi*-linear C_{Ph}-Sn···E arrangement in which angles approach 180° (**7** 170.9(3)°, **8** 170.3(4)°, **9** 162.5(5)°), while one C_{Ph}-Sn bond is arranged perpendicular to the acenaphthene backbone (type A) and the other C_{Ph}-Sn bond lies between an axial and equatorial conformation (type C). In all three structures the E-C_{Ph} bond occupies a position perpendicular to the acenaphthene skeleton giving rise to a type A conformation.

The *quasi*-linear alignment of the C_{Ph}-Sn···E three-body fragments in **7**-**9** provides a suitable geometry to promote delocalization of a chalcogen lone-pair (E) to an anti-bonding σ*(Sn−C) orbital, thus a weakly attractive 3c-4e type interaction leading to a decrease in the *peri*-distance.[2-5]

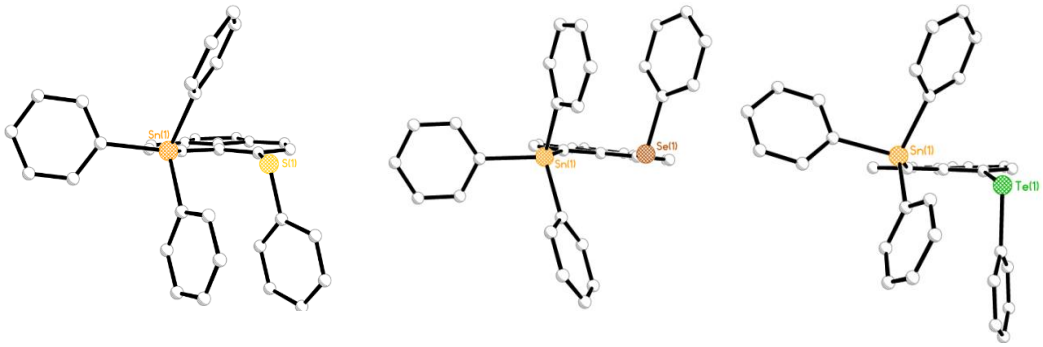

Figure 4.7 The molecular configurations of **7**-**9** showing the orientation of the substituents bound to Sn and P; all three compounds adopt similar ABC-A type conformations.

Table 4.3 Torsion angles [°] categorizing the acenaphthene and ligand conformations in **7**-**9**.

	7	**8**	**9**
C(10)-C(1)-Sn(1) C(13)	Ph: θ_1 170.9(3) equatorial-B	Ph: θ_1 -170.3(4) equatorial-B	Ph: θ_1 53.5(5) twist-C
C(10)-C(1)-Sn(1)-C(19)	Ph: θ_2 -74.5(4) axial-A	Ph: θ_2 -58.0(5) twist-C	Ph: θ1 161.5(5) equatorial-B
C(10)-C(1)-Sn(1)-C(25)	Ph: θ_3 57.8(4) twist-C	Ph: θ_3 75.8(5) axial-A	Ph: θ_3 -82.4(5) axial-A
C(10)-C(9)-E(1)-C(31)	Ph: $\theta_4$101.5(4) axial-A	Ph: θ_4-98.0(4) axial-A	Ph: θ_4 85.3(5) axial-A

The arrangement of the phenyl groups around the *peri*-substituents may be influential in the packing of the molecules and the intermolecular interactions seen within the crystal. In **7** and **8** the hydrogen atoms from both the acenaphthene and the attached phenyl rings interact with centroids of further phenyl rings from different molecules. In **7** and **8** the H atoms of C11 and C12 interact with the centroids of a separate molecule. Due to the orientation of the second molecule the C11

and C12 H atoms can interact with the centroids of the first molecule resulting in a back interaction (Figure 4.8 and 4.9). However there is no C12-H···centroid (Cg) interaction seen in a similar analogue substituted with Br **(1)**.

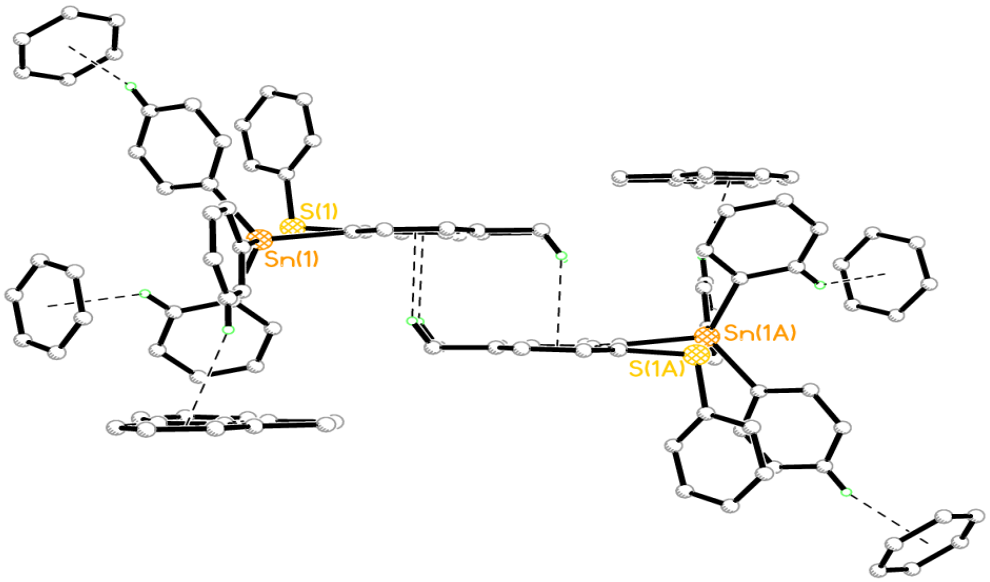

Figure 4.8 H- Centroid interactions within the structure of **7**.[10,11]

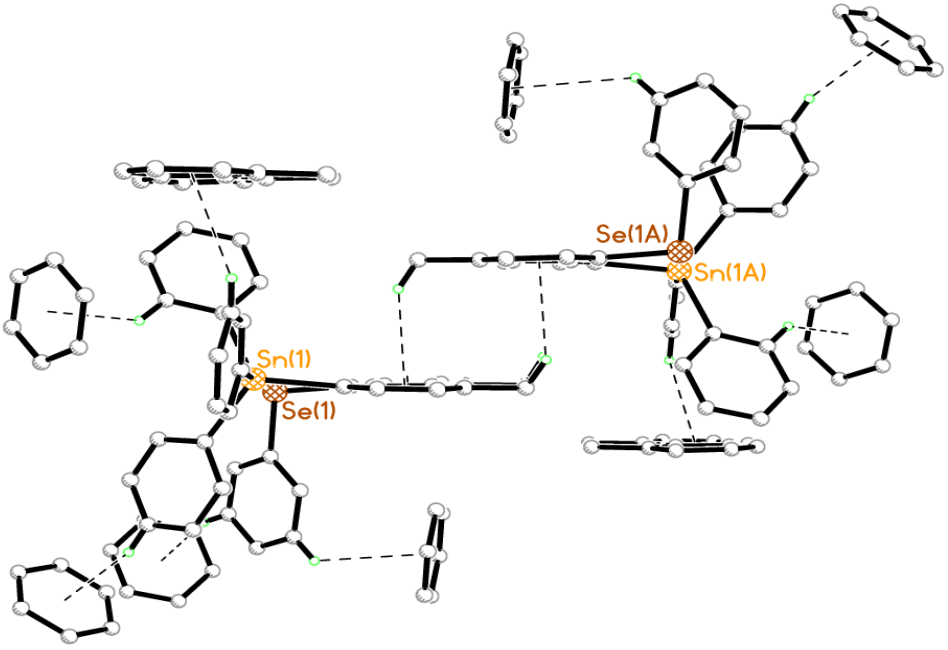

Figure 4.9 H- Centroid interactions within the structure of **8**.[10,11]

Section 2

Synthesis and Structural Study of 5-(chlorodiphenylstannyl)-6-(phenylchalcogeno) acenaphthenes

To obtain further insight into the factors associated with weak interactions between *peri*-substituents and the structural features of the acenaphthene scaffold, we decided to introduce less bulkier diphenyltin chloride and chalcogen moieties as the *peri*-substituents, which will be discussed in this section.

Synthesis

We achieved conversion of 5-bromo-6-(phenylchalcogeno)acenaphthenes, **Acenap[Br][EPh] (E = S, Se),** to the desired acenaphthene compounds **10** and **11** (*peri*-substituted with $SnPh_2Cl$ and EPh moieties), following a similar procedure to that used in section 4.1. The appropriate 5-bromo-6-(phenylchalcogeno)acenaphthene was reacted with *n*-butyllithium (1 equivalent) and diphenyltin dichloride (1 equivalent) to give the novel 5-(diphenyltinchloride)-6-(phenylchalcogeno)acenaphthenes **10** and **11** [yield: 35% (**10**), 27% (**11**); Scheme 4.3]. Compounds **10** and **11** were characterised by elemental analysis, ^{1}H, ^{13}C and ^{119}Sn NMR spectroscopy and mass spectrometry, whilst **11** was additionally characterised by ^{77}Se NMR spectroscopy.

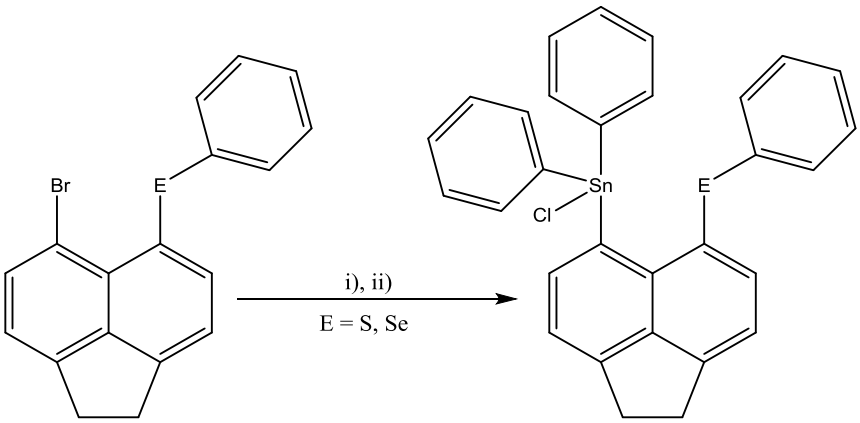

Scheme 4.3 The preparation of 6-chalcogenoacenaphth-5-yl-diphenyltin chlorides **10** and **11** from 5-bromo-6-(phenylchalcogeno)acenaphthenes. Conditions: i) *n*BuLi (1 equiv), Et_2O, -78 ºC, 1 h; ii) $SnPh_2Cl_2$ (1 equiv), Et_2O, 78 ºC, 30 min.

Suitable crystals for **10** and **11** were obtained by slow evaporation of hexane into a saturated solution of the compound in THF, the data for both compounds refined in the *P-1* space group (R1 = 5.66% (**10**); R1 = 9.31% (**11**)). Compound **10** crystallises with two independent molecules in the asymmetric unit which are chemically identical, but differ slightly crystallographically (Figure 4.10), whilst compound **11** contains one independent molecule in the asymmetric unit (Figure 4.11). Selected interatomic distances, angles and torsion angles are listed in Table 4.4, further crystallographic data for **10** and **11** can be found in Appendix 3.

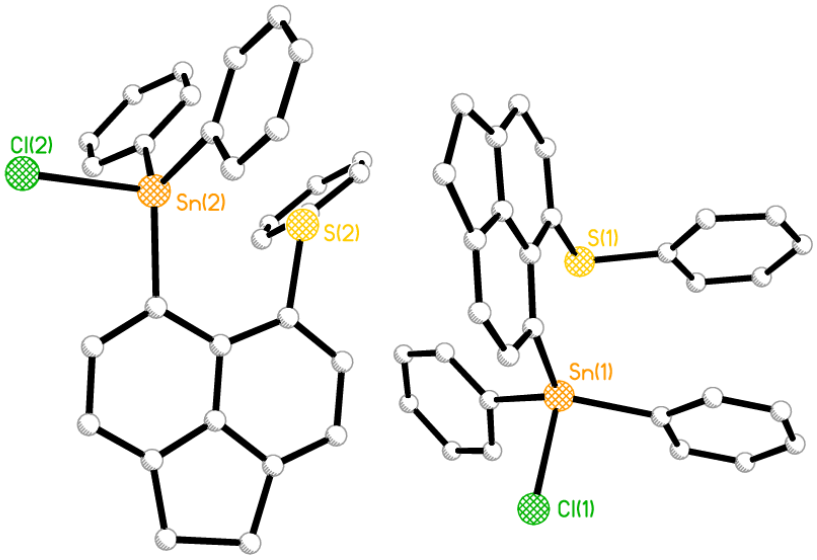

Figure 4.10 The crystal structure of *6-phenylsulfanylacenaphth-5-yl-diphenyltin chloride* **10** (hydrogen atoms omitted for clarity).

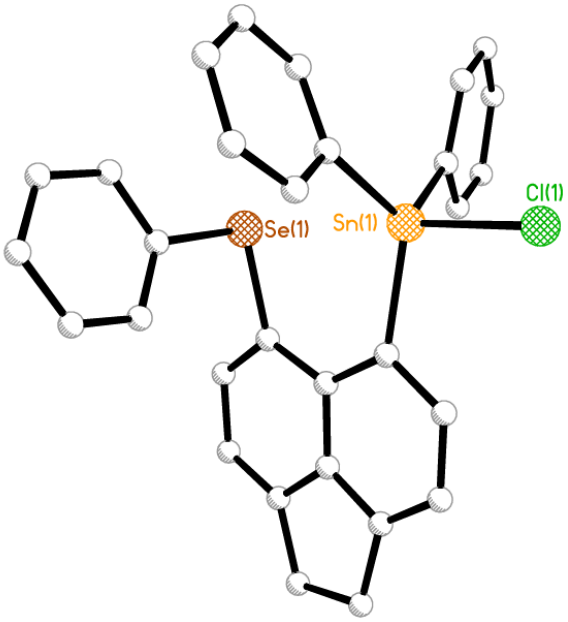

Figure 4.11 *The crystal structure of 6-phenylselanylacenaphth-5-yl-diphenyltin chloride* **11** (hydrogen atoms omitted for clarity).

The molecular structures of **10** and **11** were studied and compared to the two analogous triphenyltin (Acenap[$SnPh_3$][EPh]) (E = S **7**; E = Se **8**) by single crystal X-ray crystallography. The magnitude of deviation from the ideal acenaphthene skeleton is related to the bulkiness of the tin and size of the chalcogen functionalities which occupy the *peri*-positions in the acenaphthene molecules. Both compounds **10** and **11** show a reduction in the repulsive interactions operating between the tin and chalcogen atoms compared to **7** and **8** as indicated by the degree of geometrical deformation of the molecules. In **10** and **11**, one of the *peri*-positions is occupied by the less bulky $SnPh_2Cl$ substituent compared to $SnPh_3$ in analogous **7** and **8**, and thus the non-bonded *peri*-distances are significantly shorter than for **7** and **8**. The distances, however, naturally increase with the atomic radii of the chalcogen atom attached to the acenaphthene [**7** 3.27(14) Å, **8** 3.341(15) Å, **10** 2.978(13) Å, **11** 3.094(14) Å], but nevertheless all separations are 25-26% shorter than the sum of the van der Waals radii of the interacting atoms.

Table 4.4 Selected bond lengths (Å) and angles (°) for **10** and **11**.

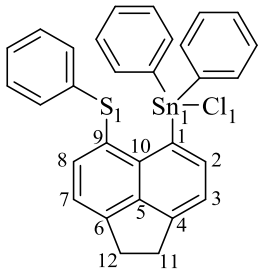

10

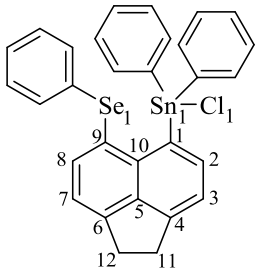

11

Peri-region-distances		
E(1)···Sn(1)	**2.978(2) [2.989(2)]**	**3.094(2)**
Σr_{vdW} - E(1)···Sn[a]	0.992[0.981]	0.976
$\%r_{vdW}$[a]	75	76
E(1)-C(9)	1.767(8) [1.779(7)]	1.926(11)
Sn(1)-C(1)	2.134(8) [2.141(7)]	2.158(10)

Acenaphthene bond lengths		
C(1)-C(2)	1.422(10) [1.382(9)]	1.396(16)
C(2)-C(3)	1.398(13) [1.419(10)]	1.420(16)
C(3)-C(4)	1.345(15) [1.370(11)]	1.363(16)
C(4)-C(5)	1.405(11) [1.389(10)]	1.390(16)
C(5)-C(10)	1.407(11) [1.407(9)]	1.438(15)
C(5)-C(6)	1.398(13) [1.420(11)]	1.395(15)
C(6)-C(7)	1.371(12) [1.374(11)]	1.380(16)
C(7)-C(8)	1.422(12) [1.407(11)]	1.405(17)
C(8)-C(9)	1.388(12) [1.378(11)]	1.387(15)
C(9)-C(10)	1.424(10) [1.426(9)]	1.424(16)
C(10)-C(1)	1.435(12) [1.426(9)]	1.430(14)
C(4)-C(11)	1.513(11) [1.498(11)]	1.515(15)
C(11)-C(12)	1.527(15) [1.574(12)]	1.563(16)
C(12)-C(6)	1.527(14) [1.509(10)]	1.517(16)
Peri-region bond angles		
E(1)-C(9)-C(10)	120.6(6) [120.2(6)]	121.0(8)
C(1)-C(10)-C(9)	126.2(7) [129.3(6)]	128.7(10)
Sn(1)-C(1)-C(10)	124.4(5) [121.5(5)]	122.9(8)
Σ of bay angles	**371.2(10) [371.0(10)]**	**372.6(15)**
Splay angle[b]	11.2 [11.0]	12.6
C(4)-C(5)-C(6)	113.5(8) [11.4(6)]	113.8(10)
In and out-of-plane displacement		
E(1)	-0.113(1) [+0.116(1)]	+0.331(1)
Sn(1)	-0.278(1) [-0.150(1)]	-0.263(1)
C:(6)-(5)-(10)-(1)	-179.9(7) [-175.1(6)]	-176.6(7)
C:(4)-(5)-(10)-(9)	179.2(6) [-177.9(6)]	-178.5(7)

[a] van der Waals radii used for calculations: rvdW(S) 1.80 Å, rvdW(Se) 1.90 Å, rvdW r_{vdW}(Sn) 2.17 Å , Splay angle: Σ of the three bay region angles – 360.

In each compound (**10** and **11)** the steric congestion imposed by the tin and chalcogen moieties is relieved by distortion of the exocyclic bonds via both out-of-plane and in-plane displacements and by distortion of the acenaphthene skeleton. The selenium and tin atoms exhibit greater deviations from the acenaphthene mean plane in **11** compared to the *peri*-atoms in **10**, with the Sn sitting 0.278(1) Å below the plane and Se lying 0.331(1) Å above due to the greater size of Se over S

which causes an increase in repulsion. In **10** the Sn and S atoms lie -0.263(1) Å and -0.113(1) Å from the acenaphthene plane, respectively (Figure 4.12).

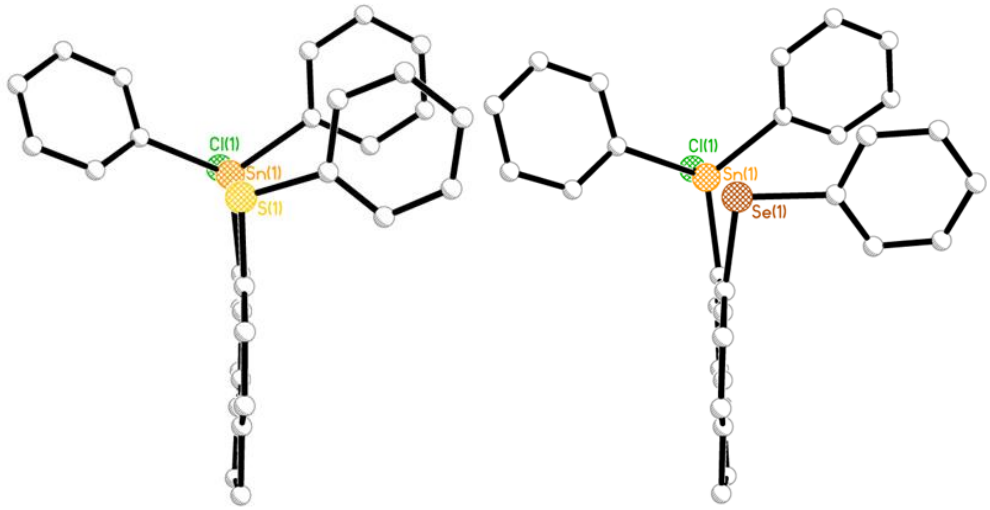

Figure 4.12 The structures **10** and **11** showing the planarity of the acenaphthene backbone.

The *peri*-substituents are further accommodated by an in-plane deviation in the C-C-C angles between the Sn and chalcogen atoms as indicated by the sum of the bay-region angles [**10** 371.2(10)°, **11** 372.6(15)°]. However, the angle change does not greatly affect the bond lengths around the bay region. **10** and **11** have similar bond lengths to that of acenaphthene (average length 1.40 Å and 1.42 Å). In **10** and **11**, the splay angles (average 12°) are much smaller than to those seen in **7** and **8** (average 20°). This indicates that the *peri*-positions are much closer when the acenaphthene is substituted with less bulkier groups. In addition, the displacement of the tin and chalcogen functionalities are accompanied by a buckling of the usually planar C5-C10 unit. This can be seen by the torsion angles associated with the central C(5)-C(10) bond (Table 4.5).

Twisting of the plane is relatively large in **11** with the angles -176.6(7)° and -178.5(7)° compared to **10**, which retains angles closer to 180° (-179.9(7)° and 179.2(6)°).

Steric strain occurring within the acenaphthene scaffold can also be relieved by the formation of non-covalent interactions between the *peri*-substituents.[3-6] Under appropriate geometric conditions this can be in the form of a three-centre four-electron interaction. In order for 3c-4e interaction to occur, a *quasi*-linear arrangement between three atoms is required.[2-5,13] Compounds **10** and **11** both exhibit *quasi*-linear conformations of the Cl-Sn···S (174.1°) and Cl-Sn···Se atoms (175.48°), respectively, thus promoting the delocalisation of a chalcogen lone-pair to the electropositive tin atom, forming a non-covalent 3c-4e type interaction (Figure 4.13). Further to that, the Cl atom in both cases aligns along the acenaphthene plane adopting an equatorial conformation (type B) which leads to the weak interaction (Table 4.5). Both the molecules show BAA-A type conformations according to the classification system defined by Nakanishi *et al.*[14] in which the E-C_{Ph} and two of the Sn-C_{Ph} bonds align perpendicular to the acenaphthene plane adopting axial type "A" conformations.

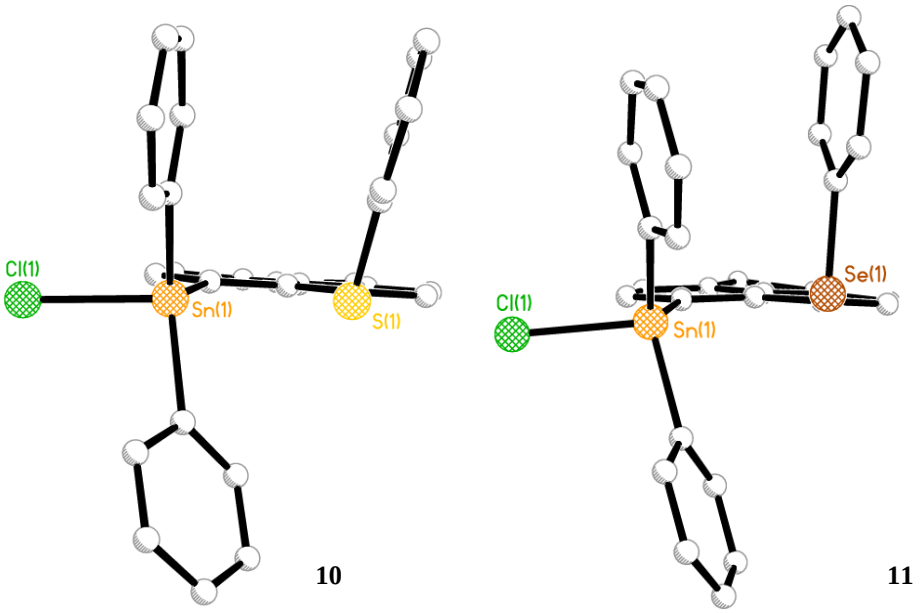

10 **11**

Figure 4.13 The molecular configurations of **10** and **11** showing the orientation of the substituents bound to Sn and Chalcogen; both compounds adopt similar BAA-A type conformations.

Table 4.5 Torsion angles [°] categorizing the acenaphthene and ligand conformations in **10** and **11**.

	10	**11**
C(10)-C(1)-Sn(1) Clb(1)	Ph: θ_1 172.0(5) equatorial-B	Ph: θ_1 172.0(6) equatorial-B
C(10)-C(1)-Sn(1)-C(19)	Ph: θ_2 -67.8(6) axial-A	Ph: θ_2 -65.3(8) axial-A
C(10)-C(1)-Sn(1)-C(13)	Ph: θ_3 86.0(6) axial-A	Ph: θ_3 82.6(6) axial-A
C(10)-C(9)-E(1)-C(25)	Ph: θ_4 -103.4(6) axial-A	Ph: θ_4-88.0(7) axial-A

As a result of the different orientation of the groups attached to the tin atom, the Cl-Sn-C and C-Sn-C angles are varied, thus the best description of the geometry around the tin in each case is a distorted tetrahedron , with the largest angle 120.7(4)° for **11** and smallest angle of 95.6(2)° for **10** (deviating from the optimal 109°). However, **11** shows a much higher deviation from tetrahedral when comparing the angles to that of analogous **7** and **8**, whose most obtuse angle is 115.37(17)° (**7**). These geometrical distortions can be explained by the rigidity of the acenaphthene and non-covalent interactions of the *peri*-substituents.

Table 4.6 Bond angles [°] categorising the geometry around Sn in **10** and **11**.

Angles around the Sn atom	**10**	**11**
C(1)-Sn(1)-C(13)	118.3(3) [118.4(3)]	120.7(4)
C(1)-Sn(1)-C(19)	115.6(3) [115.3(3)]	113.4(4)
C(13)-Sn(1)-C(19)	120.5(3) [119.5(3)]	117.8(4)
Cl(1)-Sn(1)-C(1)	99.96(19) [97.84(19)]	99.7(3)
Cl(1)-Sn(1)-C(13)	95.6(2) [98.3(2)]	97.9(3)
Cl(1)-Sn(1)-C(19)	98.2(2) [100.0(2)]	101.1(4)

An investigation into the packing and the intermolecular forces present in compounds **10** and **11** was of interest. In **11**, the molecules packed one on top of the other with a 180° rotation of the acenaphthene ring (Figure 4.14). Both molecules **10** and **11** show distinct secondary interactions with C-H···Cl type weak hydrogen bonds; the Cl atom attached to tin atom interacts with the adjacent C-H group of the acenaphthene (Figure 4.14 and 4.15). There is no π-π stacking observed in either compound as the closest ring systems are 3.83 Å apart. However, there is an H-Cg interaction present, similar to that seen in **7** and **8**.

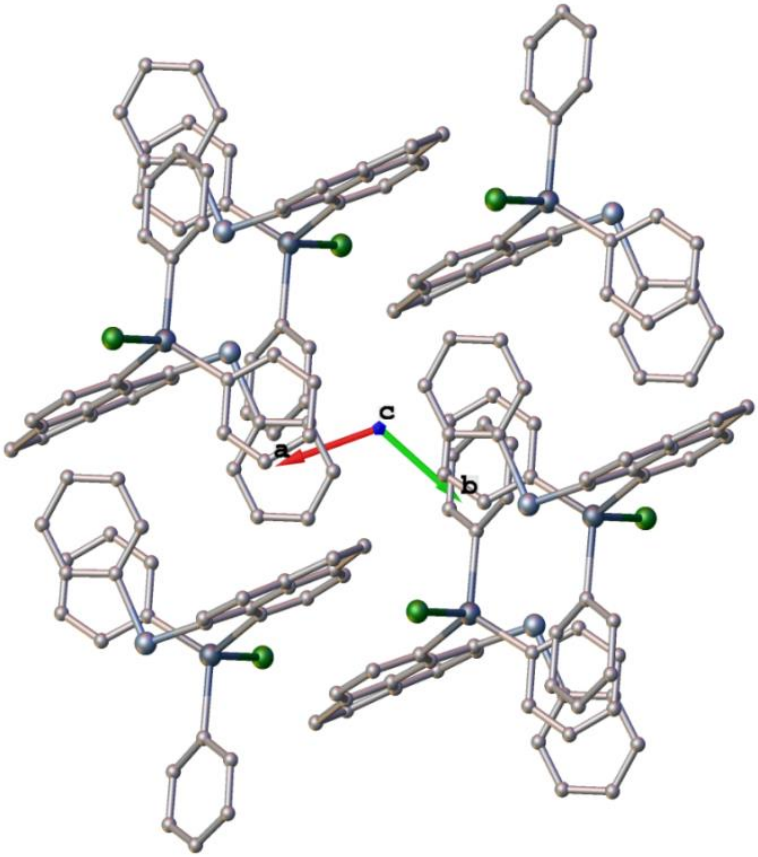

Figure 4.14 Intermolecular packing in **10**.

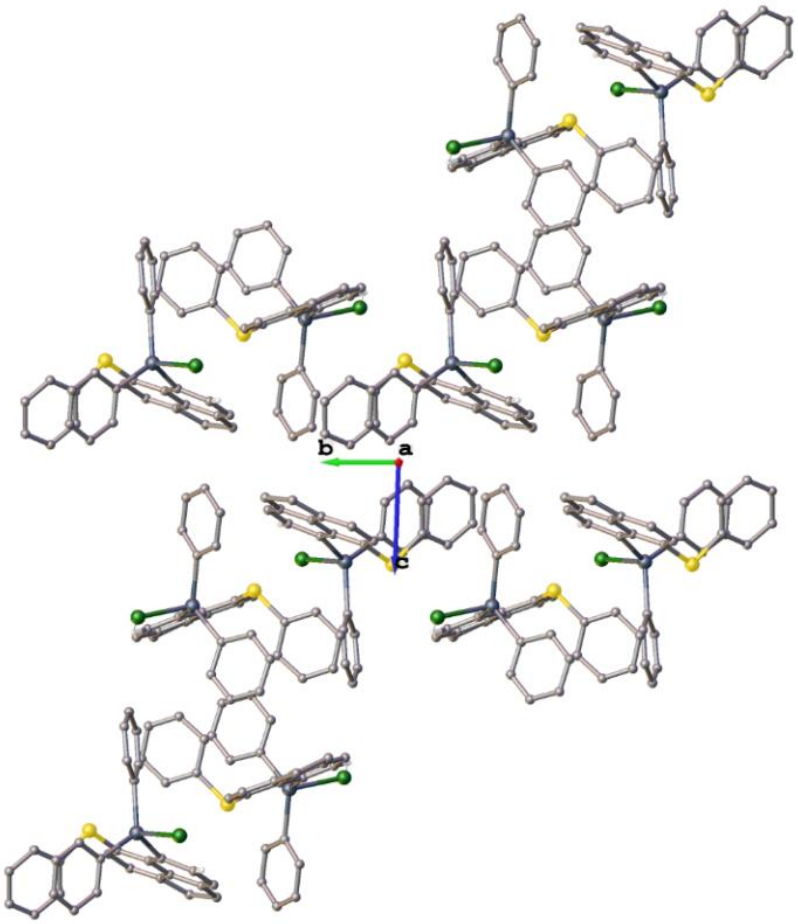

Figure 4.15 Intermolecular packing in **11**.

Section 3

Synthesis and structural studies of bis(6-phenylsulfunalyacenaphth-5-yl)tin dichloride and bis(6-phenylsulfanylcenaphth-5-yl)diphenyltin

This section focuses on the preparation and crystallographic studies of strain-induced bis-acenaphthene compounds. These systems provide exceptional insights into the effect of structural deformation on ground-state structures and on internal mobility. The compounds will be compared to the analogous structures of **3** and **5**.

Synthesis

Single substitution reactions of 5-bromo-6-(phenylsulfanyl)acenaphthene, *via* lithium halogen exchange followed by addition of $SnCl_2$ and $SnPh_2Cl_2$ afforded bis-compounds ($\{AcenapSPh\}_2SnX_2$ (X= Cl (**12**), Ph (**13**)), respectively (Scheme 4.4). For their synthesis, 5-bromo-6-(phenylsulfanyl)acenaphthene was independently reacted with *n*-butyllithium (1 equivalent) at −40 °C in diethyl ether followed by subsequent addition of a ½ equivalent of the respective tin dichloride [26% (**12**), 22% (**13**); Scheme 4.4].

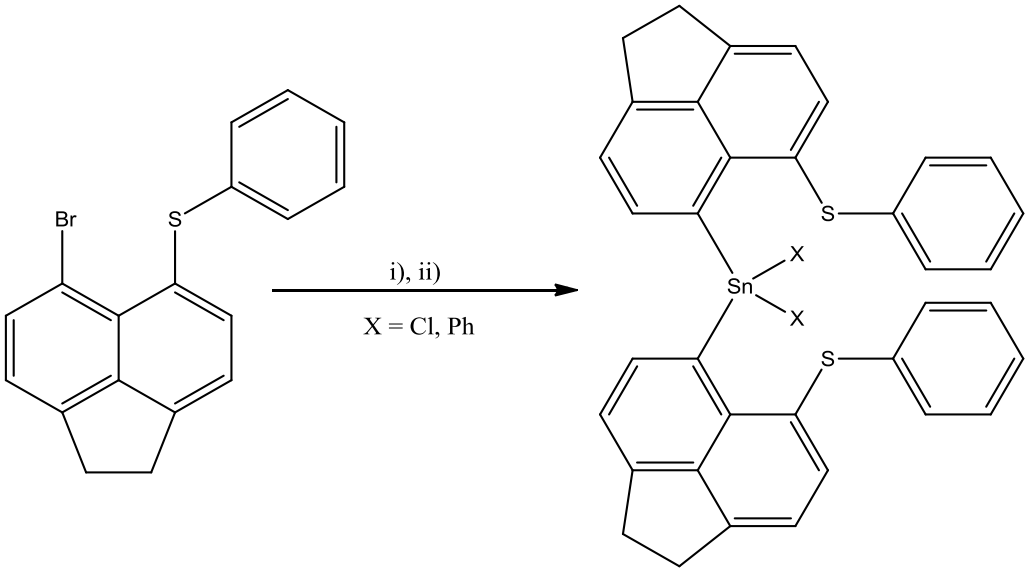

Scheme **4.4** The preparation of bis(6-phenylsulfanylacenaphth-5-yl)tin dichloride **12** and bis(6-phenylsulfanylacenaphth-5-yl)diphenyltin **13** from 5-bromo-6-(phenylsulfanyl)acenaphthene. Conditions: i) *n*BuLi (1 equiv), Et_2O, -78 ºC, 1 h; ii) $SnCl_4$ (**12**) or $SnPh_2Cl_2$ (**13**) (1 equiv), Et_2O, 78 ºC, 30 min.

Both compounds were fully characterised by elemental analysis, ^{1}H, ^{13}C and ^{119}Sn NMR spectroscopy. The ^{119}Sn NMR spectra of **12** and **13** both display single peaks, with the presence of the two highly electronegative chlorine atoms producing a substantial upfield shift at -192.04 ppm compared to the two phenyl groups (-31.4 ppm).

X ray investigations

Colourless crystals, suitable for characterisation by single crystal X-ray crystallography were obtained for **12** and **13** by hexane diffusion into a saturated solution of the product in THF. The data for both **12** and **13** refined in the $P2_1/c$ space group, with the final refinement of **12** containing one independent molecule and one solvent (THF) molecule in the asymmetric unit, whilst

compound **13** had one independent molecule in the asymmetric unit, (R1 = 10.02 **(12),** 3.33 **(13**) %). The crystal structures of **12** and **13** are shown in Figures 4.16 and 4.17. A list of interatomic bond lengths and angles is given in Table 4.7, and further crystal structure data is found in Appendix 3.

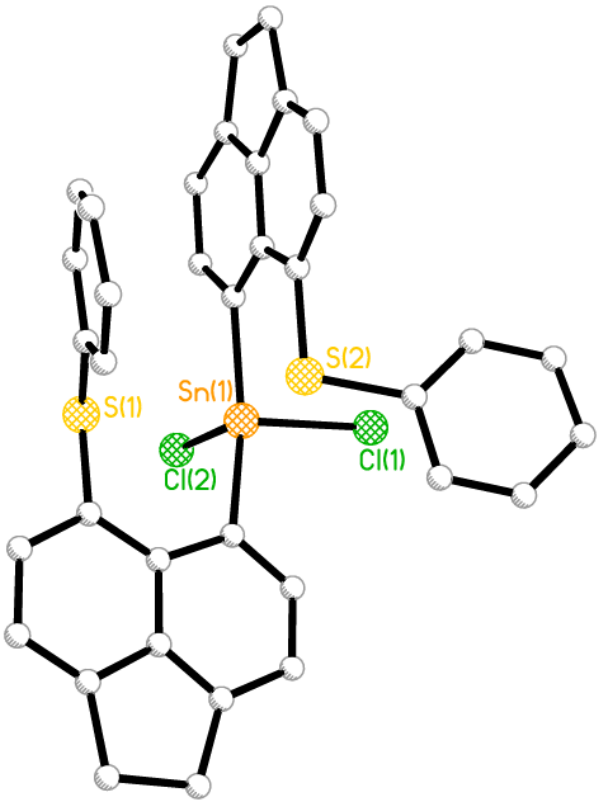

Figure 4.16 The crystal structure of *bis(6-phenylsulfanylacenaphth-5-yl)tin dichloride* **12** (hydrogen atoms omitted for clarity).

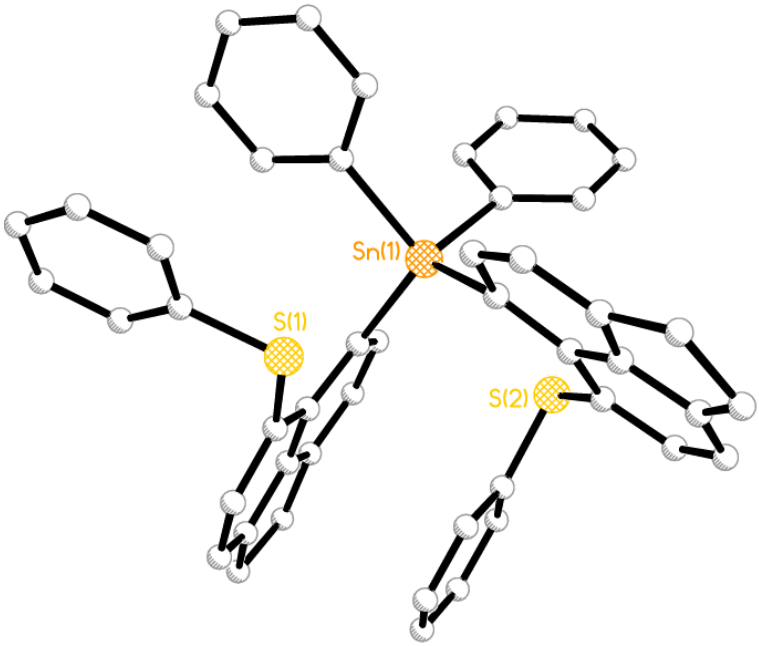

Figure 4.17 The crystal structure of *bis(6-phenylsulfanylacenaphth-5-yl)diphenyltin* **13** (hydrogen atoms omitted for clarity).

Compounds **12** and **13** adopt similar structural configurations to bromine analogues **3** and **5** described in Chapter 3, which were shown to use four different types of structural variation to stabilise the steric strain caused by the interaction between the bulky Sn and Br substituents. Since the only difference between **12** and **13** and the bromine analogues is the existence of the -SPh moiety instead of the Br atom, these four compounds are well suited for comparison to understand how the change in the *peri*-substituents affects the acenaphthene skeleton in these bis-acenaphthene compounds.

Interestingly, the *peri*-distances are notably shorter in the sulfur derivatives **12** and **13** (2.940(3) Å, 2.978(2) Å **12**, 3.281(1) Å, 3.23(1) Å **13**)) compared to bromine analogues **3** and **5** (3.174(2) Å **3**,

3.299(1) Å **5**)), expected from the reduction in size going from a Br atom to a S atom. This may indicate that addition of the –SPh group instead of Br causes the *peri*-substituents to get close enough to make a weak dative-covalent bond. However, the Sn(1)···S(1) distance increases with increasing size of the Sn group, similar to the trend observed in **3** and **5**. The *peri*-distances in **12** (2.940(3) Å, 2.978(2) Å) are smaller than in **13** (3.281(1) Å, 3.23(1) Å), but all four distances are still less than the sum of the van der Waals radii for the two interacting atoms [$\sum r_{vdw}$ (SnS) = 3.97 Å], suggesting weak interactions could be present. In addition, a linear arrangement of the S(1)···Sn(1)-Cl(1) and S(1)···Sn(1)-C_{Ph} atoms (175.59°, 171.02° **12**, 175.16°, 176.40° **13)** across the *peri*-gap, supports the existence of weak 3c-4e type interactions operating in these compounds. Furthermore, the existence of an electronegative Cl atom on the tin centre encourages a donor-acceptor interaction to occur between sulfur and tin, which explains the smaller *peri*-distance and increased linearity of the S(1)···Sn(1)-Cl(1) angles in **12** compared to **13**.

Table 4.7 Selected bond lengths (Å) and angles (°) for **12** and **13**.

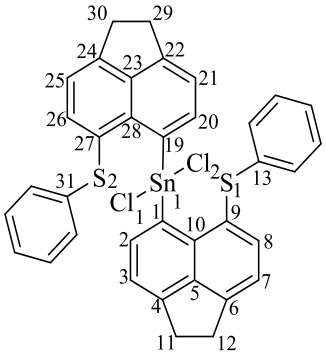

12

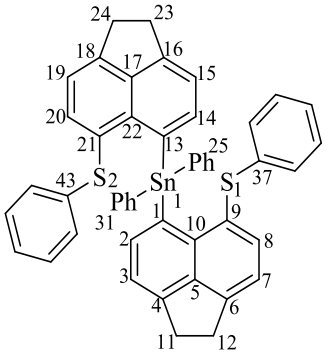

13

Fragment	**12a**	**12b**	**13a**	**13b**
Peri-region-distances				
S(1)···Sn(1)	**2.940(3)**	**2.978(2)**	**3.281(1)**	**3.23(1)**
Σr_{vdW} - S(1)···Sn[a]	1.03	0.992	0.689	0.74

%r_{vdW}[a]	74	75	83	82
S(1)-C(9)	1.788(11)	1.798(12)	1.782(4)	1.785(4)
Sn(1)-C(1)	2.141(10)	2.136(11)	2.172(3)	2.172(3)
Acenaphthene bond lengths				
C(1)-C(2)	1.364(17)	1.377(17)	1.390(5)	1.392(5)
C(2)-C(3)	1.392(16)	1.439(17)	1.420(5)	1.417(5)
C(3)-C(4)	1.416(18)	1.406(16)	1.360(5)	1.366(5)
C(4)-C(5)	1.373(17)	1.416(16)	1.412(5)	1.418(5)
C(5)-C(10)	1.440(15)	1.432(15)	1.416(4)	1.421(5)
C(5)-C(6)	1.429(16)	1.406(16)	1.412(5)	1.412(5)
C(6)-C(7)	1.366(19)	1.352(19)	1.367(6)	1.370(6)
C(7)-C(8)	1.421(17)	1.374(17)	1.383(5)	1.409(5)
C(8)-C(9)	1.392(17)	1.389(17)	1.383(5)	1.384(5)
C(9)-C(10)	1.404(17)	1.425(16)	1.422(5)	1.432(5)
C(10)-C(1)	1.447(16)	1.413(15)	1.443(5)	1.435(5)
C(4)-C(11)	1.507(16)	1.488(16)	1.513(5)	1.518(5)
C(11)-C(12)	1.556(18)	1.591(17)	1.559(5)	1.545(6)
C(12)-C(6)	1.538(17)	1.548(17)	1.520(5)	1.516(5)
Peri-region bond angles				
S(1)-C(9)-C(10)	118.7(9)	118.1(9)	121.8(3)	120.2(3)
C(1)-C(10)-C(9)	129.9(10)	129.6(10)	128.6(3)	129.3(3)
Sn(1)-C(1)-C(10)	120.2(8)	123.1(8)	126.7(3)	127.4(3)
Σ of bay angles	**368.8(16)**	**370.8(16)**	**377.1(5)**	**376.9(5)**
Splay angle[b]	8.8	10.8	17.1	16.9
C(4)-C(5)-C(6)	113.1(10)	112.6(10)	111.5(3)	111.8(3)
In and out-of-plane displacement				
S(1)	+0.218(1)	+0.206(1)	+0.493(1)	-0.037(1)
Sn(1)	+0.185(1)	-0.002(1)	-0.262(1)	-0.320(1)
C:(6)-(5)-(10)-(1)	178.6(9)	-179.6(10)	173.4(3)	-178.9(3)
C:(4)-(5)-(10)-(9)	-178.0(9)	-179.0(10)	178.6(3)	179.0(3)

[a] van der Waals radii used for calculations: rvdW(S) 1.80 Å, rvdW (Sn) 2.17 Å , Splay angle: Σ of the three bay region angles – 360.

Similar to **3** and **5**, acenaphthene structural distortions occur to accommodate the large Sn and S substituents situated across the *peri*-gap, in the form of in-plane and out-of-plane deflections of the *peri*-bonds relative to the plane of the acenaphthene ring. The degree of in-plane distortion of the tin and sulfur atoms, shown by the sum of the *peri*-region angles, is larger in **13** compared to **12**

[368.8(16)°, 370.8(16)° **12**, 377.1(5)°, 376.9(5)° **13**] and as expected, less than the distortion taking place in the bromine analogues **3** and **5**. However, the Sn–C bond distance is not greatly affected by the substitution, with distances statistically similar to other compounds studied (~2.14°).

Interestingly, compounds **12** and **13** not only display differing degrees of out-of-plane displacement, but also different locations of their *peri*-atoms in each side of the molecule. In **12a**, both the Sn and S atoms lie above the plane (+0.218(1) Å, +0.185(1) Å) whilst in the second acenaphthene fragment the S atom lies above the plane (+0.206(1) Å) and the Sn atom is essentially coplanar (-0.002(1) Å). Similarly in **13b** the S atom lies close to the plane (-0.037(1) Å) with Sn situated -0.320(1) Å below the plane, compared to fragment **13a** in which the S and Sn atoms are displaced to opposite side of the plane (+0.493(1) Å, -0.262(1) Å) (Table 4.7). In contrast to **3** and **5**, the degree of displacement of the Sn group is greater in **12** and **13** due to steric hindrance of phenyl groups.

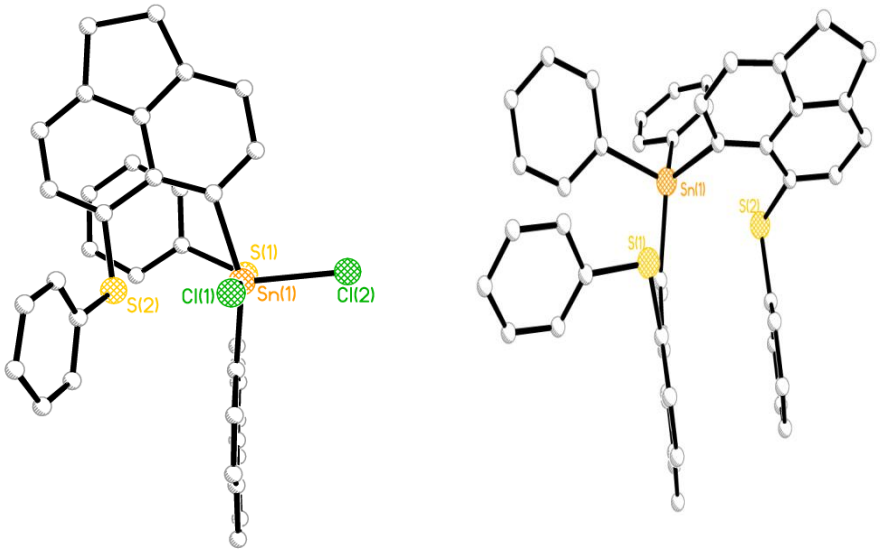

Figure 4.18 The structures of compounds **12** and **13** showing the planarity of the acenaphthene backbone.

The tin centre in the $SnCl_2$ group in **12** forms a distorted conformation, in between tetrahedral and trigonal bipyramidal, due to the additional non covalent intramolecular Sn···S interactions. The C-Sn-C angles, in each case, range from 98.3°-151.1° which demonstrates the considerable amount of distortion away from that of an optimal tetrahedron (109.5°). This deviation of the Sn geometry is most probably due to the severe congestion of the acenaphthene/phenyl groups bound to the tin centre. This phenomenon is similar to that of analogues **3** and **5**.

Table 4.8 Bond angles [°] categorising the geometry around Sn in **12** and **13**.

Angles around the Sn atom	**12**		**13**	
C(1)-Sn(1)-C(19)	151.1(4)	151.1(4)	-	-
C(1)-Sn(1)-Cl(1)	100.2(3)	100.2(3)	-	-
C(1)-Sn(1)-Cl(2)	98.3(3)	98.3(3)	-	-
Cl(1)-Sn(1)-Cl(2)	98.29(11)	98.29(11)	-	-
C(19)-Sn(1)-Cl(1)	97.0(3)	97.0(3)	-	-
C(19)-Sn(1)-Cl(2)	102.1(3)	102.1(3)	-	-
C(1)-Sn(1)-C(13)	-	-	122.59(11)	122.59(11)
C(1)-Sn(1)-C(25)	-	-	107.76(12)	107.76(12)
C(1)-Sn(1)-C(31)	-	-	105.95(12)	105.95(12)
C(13)-Sn(1)-C(25)	-	-	108.79(12)	108.79(12)
C(13)-Sn(1)-C(31)	-	-	109.55(12)	109.55(12)
C(25)-Sn(1)-C(31)	-	-	99.82(11)	99.82(11)

Both compounds display similar stacking in the way their molecules pack (Figure 4.19 and 4.20), where the acenaphthene rings align parallel to each other but slightly off-set. This is similar to the packing seen in **3** and **5**. There are no significant π-π stacking interactions seen in either of the compounds; when the molecules are packed the distances between the centroids exceed 3.80 Å[5,15]. The only difference in the packing between the two compounds is the weak H bond (soft acid-soft base) interaction between a Cl atom and the adjacent C-H bond in the neighbouring acenaphthene in **12**.

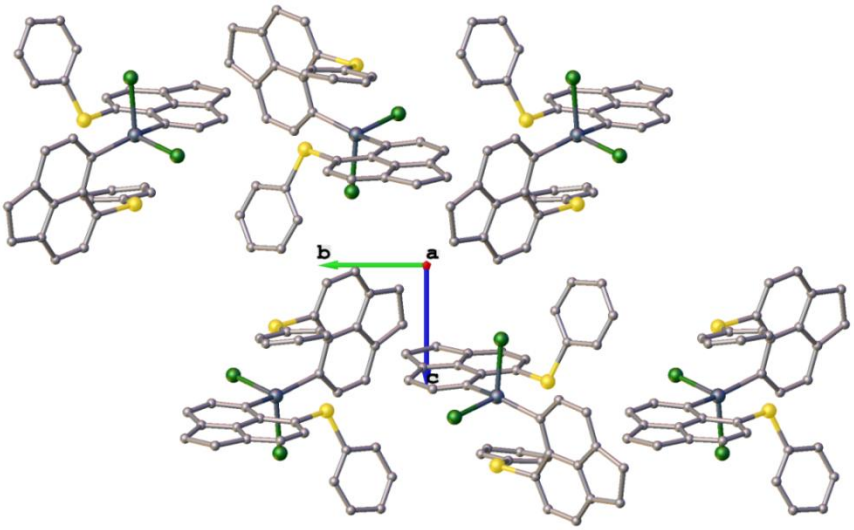

Figure 4.19 Packing in **12**.

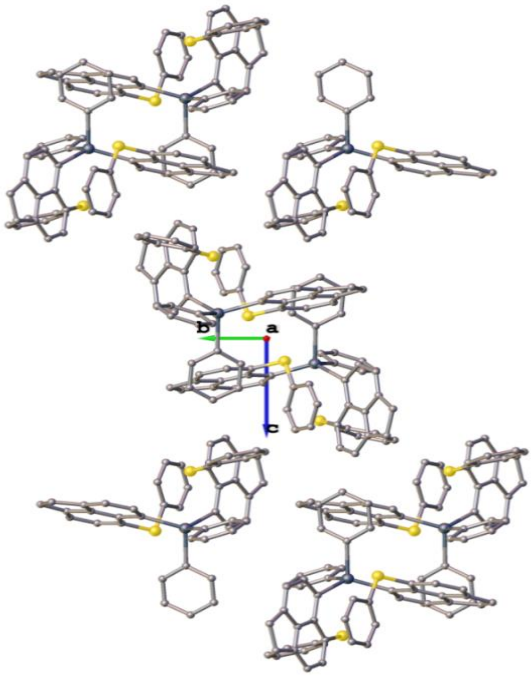

Figure 4.20 Packing in **13**.

Section 4

Synthesis and structural studies of 6-(butylchalcogeno)acenaphth-5-yl-dibutyltin chlorides

To further investigate the factors influencing the donor-acceptor interactions and intramolecular strain occurring in organotin acenaphthene compounds, less bulky dibutyltin-chalcogen *peri*-substituted systems were synthesised. This section discusses the preparation and structural distortions that occur when dibutyltin chloride and elements from group 16 (S, Se) occupy the 5,6-positions in acenaphthene.

Synthesis

We envisaged that reacting 5-bromo-6-(phenylchalcogeno)acenaphthenes, **Acenap[Br][EPh] (E = S, Se),** following a similar procedure to that used in section 4.1, would afford the desired acenaphthene compounds **14** and **15**, *peri*-substituted with $SnPh_2Cl$ and EPh moieties. For their synthesis, the appropriate 5-bromo-6-(phenylchalcogeno)acenaphthene was reacted with *n*-butyllithium (single equivalent) and dibutyltin dichloride (single equivalent) to afford the novel 6-(phenylchalcogeno)acenaphth-5-yl-dibutyltin chlorides **14** and **15** [yield: 29% (**14**), 61% (**15**); Scheme 4.5]. Compounds **14** and **15** were characterised by elemental analysis, ^{1}H, ^{13}C and ^{119}Sn NMR spectroscopy and mass spectrometry, whilst **15** was additionally characterised by ^{77}Se NMR spectroscopy.

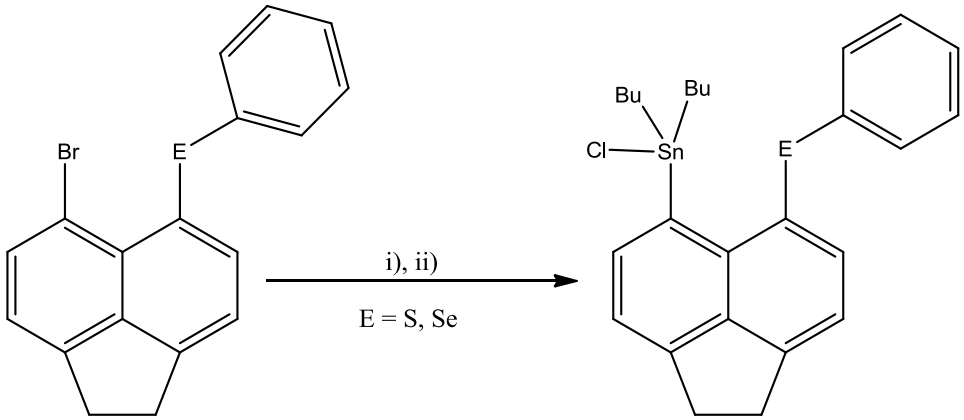

Scheme **4.5** The preparation of 6-phenylchalcogencenaphth-5-yl-dibutyltin chloride **14** and **15** from the 5-bromo-6-(phenylchalcogeno)acenaphthene. Conditions: i) *n*BuLi (1 equiv), Et_2O, -78 ºC, 1 h; ii) Bu_2SnCl_2 (1 equiv), Et_2O, 78 ºC, 30 min.

As expected, the ^{119}Sn NMR spectra of both **14** and **15** display a single peak with the signal for the sulfur derivative lying significantly upfield (−114.5 ppm) compared to that for the selenium compound (-12.4 ppm). Satellites for ^{119}Sn-^{77}Se expected in the spectrum of **15** were within the baseline and as such coupling could not be observed.

X ray investigations

Suitable single crystals were obtained for **14** and **15** by diffusion of hexane into a saturated solution of the compound in tetrahydrofuran (THF). Both the compounds crystallise in the $P2_1/n$ space group (R1 = 3.3(**14**), 5.57 (**15**), with one molecule in the asymmetric unit (Figures 4.21, 4.22). Selected interatomic distances, angles and torsion angles are listed in Table 4.9, further refinement data for **14**-**15** can be found in Appendix 3.

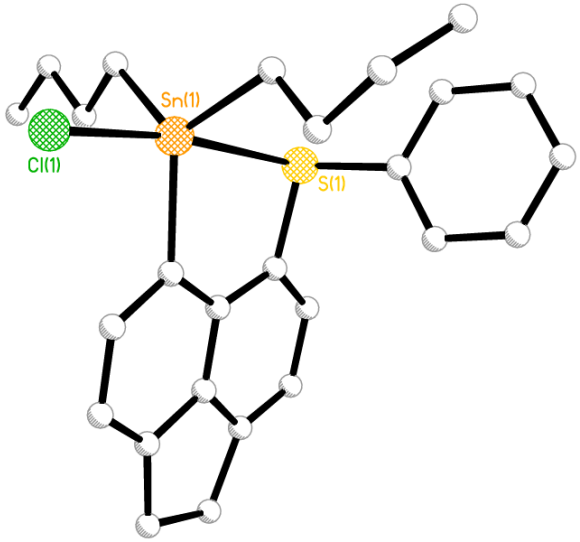

Figure 4.21 The crystal structure of *6-phenylsulfanylacenaphth-5-yl-dibutyltin chloride* **14** (hydrogen atoms omitted for clarity).

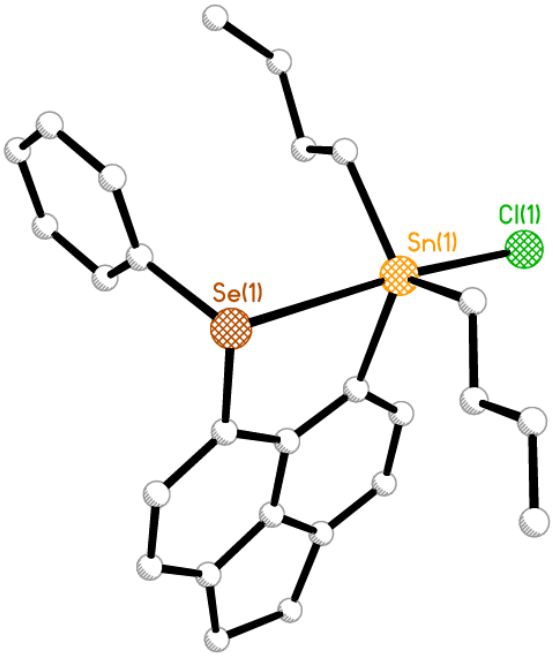

Figure 4.22 The crystal structure of *6-phenylselanylacenaphth-5-yl-dibutyltin chloride* **15** (hydrogen atoms omitted for clarity).

Positioning chalogen and butyltin chloride moieties in the *peri*-positions of acenaphthene provides an excellent system to study non-covalent interactions across the *peri*-gap. The structural deviation of **14** and **15** is thus compared to the previously discussed diphenyltin chloride analogues (**10** and **11**) in Section 2.

There is a general trend of increasing non-bonded distance with increasing size of the chalcogen atom. Unsurprisingly, the observed *peri*-distance of **14** is larger than that in **13**, displaying an increase when larger atoms are substituted at the 5,6 positions in acenaphthene (**14** 2.980(1) Å, **15** 3.0595(10) Å). This is indeed consistent with the difference in the *peri*-distance observed between **10** and **11** (**10** 2.978(13) Å, **11** 3.094(14) Å), however, the *peri*-gaps of equivalent chalcogen compounds are statistically invariant. Nevertheless, the Sn···E distances are much shorter than the $\sum r_{vdW}$ radii for the two interacting atoms in all cases (3.97-4.07 Å).

Table 4.9. Selected bond lengths (Å) and angles (°) for **14** and **15**.

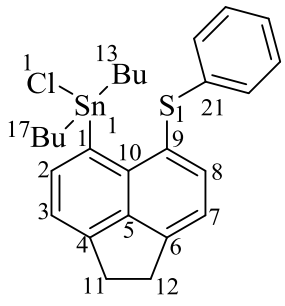

14

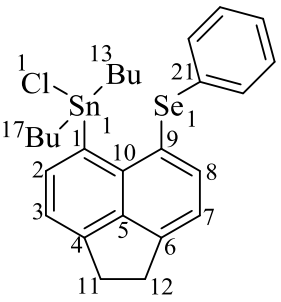

15

Peri-region-distances		
E(1)···Sn(1)	**2.980(1)**	**3.0595(10)**
Σr_{vdW} - E···Sn[a]	0.99	1.011
$\%r_{vdW}$[a]	75	75

E(1)-C(9)	1.775(4)	1.920(7)
Sn(1)-C(1)	2.168(3)	2.170(7)
Acenaphthene bond lengths		
C(1)-C(2)	1.388(5)	1.387(10)
C(2)-C(3)	1.417(5)	1.415(10)
C(3)-C(4)	1.364(5)	1.370(9)
C(4)-C(5)	1.410(5)	1.410(9)
C(5)-C(10)	1.416(5)	1.443(9)
C(5)-C(6)	1.410(4)	1.404(9)
C(6)-C(7)	1.373(5)	1.365(10)
C(7)-C(8)	1.411(5)	1.410(10)
C(8)-C(9)	1.379(5)	1.407(9)
C(9)-C(10)	1.427(5)	1.424(9)
C(10)-C(1)	1.426(4)	1.417(9)
C(4)-C(11)	1.514(5)	1.520(10)
C(11)-C(12)	1.547(5)	1.554(10)
C(12)-C(6)	1.516(5)	1.512(9)
Peri-region bond angles		
E(1)-C(9)-C(10)	119.9(3)	119.4(5)
C(1)-C(10)-C(9)	128.6(3)	130.3(6)
Sn(1)-C(1)-C(10)	122.3(3)	123.0(5)
Σ of bay angles	**370.8(5)**	**372.7(9)**
Splay angle[b]	10.8	12.7
C(4)-C(5)-C(6)	112.0(3)	112.3(6)
In and out-of-plane displacement		
E(1)	-0.132(1)	+0.207(1)
Sn(1)	-0.034(1)	-0.015(1)
C:(6)-(5)-(10)-(1)	177.8	177.8
C:(4)-(5)-(10)-(9)	-179.8	179.7

[a] van der Waals radii used for calculations: rvdW(S) 1.80 Å, rvdW (Se) 1.90 Å, rvdW (Sn) 2.17 Å, Splay angle: Σ of the three bay region angles – 360.

Both molecules adopt the 'AAB-A type' conformation with Cl-Sn and Sn-C_{acenap} bonds lying along the acenaphthene plane and approaching a *quasi*-planar arrangement of atoms (angles ranging from 172°-174°; Figure 4.23). The EPh groups in **14** and **15** sit perpendicular to the mean plane and adopt a similar (*axial*) arrangement to that observed in analogues **10** and **11**. Similarly,

the two Sn-C_{butyl} bonds also adopt an axial arrangement in **14** and **15**, similar to the diphenyl adducts, **10** and **11**. The presence of the linear E···Sn-Cl arrangement and the effect of the electron rich Cl atom on the tin centre is such that a non-covalent 3c-4e type interaction occurs between chalcogen···Sn-Cl in these systems.[5,13]

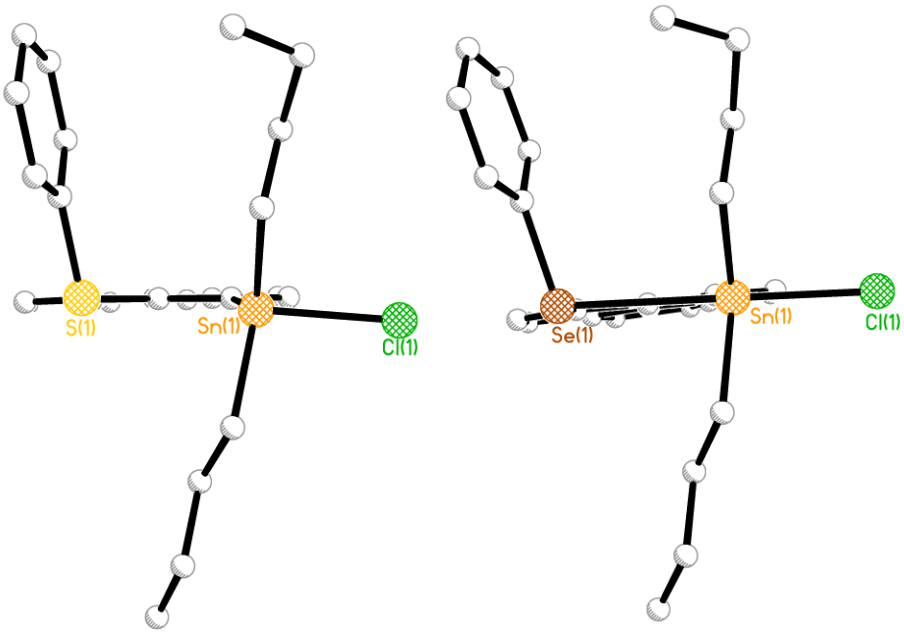

Figure 4.23 The molecular configurations of **14** and **15** showing the orientation of the substituents bound to Sn and Chalcogen; both compounds adopt similar AAB-A type conformations.

Table 4.10. Torsion angles [°] categorizing the acenaphthene and ligand conformations in **14**-**15**.

	14	**15**
C(10)-C(1)-Sn(1) C(13)	Ph: θ_1 -87.6(3) axial-A	Ph: θ_1 -87.3(5) axial-A
C(10)-C(1)-Sn(1)-C(17)	Ph: θ_2 70.3(3) axial-A	Ph: θ_2 72.5(6) axial-A
C(10)-C(1)-Sn(1)-Cl(1)	Ph: θ_3 172.6(2) equatorial-B	Ph: θ_3 174.0(5) equatorial-B
C(10)-C(9)-E(1)-C(21)	Ph: $\theta_4$100.3(3) axial-A	Ph: $\theta_4$101.6(5) axial-A

In both **14** and **15**, the acenaphthene geometry distorts from planarity to accommodate the steric congestion experienced by the chalcogen and butyltin groups. In each case, the exocyclic bonds are displaced from the plane of the backbone, with the heavier Se atom of compound **15** showing the biggest deviation from the plane (Se +0.207(1) Å, Sn -0.015(1) Å). In **14**, both *peri*-atoms sit below the mean plane (-0.132(1) Å S, -0.034(1) Å Sn).

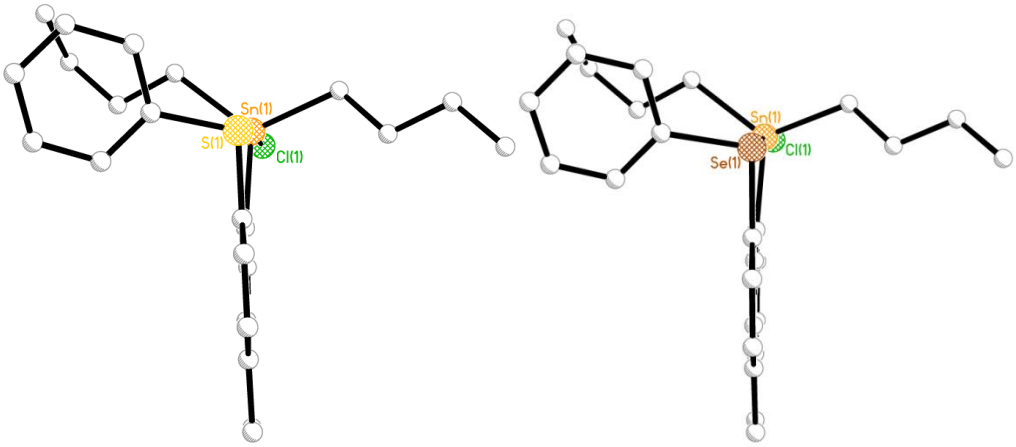

Figure 4.24 The structures **14** and **15** showing the planarity of the acenaphthene backbone.

Further reduction in strain between neighbouring substituents is partly relieved by in-plane distortions, indicated by a widening of the bay-region angles which increase from 370.8(5)° in **14** to 372.7(9)° in **15**. This is comparable to that seen in **10** and **11**. In both **14** and **15** the acenaphthene backbones are relatively planar, comparable to that observed for the phenyl tin substituents. In each compound, the C:(4)-(5)-(10)-(9) torsion angle (**14** -179.8°, **15** 179.7°) is almost planar, while the C:(6)-(5)-(10)-(1) angle deviates slightly from planarity in order to achieve a relaxed geometry (**14** 177.81° and **15** 177.8°).

Angles around the tin centre are grossly distorted from that of an optimal tetrahedron value (109.5°). As a consequence, the angles involving the butyl groups are widened to an average of 122° (Table 4.11). However, the angle associated with Cl atom is compressed to an average of 95°. These distortions are probably due to the steric influence of both the dibutyl and acnaphthyl groups attached to the tin centre.

Table 4.11 Bond angles [°] categorising the geometry around Sn in **14** and **15**.

Angles around the Sn atom	**14**	**15**
C(1)-Sn(1)-C(13)	123.83(14)	113.7(3)
C(1)-Sn(1)-Cl(1)	96.77(9)	96.89(18)
C(13)-Sn(1)-Cl(1)	94.34(10)	97.6(3)
C(1)-Sn(1)-C(17)	114.16(13)	122.6(3)
C(13)-Sn(1)-C(17)	118.30(14)	120.5(3)
C(17)-Sn(1)-Cl(1)	98.33(10)	93.5(2)

The conformation of both structures (AAB-A) may be a dominant factor in the packing of these molecules and the intermolecular interactions seen within the crystal. In **14** and **15** the hydrogen atoms from both the acenaphthene and the attached phenyl rings interact with centroids of further

phenyl rings from different molecules. In both compounds the H atoms of C11 and C12 interact with the centroids of a separate molecule. Due to the orientation of the second molecule the C11 and C12 H atoms can interact with the centroids of the first molecule resulting in a back interaction (Figure 4.25). However, there is no C12-H···centroid (Cg) interaction seen in a similar analogue substituted with $SnPh_3$ (**7-9**). In addition to that, both compounds show weak C-H···Cl H bonding due to the close proximity of the Cl and an adjacent C-H group from a neighbouring acenaphthene molecule.

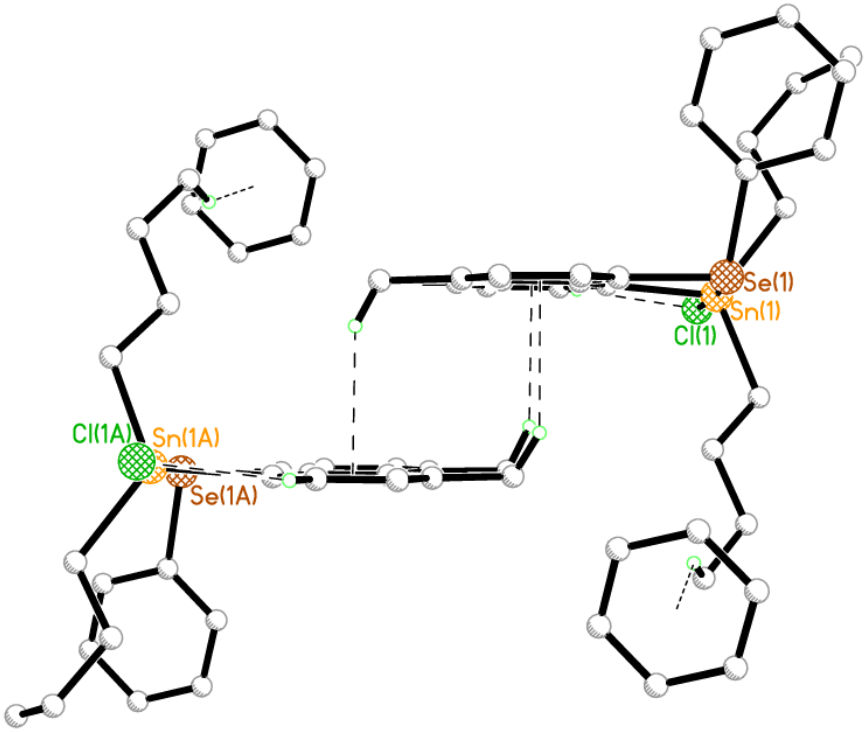

Figure 4.25 H- Centroid interactions within the structure of **14**.[10,11]

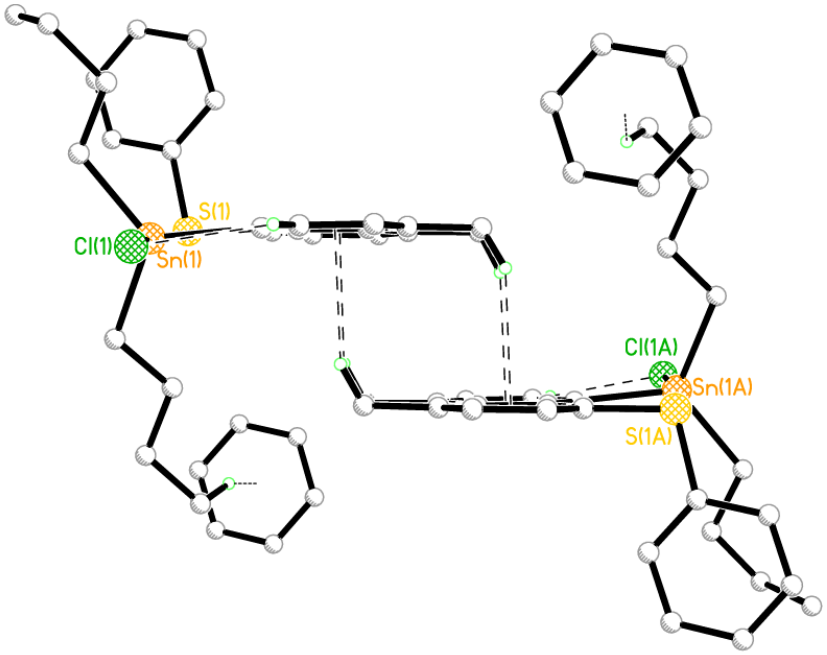

Figure 4.26 H- Centroid interactions within the structure of **15**.[10,11]

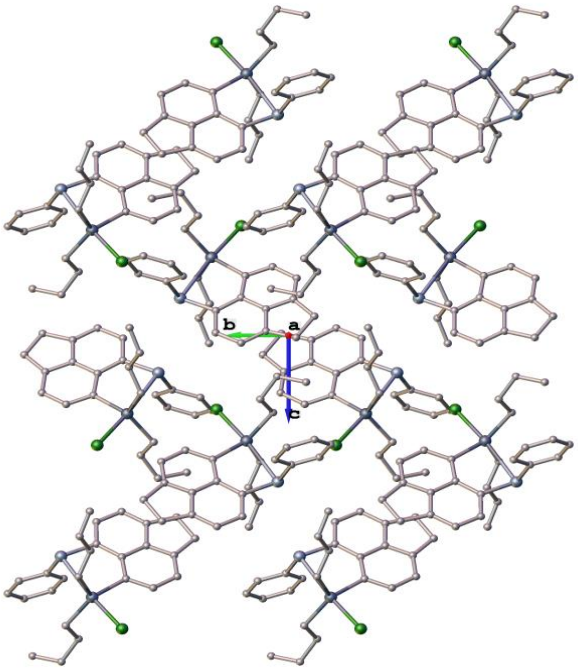

Figure 4.27 Packing in **14**.

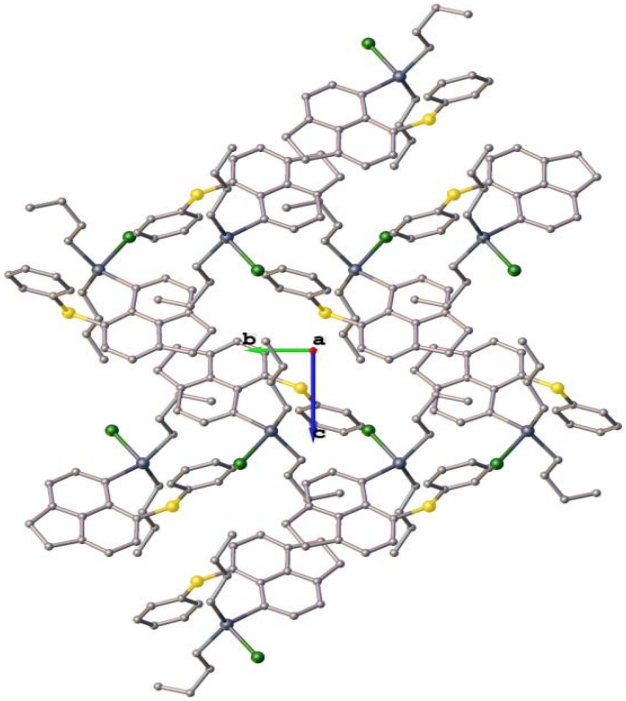

Figure 4.28 Packing in **15**.

Section 5

Synthesis and Structural Study of 5-bromo-6-(ethylsulfanyl) acenaphthenes

To understand the impact of the size of the chalcogen group and tin moieties on acenaphthene distortion we synthesised novel *peri*-substituted 5-bromo-6-(ethylsulfanyl)acenaphthene as a precursor to further react with tin chlorides. In this section, the synthesis and structural features of 5-bromo-6-(ethylsulfanyl)acenaphthene will be discussed followed by a comparison with a similar, previously reported, naphthalene analogue (1-bromo-8-(ethylsulfanyl)naphthalene (**16B**)) [5].

Synthesis

5-bromo-6-(ethylsulfanyl)acenaphthene (**16**) was synthesised by reacting 5,6-dibromoacenaphthene with one equivalent of *n*-butyllithium at −78 °C in diethyl ether, followed by subsequent addition of diethyl disulfide [34% yield (**16**); Scheme 4.6]. Compound **16** was characterised by elemental analysis, ^{1}H, ^{13}C and mass spectrometry.

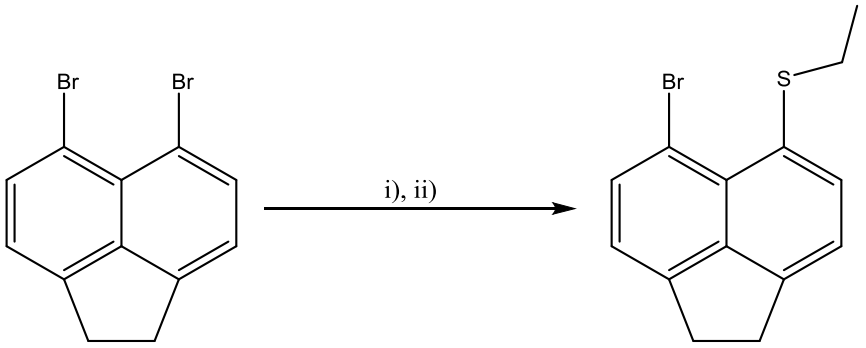

Scheme **4.6** The preparation of 5-bromo-6-(ethylsulfanyl)acenaphthene **16** from the 5,6-dibromoacenaphthene Conditions: i) *n*BuLi (1 equiv), Et_2O, -78 ºC, 1 h; ii) EtSSEt(1 equiv), Et_2O, 78 ºC, 30 min.

X ray investigations

Crystals for **16** were obtained by diffusion of hexane into a saturated solution of the product in dichloromethane (DCM), suitable for characterization by X-ray crystallography; the data refined in the *C2/c* space group (R1 = 6.56% (**16**)). Compound **16** crystallises with only one molecule in the asymmetric unit (Figures 4.29). Selected interatomic distances, angles and torsion angles are listed in Table 4.12, further crystallography data for **16** can be found in Appendix 3.

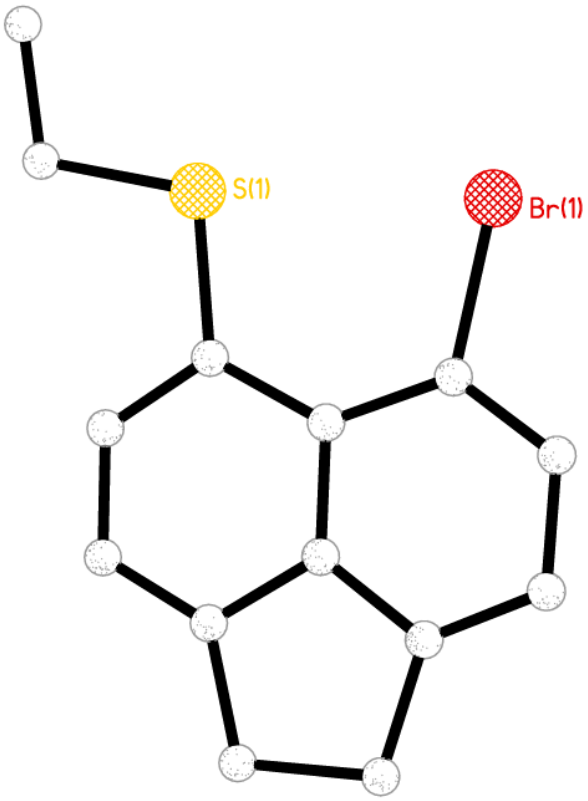

Figure 4.29 The crystal structure of *5-bromo-6-(ethylsulfanyl)acenaphthene* **16** (hydrogen atoms omitted for clarity).

Steric strain induced by introducing atoms or groups at the *peri*-positions on the naphthalene framework, is relieved by deformation of carbon skeleton.[5,13] The ideal naphthalene ring is perfectly planar with all internal angles approximately 120°.[3] The exocyclic bonds sit parallel to each other with a separation of 2.5 Å.[3] However, introducing the ethylene linker at the 1,2-positions of acenaphthene naturally reduces the planarity of the naphthalene ring system. Upon substitution, deformation of the naphthalene framework is accompanied by in- and out-of-plane distortions and deviation of the exocyclic bonds.

Comparing the intramolecular S···Br distances it can be noticed that the *peri*-distance in **16** is slightly larger than in the naphthalene analogue **16B** (**16** 3.190(3) Å, **16B** 3.056(2) Å). The reason for this is the introduction of the ethylene linker in acenaphthene, which reduces the planarity of the carbon system[1]. However, the *peri*-distance is still well within the van der Waals radii of S and Br (3.65 Å).

Table 4.12 Selected bond lengths (Å) and angles (°) for **16** and **16B**.

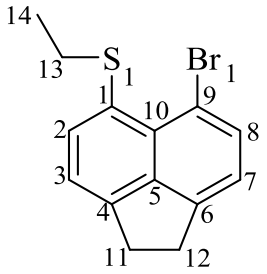

16

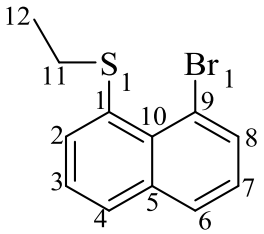

16B

Peri-region-distances		
S(1)···Br(1)	**3.190(3)**	**3.056(2)**
Σr_{vdW} - S···Br[a]	0.46	0.594
$\%r_{vdW}$[a]	87	84

Br(1)-C(9)	1.911(7)	1.901(6)
S(1)-C(1)	1.796(6)	1.770(6)
Acenaphthene bond lengths		
C(1)-C(2)	1.383(10)	1.365(9)
C(2)-C(3)	1.415(9)	1.403(10)
C(3)-C(4)	1.354(9)	1.348(9)
C(4)-C(5)	1.433(10)	1.395(9)
C(5)-C(10)	1.420(9)	1.446(8)
C(5)-C(6)	1.403(8)	1.443(9)
C(6)-C(7)	1.380(10)	1.312(9)
C(7)-C(8)	1.416(9)	1.398(8)
C(8)-C(9)	1.367(9)	1.371(9)
C(9)-C(10)	1.428(10)	1.443(8)
C(10)-C(1)	1.439(9)	1.419(8)
C(4)-C(11)	1.511(9)	-
C(11)-C(12)	1.529(11)	-
C(12)-C(6)	1.524(9)	-
Peri-region bond angles		
Br(1)-C(9)-C(10)	123.3(5)	124.5(4)
C(1)-C(10)-C(9)	131.2(6)	128.8(5)
S(1)-C(1)-C(10)	122.2(5)	121.2(4)
Σ of bay angles	**376.7(9)**	**374.5(8)**
Splay angle[b]	16.7	14.5
C(4)-C(5)-C(6)	110.8(6)	119.5(5)
In and out-of-plane displacement		
S(1)	-0.027(1)	0.040(1)
Br(1)	0.050(1)	0.010(1)
C:(6)-(5)-(10)-(1)	179.6	-179.2(5)
C:(4)-(5)-(10)-(9)	-178.5	-178.4(6)

[a] van der Waals radii used for calculations: rvdW(S) 1.80 Å, rvdW (Br) 1.85 Å, Splay angle: Σ of the three bay region angles – 360.

In both analogues the *peri*-atoms show minor out-of-plane deviations with S(1) sitting -0.027(1) Å below the mean acenaphthene plane in **16** and Br(1) lying 0.050(1) Å above the plane. Conversely,

both atoms in the naphthalene derivative **16B** are located above the plane (S +0.040(1) Å and Br +0.010(1) Å).

The increase in *peri*-distance observed in the acenaphthene compound **16** is accompanied by an increase in the bay region angles [**16** 376.7(9)°] indicating slightly greater in-plane distortion occurs in **16** compared to **16B [**374.5(8) °]. Further, distortion is observed in **16** by looking at the central acenaphthene torsion angles associated with the C5-C10 bond which deviate slightly from 180° (C: (4)-(5)-(10)-(9) -178.5°, C: (6)-(5)-(10)-(1) 179.6°).

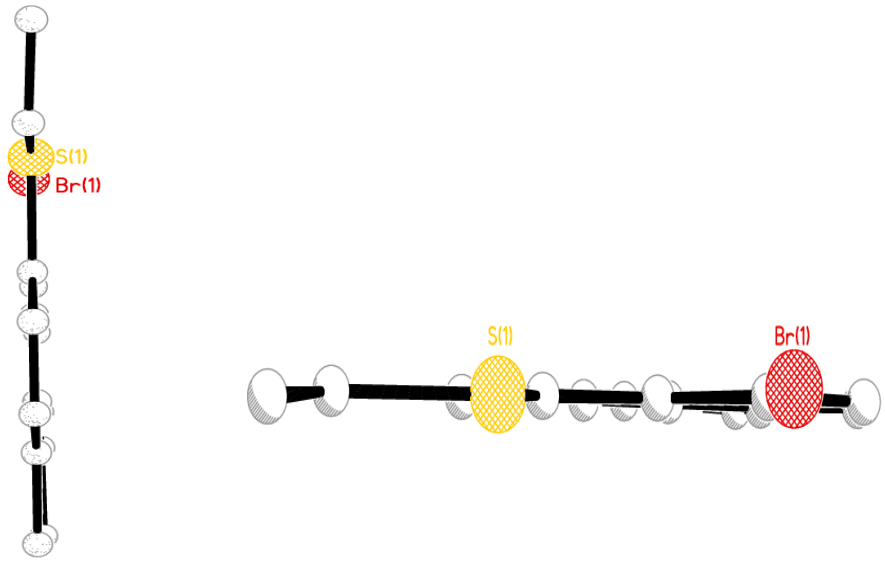

Figure 4.30 compounds **16** showing the planarity of the acenaphthene backbone.

The molecules of acenaphthene **16** pack in a back-to-back overlay arrangement with neighbouring rings rotated by 180° in comparison to one another, allowing for a significant overlap for π-π interactions to occur. The shortest intermolecular Centroid···Centroid distance is 3.7426 Å.

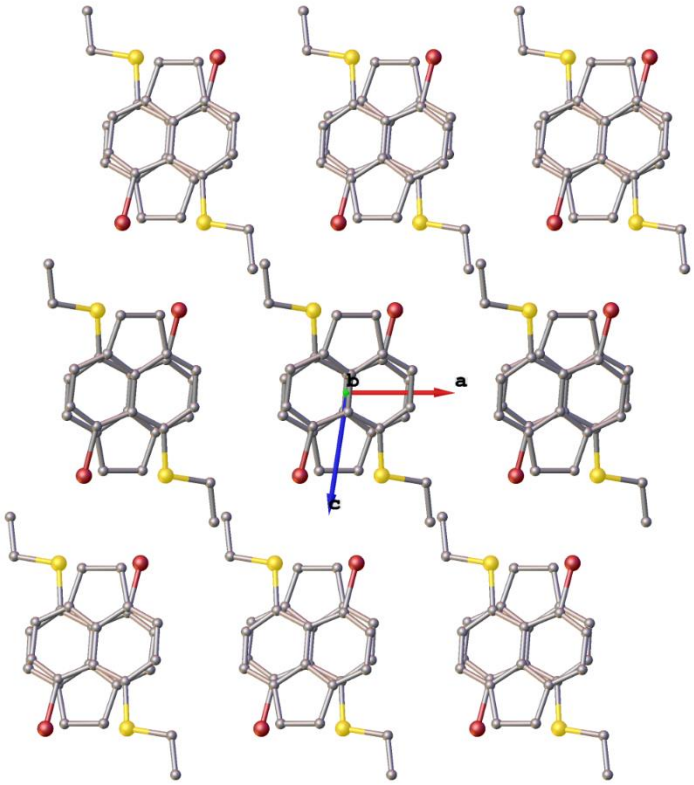

Figure 4.31 Packing in **16**.

Section 6

Synthesis and Structural Study of 5-bromo-6-(ethylsulfanyl) acenaphthenes

This section focuses on the synthesis and structural deviations of acenaphthenes substituted by less sterically demanding SEt and Bu_2Cl groups versus the more sterically crowded SEt and Ph_3Sn moieties.

Synthesis

6-ethylsulfanylacenaphth-5-yl-dibutylltin chloride (**17**) and 6-ethylsulfanylacenaphth-5-yl-triphenyltin (**18**) were synthesized by reacting 5,6-dibromoacenaphthene with a single equivalent of *n*-butyllithium at −78 °C in diethyl ether, followed by subsequent addition of $SnBu_2Cl$ and $SnPh_3Cl$, respectively [yield: 53% (**17**), 48 % (**18**); Scheme 4.7 and 4.8]

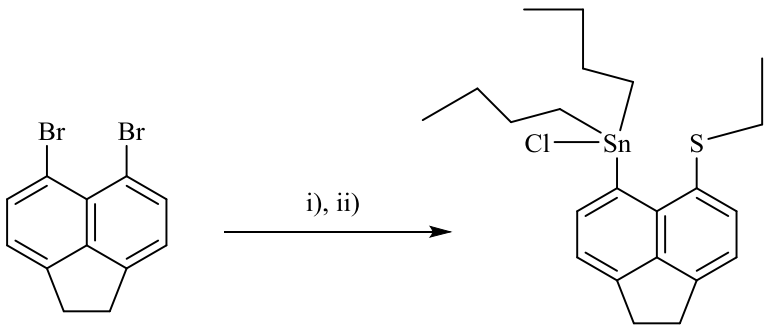

Scheme 4.7. The preparation of 6-ethylsulfanylacenaphth-5-yl-dibutylltin chloride **17.** Conditions: i) *n*BuLi (1 equiv), Et_2O, -78 ºC, 1 h; ii) $SnBu_2Cl_2$ (**17**) (1 equiv), Et_2O, 78 ºC, 30 min.

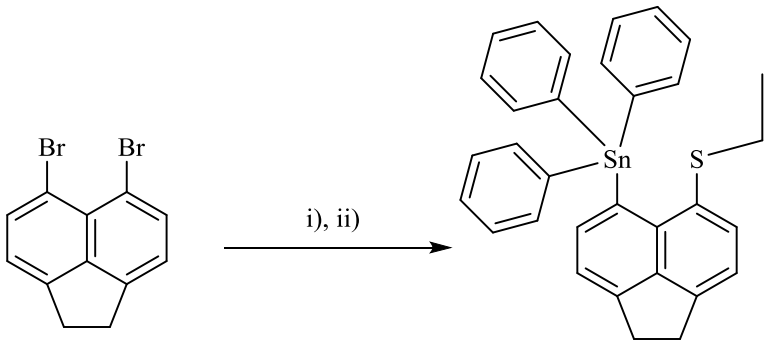

Scheme 4.8. The preparation of 6-ethylsulfanylacenaphth-5-yl-triphenyltin **18**. Conditions: i) *n*BuLi (1 equiv), Et_2O, -78 ºC, 1 h; ii) $SnPh_3Cl$ (**18**) (1 equiv), Et_2O, 78 ºC, 30 min.

X ray investigations

Crystals for **17** suitable for X-ray crystallography were obtained by recrystallisation from tetrahydrofuran (THF) at -30 °C; crystallising in the *Pbcn* space group (R1 = 4.02%). Suitable single crystals for **18** were obtained by diffusion of hexane into a saturated solution of the compound in dichloromethane; crystallising in the *Pbcn* space group (R1 = 5.93%). Both compounds crystallise with only one molecule in the asymmetric unit (Figures 4.32, 4.33), however each the molecule contains one disordered CH_3 group over symmetry elements and refined with half occupancy. Selected interatomic distances, angles and torsion angles are listed in Table 4.13, refinement data can be found in Appendix 3.

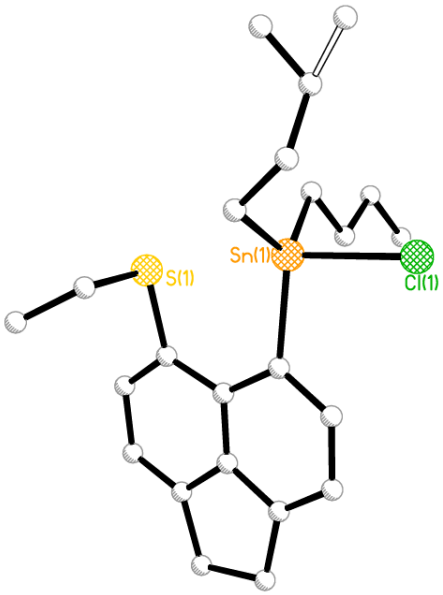

Figure 4.32 The crystal structure of *6-ethylsulfanylacenaphth-5-yl-dibutyltin chloride* **17** (hydrogen atoms omitted for clarity).

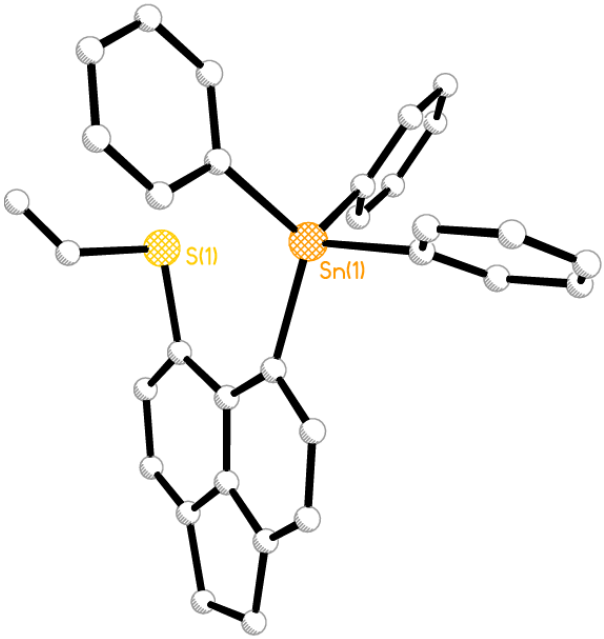

Figure 4.33 The crystal structure of *6-ethylsulfanylacenaphth-5-yl-dibutyltin chloride* **18** (hydrogen atoms omitted for clarity).

The structural differences between **17** and **18** can best be described by comparing the *peri*-distances between the Sn group and SEt, in-plane distortions, out-of-plane deflections of the substituents, and buckling of acenaphthene ring.

It has previously been shown that the amount of distortion occurring in chalcogen substituted systems, away from the optimal acenaphthene geometry, is related to the size of the substituent bound to the chalcogen atom.[3,5,12,13] Both compounds **17** and **18** show a reduction in steric hindrance operating in the *peri*-region compared to SPh analogues **14** and **7,** as displayed by the decreased geometrical distortion of these molecules. In **17** and **18**, one of the *peri*-positions is occupied by the less sterically demanding SEt substituent (compared to SPh in analogous **14** and **7**) and thus the *peri*-distances are notably shorter than for SPh analogues. They do, however, naturally increase as the bulkiness of the Sn group increases from $SnBu_2$ to $SnPh_3$ [**17** 2.98(2) Å, **18** 3.23(2) Å], but the *peri*-separations are still well within the sum of the van der Waals radii of the Sn and S atoms (3.97 Å).

Table 4.13 Selected bond lengths (Å) and angles (°) for **17** to **18**.

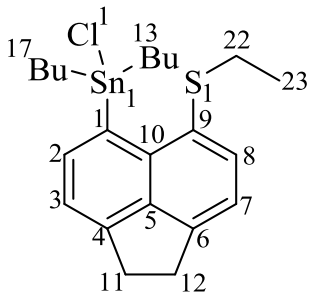

17

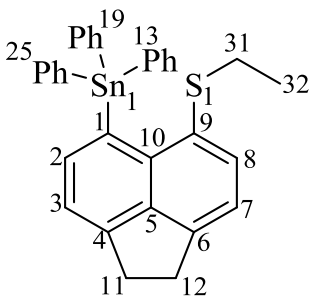

18

Peri-region-distances		
S(1)···Sn(1)	**2.98(2)**	**3.23(2)**
Σr_{vdW} - S(1)···Sn[a]	0.99	0.74
$\%r_{vdW}$[a]	75	81
S(1)-C(9)	1.785(4)	1.769(10)
Sn(1)-C(1)	2.164(4)	2.149(6)
Acenaphthene bond lengths		
C(1)-C(2)	1.382(7)	1.372(9)
C(2)-C(3)	1.426(6)	1.399(10)
C(3)-C(4)	1.376(8)	1.363(12)
C(4)-C(5)	1.413(7)	1.390(12)
C(5)-C(10)	1.419(6)	1.433(11)
C(5)-C(6)	1.428(8)	1.395(11)
C(6)-C(7)	1.364(8)	1.354(19)
C(7)-C(8)	1.426(6)	1.415(19)
C(8)-C(9)	1.399(8)	1.381(10)
C(9)-C(10)	1.420(8)	1.432(11)
C(10)-C(1)	1.438(8)	1.432(8)
C(4)-C(11)	1.528(7)	1.513(14
C(11)-C(12)	1.551(9)	1.500(17)
C(12)-C(6)	1.527(6)	1.514(19)
Peri-region bond angles		
S(1)-C(9)-C(10)	120.2(4)	121.4(5)
C(1)-C(10)-C(9)	127.9(4)	128.1(6)
Sn(1)-C(1)-C(10)	121.7(4)	126.1(6)
Σ of bay angles	**369.8(7)**	**375.6(10)**

Splay angle[b]	9.8	15.6
C(4)-C(5)-C(6)	112.0(4)	113.5(9)
In and out-of-plane displacement		
S(1)	+0.342(1)	-0.261(1)
Sn(1)	-0.229(1)	+0.495(1)
C:(6)-(5)-(10)-(1)	-176.0(4)	177.5(6)
C:(4)-(5)-(10)-(9)	-177.1(4)	175.4(6)

[a] van der Waals radii used for calculations: rvdW(S) 1.80 Å, rvdW (Sn) 2.17 Å, Splay angle: Σ of the three bay region angles – 360.

In each compound (**17** and **18)** the steric constrain induced by the tin and sulfur functionalities is released by deviation of the exocyclic bonds via both out-of-plane and in-plane displacements and augmented by deformation of the acenaphthene skeleton. In both of the compounds, the S atom is tilted in one direction from the mean plane and the Sn atom to the other side of the plane (Figure 4.34). This type of deviation may have a greater impact on the acenaphthene backbone. Furthermore, Sn deviates rather drastically from the mean plane by 0.495(1) Å in **18**, this may be due to steric crowding from the Ph groups bound to Sn, causing the additional distortion from the plane.

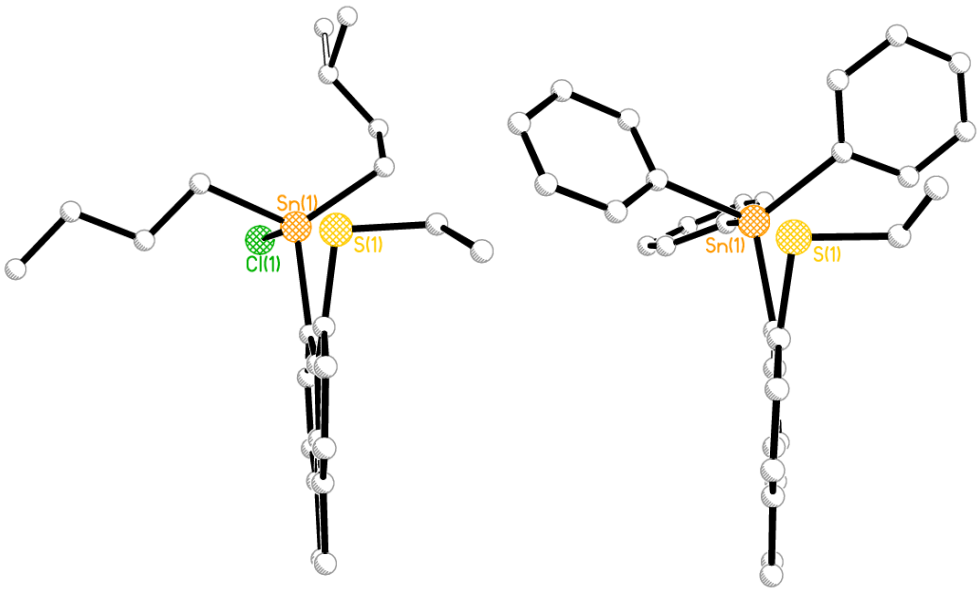

Figure 4.34 The structures of compounds **17** and **18** showing the planarity of the acenaphthene backbone.

Further distortion is achieved by in-plane deviation of the angles in the bay region which sum to 369.8(7)° (**17**) and 375.6(10)° (**18**). Lastly, the acenaphthene ring distortions of the dihedral angle C:(6)-(5)-(10)-(1) is larger in **17** but the C:(4)-(5)-(10)-(9) angle is less distorted compared to **18** (Table 4.13).

A non-covalent 3c-4e type interaction seems possible in both compounds since the Sn···S distances are shorter than the sum of the van der Waals radii of two atoms (3.97 Å) and there is a *quasi*-linear three body fragment in each compound; S···Sn-Cl (173.31°) for **17** and S···Sn-C_{Ph} (171.58°) for **18** (Figure 4.35).

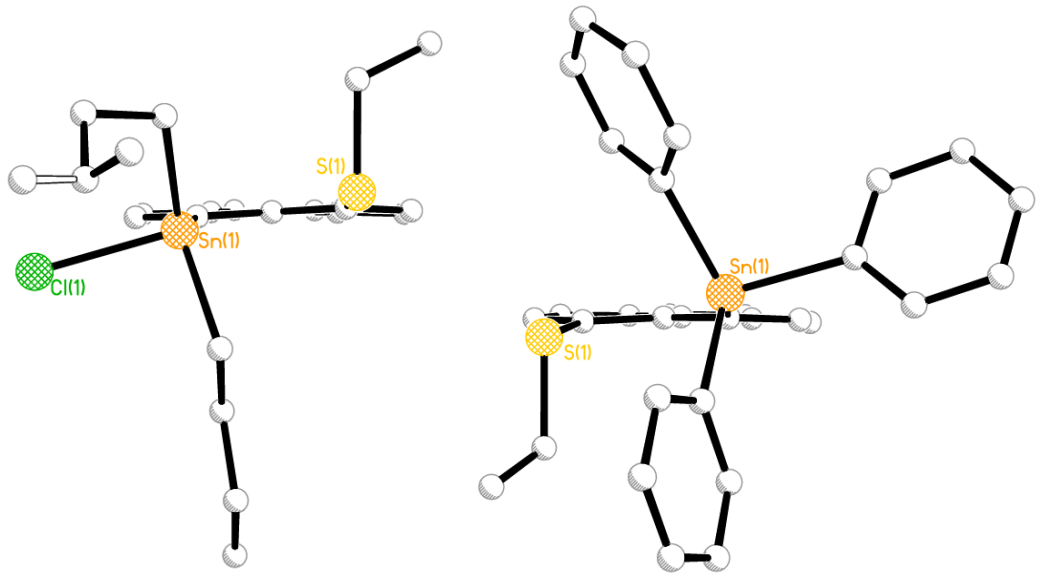

Figure 4.35 The structures of compounds **17** and **18** showing the linear arrangement of the substituents.

In both compounds **17** and **18**, the molecules pack one on top of the other with a 180° rotation of the acenaphthene ring (Figure 4.36 and 4.37), with **18** showing "butterfly type" packing due to the orientation of phenyl groups. There is no π-π stacking observed in either compound as the closest ring systems are 3.90 Å apart.

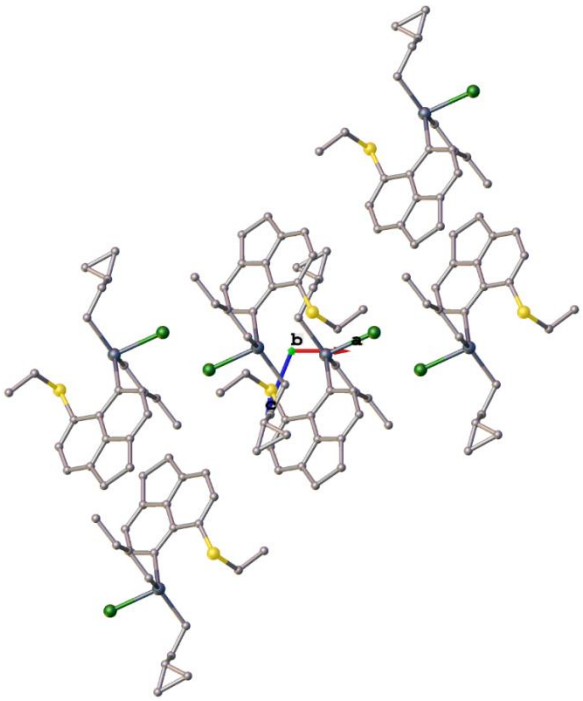

Figure 4.36 Packing in **17**.

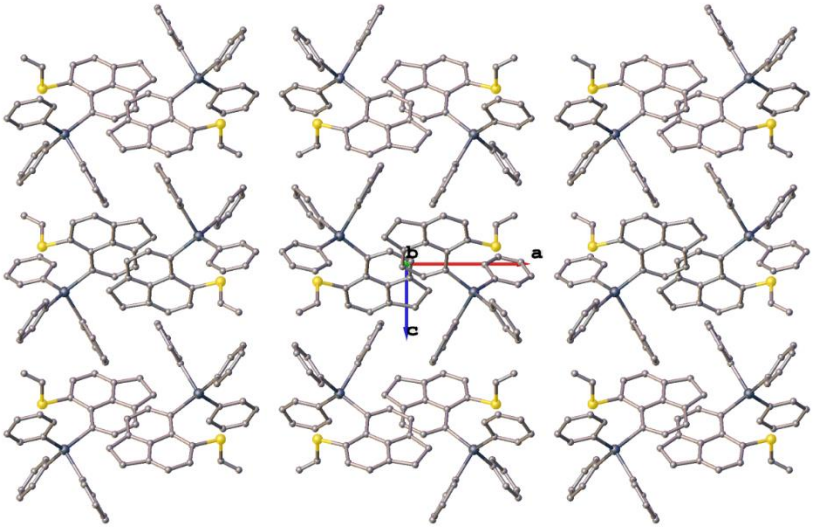

Figure 4.37 Packing in **18**.

Conclusion

A series of mixed tin-chalcogen *peri*-substituted acenaphthenes have been prepared and crystallographically characterised. It has been found that even subtle changes in the *peri*-substituents can cause significant changes in the amount of distortion of the acenaphthene backbone. In **7-18**, the *peri*-distance increases as the size of the chalcogen atoms and Sn moieties increases. Therefore the largest *peri*-distance occurred in $SnPh_3$/TePh substituent (**9**) and the smallest *peri*-distance occurred in $SnCl_2$/SPh (**12**).

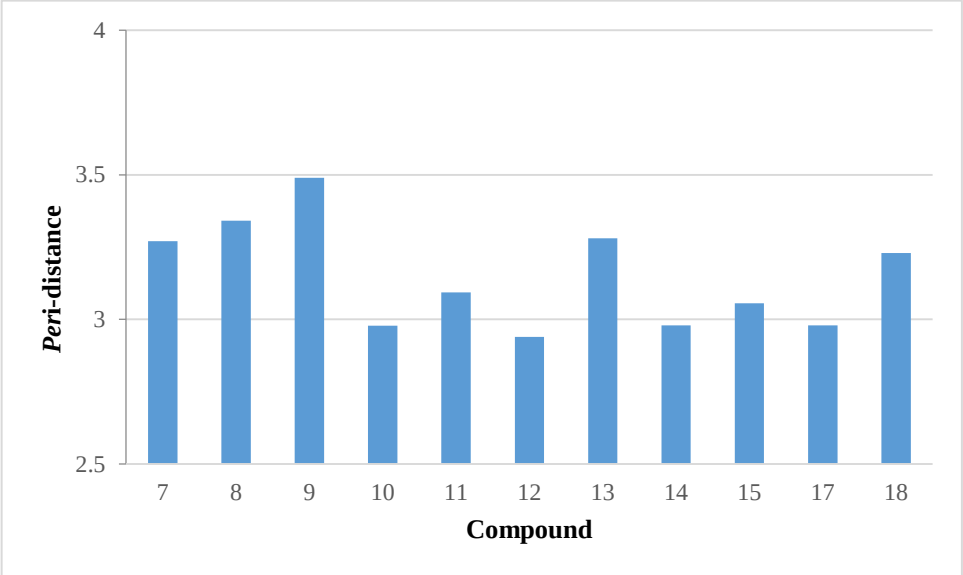

Figure 4.38 Graph of Sn(1)···E(1) *peri*-distances for **7-18**.

In all of the compounds, at least one Sn-C_R/Sn-Cl bond align along the acenaphthene plane producing a *quasi*-linear Y-Sn···E three-body fragment which provides the correct geometry for promoting delocalization of the chalcogen lone-pair to an anti-bonding σ*(Sn−Y) orbital to form a donor-acceptor three-center four-electron (3c-4e) type interaction.

Experimental

All experiments were carried out under an oxygen- and moisture-free nitrogen atmosphere using standard Schlenk techniques and glassware. Reagents were obtained from commercial sources and used as received. Dry solvents were collected from a MBraun solvent system. 5,6-Dibromoacenaphthene was prepared following standard literature procedures starting from acenaphthene.[2-4] Elemental analyses were performed by the London Metropolitan University School of Human Sciences Microanalysis Service. ^{1}H and ^{13}C NMR spectra were recorded on a Bruker Avance 300 MHz spectrometer. ^{77}Se and ^{119}Sn NMR spectra were recorded on a JEOL GSX 270 MHz spectrometer. δ(H) and δ(C) were referenced to external Me_4Si. δ(Se) and δ(Sn) were referenced to external Me_2Se and Me_4Sn, respectively. Assignments of ^{13}C and ^{1}H NMR spectra were made with the help of H−H COSY and HSQC experiments, performed on a Bruker Avance 300 MHz spectrometer. All NMR shifts (δ) are given in ppm, and all couplings (J) are given in Hz.

6-(phenylsulfanyl)acenaphth-5-yl-triphenyltin (7):

To a solution of 5-bromo-6-(phenylsulfanyl)acenaphthene (0.5 g, 1.5 mmol) in dry diethyl ether (30 mL) at −78 °C was added dropwise a 2.5 M solution of *n*-butyllithium in hexane (0.6 mL, 1.5 mmol). The reaction mixture was stirred for 1 h after which a solution of Ph_3SnCl (0.58 g, 1.5 mmol) in diethyl ether (15 mL) was added dropwise to the reaction solution at -78 °C. After stirring at this temperature for 30 min, the reaction mixture was allowed to warm to room temperature and then stirred overnight. The solvent was evaporated *in vacuo* and toluene was added. The mixture was filtered and the toluene was removed *in vacuo*. Colourless crystals were obtained after recrystallization from THF/hexane via the diffusion method (0.31g, 39%); m.p. 170-

172 °C; elemental analysis (Found: C, 70.7; H, 4.5. Calc. for $C_{36}H_{28}SnS$: C, 70.7; H, 4.6; S, 5.2%); ^{1}H NMR (270 MHz, $CDCl_3$, Me_4Si): δ 7.80 (1 H, d, $^{3}J_{HH}$ = 6.7, $^{3}J_{HSn}$ = 66/63, Acenap 4-H), 7.75 (1 H, d, $^{3}J_{HH}$ = 7.2, Acenap 7-H), 7.60-7.40 (6 H, m, Sn*Ph-o*), 7.37 (1 H, d, $^{3}J_{HH}$ = 7.2, Acenap 8-H), 7.34 (1 H, d, $^{3}J_{HH}$ = 6.7, Acenap 3-H), 7.29-7.18 (9 H, m, Sn*Ph-m,p*), 6.92-6.78 (3 H, m, S*Ph-m,p*), 6.38-6.33 (2 H, m, S*Ph-o*), 3.57-3.45 (4 H, m, Acenap 2xCH_2); ^{13}C NMR (67.9 MHz, $CDCl_3$, Me_4Si): δ 150.0(q), 149.1(q), 142.6(q), 142.5(s, $^{2}J_{CSn}$ = 46), 141.1(q), 139.9(q), 138.8(s), 137.4(s, $^{2}J_{CSn}$ = 36), 130.8(q), 128.7(s), 128.6(s, $^{2}J_{CSn}$ = 52), 128.5(s), 127.0(s), 126.8(q), 125.0(s), 121.0(s), 120.9(s), 30.6(s, Acenap CH$_2$), 30.5(s, Acenap CH$_2$); ^{119}Sn NMR (100.76 MHz, $CDCl_3$, Me_4Sn): δ -130.1(s).

6-(phenylselanyl)acenaphth-5-yl-triphenyltin (8):

Experimental as for compound **7** but with [Acenap(Br)(SePh)] (0.5 g, 1.3 mmol), 2.5 M *n*-butyllithium (0.5 mL, 1.3 mmol) and Ph_3SnCl (0.50 g, 1.3 mmol). Colourless crystals were obtained after recrystallization from THF/hexane via the diffusion method (0.42 g, 44%); m.p. 188-190 °C; elemental analysis (Found: C, 65.8; H, 4.2. Calc. for $C_{36}H_{28}SnSe$: C, 65.7; 4.3 H, %); ^{1}H NMR (270 MHz, $CDCl_3$, Me_4Si): δ 7.88 (1 H, d, $^{3}J_{HH}$ = 5.5, Acenap 4-H), 7.76 (1 H, d, $^{3}J_{HH}$ = 6.8, Acenap-7-H), 7.48-7.27 (6 H, m, Sn*Ph-o*), 7.27-7.05 (11 H, m, Acenap 3,8-H, Sn*Ph-m,p*) 6.87-6.78 (1 H, m, Se*Ph-p*), 6.76-6.68 (2 H, m, Se*Ph-m*), 6.36-6.28 (2 H, m, Se*Ph-o*), 3.45-3.32 (2 H, m, Acenap 2xCH_2); ^{13}C NMR (67.9 MHz, $CDCl_3$, Me_4Si): δ 150.2(q), 149.2(q), 143.3(q), 142.8(s, $^{2}J_{CSn}$ = 45), 141.2(q), 140.9(s), 140.3(q), 137.3(s, $^{2}J_{CSn}$ = 36), 136.0(q), 133.2(q), 129.0(s), 128.8(s), 128.6(s), 128.5(s), 125.6(s), 124.9(q), 121.1(s), 120.9(s), 30.7(s, Acenap CH$_2$), 30.5(s, Acenap CH$_2$); ^{119}Sn NMR (100.76 MHz, $CDCl_3$, Me_4Sn): δ -134.8(s, $^{4}J_{SnSe}$ = 68); ^{77}Se NMR (51.4 MHz, $CDCl_3$, Me_2Se): δ 318.2 (s, $^{4}J_{SeSn}$ = 64).

6-(phenyltelluro)acenaphth-5-yl-triphenyltin (9):

Experimental as for compound **7** but with [Acenap(Br)($SnPh_3$)] (0.5 g, 1.3 mmol), 2.5 M *n*-butyllithium (0.5 mL, 1.3 mmol) and PhTeTePh (0.53 g, 1.3 mmol). Red crystals were obtained after recrystallization from THF/hexane via the diffusion method (0.48 g, 79%); m.p. 223-225 °C; elemental analysis (Found: C, 61.0; H, 4.0. Calc. for $C_{26}H_{31}SnSeCl$: C, 61.2; H, 4.0%); ^{1}H NMR (270 MHz, $CDCl_3$, Me_4Si): δ 8.21 (1 H, d, $^{3}J_{HH}$ = 7.1, Acenap 7-H, 7.70 (1 H, d, $^{3}J_{HH}$ = 6.9, $^{3}J_{HSn}$ = 66/63, Acenap 4-H, 7.59-7.24 (9 H, m, Sn*Ph-o,p*), 7.24-7.08 (6 H, m, Sn*Ph-m*), 6.96-6.88 (1 H, m, Te*Ph-p*), 6.82-6.74 (2 H, m, Te*Ph-m*), 6.64-6.58 (2 H, m, Te*Ph-o*), 3.43-3.30 (4 H, m, Acenap 2xCH_2); ^{13}C NMR (67.9 MHz, $CDCl_3$, Me_4Si): δ 147.1(s), 143.4(s), 137.4(s), 137.4(s), 134.1(s), 129.2(s), 129.2(s), 129.1(s), 128.7(s), 128.6(s), 121.7(s), 30.8(s, Acenap *C*H_2), 30.4(s, Acenap *C*H_2); ^{119}Sn NMR (100.76 MHz, $CDCl_3$, Me_4Sn): δ -146.8; ^{125}Te NMR (85.2 MHz, $CDCl_3$, Me_2Te): δ 507.1.

6-(phenylsulfanyl)acenaphth-5-yl-diphenyltin chloride (10):

Experimental as for compound **7** but with [Acenap(Br)(SPh)] (0.5 g, 1.5 mmol), 2.5 M *n*-butyllithium (0.6 mL, 1.5 mmol) and Ph_2SnCl_2 (0.52 g, 1.5 mmol). Colourless crystals were obtained after recrystallization from THF/hexane via the diffusion method (0.33 g, 40%); m.p. 75-77 °C; ^{1}H NMR (270 MHz, $CDCl_3$, Me_4Si): δ 8.84 (1 H, d, $^{3}J_{HH}$ = 7.0, $^{3}J_{HSn}$ = 77/74, Acenap 4-H), 7.91 (1 H, d, $^{3}J_{HH}$ = 8.3, Acenap 7-H), 7.66 (1 H, d, $^{3}J_{HH}$ = 7.0, Acenap 3-H), 7.61-7.53 (6 H, m, Sn*Ph-o*), 7.52-7.47 (1 H, m, Acenap 8-H), 7.29-7.09 (9 H, m, Sn*Ph-m,p*), 6.97-6.91 (1 H, m, S*Ph-p*), 6.88-6.80 (2 H, m, S*Ph-m*), 6.49-6.43 (2 H, m, S*Ph-o*), 3.61-3.49 (4 H, m, Acenap 2xCH_2); ^{13}C NMR (67.9 MHz, $CDCl_3$, Me_4Si): δ 150.7(q), 149.7(q), 141.3(s, $^{2}J_{CSn}$ = 39), 141.2(q), 140.7(q), 139.1(q), 136.3(q), 135.8(s, $^{2}J_{CSn}$ = 47), 132.8(q), 129.1(s), 128.7(s), 128.5(s), 127.6(s), 127.2(s),

126.1(s), 123.5(q), 121.5(s), 121.1(s), 30.2(s, Acenap *C*H_2), 30.4(s, Acenap *C*H_2); ^{119}Sn NMR (100.76 MHz, $CDCl_3$, Me_4Sn): δ -116.9.

6-(phenylselanyl)acenaphth-5-yl-diphenyltin chloride (11):

Experimental as for compound **7** but with [Acenap(Br)(SePh)] (0.5 g, 1.3 mmol), 2.5 M *n*-butyllithium (0.5 mL, 1.3 mmol) and Ph_2SnCl_2 (0.45 g, 1.3 mmol). Colourless crystals were obtained after recrystallization from THF/hexane via the diffusion method (0.31 g, 39%); m.p. 152-154 °C; elemental analysis (Found: C, 58.4; H, 3.9. Calc. for $C_{26}H_{31}SnSeCl$: C, 58.4; H, 3.8%); ^{1}H NMR (270 MHz, $CDCl_3$, Me_4Si): δ 8.75 (1 H, d, $^3J_{HH}$ = 7.1, $^3J_{HSn}$ = 78/75, Acenap 4-H), 7.72 (1 H, d, $^3J_{HH}$ = 7.1, Acenap 7-H), 7.51 (1 H, d, $^3J_{HH}$ = 7.1, Acenap 3-H), 7.49-7.42 (6 H, m, Sn*Ph-o*), 7.29-6.99 (10 H, m, Acenap 8-H, Sn*Ph-m,p*), 6.89-6.78 (1 H, m, Se*Ph-p*), 6.74-6.63 (2 H, m, Se*Ph-m*), 6.35-6.24 (2 H, m, Se*Ph-o*), 3.48-3.34 (4 H, m, Acenap 2xCH_2); ^{13}C NMR (67.9 MHz, $CDCl_3$, Me_4Si): δ 151.3(q), 150.1(q), 146.9(q), 142.8(q), 142.2(s), 141.3(q), 137.3(s), 136.1(s), 133.2(q), 132.0(q), 130.9(s), 129.6(s), 129.0(s), 128.8(s), 126.8(s), 122.5(q), 121.9(s), 120.4(s), 30.8(s, Acenap *C*H_2), 30.6(s, Acenap *C*H_2); ^{119}Sn NMR (100.76 MHz, $CDCl_3$, Me_4Sn): δ -131.3(s, $^4J_{SnSe}$ = 163); ^{77}Se NMR (51.4 MHz, $CDCl_3$, Me_2Se): δ 267.5(s, $^4J_{SeSn}$ = 160).

Bis(6-(phenylsulfanyl)acenaphthen-5-yl)dichlorostannane (12):

Experimental as for compound **7** but with [Acenap(Br)(SPh)] (0.5 g, 1.5 mmol), 2.5 M *n*-butyllithium (0.6 mL, 1.5 mmol) and $SnCl_4$ (0.39 g, 1.5 mmol) in hexane (15 mL). Colourless crystals were obtained after recrystallization out of THF/hexane via diffusion method (0.1 g, 19%); m.p. 224-226 °C; Elemental analysis (Found: C, 54.7; H, 4.2. Calc. for $C_{28}H_{26}SnS_2Cl_2$: C, 54.6; H, 4.3%); ^{1}H NMR (270 MHz, $CDCl_3$, Me_4Si): δ 8.54 (2 H, d, $^3J_{HH}$ = 7.1, $^3J_{HSn}$ = 120/114, Acenap 2x4-H), 7.53 (2 H, d, $^3J_{HH}$ = 7.1, $^4J_{HSn}$ = 26, Acenap 2x3-H), 7.45 (2 H, d, $^3J_{HH}$ = 7.1, Acenap 2x7-

H), 7.21 (2 H, d, $^{3}J_{HH}$ = 7.1, Acenap 2x8-H), 6.77-6.66 (6 H, m, S*Ph-m,p*), 6.23-6.20 (4 H, m, S*Ph-o*), 3.52-3.37 (8 H, m, Acenap 4xCH_2); ^{13}C NMR (67.9 MHz, $CDCl_3$, Me_4Si): δ 150.5(q), 149.6(q), 140.8(q), 137.9(s), 137.2(s), 137.1(q), 136.1(q), 135.7(q), 128.6(s), 126.6(s), 126.3(q), 122.1(s), 121.7(s), 120.8(s), 30.9(s, Acenap 2xCH$_2$), 26.0(s, Acenap 2xCH$_2$); ^{119}Sn NMR (100.76 MHz, $CDCl_3$, Me_4Sn): δ -192.04(s).

Bis(6-(phenylsulfanyl)acenaphthen-5-yl)diphenylstannane (13):

Experimental as for compound **7** but with [Acenap(Br)(SPh)] (0.5 g, 1.5 mmol), 2.5 M *n*-butyllithium (0.6 mL, 1.5 mmol) and Ph_2SnCl_2 (0.52 g, 1.5 mmol). Colourless crystals were obtained after recrystallization from THF/hexane via the diffusion method (0.26 g, 44%); m.p. 220-222 °C; elemental analysis (Found: C, 72.4; H, 4.6. Calc. for $C_{48}H_{36}SnS_2$: C, 72.5; H, 4.6%;); ^{1}H NMR (270 MHz, $CDCl_3$, Me_4Si): δ 8.71 (2 H, d, $^{3}J_{HH}$ = 7.1, $^{3}J_{HSn}$ = 63/60, Acenap 2x4-H), 7.66 (2 H, d, $^{3}J_{HH}$ = 7.2, Acenap 2x7-H), 7.55 (2 H, d, $^{3}J_{HH}$ = 7.0, Acenap 2x3-H), 7.49-7.42 (4 H, m, Sn*Ph-o*), 7.30-7.23 (2 H, m, Acenap 2x8-H), 7.17-7.07 (6 H, m, S*Ph-m,p*), 6.87-6.77 (2 H, m, S*Ph-p*), 6.77-6.68 (4 H, m, S*Ph-m*), 6.40-6.31 (4 H, m, S*Ph-o*), 3.53-3.38 (8 H, m, Acenap 4xCH_2); ^{13}C NMR (67.9 MHz, $CDCl_3$, Me_4Si): δ 151.0(q), 149.9(q), 142.0(q), 141.6(s), 140.1(q), 138.0(s), 136.7(q), 136.2(s), 131.5(q), 129.1(s), 128.9(s), 128.7(s), 127.6(s), 126.5(s), 125.3(q), 121.9(s), 121.0(s), 30.9(s, Acenap 2xCH$_2$), 30.8(s, Acenap 2xCH$_2$); ^{119}Sn NMR (100.76 MHz, CDCl3, Me4Sn): δ .-166.9(s).

6-(phenylsulfanyl)acenaphth-5-yl-dibutyltin chloride (14):

Experimental as for compound **7** but with [Acenap(Br)(SPh)] (0.5 g, 1.5 mmol), 2.5 M *n*-butyllithium (0.6 mL, 1.5 mmol) and Bu_2SnCl_2 (0.46 g, 1.5 mmol). Colourless crystals were obtained after recrystallization from THF/hexane via the diffusion method (0.18 g, 23%); m.p. 82-

84 °C; elemental analysis (Found: C, 58.8; H, 5.8. Calc. for $C_{26}H_{31}SnSCl$: C, 58.9; H, 5.9%); ^{1}H NMR (270 MHz, $CDCl_3$, Me_4Si): δ 8.44 (1 H, d, $^{3}J_{HH}$ = 7.0, $^{3}J_{HSn}$ = 64/61, Acenap 4-H), 7.70 (1 H, d, $^{3}J_{HH}$ = 6.4, Acenap 7-H), 7.44 (1 H, d, $^{3}J_{HH}$ = 7.8, Acenap 3-H), 7.27 (1 H, d, $^{3}J_{HH}$ = 7.1, Acenap 8-H), 7.12-7.02 (3 H, m, S*Ph-m,p*), 6.84-6.81 (2 H, m, S*Ph-o*), 3.40-3.30 (4 H, m, Acenap 2xCH_2), 1.50-1.25 (8 H, m, 2xCH_2-α, 2xCH_2-β), 1.04 (4 H, h, $^{3}J_{HH}$ = 7.3, 2xCH_2-γ), 0.65 (6 H, t, $^{3}J_{HH}$ = 7.2, 2xCH_3-δ); ^{13}C NMR (67.9 MHz, $CDCl_3$, Me_4Si): δ 151.1(q), 148.8(q), 140.9(s), 139.7(q), 137.8(s), 137.3(q), 132.9(q), 129.7(s), 129.5(s), 127.3(s), 126.3(q), 123.6(q), 121.7(s), 120.7(s), 30.8(s, Acenap *C*H_2), 30.6(s, Acenap *C*H_2), 28.7(s, 2x*C*H_2-β), 26.9(s, 2x*C*H_2-γ), 22.1(s, 2x*C*H_2-α), 13.9(s, 2x*C*H_3-δ); ^{119}Sn NMR (100.76 MHz, $CDCl_3$, Me_4Sn): δ 3.56.

6-(phenylselanyl)acenaphth-5-yl-dibutyltin chloride (15):

Experimental as for compound **7** but with [Acenap(Br)(SePh)] (0.5 g, 1.3 mmol), 2.5 M *n*-butyllithium (0.5 mL, 1.3 mmol) and Bu_2SnCl_2 (0.39 g, 1.3 mmol). Yellow crystals were obtained after recrystallization from THF/hexane via the diffusion method (0.46 g, 62%); m.p. 108-110 °C; elemental analysis (Found: C, 54.3; H, 5.3. Calc for $C_{26}H_{31}SnSeCl$: C, 54.2; H, 5.4%); ^{1}H NMR (270 MHz, $CDCl_3$, Me_4Si): δ 8.50 (1 H, d, $^{3}J_{HH}$ = 7.1, $^{3}J_{HSn}$ = 64/61, Acenap 4-H), 7.83 (1 H, d, $^{3}J_{HH}$ = 7.1, Acenap 7-H), 7.43 (1 H, d, $^{3}J_{HH}$ = 7.0, Acenap 3-H), 7.25 (1 H, d, $^{3}J_{HH}$ = 7.2, Acenap 8-H), 7.12-7.03 (3 H, m, Se*Ph-m,p*), 6.88-6.81 (2 H, m, Se*Ph-o*), 3.45-3.33 (4 H, m, Acenap 2xCH_2), 1.50-1.25 (8 H, m, 2xCH_2-α, 2xCH_2-β), 1.05 (4 H, h, $^{3}J_{HH}$ = 7.4, 2xCH_2-γ), 0.65 (6 H, t, $^{3}J_{HH}$ = 7.2, 2xCH_3-δ); ^{13}C NMR (67.9 MHz, $CDCl_3$, Me_4Si): δ 151.3(q), 148.9(q), 141.4(s), 141.2(q), 140.2(q), 139.6(s), 135.3(q), 133.1(q), 130.0(s), 128.8(s), 127.5(s), 122.1(q), 121.6(s), 120.8(s), 30.7(s, Acenap *C*H_2), 30.6(s, Acenap *C*H_2), 28.9(s, 2x*C*H_2-β), 26.9(s, 2x*C*H_2-γ), 23.2(s, 2x*C*H_2-α), 13.9(s, 2x*C*H_3-δ); ^{119}Sn NMR (100.76 MHz, $CDCl_3$, Me_4Sn): δ -12.4.

5-bromo-6-ethylsulfanylacenaphthene (16):

To a solution of 5,6-dibromoacenaphthene (10.0 g, 32.0 mmol) in dry diethyl ether (60 mL) at −78 °C was added dropwise a 2.5 M solution of *n*-butyllithium in hexane (12.1 mL, 32.2 mmol). The reaction mixture was stirred for 1 h after which a solution of diethyl disulfide (4 mL, 32.2 mmol) in diethyl ether (10 mL) was added dropwise to the reaction solution at -78 °C. After stirring at this temperature for 30 min, the reaction mixture was allowed to warm to room temperature and then washed with a 0.1 N NaOH solution (2 x 50 mL). The organic layer was the collected, dried over $MgSO_4$ and concentrated under reduced pressure to afford the title compound as a yellow powder. Colourless crystals were obtained after recrystallization from DCM/hexane via the diffusion method (2.99 g, 34%); m.p. 79-81 °C; elemental analysis (Found: C, 57.4; H, 4.3. Calc. for $C_{14}H_{13}SBr$: C, 57.3; H, 4.5%); ^{1}H NMR (270 MHz, $CDCl_3$, Me_4Si): δ 7.70 (1 H, d, $^3J_{HH}$ = 7.4, Acenap 4-H), 7.49 (1 H, d, $^3J_{HH}$ = 7.4, Acenap 7-H), 7.18 (1 H, d, $^3J_{HH}$ = 7.4, Acenap 8-H), 7.05 (1 H, d, $^3J_{HH}$ = 7.4, Acenap 3-H), 3.29 (4 H, s, Acenap 2xCH_2), 2.96 (2 H, q, $^3J_{HH}$ = 7.5, S$CH_2$$CH_3$,), 1.33 (3 H, t, $^3J_{HH}$ = 7.5, SCH_2CH_3,); ^{13}C NMR (67.9 MHz, $CDCl_3$, Me_4Si): δ 146.9(q), 145.7(q), 141.9(q), 135.9(q), 135.0(s), 132.0(s), 129.6(q), 120.7(s), 120.2(s), 114.5(q), 30.4(s, S$CH_2$$CH_3$), 30.1(s, Acenap CH_2), 30.0(s, Acenap CH_2), 13.6(s, SCH_2CH_3).

6-ethylsulfanylacenaphth-5-yl-dibutyltin chloride (17):

Experimental as for compound **7** but with [Acenap(Br)(SEt)] (0.5 g, 1.7 mmol), 2.5 M *n*-butyllithium (0.7 mL, 1.7 mmol) and Bu_2SnCl_2 (0.52 g, 1.7 mmol). Colourless crystals were obtained after recrystallization out of THF at -30 °C (0.43 g, 53%); m.p. 54-56 °C; elemental analysis (Found: C, 55.0; H, 6.4. Calc. for $C_{22}H_{31}ClSSn$: C, 54.9; H, 6.5%); ^{1}H NMR (270 MHz, $CDCl_3$, Me_4Si): δ 8.43 (1 H, d, $^3J_{HH}$ = 7.1, $^3J_{HSn}$ = 66/63, Acenap 4-H), 7.66 (1 H, d, $^3J_{HH}$ = 7.1, Acenap 7-H), 7.38 (1 H, d, $^3J_{HH}$ = 6.8, Acenap 3-H), 7.22 (1 H, d, $^3J_{HH}$ = 7.5, Acenap 8-H), 3.42-

3.29 (4 H, m, Acenap 2xCH_2), 2.68 (2 H, q, $^3J_{HH}$ = 6.8, SCH_2CH$_3$), 1.17 (3 H, t, $^3J_{HH}$ = 7.7, SCH$_2$CH_3), 1.77-1.53 (8 H, m, 2xCH_2-α, 2xCH_2-β), 1.25 (4 H, h, $^3J_{HH}$ = 7.0, 2xCH_2-γ), 0.77 (6 H, t, $^3J_{HH}$ = 7.7, 2xCH_3-δ); ^{13}C NMR (67.9 MHz, CDCl$_3$, Me$_4$Si): δ 150.0(q), 148.7(q), 140.8(q), 140.4(s), 138.8(q), 136.6(s), 133.6(q), 125.5(q), 121.4(s), 119.7(s), 33.7(s, SCH_2CH$_3$), 30.7(s, Acenap CH$_2$), 30.6(s, Acenap CH$_2$), 28.9(s, $^1J_{CSn}$ = 31.0, 2xCH$_2$-β,), 27.1(s, 2xCH$_2$-α), 22.3(s, 2xCH$_2$-γ), 14.3(s, SCH$_2$$CH_3$), 14.0(s, 2x$CH_3$-δ); ^{119}Sn NMR (100.76 MHz, CDCl$_3$, Me$_4$Sn): -12.3(s).

6-ethylsulfanylacenaphth-5-yl-triphenyltin (18):

Experimental as for compound **7** but with [Acenap(Br)(SEt)] (0.5 g, 1.7 mmol), 2.5 M *n*-butyllithium (0.7 mL, 1.7 mmol) and Ph$_3$SnCl (0.66 g, 1.7 mmol). Colourless crystals were obtained after recrystallization from DCM/hexane via diffusion method (0.39 g, 41%) m.p. 120-122 °C; elemental analysis (Found: C, 68.2; H, 5.1. Calc. for C$_{22}$H$_{31}$ClSSn: C, 68.2; H, 5.0%); ^{1}H NMR (270 MHz, CDCl$_3$, Me$_4$Si): δ 8.06 (1 H, d, $^3J_{HH}$ = 6.9, Acenap 4-H), 7.93 (1 H, d, $^3J_{HH}$ = 7.2, Acenap 7-H), 7.90-7.65 (6 H, m, Sn*Ph-o*), 7.60-7.30 (11 H, m, Acenap 3,8-H, Sn*Ph-m,p*), 3.61-3.42 (4 H, m, Acenap 2xCH_2), 2.21 (2 H, q, $^3J_{HH}$ = 7.4, SCH_2CH$_3$), 0.83 (3 H, t, $^3J_{HH}$ = 7.4, SCH$_2$CH_3); ^{13}C NMR (67.9 MHz, CDCl$_3$, Me$_4$Si): δ 148.8(q), 148.5(q), 143.5(q), 141.8(s), 140.9(q), 139.4(q), 139.1(q), 137.4(s, $^2J_{CSn}$ = 35 Hz), 136.7(s), 132.0(q), 131.2(q), 128.8(s), 128.5(s), 120.5(s), 119.9(s), 33.3(s, SCH_2CH$_3$), 30.9(s, Acenap CH$_2$), 30.6(s, Acenap CH$_2$), 14.5(s, SCH$_2$$CH_3$); ^{119}Sn NMR (100.76 MHz, CDCl$_3$, Me$_4$Sn): δ -135.5(s).

X-ray Structure Analysis

X-ray crystal structures for **9**, **10**, **16** and **18** were determined at −148(1) °C on the St Andrews Robotic Diffractometer,[15] a Rigaku ACTOR-SM, Saturn 724 CCD area detector with graphite-

monochromated Mo Kα radiation (λ = 0.710 73 Å). Data for compound **17** was collected at −180(1) °C by using a Rigaku MM007 high brilliance RA generator (Mo Kα radiation, confocal optic) and Mercury CCD system. Data for compounds **7**, **8**, **11**, **12**, **13**, **14** and **15** were collected at −148(1) °C on a Rigaku SCX Mini instrument with graphite-monochromated Mo Kα radiation (λ = 0.710 73 Å). All data had intensities corrected for Lorentz, polarization, and absorption. The data for the complexes was collected and processed using CrystalClear[14,15] (Rigaku). The structures were solved by Patterson or direct methods and expanded using Fourier techniques. Non-hydrogen atoms were refined anisotropically, and hydrogen atoms were refined using a riding model. All calculations were performed using CrystalStructure[16] and SHELXL-97[17].

References

1. F. R. Knight, A. L Fuller, M Bühl, A. M. Z Slawin and J. D. Woollins., *Inorg. Chem*. 2010, **49**, 7577.

2. L. M. Diamond, F. R. Knight, K. S. Athukorala Arachchige, R. A. M. Randall, M. Bühl, A. M. Z. Slawin and J. D. Woollins., *Eur. J. Inorg. Chem*. 2014, 1512.

3. L. K. Aschenbach, F. R. Knight, R. A. M. Randall, D. B. Cordes, A. Baggott, M. Bühl, A. M. Z. Slawin and J. D. Woollins, *Dalton Trans*., 2012, **41**, 3141.

4. F. R. Knight, R. A. M. Randall, K. S. Athukorala Arachchige, L. Wakefield, J. M. Griffin, S. E. Ashbrook, M. Bühl, A. M. Z. Slawin and J. D. Woollins, *Inorg. Chem.*, 2012, **51**, 11087.

5. F. R. Knight, "*Synthesis and structural studies of group 16 peri-substituted naphthalenes and related compounds*" Ph.D. Thesis, University of St Andrews, 2010.

6. M.-L. Lechner, K. S. Athukorala Arachchige, R. A. M. Randall, F. R. Knight, M. Bühl, A. M. Z. Slawin and J. D. Woollins, *Organometallics*, 2012, **31**, 2922.

7. P. Wawrzyniak, A. M. Z. Slawin, J. D. Woollins and P. Kilian, *Dalton Trans*., 2010, **39**, 85.

8. W. Nakanishi, S. Hayashi and S. Toyota, *J. Org. Chem.*, 1998, **63**, 8790.

9. W. Nakanishi and S. Hayashi, *J. Org. Chem*., 2002, **67**, 38.

10. A. L. Spek, *J. Appl. Cryst.*, 2003**, 36**, 7.

11. A. L. Spek, *Acta Crystallogr. Sect. D*, 2009**, 65**, 148.

12. A. L. Fuller, "*Synthesis and Structural studies of group 16 peri-substituted naphthalenes and related compounds*", Ph.D. Thesis, University of St Andrews, 2010.

13. M. W. Stanford, F. R. Knight, K. S. Athukorala Arachchige, P. S. Camacho, S. E Ashbrook, M. Bühl, A. M. Z. Slawin, J. D. Woollins., *Dalton Trans*,. 2014, **43**, 6548.

14. CrystalClear 2.0; Rigaku Corp., Tokyo, 2010. *CrystalClear Software User's Guide; Molecular Structure Corp.*: The Woodlands, TX, 2011.

15. J. W. P. Flugrath, *Acta Crystallogr., Sect. D*, 1999, **D55**, 1718.

16. CrystalStructure 4.0: *Crystal Structure Analysis Package; Rigaku and Rigaku/MSC*, The Woodlands, TX 77381, 200.

17. G. M. Sheldrick, *SHELX97, Acta Crystallogr., Sect. A: Fundam. Crystallogr*., 2008, **64**, 112.

Chapter 5

Sterically crowded tin-phosphines, stabilized by weak intramolecular donor-acceptor interactions

Introduction

Extensive research has been conducted on acenaphthene systems in which the *peri*-positions are occupied by large chalcogen, pnictogen and halogen congeners.[1] In these systems the bulky heteroatoms are located in close proximity, with separations shorter than the sum of their van der Waals radii, resulting in both repulsive and attractive intramolecular interactions across the *peri*-gap due to the overlap of their orbitals.[1-3]

The ability to relieve steric hindrance by forming weak or strong bonding interactions is a distinctive feature of *peri*-substituted systems and accounts for their unusual reactivity and bonding.[1,2,4,5] For compounds which are clearly non-bonded, and similarly for compounds containing a direct covalent bond, the intramolecular *peri*-interactions are well defined as either repulsive or attractive. There are, however, a number of cases where the bonding situation is less clear-cut and both weakly attractive and repulsive interactions exist simultaneously, making interpretation of the bonding situation quite challenging.[6]

There are many examples of *peri*-substituted compounds in the literature which are stabilised by weakly attractive donor-acceptor type interactions which operate between electronically different moieties across the *peri*-gap.[1,7-11] Based on the renowned donor ability of phosphines (PR_3), coupled with the electropositivity of tin, we postulated that positioning these two functionalities in close proximity, on the acenaphthene backbone could provide good systems for promoting such weakly attractive P→Sn donor-acceptor type interactions to occur.

In this chapter, we investigate how the substituents around the tin center affect the strength of the P→Sn donor-acceptor interactions in a series of mixed Sn,P acenaphthenes; Acenap(SnR_3)(P^iPr_2) (R_3 = Ph_3 **19**; Ph_2Cl **20**; Me_2Cl **21**; Bu_2Cl **22**; Cl_2Acenap(P^iPr_2) **23**; Figure 5.1).

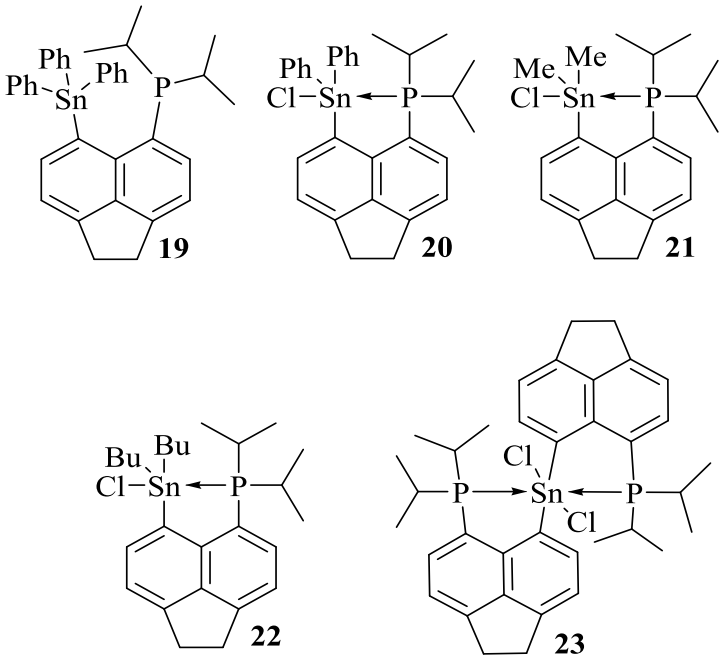

Figure 5.1 6-diisopropylphosphinoacenaphth-5-yl-tin derivatives **19**-**23**.

Synthesis

Initially, 5-bromo-6-(diisopropylphosphino)acenaphthene [Acenap(Br)(P^iPr_2)] was prepared following a previously reported literature procedure.[10] Subsequent treatment with a single equivalent of *n*-butyllithium in diethyl ether at -78 °C, afforded the air stable precursor 5-(lithio)-6-(diisopropylphosphino)acenaphthene, which when treated with the appropriate tin chloride [Ph_3ClSn, Ph_2Cl_2Sn, Me_2Cl_2Sn, Bu_2Cl_2Sn, $SnCl_4$] afforded mixed phosphorus-tin acenaphthenes [Acenap(SnR_3)(P^iPr_2)] (R_3 = Ph_3 **19**; Ph_2Cl **20**; Me_2Cl **21**; Bu_2Cl **22**; Cl_2Acenap(P^iPr_2) **23)** in moderate to good yield [yield: 72 (**1**), 65 (**2**), 46 (**3**), 93 (**4**), 71% (**5**); Scheme 5.1].

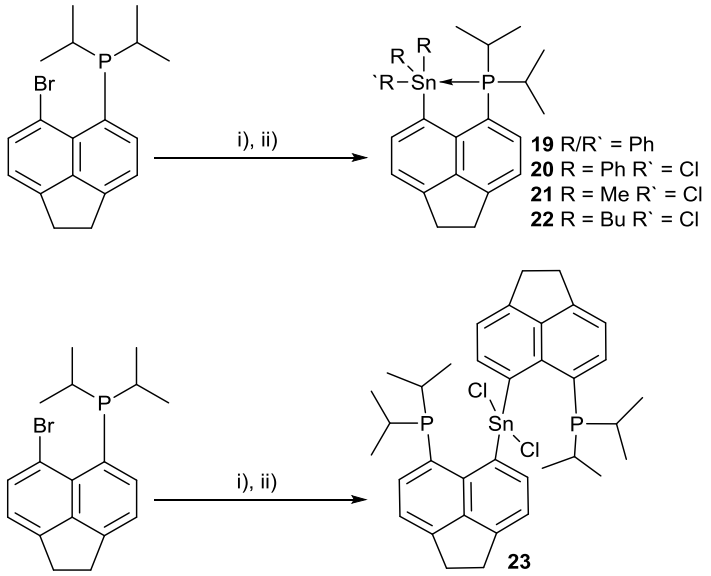

Scheme 5.1 The preparation of phosphorus-tin *peri*-substituted acenaphthenes **19**-**23**: (i) *n*BuLi (1 equiv), Et_2O, −78 °C, 2 h; (ii) Ph_3ClSn (**19**)/Ph_2Cl_2Sn (**20**)/Me_2Cl_2Sn (**21**)/Bu_2Cl_2Sn (**22**)/$SnCl_4$ (**23**) (1 equiv), Et_2O, −78 °C, 1 h; RT, 16 h.

All five compounds were characterized by ^{1}H, ^{13}C, ^{31}P and ^{119}Sn NMR and mass spectrometry, and the homogeneity of the new compounds was where possible confirmed by microanalysis. As expected, the ^{119}Sn NMR spectra for **19**-**22** all display doublets with the splitting attributed to $J(^{119}Sn,^{31}P)$ coupling. The NMR signal for tin chloride **20** (-241.0 ppm) lies notably upfield, at a much lower chemical shift, compared to the triphenyl tin analogue **19** (-183.7 ppm). In addition, within the tin chloride series, chemical shifts increase going from **20** (Ph_2Cl -241.0 ppm) to **21** (Me_2Cl –143.1 ppm) to **22** (Bu_2Cl -118.4 ppm). Due to poor solubility, no ^{31}P or ^{119}Sn NMR spectrum was obtained for tin dichloride **23**. The ^{31}P NMR spectra for tin compounds **19**-**22** display single peaks, but with satellites attributed to ^{31}P-^{119}Sn and ^{31}P-^{117}Sn coupling. Chemical shifts move downfield with a reduction in the electron density at the tin centre, with signals at -31.5 ppm (**19**), 27.3 ppm (**20**), -24.4 ppm (**21**) and -23.9 ppm (**22**).

X-ray investigations

Suitable single crystals were obtained for **19**, **22** and **23** by recrystallisation from a saturated hexane solution of the respective compound (R1 = 6.29 (**19**), 5.55 (**22**), 11.73% (**23**)). Crystals for **20** and **21** were obtained by diffusion of hexane into saturated THF and DCM solutions of the compounds, respectively (R1 = 9.99% (**20**), 8.89% (**21**)). All five compounds crystallize with only one molecule in the asymmetric unit (Figures 5.2-5.6). Selected interatomic distances, angles and torsion angles are listed in Tables 5.2-5.4, further refinement data can be found in the Appendix 3.

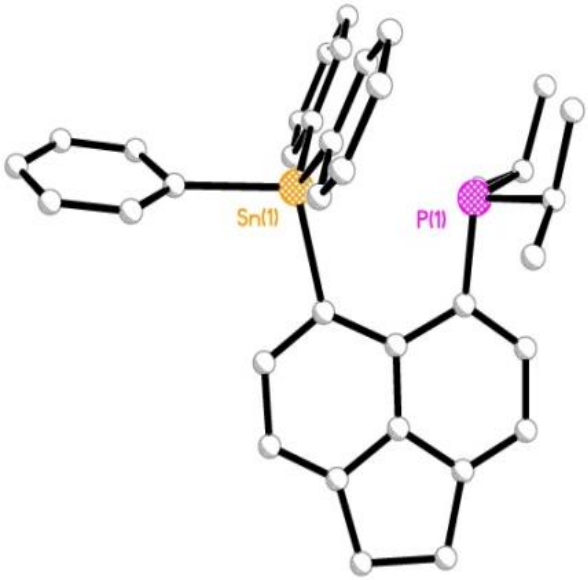

Figure 5.2 The crystal structure of *6-diisopropylphosphinoacenaphth-5-yl-triphenyltin* **19** (hydrogen atoms omitted for clarity).

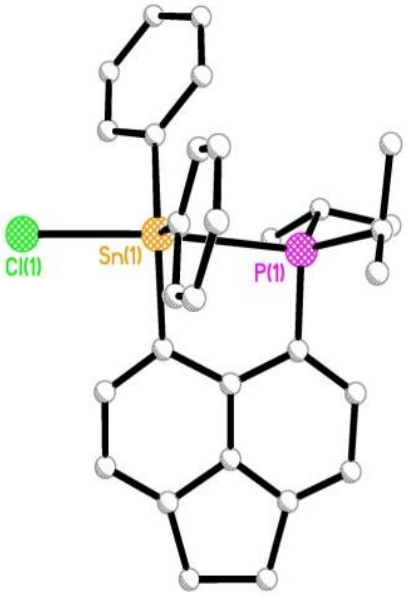

Figure 5.3 *The crystal structure of 6-diisopropylphosphinoacenaphth-5-yl-diphenyltin chloride* **20** (hydrogen atoms omitted for clarity).

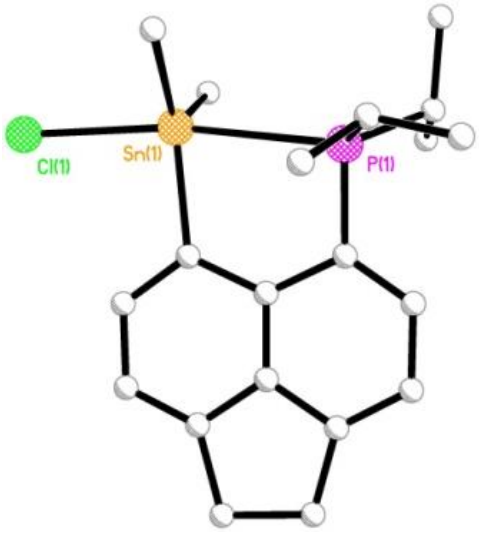

Figure 5.4 The crystal structure of *6-diisopropylphosphinoacenaphth-5-yl-dimethyltin chloride* **21** (hydrogen atoms omitted for clarity).

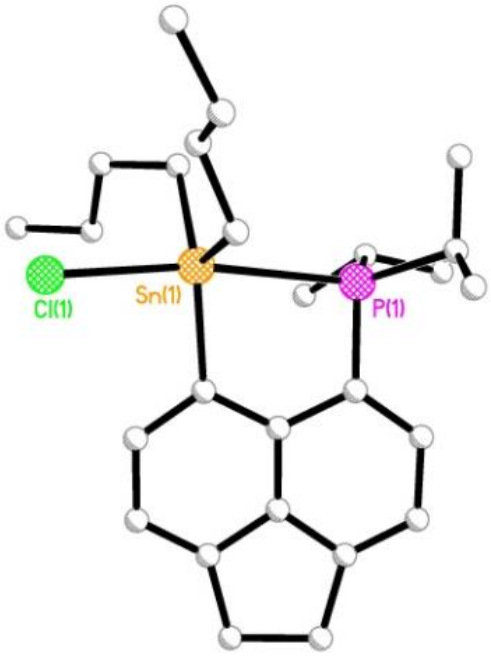

Figure 5.5 The crystal structure of *6-diisopropylphosphinoacenaphth-5-yl-dibutyltin chloride* **22** (hydrogen atoms omitted for clarity).

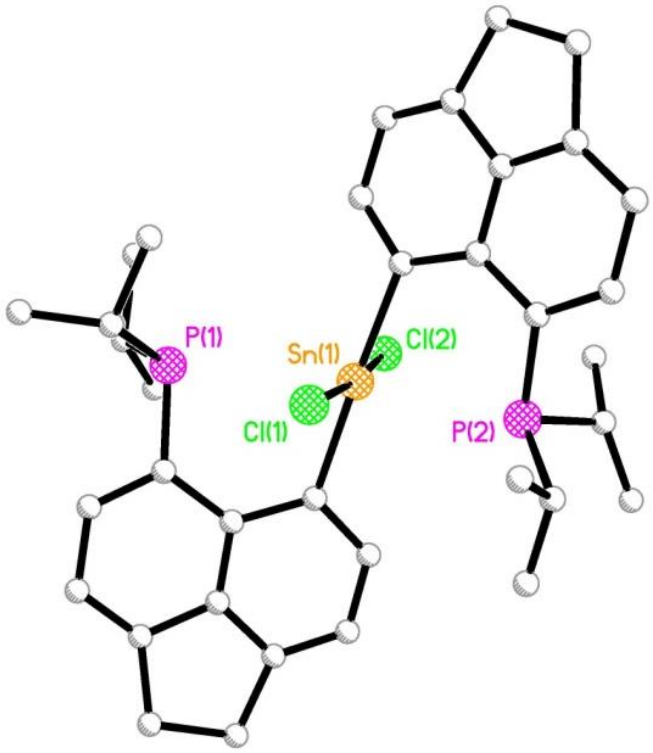

Figure 5.6 The crystal structure of *bis(6-diisopropylphosphino-5-yl)tin dichloride* **23** (hydrogen atoms omitted for clarity).

Similar to the chalcogen-tin derivatives discussed in Chapter 4, the molecular structures of the mixed tin-phosphorus systems **19**-**23** can be classified by the conformations adopted by their alkyl and aryl substituents with respect to the mean acenaphthene plane. The mono-systems **19**-**22** crystallize with similar configurations, classified as type BAA-CC for **1** and BAA-AC for **20**-**23** (Figure 4).[9,12,13]

In all four compounds, two of the Sn-C_R bonds are displaced on opposite sides and perpendicular to the mean acenaphthene plane (type A), with the last Sn-C_{Ph} bond in **19** and the Sn-Cl bonds in **20**-**22** lying parallel with the plane (type B). This affords a *quasi*-linear three-body fragment in

each case (C_{Ph}-Sn···P **19**; Cl-Sn-P **20**-**22**) with angles close to 180° (**19** 177.63(1)°, **20** 171.62(9)°, **21** 168.93(8)°, **22** 171.23(3)°). As a consequence of the phosphorus geometry and to minimize steric repulsion, the two P-C_{iPr} bonds in triphenyltin derivative **19** are displaced to opposite sides of the acenaphthene plane, each intermediate between an axial and equatorial configuration (type CC).

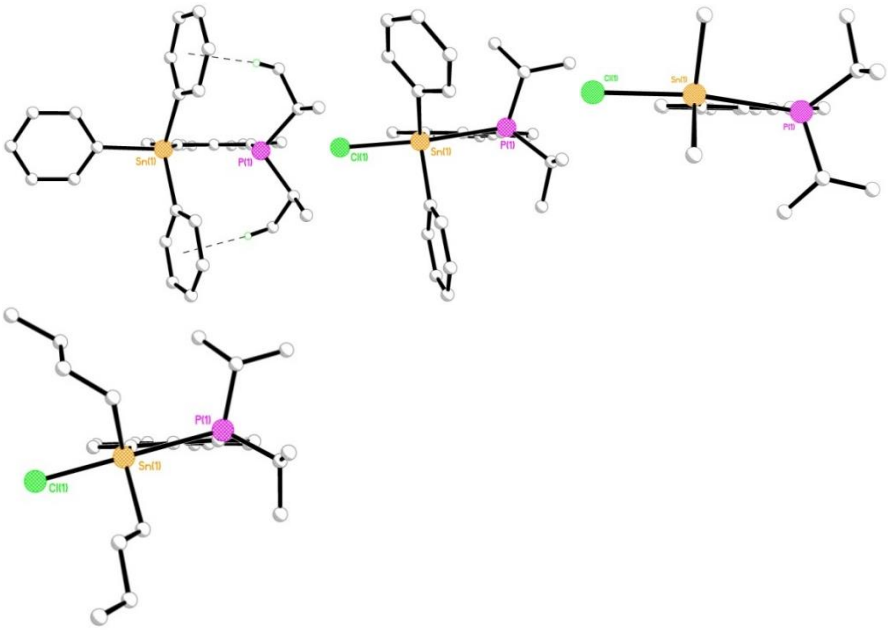

Figure 5.7 The molecular conformations of **19**-**22** showing the orientation of the substituents bound to Sn and P; **19** adopts a BAA-CC conformation with CH···π interactions between neighboring phenyl and isopropyl moieties whilst **20**-**22** adopt similar BAA-AC conformations.

This positions two H atoms, one on each ^{i}Pr moiety, in close proximity to the two phenyl groups on Sn located axially with respect the mean plane, allowing two intramolecular CH···π interactions to occur [H36B···Cg(13-18) 2.60 Å; H33A···Cg(25-30) 2.93 Å; Figure 5.7]. Whilst the phosphorus

moieties in tin chlorides **20**-**22** adopt similar conformations to **19** (type AC), no CH···π interactions are present in any of these molecules. Instead, the dominating factor controlling all four molecular conformations is the location of the phosphorus lone-pair, which in all cases points directly at the electropositive Sn center across the *peri*-gap.

Table 5.1 Torsion angles [°] categorizing the acenaphthene and ligand conformations in **19**-**23**.

1	**C(10)-C(1)-Sn(1)-C(13)**	**C(10)-C(1)-Sn(1)-C(19)**	**C(10)-C(1)-Sn(1)-C(25)**	**C(10)-C(9)-P(1) C(31)**	**C(10)-C(9)-P(1)-C(34)**
	Ph: θ_1 70.6(4) axial-A	Ph: θ_2 -179.6(4) equatorial-B	Ph: θ_3 -71.0(4) axial-A	^{i}Pr: $\theta_4$121.3(4) twist-C	^{i}Pr: θ_5 -133.6(4) twist-C
2	**C(10)-C(1)-Sn(1)-C(13)**	**C(10)-C(1)-Sn(1)-C(19)**	**C(10)-C(1)-Sn(1)-Cl(1)**	**C(10)-C(9)-P(1)-C(25)**	**C(10)-C(9)-P(1)-C(28)**
	Ph: θ_1 92.6(8) axial-A	Ph: θ_2 -75.5(8) axial-A	Cl: θ_3 -171.9(6) equatorial-B	^{i}Pr: $\theta_4$141.2(8) twist-C	^{i}Pr: θ_5 -105.2(8) axial-A
3	**C(10)-C(1)-Sn(1)-C(13)**	**C(10)-C(1)-Sn(1)-C(14)**	**C(10)-C(1)-Sn(1)-Cl(1)**	**C(10)-C(9)-P(1)-C(15)**	**C(10)-C(9)-P(1)-C(18)**
	Me: θ_1 -78.3(7) axial-A	Me: θ_2 -89.4(7) axial-A	Cl: θ_3 176.5(6) equatorial-B	^{i}Pr: θ_4-142.1(7) twist-C	^{i}Pr: θ_5 105.3(7) axial-A
4	**C(10)-C(1)-Sn(1)-C(13)**	**C(10)-C(1)-Sn(1)-C(17)**	**C(10)-C(1)-Sn(1)-Cl(1)**	**C(10)-C(9)-P(1)-C(21)**	**C(10)-C(9)-P(1)-C(24)**
	Bu: θ_1 -72.3(2) axial-A	Bu: θ_2 94.9(2) axial-A	Cl: θ_3 -165.4(2) equatorial-B	^{i}Pr: $\theta_4$148.8(2) twist-C	^{i}Pr: θ_5 -100.5(2) axial-A
5	**C(10)-C(1)-Sn(1)-C(19)**	**C(10)-C(1)-Sn(1)-Cl(1)**	**C(10)-C(1)-Sn(1)-Cl(2)**	**C(10)-C(9)-P(1)-C(13)**	**C(10)-C(9)-P(1)-C(16)**
	θ_1 160.6(10) equatorial-B	Cl: θ_2 60.7(9) twist-C	Cl: θ_3 -114.1(9) twist-C	^{i}Pr: θ_4-135.4(11) twist-C	^{i}Pr: θ_5 105.0(12) axial-A
	C(28)-C(19)-Sn(1)-C(1)	**C(28)-C(19)-Sn(1)-Cl(1)**	**C(28)-C(19)-Sn(1)-Cl(2)**	**C(28)-C(27)-P(2)-C(31)**	**C(28)-C(27)-P(2)-C(34)**

θ_6 -26.6(9) twist-C	Cl: θ_7 73.3(9) axial-A	Cl: θ_8 -111.9(9) twist-C	^{i}Pr: θ_9-141.0(12) twist-C	^{i}Pr: θ_{10} 109.6(13) axial-A

Similar to the chalcogen derivatives of Chapter 4, the *quasi*-linear alignment of the C_{Ph}-Sn···P and Cl-Sn-P three-body fragments in **19**-**22** provides a suitable geometry to promote delocalization of a phosphorus lone-pair (G) to an antibonding σ*(Sn−Y) orbital, forming a weak donor-acceptor three-centre four-electron (3c-4e) type interaction which stabilizes the molecule. In all cases Sn···P *peri*-distances are shorter than the sum of van der Waals radii of the Sn and P atoms (3.97 Å), with distances for the tin chlorides (**20** 2.815(3) Å, **21** 2.912(3) Å, **22** 2.8721(10) Å) notably smaller compared to the triphenyltin derivative (**19** 3.2511(19) Å). This suggests the donor-acceptor interactions in the tin chlorides are much stronger because of the presence of the highly electronegative chlorine atom which increases the Lewis acidity of Sn.

Table 5.2 Selected interatomic distances [Å] and angles [°] for **19**-**21**.

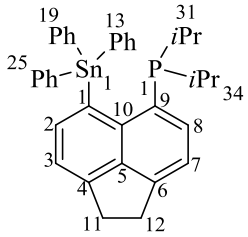

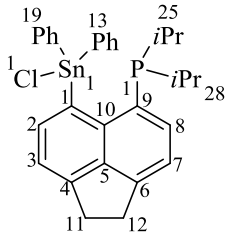

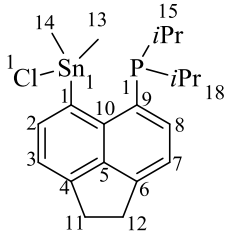

Peri-region distances	**19 $SnPh_3$**	**20 $SnPh_2Cl$**	**21 $SnMe_2Cl$**
Sn(1)···P(1)	**3.2511(19)**	**2.815(3)**	**2.912(3)**
Σr_{vdW} -Sn···P[a]	0.7189	1.155	1.058
$\%r_{vdW}$[a]	82	71	73
Sn(1)-Cl(1)	-	2.525(3)	2.626(2)
Sn(1)-C(1)	2.172(6)	2.164(11)	2.171(9)

P(1)-C(9)	1.834(6)	1.806(12)	1.820(10)
Acenaphthene bond lengths			
C(1)-C(2)	1.373(8)	1.362(16)	1.368(14)
C(2)-C(3)	1.422(8)	1.399(16)	1.400(15)
C(3)-C(4)	1.359(9)	1.383(16)	1.358(16)
C(4)-C(5)	1.409(9)	1.454(15)	1.391(14)
C(5)-C(10)	1.416(8)	1.397(14)	1.423(13)
C(5)-C(6)	1.417(9)	1.384(16)	1.403(14)
C(6)-C(7)	1.361(10)	1.339(16)	1.374(16)
C(7)-C(8)	1.412(10)	1.440(16)	1.415(17)
C(8)-C(9)	1.386(9)	1.378(17)	1.357(15)
C(9)-C(10)	1.432(9)	1.429(16)	1.445(13)
C(10)-C(1)	1.447(8)	1.458(16)	1.440(12)
C(4)-C(11)	1.515(9)	1.517(16)	1.553(15)
C(6)-C(12)	1.518(9)	1.511(15)	1.493(16)
C(11)-C(12)	1.565(10)	1.519(19)	1.521(18)
Peri-region bond angles			
Sn(1)-C(1)-C(10)	127.1(4)	119.2(7)	121.6(6)
C(1)-C(10)-C(9)	128.5(5)	128.1(9)	129.5(9)
P(1)-C(9)-C(10)	122.2(4)	116.8(9)	115.6(7)
Σ of bay angles	**377.8(8)**	**364.1(15)**	**366.7(13)**
Splay angle[b]	17.8	4.1	6.7
C(4)-C(5)-C(6)	111.3(5)	111.1(9)	112.2(9)
Out-of-plane displacement			
Sn(1)	-0.193(1)	-0.376(1)	-0.265(1)
P(1)	-0.275(1)	0.130(1)	0.142(1)
Central naphthalene ring torsion angles			
C:(6)-(5)-(10)-(1)	178.9(5)	-177.8(9)	-178.4(9)
C:(4)-(5)-(10)-(9)	-179.6(5)	-179.8(8)	179.9(9)

[a] van der Waals radii used for calculations: rvdW (Sn) 2.17 Å, rvdW (P) 1.80 Å [b] Splay angle: Σ of the three bay region angles – 360.

Table 5.2 Selected interatomic distances [Å] and angles [°] for **22-23**.

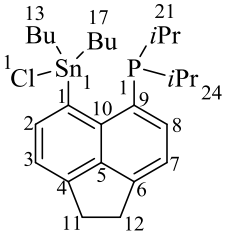

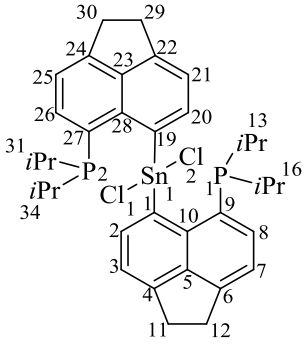

Peri-region distances	**22 $SnBu_2Cl$**	**23a $SnCl_2$**	**23b $SnCl_2$**
Sn(1)···P(1)	**2.8721(10)**	**3.141(6)**	**2.954(7)**
Σr_{vdW} -Sn···P[a]	1.0979	0.829	1.016
$\%r_{vdW}$[a]	72	79	74
Sn(1)-Cl(1)	2.5317(9)	2.625(4)	2.623(4)
Sn(1)-C(1)	2.166(3)	2.151(18)	2.142(17)
P(1)-C(9)	1.815(4)	1.77(2)	1.79(2)
Acenaphthene bond lengths			
C(1)-C(2)	1.393(5)	1.38(3)	1.34(3)
C(2)-C(3)	1.418(5)	1.38(3)	1.36(3)
C(3)-C(4)	1.369(5)	1.33(3)	1.36(3)
C(4)-C(5)	1.419(5)	1.38(3)	1.38(4)
C(5)-C(10)	1.409(5)	1.40(3)	1.45(3)
C(5)-C(6)	1.404(5)	1.41(3)	1.37(3)
C(6)-C(7)	1.375(5)	1.34(3)	1.34(4)
C(7)-C(8)	1.411(5)	1.42(3)	1.46(3)
C(8)-C(9)	1.387(5)	1.37(3)	1.37(3)
C(9)-C(10)	1.444(5)	1.44(3)	1.42(3)
C(10)-C(1)	1.432(5)	1.45(2)	1.43(2)
C(4)-C(11)	1.515(5)	1.52(3)	1.52(3)
C(6)-C(12)	1.509(5)	1.50(3)	1.52(4)
C(11)-C(12)	1.553(5)	1.55(3)	1.50(3)
Peri-region bond angles			
Sn(1)-C(1)-C(10)	121.8(2)	121.3(13)	120.3(14)
C(1)-C(10)-C(9)	127.1(3)	127.2(16)	129.7(18)
P(1)-C(9)-C(10)	116.5(2)	123.9(12)	119.0(12)
Σ of bay angles	**365.4(4)**	**372.4(24)**	**369.0(26)**

Splay angle[b]	5.4	12.4	9.0
C(4)-C(5)-C(6)	111.8(3)	112.3(18)	114.8(19)
Out-of-plane displacement			
Sn(1)	-0.339(1)	0.438(1)	0.195(1)
P(1)	0.345(1)	-0.367(1)	-0.345(1)
Central naphthalene ring torsion angles			
C:(6)-(5)-(10)-(1)	-174.5(3)	177.5(12)	177.7(14)
C:(4)-(5)-(10)-(9)	-176.7(3)	176.0(12)	176.3(14)

[a] van der Waals radii used for calculations: rvdW (Sn) 2.17 Å, rvdW (P) 1.80 Å [b] Splay angle: Σ of the three bay region angles – 360.

When heavy atoms occupy the *peri*-positions, at distances less than the van der Waals radii of the two interacting atoms, they will experience a considerable amount of steric tension across the *peri*-space. These repulsive interactions can cause the rigid organic backbone to deform from its ideal geometry in order to reduce the steric pressure, *via* in-plane and out-of-plane deflections of the substituents and buckling of the aromatic ring system.

Steric compression can also be released by the formation of weak or strong bonding due to attractive interactions operating across the *peri*-gap. This can be observed by looking at the distances in tin chlorides **20**-**22**, which show somewhat lesser steric congestion compared to triphenyltin derivative **19** due to the presence of weak hypervalent 3c-4e type interactions in the *peri*-region. Therefore this type of interaction helps to minimize the steric effects between Sn and P and thus reduces the molecular deformation within the acenaphthene skeleton. This can be observed in the phosphours-tin species by comparing the splay angles with similar tin-bromine compounds from Chapter 3. For example, a non-bonded tin-bromine analogue [Acenap(Br)($SnPh_3$)][24] splays to 22.1° whereas in **19** the angle is 17.1° and in **20**-**22** the presence of an attractive P···Sn interaction is supported by splay angles of only 4.1°, 6.7° and 5.4°,

respectively. This signifies that the bay-region angles have become more acute as the *peri*-atoms have come together as a result of bond formation (Figure 5.8).

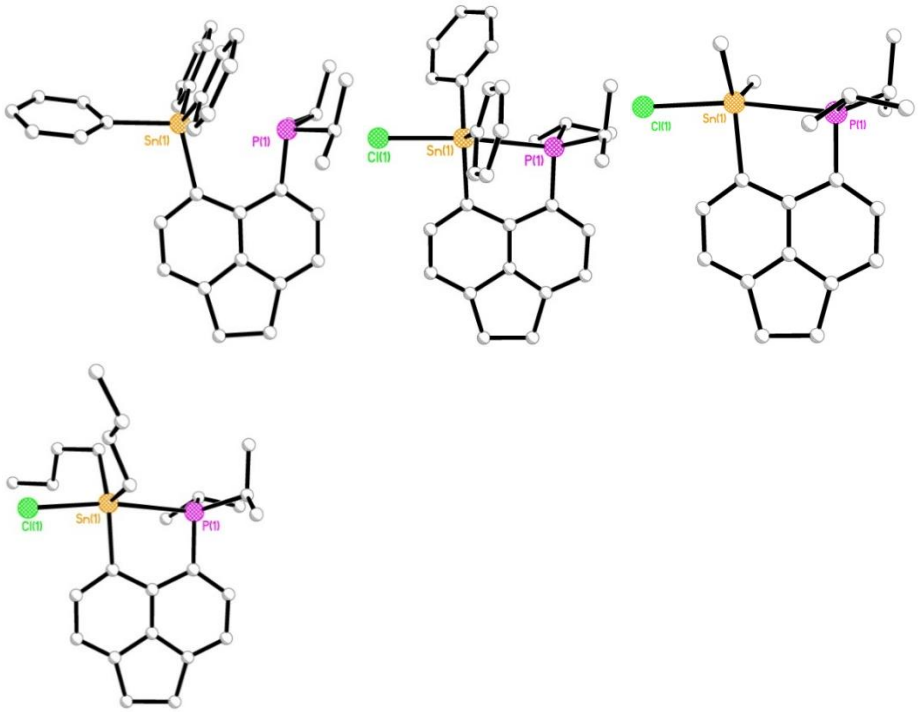

Figure 5.8 The molecular structures of **19**-**22**, showing the difference in in-plane distortion within the bay-region between the weakly bonded triphenyl tin derivative **19,** and tin chlorides **20**-**23**.

As a result of the Sn···P interaction, the environment around the tin atom in the triphenyltin derivative **19** distorts, with angles suggesting a geometry in-between tetrahedral and trigonal bipyramidal. The sum of the C1-Sn1-C13, C1-Sn1-C25 and C13-Sn1-C25 bond angles (346.3°) is thus larger than in an ideal tetrahedron (328.5°), but still less than that of a perfect trigonal

bipyramid (360°). The phosphorus atom similarly adopts a distorted trigonal pyramidal geometry, with C-P-C angles shortened from an ideal 107° to an average of 101°.

However, in tin chlorides **20**-**22**, displaying much stronger interactions between P and Sn, the geometry around the tin atom approaches that of a trigonal bipyramid, with C-Sn-C bond angles increased to 359° in all the three compounds. Similarly, the C-P-C angles around P atom are also larger (105°-107°), thus resulting in a distorted tetrahedral geometry.

Table 5.3 Bond angles [°] categorising the geometry around Sn and P in **19**-**21**.

Angles around the Sn atom	**19**	**20**	**21**
C(1)-Sn(1)-C(13)	113.1(2)	126.7(4)	114.5(4)
C(1)-Sn(1)-C(19)	104.7(2)	113.1(4)	-
C(1)-Sn(1)-C(25)	111.0(2)	-	-
C(13)-Sn(1)-C(19)	101.0(2)	119.1(4)	-
C(13)-Sn(1)-C(25)	122.2(2)	-	-
C(19)-Sn(1)-C(25)	102.0(2)	-	-
C(19)-Sn(1)···P(1)	177.63(1)	92.5(3)	-
C(9)-P(1)-C(31)	98.7(3)	-	-
C(9)-P(1)-C(34)	100.8(3)	-	-
C(31)-P(1)-C(34)	103.0(3)	-	-
C(19)-Sn(1)···P(1)	177.63(1)	-	-
C(9)-P(1)-C(31)	98.7(3)	-	-
C(1)-Sn(1)-Cl(1)	-	94.5(3)	94.6(2)
C(1)-Sn(1)-P(1)	-	78.1(3)	76.3(2)

C(13)-Sn(1)-Cl(1)	-	91.7(3)	95.5(3)
C(13)-Sn(1)-P(1)	-	89.6(3)	94.3(4)
C(19)-Sn(1)-Cl(1)	-	94.1(3)	-
Cl(1)-Sn(1)-P(1)	-	171.62(9)	168.93(8)
C(9)-P(1)-C(25)	-	106.2(6)	-
C(9)-P(1)-C(28)	-	106.9(5)	-
C(25)-P(1)-C(28)	-	106.8(6)	-
Sn(1)-P(1)-C(9)	-	95.6(4)	95.5(3)
Sn(1)-P(1)-C(25)	-	125.8(5)	-
Sn(1)-P(1)-C(28)	-	113.5(4)	-
C(1)-Sn(1)-C(14)	-	-	127.8(4)
C(13)-Sn(1)-C(14)	-	-	116.7(5)
C(14)-Sn(1)-Cl(1)	-	-	90.4(3)
C(14)-Sn(1)-P(1)	-	-	90.2(3)
C(9)-P(1)-C(15)	-	-	105.9(5)
C(9)-P(1)-C(18)	-	-	105.4(5)
C(15)-P(1)-C(18)	-	-	106.5(6)
Sn(1)-P(1)-C(15)	-	-	128.1(4)
Sn(1)-P(1)-C(18)	-	-	112.6(4)

Table 5.4 Bond angles [°] categorising the geometry around Sn and P in **21-23**.

Angles around the Sn atom	**22**	**23**
C(1)-Sn(1)-C(13)	118.40(13)	-
C(1)-Sn(1)-C(17)	125.54(13)	-
C(1)-Sn(1)-Cl(1)	94.84(9)	91.3(4)
C(1)-Sn(1)-P(1)	76.45(9)	-
C(13)-Sn(1)-C(17)	114.93(14)	-
C(13)-Sn(1)-Cl(1)	90.42(10)	-
C(13)-Sn(1)-P(1)	92.80(10)	-
C(17)-Sn(1)-Cl(1)	95.02(10)	-
C(17)-Sn(1)-P(1)	91.01(10)	-
Cl(1)-Sn(1)-P(1)	171.23(3)	-
C(9)-P(1)-C(21)	106.95(17)	-
C(9)-P(1)-C(24)	104.14(16)	-
C(21)-P(1)-C(24)	104.89(16)	-
Sn(1)-P(1)-C(9)	94.46(18)	-
Sn(1)-P(1)-C(21)	128.06(12)	-
Sn(1)-P(1)-C(24)	114.91(12)	-
C(1)-Sn(1)-C(19)	-	177.9(7)
C(1)-Sn(1)-Cl(2)	-	89.8(4)
C(1)-Sn(1)-P(2)	-	100.9(5)
C(19)-Sn(1)-Cl(1)	-	89.0(4)
C(19)-Sn(1)-Cl(2)	-	90.0(4)
C(19)-Sn(1)-P(2)	-	77.1(5)
Cl(1)-Sn(1)-P(2)	-	83.79(15)

Cl(1)-Sn(1)-Cl(2)	-	174.67(16)
Cl(2)-Sn(1)-P(2)	-	101.09(15)
C(9)-P(1)-C(13)	-	107.3(9)
C(9)-P(1)-C(16)	-	105.9(9)
C(13)-P(1)-C(16)	-	111.8(10)
C(27)-P(2)-C(31)	-	109.0(9)
C(27)-P(2)-C(34)	-	100.4(11)
C(31)-P(2)-C(34)	-	104.5(12)
Sn(1)-P(2)-C(27)	-	91.6(7)
Sn(1)-P(2)-C(31)	-	124.4(8)
Sn(1)-P(2)-C(34)	-	122.2(9)

The molecular structure of tin dichloride **23** is constructed from two crystallographically unique acenaphthene fragments, which are bonded to the tin center in a pseudo-hexacoordinated fashion. The acenaphthene rings align with an angle of 44° between the two mean planes, which creates an environment in which the tin and phosphorus atoms are located in close proximity in the *peri*-region. The geometric restrictions imposed by the planar rigid acenaphthene carbon skeletons, and the *peri*-functionalities of the molecule promotes an attractive donor-acceptor type interaction between the closely accommodated phosphorus lone-pairs and the electropositive Sn atom. This results in Sn-P distances notably shorter than the sum of van der Waals radii (Sn1-P2 2.954(7) Å, Sn1-P1 3.141(6) Å). The AC-type conformation adopted by the two P-C_{iPr} bonds in each acenaphthene fragment ensures both phosphorus lone-pairs are directed towards the tin atom and subsequently affords a distorted tetrahedral geometry around each phosphorus atom (C-P-C angles 100°-112°).

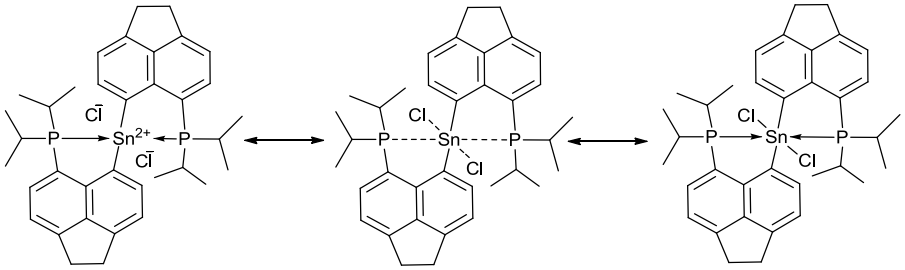

Figure 5.9 The unusual bonding situation around the *pseudo*-hexacoordinated tin centre in **23**.

In **23**, the tin geometry is somewhat complex, and can be described as either 2-coordinate (linear), 4-coordinate (square planar) or 6-coordinate (octahedral) depending upon the interpretation of the Sn-Y bonding interactions (Figure 5.9). If the two Sn-P interactions are classified as non-bonding and the Sn-Cl bonds thought of as having ionic character due to the electronegativity difference between the Sn and Cl atoms, the tin center would be coordinated to just the two acenaphthene fragments, with a C_{acenap}-Sn-C_{acenap} bond angle of 177.9(7)° (linear geometry). However, if we consider the Sn-Cl interaction as a covalent bond the arrangement of atoms around Sn is now best described as square-planar. Finally, the weakly attractive donor-acceptor interactions between P and Sn complete a distorted octahedral geometry around the tin center.

Conclusion

A series of tin-phosphorous *peri*-substituted acenaphthenes [Acenap(SnR_3)($PiPr_2$) (R_3 = Ph_3 **19**; Ph_2Cl **20**; Me_2Cl **21**; Bu_2Cl **22**; Cl_2Acenap($PiPr_2$) **23**] have been prepared and their structures investigated, in order to see how substituents bound to tin affect the strength of the intramolecular lone-pair P→Sn donor-acceptor interactions..

Mono-systems **19**-**22** adopt similar conformations, classified as type BAA-CC for **19** and BAA-AC for **20**-**22**. In all four compounds, two Sn-CR bonds align perpendicular and on opposing sides of the mean acenaphthene plane (type A) leaving the remaining Sn-C_{Ph} bond in **19** and the Sn-Cl bonds in **20**-**22** along the acenaphthene plane (type B). In each case this produces a *quasi*-linear Y-Sn···P three-body fragment which provides the correct geometry for promoting delocalization of the phosphorus lone-pair to an antibonding σ*(Sn−Y) orbital to form a donor-acceptor three-centre four-electron (3c-4e) type interaction. *Peri*-distances in tin dichlorides **20**-**22** (2 2.815(3) Å, 3 2.912(3) Å, 4 2.8721(10) Å) are notably shorter than in triphenyl derivative **19** (3.2511(19) Å) suggesting the lone-pair interaction is more predominant in these compounds due to the presence of the highly electronegative chlorine atoms, which naturally increases the Lewis-acidity of the tin centre.

The pseudo-hexacoordinate tin dichloride **23** is constructed from two acenaphthene fragments and positions two basic P^iPr_2 moieties in close proximity to the electropositive tin centre. This promotes two weakly attractive P→Sn donor-acceptor type interactions to occur, with significant covalent character predicted based on the small *peri*-separations observed (Sn1-P2 2.954(7) Å, Sn1-P1 3.141(6) Å). The geometry around the tin is unusual and can be classed as 2- 4- or 6-coordinate depending upon the interpretation of the Sn-substituent bonding interactions.

Experimental Section

All experiments were carried out under an oxygen- and moisture-free nitrogen atmosphere using standard Schlenk techniques and glassware. Reagents were obtained from commercial sources and used as received. Dry solvents were collected from a MBraun solvent system. Elemental analyses were performed by Stephen Boyer at the London Metropolitan University. ^{1}H and ^{13}C NMR spectra were recorded on a Bruker AVANCE 300 MHz spectrometer with δ(H) and δ(C) referenced to external tetramethylsilane. ^{31}P and ^{119}Sn NMR spectra were recorded on a Jeol GSX 270 MHz spectrometer with δ(P) and δ(Sn) referenced to external phosphoric acid and tetramethylstannane, respectively. Assignments of ^{13}C and ^{1}H NMR spectra were made with the help of H-H COSY and HSQC experiments. All measurements were performed at 25 °C. All values reported for NMR spectroscopy are in parts per million (ppm). Coupling constants (*J*) are given in Hertz (Hz). Mass spectrometry was performed by the University of St Andrews Mass Spectrometry Service. Electrospray Mass Spectrometry (ESMS) was carried out on a Micromass LCT orthogonal accelerator time of flight mass spectrometer. 5-(bromo)-6-(diisopropylphosphino)acenaphthene was prepared following a previously reported procedure.[10]

6-Diisopropylphosphinoacenaphth-5-yl-triphenyltin [Acenap(SnPh$_3$)(P^{i}Pr$_2$)] (19): To a solution of 5-bromo-6-diisopropylphosphinoacenapthene [Acenap(Br)(P^{i}Pr$_2$)] (0.5 g, 1.43 mmol) in diethyl ether (15 mL) at -78 ºC was added dropwise a 2.5 M solution of *n*-butyllithium in hexane (0.6 mL, 1.43 mmol). The mixture was stirred at this temperature for 1 h after which a solution of triphenyltin chloride Ph$_3$ClSn (0.5 g, 1.43 mmol) in diethyl ether (5 mL) was added dropwise. The solution was then allowed to warm to room temperature and stirred overnight. The resulting orange suspension was washed with degassed water and the organic layer was separated,

dried over magnesium sulfate and concentrated under reduced pressure. Removal of solvents *in vacuo* gave a yellow oil, which was washed with diethyl ether (5 mL) to give the title compound as a colourless solid. An analytically pure sample was obtained by recrystallisation from a saturated solution of the compound in hexane (0.64 g, 72%); m.p. 222-224 °C; elemental analysis (Found: C, 69.7; H, 6.0. Calc. for $C_{36}H_{37}PSn$: C, 69.8; H, 6.0%); ^{1}H NMR (300 MHz, $CDCl_3$, 25°C, Me_4Si): δ = 7.84 (1 H, d, $^{3}J_{HH}$ = 6.9, $^{3}J_{HSn}$ = 70/67, Acenap 4-H), 7.65-7.57 (6 H, m, Sn*Ph*), 7.46 (1 H, dd, $^{3}J_{HH}$ = 7.0, $^{3}J_{HP}$ = 3.6, Acenap 7-H), 7.28-7.15 (11 H, m, Acenap 3,8-H, Sn*Ph*), 3.35 (4 H, s, Acenap 2xCH_2), 1.80-1.61 (2 H, m, 2xP*CH*), 0.57 (6 H, dd, $^{3}J_{HH}$ = 6.9, $^{3}J_{HP}$ = 14.6 Hz, 2xCH_3), 0.25 (6 H, dd, $^{3}J_{HH}$ = 7.0, $^{3}J_{HP}$ = 11.8, 2xCH_3); ^{13}C NMR (75.5 MHz; $CDCl_3$; 25ºC; Me_4Si): δ = 141.5(s), 137.7(s, $^{2}J_{CSn}$ = 33.3), 133.6(d, $^{2}J_{CP}$ = 2.7, C-7), 128.5(s), 128.1(s), 120.0(s), 119.4(s), 30.6(s, Acenap CH_2), 30.4(s, Acenap CH_2), 25.6(d, $^{1}J_{CP}$ = 10.4, 2xP*C*H), 19.7(d, $^{2}J_{CP}$ = 14.6, 2xCH_3), 18.5(d, $^{2}J_{CP}$ = 6.5, 2xCH_3); ^{31}P NMR (109.4 MHz; $CDCl_3$; 25ºC; H_3PO_4): δ = -31.5 (s, $^{4}J_{PSn}$ = 373/355); ^{119}Sn NMR (100.7 MHz; $CDCl_3$; 25ºC; Me_4Sn): δ = -183.7 (d, $^{4}J_{SnP}$ = 373); MS (ES^+): *m/z* 642.57 (100%, M + Na).

6-Diisopropylphosphinoacenaphth-5-yl-diphenyltin chloride [Acenap(SnPh$_2$Cl)(P^{i}Pr$_2$)] (20): Experimental as for compound **1** but with [Acenap(Br)(P^{i}Pr$_2$)] (0.5 g, 1.43mmol), 2.5 M solution of *n*-butyllithium in hexane (0.6 mL, 1.43 mmol) and Ph_2Cl_2Sn (0.49 g, 1.43 mmol). The crude product was washed with toluene, the mixture was filtered and the toluene was removed *in vacuo*. An analytically pure sample was obtained from recrystallisation by diffusion of hexane into a saturated solution of the compound in THF (0.54 g, 65%); m.p. 214-216°C; elemental analysis (Found: C, 62.3; H, 5.6. Calc. for $C_{30}H_{32}PSnCl$: C, 62.4; H, 5.5%); ^{1}H NMR (300 MHz, $CDCl_3$, 25°C, Me_4Si): δ = 8.94 (1 H, d, $^{3}J_{HH}$ = 7.1, $^{3}J_{HSn}$ = 83, Acenap 4-H), 7.76-7.63 (6 H, m, Sn*Ph*), 7.52-7.35 (4 H, m, Acenap 3,7-H, Sn*Ph*), 7.29-7.11 (5 H, m, Acenap 8-H, Sn*Ph*), 3.33 (4 H, s,

Acenap 2xCH_2), 2.14-1.93 (2 H, m, 2xP*CH*), 0.57 (6 H, dd, $^3J_{HH}$ = 7.0, $^3J_{HP}$ = 16.8, 2x*CH*$_3$), 0.46 (6 H, dd, $^3J_{HH}$ = 7.0, $^3J_{HP}$ = 13.0, 2x*CH*$_3$); ^{13}C NMR (75.5 MHz; $CDCl_3$; 25ºC; Me_4Si): δ = 141.3(d, $^4J_{CP}$ = 6.8, $^2J_{CSn}$ = 50.0, C-4), 136.4(s, $^2J_{CSn}$ = 43.9), 133.6(d, $^2J_{CP}$ = 2.5, C-7), 129.3(s), 129.1(s), 121.3(d, $^5J_{CP}$ = 3.4, C-3), 119.7(d, $^3J_{CP}$ = 4.1, C-8), 31.1(s, Acenap *C*H_2), 30.6(s, Acenap *C*H_2), 23.7(d, $^1J_{CP}$ = 5.1, 2xP*C*H), 18.6(d, $^2J_{CP}$ = 5.1, 2x*C*H_3), 17.1(br s, 2x*C*H_3); ^{31}P NMR (109.4 MHz; $CDCl_3$; 25ºC; H_3PO_4): δ = -27.3 (s, $^4J_{PSn}$ = 754/721); ^{119}Sn NMR (100.7 MHz; $CDCl_3$; 25ºC; Me_4Sn): δ = -241.0 (d, $^4J_{SnP}$ = 754); MS (ES^+): *m/z* 542.60 (100%, M - Cl + Na).

6-Diisopropylphosphinoacenaphth-5-yl-dimethyltin chloride [Acenap($SnMe_2Cl$)(P^iPr_2)] (21): Experimental as for compound **1** but with [Acenap(Br)(P^iPr_2)] (0.5 g, 1.43mmol), 2.5 M solution of *n*-butyllithium in hexane (0.6 mL, 1.43 mmol) and Me_2Cl_2Sn (0.31 g, 1.43 mmol). The crude product was washed with toluene, the mixture was filtered and the toluene was removed *in vacuo*. An analytically pure sample was obtained from recrystallisation by diffusion of hexane into a saturated solution of the compound in dichloromethane (0.3 g, 46%); m.p. 174-176°C; elemental analysis (Found: C, 53.2; H, 6.35. Calc. for $C_{20}H_{28}PSnCl$: C, 53.0; H, 6.2%); ^{1}H NMR (300 MHz, $CDCl_3$, 25°C, Me_4Si): δ = 8.67 (1 H, d, $^3J_{HH}$ = 7.0, $^3J_{HSn}$ = 78, Acenap 4-H), 7.54-7.42 (1 H, m, Acenap 7-H), 7.34 (1 H, d, $^3J_{HH}$ = 7.0, Acenap 3-H), 7.26 (1 H, d, $^3J_{HH}$ = 7.1, Acenap 8-H), 3.29 (4 H, s, Acenap 2xCH_2), 2.42-2.25 (2 H, m, 2xP*CH*), 1.10-0.86 (18 H, m, 2xPCH(*CH*$_3$)$_2$, 2xSnCH_3); ^{13}C NMR (75.5 MHz; $CDCl_3$; 25ºC; Me_4Si): δ = 140.4(d, $^4J_{CP}$ = 6.7, C-4), 133.1(d, $^2J_{CP}$ = 2.5, C-7), 121.5(d, $^5J_{CP}$ = 2.9, C-3), 119.5(d, $^3J_{CP}$ = 4.3, C-8), 31.0(s, Acenap *C*H_2), 30.5(s, Acenap *C*H_2), 23.9(d, $^1J_{CP}$ = 5.2, 2xP*C*H), 19.7(br s, 2xPCH(*C*H_3)$_2$), 19.6 (br s, 2xPCH(*C*H_3)$_2$), 18.3(s, 2xSn*C*H_3); ^{31}P NMR (109.4 MHz; $CDCl_3$; 25ºC; H_3PO_4): δ = -24.4 (s, $^4J_{PSn}$ = 742/709); ^{119}Sn NMR (100.7 MHz; $CDCl_3$; 25ºC; Me_4Sn): δ = -143.1 (d, $^4J_{SnP}$ = 742); MS (ES^+): *m/z* 419.09 (100%, M-Cl).

6-Diisopropylphosphinoacenaphth-5-yl-dibutyltin chloride [Acenap(SnBu$_2$Cl)(P^{i}Pr$_2$)] (22): Experimental as for compound **1** but with [Acenap(Br)(P^{i}Pr$_2$)] (1.0 g, 2.86 mmol), 2.5 M solution of *n*-butyllithium in hexane (1.14 mL, 2.86 mmol) and Bu_2Cl_2Sn (0.87 g, 2.86 mmol). The resulting orange oil was washed with MeCN (5 mL) to give the title compound as a cream solid. An analytically pure sample was obtained by recrystallisation from a saturated solution of the compound in hexane (1.54 g, 93%); m.p. 186-188°C; elemental analysis (Found: C, 58.0; H, 7.6. Calc. for $C_{26}H_{40}PSnCl$: C, 58.1; H, 7.5%); ^{1}H NMR (300 MHz, $CDCl_3$, 25°C, Me_4Si): δ = 8.65 (1 H, d, $^3J_{HH}$ = 7.0, $^3J_{HSn}$ = 70/67, Acenap 4-H), 7.51 (1 H, dd, $^3J_{HH}$ = 7.0, $^3J_{HP}$ = 5.7, Acenap 7-H), 7.37 (1 H, d, $^3J_{HH}$ = 7.0, Acenap 3-H), 7.28 (1 H, d, $^3J_{HH}$ = 7.0, Acenap 8-H), 3.35 (4 H, s, Acenap 2xCH_2), 2.42-2.30 (2 H, m, 2xP*CH*), 1.82-1.45 (8 H, m, 2xCH_2-α, 2xCH_2-β), 1.36-1.20 (4 H, m, 2xCH_2-γ), 1.06-0.92 (12 H, m, 2xPCH(*CH*$_3$)$_2$), 0.79 (6 H, t, $^3J_{HH}$ = 7.3, 2x*CH*$_3$-δ); ^{13}C NMR (75.5 MHz; $CDCl_3$; 25ºC; Me_4Si): δ = 140.6(d, $^4J_{CP}$ = 6.4, C-4), 132.8(d, $^2J_{CP}$ = 2.7, C-7), 121.1(d, $^5J_{CP}$ = 2.8, C-3), 119.2(d, $^3J_{CP}$ = 4.0, C-8), 30.9(s, Acenap *C*H$_2$), 30.4(s, Acenap *C*H$_2$), 29.0(s, $^2J_{CSn}$ = 31.8, 2x*C*H$_2$-β), 27.3(s, $^3J_{CSn}$ = 38.3, 2x*C*H$_2$-γ), 24.0(d, $^1J_{CP}$ = 3.4, 2xP*C*H), 23.7(d, $^3J_{CP}$ = 25.6, 2x*C*H$_2$-α), 19.7(d, $^2J_{CP}$ = 10.1, 2xPCH(*C*H$_3$)$_2$), 18.2 (br s, 2xPCH(*C*H$_3$)$_2$), 14.1(s, 2x*C*H$_3$-δ); ^{31}P NMR (109.4 MHz; $CDCl_3$; 25ºC; H_3PO_4): δ = -23.9 (s, $^4J_{PSn}$ = 740/707); ^{119}Sn NMR (100.7 MHz; $CDCl_3$; 25ºC; Me_4Sn): δ = -118.4 (d, $^4J_{SnP}$ = 740); MS (ES$^+$): *m/z* 503.19 (100%, M-Cl).

Bis(6-diisopropylphosphino-5-yl)tin dichloride [{Acenap(P^{i}Pr$_2$)}$_2$SnCl$_2$] (23): Experimental as for compound **1** but with [Acenap(Br)(P^{i}Pr$_2$)] (0.5 g, 1.43mmol), 2.5 M solution of *n*-butyllithium in hexane (0.6 mL, 1.43 mmol) and $SnCl_4$ (0.37 g, 1.43 mmol). The resulting orange oil was washed with MeCN (5 mL) to give the title compound as a cream solid. An analytically pure sample was obtained by recrystallisation from a saturated solution of the compound in hexane (0.37 g, 71 %); m.p. 220-222°C (decomp); ^{1}H NMR (300 MHz, $CDCl_3$, 25°C, Me_4Si): δ = 8.36 (1

H, d, $^{3}J_{HH}$ = 8.2, $^{4}J_{HP}$ = 3.6, Acenap 4-H), 7.47 (1 H, m, Acenap 7-H), 7.38-7.22 (2 H, m, Acenap 3,8-H), 3.38 (4 H, s, Acenap 2xCH_2), 2.44-2.20 (2 H, m, 2xP*CH*), 1.15 (6 H, dd, $^{3}J_{HH}$ = 7.0, $^{3}J_{HP}$ = 15.1, 2xCH_3), 0.96 (6 H, dd, $^{3}J_{HH}$ = 6.9, $^{3}J_{HP}$ = 11.6, 2xCH_3).

X-ray Structure Analysis

X-ray crystal structures for **19** and **20** were determined at −148(1) °C using a Rigaku MM007 high-brilliance RA generator (Mo Kα radiation, confocal optic) and Saturn CCD system. At least a full hemisphere of data was collected using ω scans. Intensities were corrected for Lorentz, polarization, and absorption. Data for compounds **21-23** were collected at −180(1) °C using a Rigaku MM007 high-brilliance RA generator (Mo Kα radiation, confocal optic) and Mercury CCD system. At least a full hemisphere of data was collected using ω scans. Data for the complexes analyzed was collected and processed using CrystalClear (Rigaku).[14] Structures were solved by direct methods[15] and expanded using Fourier techniques.[16] Non-hydrogen atoms were refined anisotropically. Hydrogen atoms were refined using the riding model. All calculations were performed using the CrystalStructure[17] crystallographic software package except for refinement, which was performed using SHELXL-97.[18]

References

1. P. Kilian, F. R. Knight and J. D. Woollins, *Chem. Eur. J.*, 2011, **17**, 2302.

2. V. Balasubramaniyan, *Chem. Rev*., 1966, **66**, 567.

3. A. C. Hazell, R. G. Hazell, L. Norskov-Lauritsen, C. E. Briant and D. W. Jones, *Acta Crystallogr., Sect. C*, 1986, **42**, 690.

4. (a) J. Meinwald, D. Dauplaise, F. Wudl and J. J. Hauser, *J. Am. Chem. Soc*., 1977, **99**, 255. (b) A. J. Ashe III, J. W. Kampf and P. M. Savla, *Heteroatom Chem*., 1994, **5**, 113. (c) M. C. R. Lanfrey, *Acad. Sci*., 1911, **152**, 92. (d) W. B. Price and S. J. Smiles, *Chem. Soc*., 1928, 2372. (e) A. Zweig and A. K. Hoffman, *J. Org. Chem*., 1965, **30**, 3997. (f) P. Kilian, A. M. Z. Slawin and J. D. Woollins, *Dalton Trans*., 2006, 2175. (g) P. Kilian, D. Philp, A. M. Z. Slawin and J. D. Woollins, *Eur. J. Inorg. Chem*., 2003, 249.

5. P. Kilian, F. R. Knight and J. D. Woollins, *Coord. Chem. Rev*., 2011, **255**, 1387.

6. For example: (a) C. Chuit and C. Reyé, *Eur. J. Inorg. Chem*., 1998, 1847. (b) G. P. Schiemenz, *Z. Anorg. Allg. Chem*., 2002, **628**, 2597. (c) F. H. Carré, C. Chuit, R. J. P. Corriu, W. E. Douglas, D. M. H. Guy and C. Reyé, *Eur. J. Inorg. Chem*., 2000, 647. (d) D. Hellwinkel, W. Lindner and H. –J. Wilfinger, *Tetrahedron Lett*., 1969, **10**, 3423.

7. (a) J. Beckmann, J. Bolsinger, A. Duthie and P. Finke, *Dalton. Trans*., 2013, **42**, 12193. (b) J. Beckmann, J. Bolsinger and A. Duthie, *Chem. Eur. J*., 2011, **17**, 930.

8. A. Panda, G. Mugesh, H. B. Singh and R. Butcher, *Organometallics*, 1999, **18**, 1986.

9. For example: S. Hayashi and W. Nakanishi, *J. Org. Chem*., 2002, **67**, 38.

10. (a) P. Wawrzyniak, A. M. Z. Slawin, J. D. Woollins and P. Kilian, *Dalton Trans*., 2010, **39**, 85. (b) P. Wawrzyniak, A. L. Fuller, A. M. Z. Slawin and P. Kilian, *Inorg. Chem*., 2009, **48**, 2500. (c) B. A. Surgenor, M. Bühl, A. M. Z. Slawin, J. D. Woollins and P. Kilian, *Angew. Chem. Int. Ed*., 2012, **51**, 10150.

11. J. T. B. H. Jastrzebski, J. Boersma, P. M. Esch, G. van Koten, *Organometallics*, 1991, **10**, 930.

12. L. K. Aschenbach, F. R. Knight, R. A. M. Randall, D. B. Cordes, A. Baggott, M. Bühl, A. M. Z. Slawin and J. D. Woollins, *Dalton Trans*., 2012, **41**, 3141.

13. P. Nagy, D. Szabó, I. Kapovits, Á. Kucsman, G. Argay and A. Kálmán, *J. Mol. Struct*., 2002, **606**, 61.

14. *CrystalClear 1.6*, Rigaku Corporation. CrystalClear Software User's Guide, Molecular Structure Corporation, © 2000, 1999; J. W. P. Flugrath, *Acta Crystallogr., Sect. D: Biol. Crystallogr*., 1999, **55**, 1718.

15. SIR97: A. Altomare, M. Burla, M. Camalli, G. Cascarano, C. Giacovazzo, A. Guagliardi, A. Moliterni, G. Polidori and R. Spagna, *J. Appl. Crystallogr*., 1999, **32**, 115.

16. DIRDIF99: P. T. Beurskens, G. Admiraal, G. Beurskens, W. P. Bosman, R. de Gelder, R. Israel and J. M. M. Smits, *The DIRDIF-99 program system, Technical Report of the Crystallography Laboratory*, University of Nijmegen, The Netherlands, 1999.

17. *CrystalStructure 3.8.1: Crystal Structure Analysis Package*, Rigaku and Rigaku/MSC (2000-2006). 9009 New Trails Dr. The Woodlands TX 77381 USA.

18. G. M. Sheldrick, *SHELX97, Acta Crystallogr., Sect. A: Fundam. Crystallogr*., 2008, **64**, 112.

Chapter 6

Sterically crowded distannyl acenaphthenes

Introduction

A important geometric feature of naphthalenes and acenaphthenes is the short 'natural' *peri* distance of *ca*. 2.44 Å.[1-4] As a consequence of this *peri* geometry, substituents experience considerable strain.[5] Only the hydrogen substituted naphthalene and acenaphthene is relaxed.[1,2] Out-of-plane as well as in-plane distortion can be observed (Figure 6.1), leading to a significant change in the naphthalene and acenaphthene geometry.[5] In addition, weak interatomic interactions, as well as strong formal bonds between the *peri*-substituents help to release some of the geometric strain..[6-13]

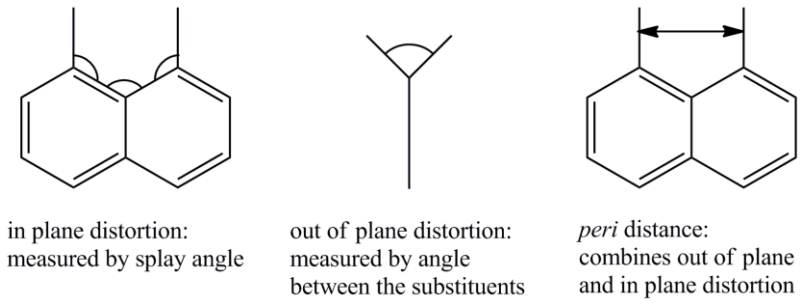

Figure 6.1 Geometric distortion found in *peri*-substituted naphthalenes and acenaphthenes; splay angle is the sum of the bay angles minus 360°.

Due to the large van der Waals radii of tin (2.17 Å), large distortions are expected in distannyl substituted naphthalenes and acenaphthenes and were indeed found in the first reported *peri*-substituted system of this type, 1,8-bis(trimethylstannyl)naphthalene.[10] The *peri*-distance of 1,8-bis(trimethylstannyl)naphthalene at 3.86 Å is the largest *peri*-distance known for tin containing naphthalene systems, and one of the largest ever *peri*-distances reported for any *peri*-system. Correspondingly, significant out-of-plane distortion is observed, with the angle between the C-Sn

bonds being over 50°, whilst a splay angle (sum of the *peri* angles minus 360°) of 16.6°, suggests the exocyclic *peri*-bonds are moving away from each other to minimise the steric strain.

Due to this geometric strain the synthesis of distannyl substituted naphthalenes and acenaphthenes is rather challenging. Prior to this work, the crystal structure of 1,8-bis(trimethylstannyl)naphthalene was the only known example of a distannyl substituted naphthalene structurally characterised. In 1977, Meinwald *et al*. reported on the synthesis of 7,7,14,14-tetraorganyldinaphtho[1,8-*bc*:1',8'-*fg*][1-5] distannocin using dilithionaphthalene and dimethyldichlorostannane and diphenyldichlorostannane as starting materials.[14] The acenaphthene analogue: 5,5,12,12-tetramethyldiacenaphtho[5,6-*bc*:5',6'-*fg*]-(1,5)distannocin was first described by Fry *et al*. in 1991.[15] 1,8-diallylstannylnaphthalenes are mentioned as alkylation agents by Maruoka *et al*. in 1997.[16]

Deformation of sterically crowded homologous molecules have been of continuing interest in organic chemistry; these overcrowded molecules provide a deeper understanding of the special features of distorted molecules, such as the geometry around the *peri*-substituents and molecular strain occurring in the backbone. This chapter focuses on synthesising sterically overcrowded homologous tin-tin acenaphthene compounds with the aim of producing the largest ever *peri*-distance and therefore the most distorted acenaphthene structure.

We herein report the synthesis of three new distannyl substituted acenaphthenes containing homonuclear tin-tin moieties at the 5,6-positions in **24**-**26** (Acenap[$SnMe_3$]$_2$ **24**, Acenap[$SnPh_3$]$_2$ **25**, Bis-acenap[$SnMe_2$]$_2$ **26**, Figure 6.2). These three structures are compared with the structure of 1,8-bis(trimethylstannyl)naphthalene.[1] Geometric optimisation and NBO calculations of the compounds have also been made in order to identify any potential intramolecular interactions.

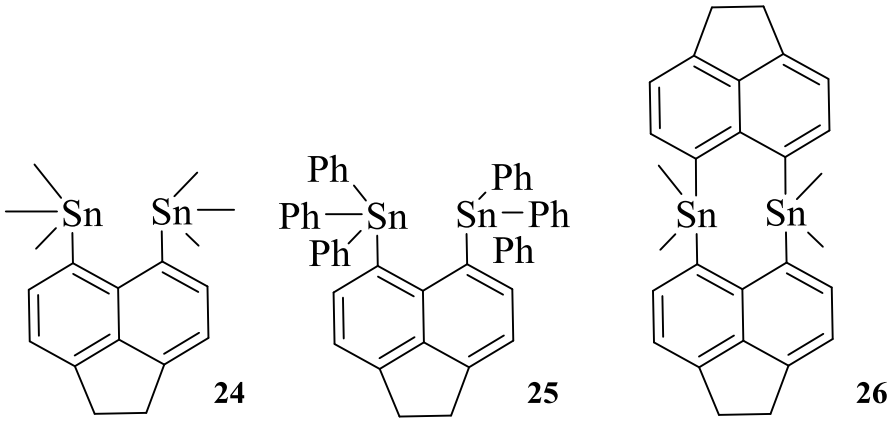

Figure 6.2 Compounds **24-26**, which will be discussed in this chapter.

Synthesis

The desired acenaphthene compounds **24** and **25** (*peri*-substituted with $SnMe_3$ and $SnPh_3$ moieties), were prepared from 5,6-dibromoacenaphthene. For their synthesis, 5,6-dibromoacenaphthene was initially reacted with TMEDA and *n*-butyllithium (2 equivalents), before being treated with the appropriate tin chloride (Me_3SnCl **24**; Ph_3SnCl **25**; 2 equivalents) to give 5,6-bis(trimethylstannyl)acenaphthene **24** and 5,6-bis(phenylstannyl)acenaphthene **25** in good to moderate yield [yield: 65% (**24**), 48% (**25**); Scheme 6.1]. Bis(μ-5,6-acenaphthenediyl)trimethyltin **26** was synthesized by a similar reaction of 5,6-dibromoacenaphthene; again treatment with TMEDA and two equivalents of *n*-butyllithium at −10 °C in diethyl ether, with subsequent addition of $SnMe_2Cl_2$ yielding the title compound [yield: 30% **26**; Scheme 6.2]. Compounds **24, 25** and **26** were characterised by elemental analysis, ^{1}H, ^{13}C and ^{119}Sn NMR spectroscopy and mass spectrometry.

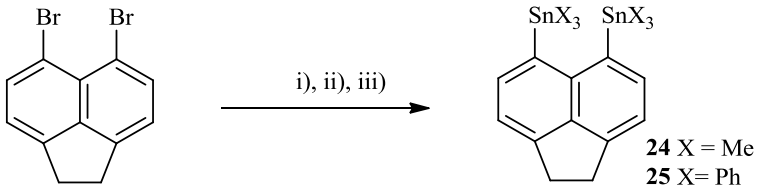

Scheme **6.1** The preparation of 5,6-bis(trimethylstannyl)acenaphthene **24** and 5,6-bis(phenylstannyl)acenaphthene **25** from 5,6-dibromoacenaphthene. Conditions: i) TMEDA (1 equiv), Et_2O, -10 – 0 °C, 15 min; ii) *n*BuLi (1 equiv), Et_2O, -10 – 0 °C, 1 h; X_3SnCl (1 equiv; X = Me, Ph), Et_2O, -10 – 0 °C

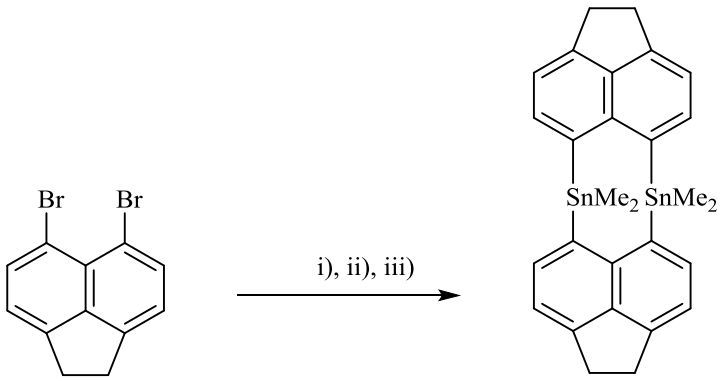

Scheme **6.2** The preparation of Bis(μ-5,6-acenaphthenediyl)trimethyltin **26** from 5,6-dibromoacenaphthene. Conditions: i) TMEDA (1 equiv), Et_2O, -10 – 0 °C, 15 min; ii) *n*BuLi (1 equiv), Et_2O, -10 – 0 °C, 1 h; Me_2SnCl_2 (1 equiv), Et_2O, -10 – 0 °C.

X ray investigations

Suitable single crystals were obtained for **24** by recrystallisation from a saturated solution of the compound in tetrahydrofuran (THF). Colourless crystals, suitable for characterisation by single crystal X-ray crystallography were obtained for **25** from recrystallisation by hexane diffusion into a saturated solution of the product in THF. Crystals for **26** were obtained by recrystallisation from a saturated solution of the product in chloroform ($CHCl_3$). All three compounds crystallise with

one molecule in the asymmetric unit cell (R1 = 6.59 (**24**), 3.2 (**25**) 3.1% (**26**); Figures 6.3, 6.4, 6.5). Selected interatomic distances, angles and torsion angles are listed in Table 6.1, further refinement data for **24**-**26** can be found in Appendix 3.

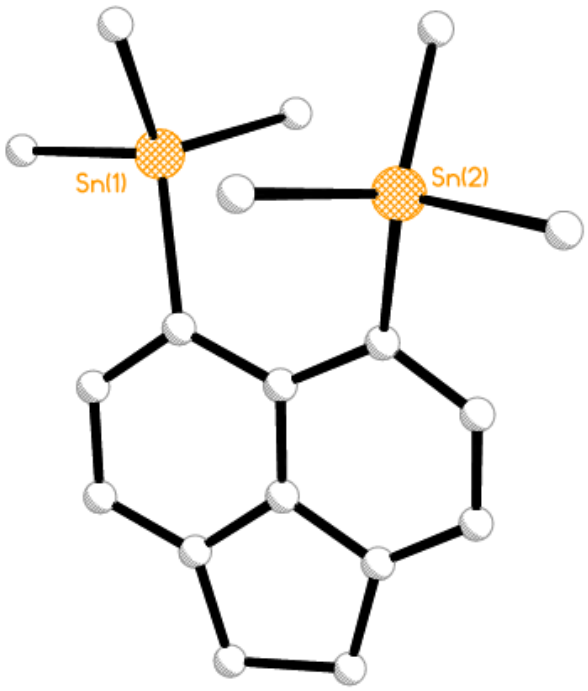

Figure 6.3 The crystal structure of *5,6-bis(trimethylstannyl)acenaphthene* **24** (hydrogen atoms omitted for clarity).

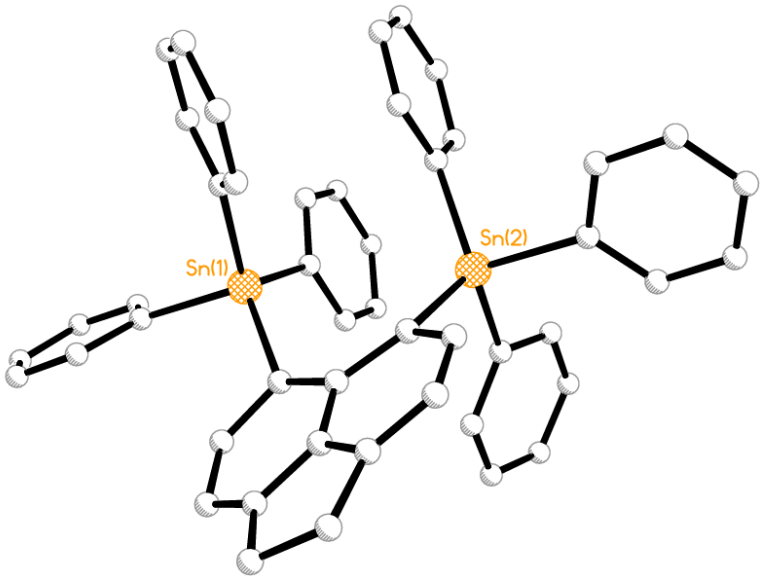

Figure 6.4 The crystal structure of *5,6-bis(phenylstannyl)acenaphthene* **25** (hydrogen atoms omitted for clarity).

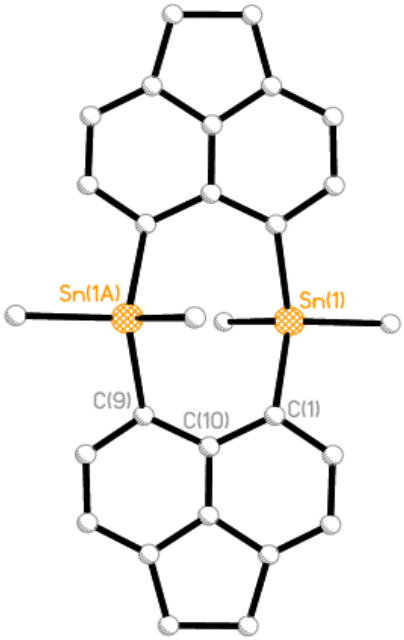

Figure 6.5 The crystal structure of *bis(μ-5,6-acenaphthenediyl)trimethyltin* **26** (hydrogen atoms omitted for clarity).

The severe distortions induced by crowding the *peri*-positions of acenaphthene with bulky substituents, such as aryl- and alkytin moieties, are best highlighted by comparing in- and out-of-plane displacements of the exocyclic bonds and the degree of buckling in the acenaphthene backbone. The degree of geometrical distortion is related to the bulkiness of the tin functionalities which occupy the *peri*-positions and is best illustrated by comparing *peri*-distances. In bis-trimethyltin derivative **24**, the *peri*-substituents align far apart, with a non-bonded distance of 3.874(3) Å, marginally longer than the naphthalene analogue (3.86 Å). The larger triphenyltin moiety in **25** naturally increases the Sn···Sn separation, displaying a much larger *peri*-distance of 4.0659(9) Å, which, to the best of our knowledge, is the largest ever *peri*-distance known to date. Due to the cyclic structure of the molecule, compound **26** exhibits a somewhat smaller *peri*-distance (3.657(6) Å)) compared to **24** and **25**. This can be explained by the presence of two rigid acenaphthene backbones which fixes the Sn atoms in closer proximity. Despite the increase in steric strain and corresponding distortion of the acenaphthene geometry, the Sn···Sn distances are still all shorter than the $\sum r_{vdW}$ radii for the two interacting Sn atoms (4.34 Å).

Table 6.1 Selected bond lengths (Å) and angles (°) for **24**.

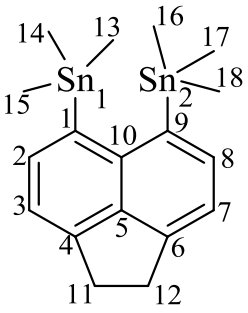

24

Peri-region-distances	
Sn(1)···Sn(2)	**3.874(1)**
Σr_{vdW} - Sn···Sn[a]	0.466
$\%r_{vdW}$[a]	89

Sn(1)-C(1)	2.161(10)
Sn(2)-C(9)	2.120(10)
Acenaphthene bond lengths	
C(1)-C(2)	1.368(15)
C(2)-C(3)	1.404(15)
C(3)-C(4)	1.360(15)
C(4)-C(5)	1.390(15)
C(5)-C(10)	1.408(14)
C(5)-C(6)	1.408(15)
C(6)-C(7)	1.349(16)
C(7)-C(8)	1.397(16)
C(8)-C(9)	1.381(15)
C(9)-C(10)	1.443(14)
C(10)-C(1)	1.422(14)
C(4)-C(11)	1.493(14)
C(11)-C(12)	1.520(16)
C(12)-C(6)	1.496(15)
Peri-region bond angles	
Sn(2)-C(9)-C(10)	127.1(7)
C(1)-C(10)-C(9)	128.8(9)
Sn(1)-C(1)-C(10)	126.8(7)
Σ of bay angles	**382.7(13)**
Splay angle[b]	22.7
C(4)-C(5)-C(6)	110.9(9)
In and out-of-plane displacement	
Sn(1)	+0.984(1)
Sn(2)	-0.795(1)
C:(6)-(5)-(10)-(1)	173.6(8)
C:(4)-(5)-(10)-(9)	173.2(9)

[a] van der Waals radii used for calculations: rvdW (Sn) 2.17 Å, Splay angle: Σ of the three bay region angles – 360.

Table 6.2 Selected bond lengths (Å) and angles (°) for **25**.

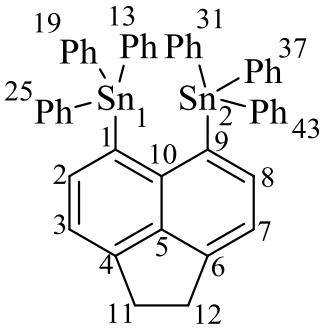

25

Peri-region-distances	
Sn(1)···Sn(2)	**4.0659(9)**
Σr_{vdW} - Sn···Sn[a]	0.2741
$\%r_{vdW}$[a]	94
Sn(1)-C(1)	2.165(3)
Sn(2)-C(9)	2.164(4)
Acenaphthene bond lengths	
C(1)-C(2)	1.401(5)
C(2)-C(3)	1.415(5)
C(3)-C(4)	1.379(5)
C(4)-C(5)	1.406(5)
C(5)-C(10)	1.425(5)
C(5)-C(6)	1.419(5)
C(6)-C(7)	1.349(5)
C(7)-C(8)	1.413(5)
C(8)-C(9)	1.385(5)
C(9)-C(10)	1.436(5)
C(10)-C(1)	1.447(5)
C(4)-C(11)	1.514(5)
C(11)-C(12)	1.552(5)
C(12)-C(6)	1.509(5)
Peri-region bond angles	
Sn(2)-C(9)-C(10)	128.5(2)
C(1)-C(10)-C(9)	129.5(3)
Sn(1)-C(1)-C(10)	128.8(2)
Σ of bay angles	**386.8(4)**
Splay angle[b]	26.8

C(4)-C(5)-C(6)	111.1(3)
In and out-of-plane displacement	
Sn(1)	-1.045(1)
Sn(2)	+0.725(1)
C:(6)-(5)-(10)-(1)	-174.3(3)
C:(4)-(5)-(10)-(9)	-175.7(3)

[a] van der Waals radii used for calculations: rvdW (Sn) 2.17 Å, Splay angle: Σ of the three bay region angles – 360.

Table 6.3 Selected bond lengths (Å) and angles (°) for **26**

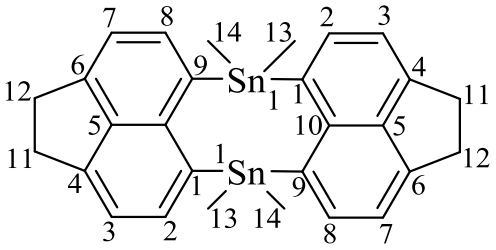

26

Peri-region-distances	
Sn(1)···Sn(1)	**3.657(6)**
Σr_{vdW} - Sn···Sn[a]	0.683
$\%r_{vdW}$[a]	84
Sn(1)-C(1)	2.164(5)
Sn(1)-C(9)	2.161(6)
Acenaphthene bond lengths	
C(1)-C(2)	1.401(8)
C(2)-C(3)	1.424(8)
C(3)-C(4)	1.357(6)
C(4)-C(5)	1.431(8)
C(5)-C(10)	1.414(8)
C(5)-C(6)	1.414(6)
C(6)-C(7)	1.366(8)
C(7)-C(8)	1.411(8)
C(8)-C(9)	1.394(6)
C(9)-C(10)	1.437(8)
C(10)-C(1)	1.434(5)

C(4)-C(11)	1.525(8)
C(11)-C(12)	1.555(7)
C(12)-C(6)	1.515(9)
Peri-region bond angles	
Sn(1)-C(9)-C(10)	123.1(3)
C(1)-C(10)-C(9)	127.1(5)
Sn(1)-C(1)-C(10)	123.6(4)
Σ of bay angles	**373.8(7)**
Splay angle[b]	13.8
C(4)-C(5)-C(6)	111.4(5)
In and out-of-plane displacement	
Sn(1)	+0.962(1)
Sn(1)	-0.845(1)
C:(6)-(5)-(10)-(1)	-175.2(5)
C:(4)-(5)-(10)-(9)	-176.5(5)

[a] van der Waals radii used for calculations: rvdW (Sn) 2.17 Å, Splay angle: Σ of the three bay region angles – 360.

The increase in *peri*-distance observed in the studied molecules is accompanied by a considerable increase in the splay angles, although in-plane distortion is much more significant in the non-cyclic compounds [**24** 22.7°, **25** 26.8°] compared to **26 [**13.8°]. It is interesting to compare analogous 1,8-bis(trimethylstannyl)naphthalene (**a**) with the acenaphthene structure **24**; the splay angle of **a** is significantly smaller (16.6°), but the degree of out-of-plane distortion is larger. The bis(ethylene) bridge in the acenaphthene stabilises the aromatic ring structure and inhibits buckling of the ring system. As a consequence, in-plane distortion is more pronounced.

Further distortion can be achieved through-out-of-plane deflections of the Sn atoms away from the mean acenaphthene plane. In analogues **24** and **25**, the *peri*-atoms show significant out-of-plane deviations with Sn(1) sitting 0.984(1) Å above the mean acenaphthene plane in **24** and Sn(2) lying -0.795(1) Å below the plane. Due to the greater steric repulsion caused by the larger size of the

phenyl groups in **25**, the Sn atoms are forced to lie further from the plane, with distances 0.725 Å (Sn(1)) and -1.045 Å (Sn(2)). Compound **26** shows similar out-of-plane distortion, with Sn(1) 0.962(1) Å and Sn(2) 0.845 Å, from the mean plane respectively.

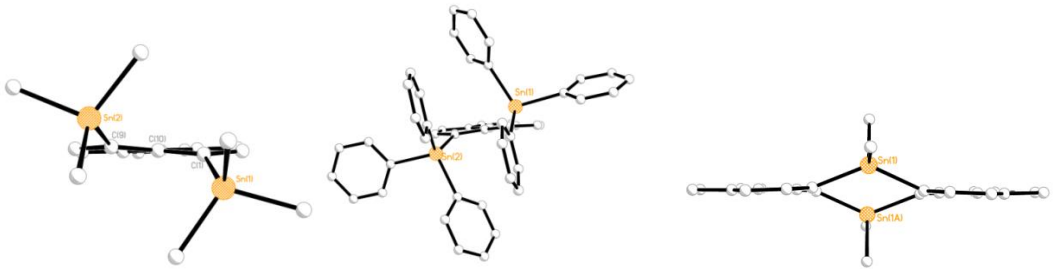

24 **25** **26**

Figure 6.6 Compounds **24**, **25** and **26** showing the planarity of the acenaphthene backbone.

The coordination geometry around the tin centre in each structure significantly deviates from that of an ideal tetrahedron value (109.5°) with angles in the range 99.64°-131.21° (Table 6.4, 6.5, 6.6). These distortions are probably due to the steric pressure of the crowded *peri*-groups attached to the tin centre.

Table 6.4 Bond angles [°] categorising the geometry around Sn in **24**.

Angles around the Sn atom	**24**
C(1)-Sn(1)-C(13)	121.7(5)
C(1)-Sn(1)-C(14)	106.1(4)
C(1)-Sn(1)-C(15)	104.3(5)
C(13)-Sn(1)-C(14)	112.8(5)
C(13)-Sn(1)-C(15)	101.2(5)
C(14)-Sn(1)-C(15)	109.8(5)
C(9)-Sn(2)-C(16)	117.9(4)
C(9)-Sn(2)-C(17)	104.6(5)
C(16)-Sn(2)-C(17)	104.5(5)
C(16)-Sn(2)-C(18)	115.2(5)
C(17)-Sn(2)-C(18)	107.1(5)

Table 6.5 Bond angles [°] categorising the geometry around Sn in **25**.

Angles around the Sn atom	**25**
C(1)-Sn(1)-C(9)	131.21(19)
C(1)-Sn(1)-C(13)	102.8(2)
C(1)-Sn(1)-C(14)	103.28(17)
C(9)-Sn(1)-C(13)	104.03(19)
C(9)-Sn(1)-C(14)	102.3(2)
C(13)-Sn(1)-C(14)	113.4(2)

Table 6.6 Bond angles [°] categorising the geometry around Sn in **26**.

Angles around the Sn atom	**26**
C(1)-Sn(1)-C(13)	107.87(12)
C(1)-Sn(1)-C(19)	106.69(13)
C(1)-Sn(1)-C(25)	119.43(15)
C(13)-Sn(1)-C(19)	107.31(14)
C(13)-Sn(1)-C(25)	99.64(14)

C(19)-Sn(1)-C(25)	114.93(13)
C(9)-Sn(2)-C(31)	108.84(13)
C(9)-Sn(2)-C(37)	120.86(15)
C(9)-Sn(2)-C(43)	104.31(13)
C(31)-Sn(2)-C(37)	115.51(14)
C(31)-Sn(2)-C(43)	104.97(15)
C(37)-Sn(2)-C(43)	99.98(13)

DFT Calculations

Geometry optimisations were performed for **24**-**26**. Wiberg bonding indices (WBI),[17] which measure the covalent bond order, of 0.01 were found for **24** and **25**, indicating that hardly any interaction exists between the two tin atoms. A slightly higher WBI index of 0.03 was found for the cyclic structure **26**, however the value still implies minimal interaction. We recently showed that the *peri*-distance to van der Waals (vdW) radius ratio can be an indicator for interactions between the *peri*-substituents on acenaphthenes and naphthalenes. The somewhat smaller WBI values obtained for **24**-**26** in comparison to the other tin substituted acenaphthenes is consistent with the much larger peri-distances observed in these tin-tin derivatives.

In Chapter 3 the synthesis of a series of bromo-tin acenaphthenes was described, and similar WBIs were observed between the bromine and the tin (0.06-0.08) in that case. We can conclude that due to the severe steric hindrance and the Sn···Sn repulsion across the *peri*-gap, the *peri*-substituents are forced to lie further away from each other, minimising the chance for intramolecular interactions to occur and subsequently affording the negligible WBIs observed.

Conclusion

Three different sterically crowded homonulcear tin-tin acenaphthenes have been prepared, and investigated to see how the size of the groups attached to the *peri*-atoms affects the degree of deformation of the acenaphthene backbone. The deformation of the exocyclic bonds is naturally dependent on the size of the *peri*-substituents. Thus, in **24** and **25**, exceptionally large splay angles are observed compared to other compounds observed in this thesis (**24** 22.7°, **25** 26.8°) with the effects of steric strain much more pronounced in these two systems. However, in the cyclic derivative **26**, a smaller deformation of the carbon system is observed due to the fused structure and the steric tension is localized around the acenaphthyl groups. Thus it appears that molecular deformations in the homonuclear series of distannylacenapthenes follow the order **25** (Ph_3Sn) >> **24** (Me_3Sn) > **26** (Me_3Sn). It is also noteworthy that all the three compounds have negligible WBI values, implying the repulsion operating between the sterically crowded tin substituents dominates the structure of these molecules.

Experimental Section

All experiments were carried out under an oxygen- and moisture-free nitrogen atmosphere using standard Schlenk techniques and glassware. Reagents were obtained from commercial sources and used as received. Dry solvents were collected from a MBraun solvent system. Elemental analyses were performed by Stephen Boyer at the London Metropolitan University. Infra-red spectra were recorded as KBr discs in the range 4000-300 cm^{-1} on a Perkin-Elmer System 2000 Fourier transform spectrometer. ^{1}H, ^{13}C and ^{119}Sn NMR spectra were recorded on a Jeol GSX 270 MHz spectrometer with δ(H), δ(C) and δ(Sn) referenced to external tetramethylsilane and external tetramethylstannane. Assignments of ^{13}C and ^{1}H NMR spectra were made with the help of H-H COSY and HSQC experiments. All measurements were performed at 25 °C. All values reported for NMR spectroscopy are in parts per million (ppm). Coupling constants (*J*) are given in Hertz (Hz). Mass spectrometry was performed by the University of St Andrews Mass Spectrometry Service. Electrospray Mass Spectrometry (ESMS) was carried out on a Micromass LCT orthogonal accelerator time of flight mass spectrometer. 5,6-dibromoacenaphthene and 5-bromoacenaphth-6-yl-triphenyltin was prepared following a previously reported procedure.[18]

5,6-bis(trimethylstannyl)acenaphthene [Acenap($SnMe_3$)$_2$] (24): A solution of 5,6-dibromoacenaphthene (1.03 g, 3.31 mmol) in diethyl ether (100 mL) was cooled to -10 – 0 °C on an ice-ethanol bath and to this was added a solution of TMEDA (1.4 mL, 8.93 mmol). The mixture was allowed to stir for 15 min before a solution of *n*-butyllithium (2.5 M) in hexane (2.9 mL, 7.28 mmol) was added dropwise over a period of 15 min. During these operations, the temperature of the mixture was maintained at -10 – 0 °C. The mixture was stirred at this temperature for a further 1 h, before a solution Me_3SnCl (1.7 mL, 1.32 g, 6.62 mmol) in diethyl ether (100 mL) was added dropwise. The mixture was allowed to warm to room temperature and then stirred overnight before

being washed with 0.1 N sodium hydroxide (2 x 60 mL). The organic layer was dried over magnesium sulfate and concentrated under reduced pressure to afford a white solid. The crude product was washed with ethanol and the title compound was collected by filtration as a white solid. An analytically pure sample was obtained from recrystallisation in THF at -30 °C (1.04 g, 65%); m.p. 132-134 °C; elemental analysis (Found: C, 45.2; H, 5.5. Calc. for $C_{18}H_{26}Sn_2$: C, 45.1; H, 5.5%); ^{1}H NMR (270 MHz, $CDCl_3$, 25 °C, Me_4Si): δ = 7.67 (2 H, d, $^3J_{HH}$ = 6.6, $^3J_{HSn}$ = 58/56, Acenap 4,7-H), 7.24 (2 H, d, $^3J_{HH}$ = 6.6, Acenap 3,8-H), 3.34 (4 H, s, Acenap 2xCH_2), 0.34 (18 H, s, $^3J_{HSn}$ = 53/51, 6xCH_3); ^{13}C NMR (75.5 MHz; $CDCl_3$; 25 ºC; Me_4Si): δ = 148.1(q), 139.3(s, $^3J_{CSn}$ = 32), 138.6(q), 119.0(s, $^4J_{CSn}$ = 53), 58.5(q), 29.9(s), 18.5(q), -4.5(s, $^2J_{CSn}$ = 347/331); ^{119}Sn NMR (100.7 MHz; $CDCl_3$; 25 ºC; Me_4Sn): δ = -24.3 (s, $^4J_{SnSn}$ = 37 Hz); MS (ES^+): *m/z* 134.93 (100%, SnMe), 164.97 (28, $SnMe_3$), 197.00 (24, $SnMe_3OMe$), 303.02 (5, $C_{12}H_8SnMe_3$), 349.02 (7, M^+ - $SnMe_3$ + OMe).

5,6-bis(triphenylstannyl)acenaphthene [Acenap($SnPh_3$)$_2$] (25): Experimental as for compound **24** but with 5,6-dibromoacenaphthene (1.09 g, 3.49 mmol), TMEDA (1.5 mL, 9.44 mmol), *n*-butyllithium (2.5 M) in hexane (3.1 mL, 7.69 mmol) and triphenyltin chloride (2.69 g, 6.98 mmol). The crude product was refluxed with hexane for 30 min affording a white solid precipitate which was collected by filtration. An analytically pure sample was obtained from recrystallisation by diffusion of hexane into a saturated solution of the compound in tetrahydrofuran (1.43 g, 48%); m.p. 193-195 °C; ^{1}H NMR (270 MHz, $CDCl_3$, 25 °C, Me_4Si): δ = 7.80 (2 H, d, $^3J(^1H,^1H)$ = 6.9 Hz, $^3J(^1H,^{119/117}Sn)$ = 63/59, Acenap 4,7-H), 7.32 (2 H, d, $^3J(^1H,^1H)$ = 6.9 Hz, Acenap 3,8-H), 7.27-7.14 (6 H, m, Sn*Ph-p*), 7.14-6.96 (24 H, m, 6 H, m, Sn*Ph-o,m*), 3.49 (4 H, s, Acenap 2xCH_2); ^{13}C NMR (75.5 MHz; $CDCl_3$; 25 ºC; Me_4Si): δ = 149.4(q), 142.8(s, $^2J(^{13}C,^{119/117}Sn)$ = 33 Hz, 4,7-C), 141.8(q), 137.3(s, $^2J(^{13}C,^{119/117}Sn)$ = 36 Hz), 134.2(q), 129.3(q), 128.8(q), 128.3(s), 128.2(s, $^3J(^{13}C,^{119/117}Sn)$ = 52 Hz), 119.9(s, $^2J(^{13}C,^{119/117}Sn)$ = 59 Hz, 3,8-C), 30.1(s, Acenap 2xCH_2); ^{119}Sn

NMR (100.7 MHz; $CDCl_3$; 25 ºC; Me_4Sn): δ = -120.8 (s, $^4J(^{119}Sn,^{117}Sn)$ = 31 Hz); MS (ES^+): *m/z* 351.02 (70%, $SnPh_3$), 383.05 (100, $SnPh_3OMe$), 503.08 (30, M^+-$SnPh_3$), 875.09 (21, M+ Na).

Bis(μ-5,6-acenaphthenediyl)trimethyltin [$Acenap_2(SnMe_2)_2$] (26):

Experimental as for compound **24** but with [$AcenapBr_2$] (0.79 g, 2.5 mmol), TMEDA (1.0 mL, 6.7 mmol), 2.5 M *n*-butyllithium (2.0 mL, 5.0 mmol) and Me_2SnCl_2 (1.1 g, 5 mmol). Colourless crystals were obtained by recrystallisation from chloroform (0.23 g, 30%); elemental analysis (Found: C, 55.9; H, 4.8. Calc. for $C_{18}H_{26}Sn_2$: C, 55.9; H, 4.7%); ^{1}H NMR (300 MHz, $CDCl_3$, Me_4Si): δ 7.66 (4 H, d, $^3J_{HH}$ = 6.7, $^3J_{HSn}$ = 61/58, Acenap 4,7-H), 7.22 (4 H, d, $^3J_{HH}$ = 6.8, Acenap 3,8-H), 3.30 (8 H, s, Acenap 4xCH_2), 0.51 (12 H, s, $^2J_{HSn}$ = 53/51, 4xCH_3); ^{13}C NMR (75.5 MHz, $CDCl_3$, Me_4Si): δ 148.6(q), 139.9(q), 138.7(s), 119.7(s), 30.3(s, Acenap 4xCH_2), -2.73(s, 4xCH_3); ^{119}Sn NMR (100.76 MHz, $CDCl_3$, Me_4Sn): δ -60.4(s).

X-ray Structure Analysis

X-ray crystal structure for **24** was determined at −148(1) °C on a Rigaku SCX Mini instrument with graphite-monochromated Mo Kα radiation (λ = 0.710 73 Å). Data for compound **25** was collected at -100(1) °C on a Rigaku XtaLAB P200 diffractometer Mo-Ka radiation (λ = 0.710 73 Å). Data for compound **26** was collected at −180(1) °C by using a Rigaku MM007 high brilliance RA generator (Mo Kα radiation, confocal optic) and Mercury CCD system. All data had intensities corrected for Lorentz, polarization, and absorption. The data for the complexes was collected and processed using CrystalClear[19,20] (Rigaku). The structures were solved by Patterson or direct methods and expanded using Fourier techniques. Non-hydrogen atoms were refined anisotropically, and hydrogen atoms were refined using a riding model. All calculations were performed using CrystalStructure[21] and SHELXL-97.

References

1. C. A. Coulson, R. Daudel and J. M. Robertson, *Proc. R. Soc. A*, 1951, **207**, 306.

2. D. W. J. Cruickshank, *Acta Crystallogr*., 1957, **10**, 504.

3. C. P. Brock and J. D. Dunitz, *Acta Crystallogr. Sect. B*, 1982, **38**, 2218.

4. J. Oddershede and S. Larsen, *J. Phys. Chem*., 2004, **108**, 1057.

5. V. Balasubramaniyan, *Chem. Rev*., 1966, **66**, 567.

6. H. Schmidbaur, H. -J. Öller, D. L. Wilkinson, B. Huber and G. Müller, *Chem. Ber*., 1989, **122**, 31.

7. H. Fujihara, R. Akaishi, T. Erata and N. Furukawa, *J. Chem. Soc. Chem. Commun*., 1989, 1789.

8. H. Fujihara and N. Furukawa, *J. Mol. Struct*., 1989, **261**, 192.

9. J. Handal, J. G. White, R. W. Franck, Y. H. Yuh and N. L. Allinger, *J. Am. Chem. Soc.*, 1977, **99**, 3345.

10. J. F. Blount, F. Cozzi, J. R. Damewood, D. L. Iroff, U. Sjöstrand and K. Mislow, *J. Am. Chem. Soc.*, 1980, **102**, 99.

11. F. A. L. Anet, D. Donovan, U. Sjöstrand, F. Cozzi and K. Mislow, *J. Am. Chem. Soc*., 1980, **103**, 1748.

12. W. D. Hounshell, F. A. L. Anet, F. Cozzi, J. R. Damewood, C. A. Johnson, U. Sjöstrand and K. Mislow, *J. Am. Chem. Soc*., 1980, **102**, 5941.

13. R. Schroeck, K. Angermaier, A. Sladek and H. Schmidbaur, *Organometallics*, 1994, **13**, 3399.

14. J. Meinwald, S. Knapp and T. Tatsuoka, *Tetrahedron letters*, 1977, **26**, 2247.

15. R. H. Mitchell, M. Chaudhary, R. V. Williams, R. Fyles, J. Gibson, M. J. Ashwood-Smith and A. J. Fry, *Can. J. Chem*., 1992, **10**, 1015.

16. N. Asao, P. Liu and K. Maruoka, *Angew. Chem. Int. Ed. Engl*., 1997, **36**, 2507.

17. K. B. Wiberg, *Tetrahedron*, 1968, **24**, 1083.

18. 1. M.-L. Lechner, K. S. Athukorala Arachchige, R. A. M. Randall, F. R. Knight, M. Bühl, A. M. Z. Slawin and J. D. Woollins, *Organometallics*, 2012, **31**, 2922.

19. CrystalClear 2.0; Rigaku Corp., Tokyo, 2010. CrystalClear Software User's Guide; Molecular Structure Corp.: The Woodlands, TX, 2011.

20. J. W. P. Flugrath, *Acta Crystallogr., Sect. D*, 1999, **D55**, 1718.

21. CrystalStructure 4.0: Crystal Structure Analysis Package; Rigaku and Rigaku/MSC, The Woodlands, TX 77381, 200.

APPENDIX 1

PUBLICATIONS TO DATE

1. Fergus R. Knight, **Kasun S. Athukorala Arachchige**, Rebecca A. M. Randall, Michael Bühl, Alexandra M. Z. Slawin, and J. Derek Woollins., *Dalton Trans.*, 2012**, 41,** 3154-3165.

2. Fergus R. Knight, Rebecca A. M. Randall, **Kasun S. Athukorala Arachchige,** Lucy Wakefield, John M. Griffin, Sharon E. Ashbrook, Michael Bühl, Alexandra M. Z. Slawin, and J. Derek Woollins, *Inorg. Chem.*, 2012, **51**(20), 11087-11097.

3. Marie-Luise Lechner, **Kasun S. Athukorala Arachchige**, Fergus R. Knight, Michael Bühl, Alexandra M. Z. Slawin and J. Derek Woollins, *Organometallics*, 2012**, 31**(7), 2922-2930.

4. Guoxiong Hua, **Kasun S. Athukorala Arachchige**, Alexandra M. Z. Slawin and J. Derek Woollins, *Eur. J. Org. Chem.*, 2013, **32**, 7402-7410.

5. Conor G. E. Fleming, **Kasun S. Athukorala Arachchige**, Michael Bühl, Rebecca Randall, Alexandra M. Z. Slawin and Petr Kilian., *Dalton Trans*, 2013**, 42**(5),1437-1450.

6. Matthew J. Ray, Rebecca A. M. Randall, **Kasun S. Athukorala Arachchige**, Alexandra M. Z. Slawin, Michael Bühl, Tomas Lebl and Petr Kilian., *Inorg. Chem.*, 2013**, 52**(8)**,** 4346-4359.

7. Andreas Nordheider, Tristram Chivers, Ramalingam Thirumoorthi, **Kasun S. Athukorala Arachchige**, Alexandra M. Z. Slawin, J. Derek Woollins and Ignacio Vargas-Baca, *Dalton Trans.*, 2013, **42**, 3291-3294.

8. Sebastien Meiries, Gaetan Le Duc, Anthony Chartoire, Alba Collado, Klaus Speck, **Kasun S. Athukorala Arachchige**, Alexandra M. Z. Slawin and Steven P. Nolan., *Chem. Eur. J*., 2013, **19**(51), 17358-17368.

9. Farida H. Aidoudi, Cameron Black, **Kasun S. Athukorala Arachchige**, Alexandra M. Z. Slawin, Russell E. Morris and Philip Lightfoot, *Dalton Trans*., 2014, **43**(2), 568-575.

10. Louise M. Diamond, Fergus R. Knight, Rebecca A. M. Randall**, Kasun S. A. Arachchige**, Michael Bühl, Alexandra M. Z. Slawin and J. Derek Woollins., *Eur. J. Inorg. Chem.*, 2014, 1512-1523.

11. Martin W. Stanford, Fergus R. Knight, **Kasun S. Athukorala Arachchige**, Paula Sanz Camacho, Sharon E. Ashbrook, Michael Bühl, Alexandra M. Z. Slawin and J. Derek Woollins, *Dalton Trans*., 2014, **43**, 6548-6560.

12. Andreas Nordheider, Tristram Chivers, Oliver Schön, Konstantin Karaghiosoff, **K. S. Athukorala Arachchige**, Alexandra M. Z. Slawin and J. Derek Woollins, *Chem. Eur. J.*, 2014, **20**, 704-712.

13. Laura Ascherl, Andreas Nordheider**, Kasun S. Athukorala Arachchige**, David B. Cordes, Konstantin Karaghiosoff, Michael Bühl, Alexandra M. Z. Slawin and J. Derek Woollins, *Chem. Commun*., 2014, accepted.

14. Brian A. Chalmers, Michael Bühl, **K. S. Athukorala Arachchige**, A. M. Z. Slawin and P. Kilian, *J. Am. Chem. Soc*., 2014, accepted.

15. **Kasun S. Athukorala Arachchige**, Paula Sanz Camacho, Matthew J. Ray, Brian A. Chalmers, Fergus R. Knight, Sharon E. Ashbrook, Michael Bühl, Petr Kilian, Alexandra M. Z. Slawin and J. Derek Woollins, *Organometallics*, 2014**,** accepted.